LABORATÓRIO NACIONAL
DE ENGENHARIA CIVIL

DEPARTAMENTO DE ESTRUTURAS
Núcleo de Engenharia Sísmica e Dinâmica
de Estruturas

Proc. 0305/17/14529

NEFOREEE PROJECT – TASK 2

Complementary nature of shaking tables and reaction walls: LNEC experimental program over Dorka and Jarret energy dissipation devices

Lisbon • February 2009

I&D ESTRUTURAS

RELATÓRIO 27/**2009 – NESDE/DE**

PROJECTO NEFOREEE – TASK 2

Complementaridade entre ensaios em mesa sísmica e em paredes de reacção: Programa experimental desenvolvido no LNEC em dispositivos dissipadores de energia do tipo Dorka e Jarret

O presente Relatório refere-se à Task 2 do Projecto NEFOREEE (New Fields of Research in Earthquake Engineering Experimentation) e compreende a descrição da plataforma sísmica triaxial do LNEC e o programa experimental desenvolvido no âmbito do Projecto em causa.

Apresenta-se a descrição da mesa sísmica com suporte gráfico, desenhos de dimensionamento e fotografias, bem como o seu sistema de controlo. Inclui-se ainda a instrumentação disponível no NESDE e a utilizada em particular para estes ensaios.

Descreve-se o modelo ensaiado, a sequência de ensaios e por fim apresentam-se os resultados obtidos. Para finalizar é feita uma breve análise de resultados.

Lisboa, Laboratório Nacional de Engenharia Civil, Janeiro de 2009

NEFOREEE PROJECT – TASK 2

Complementary Nature of Shaking Tables and Reaction Walls:

LNEC experimental program over Dorka and Jarret energy dissipation devices

This Report corresponds to Task 2 of the NEFOREEE (New Fields of Research in Earthquake Engineering Experimentation) Project and comprises the description of the LNEC triaxial seismic platform and a presentation of the experimental program developed in the scope of this Project.

It is presented a description of the facility and the 3D seismic table with graphical support, drawings of sizing and photographs, as well as its control system. The main instrumentation available at the NESDE laboratory and used for this test is also included in this report.

The model tested is described as well as the sequence of tests and the corresponding obtained results. Finally a brief analysis of the results is made.

Lisbon, Laboratório Nacional de Engenharia Civil, Janeiro 2009

Laboratório Nacional da Engenharia Civil, Janeiro de 2009

VISTOS

A Chefe do Núcleo de Engenharia Sísmica e Dinâmica de Estruturas

Ema Coelho

O Director
do Departamento de Estruturas

João Almeida Fernandes

AUTORIA

Maria João Falcão Silva
Bolseira de Doutoramento

Alfredo Campos Costa
Investigador Principal

Rogério Bairrão
Investigador Principal

INDEX

INDEX OF FIGURES

INDEX OF TABLES

1. Introduction

This report provides a detailed account of a series of shaking table tests performed on a very specific specimen at the Portuguese National Laboratory of Civil Engineering (LNEC). The object of this research report corresponds to a part of TASK1 of NEFOREEE project (New Fields of Research in Earthquake Engineering Experimentation), named “Complementarity of shaking tables and reaction walls”.

The main objectives of the NEFOREE Project are to pursue research in the following six areas of earthquake engineering:

1. Controlled testing in the non-linear range of material behaviour.
2. The complementarity of shaking tables and reaction walls.
3. Reliability of qualification tests performed on shaking tables.
4. Sub-structuring methods on shaking tables.
5. Multiple support input to large structures.
6. Continuous pseudodynamic (CPsD) testing with substructuring.

Each of the referred objectives was linked to a given Task, being LNEC involved in TASK 1 (Controlled Testing in the Non-Linear Range), and TASK 2 (Complementary Nature of Shaking Tables and Reaction Walls. For each one of the Tasks the lead partner was responsible for setting the objectives [1]

In what concerns TASK2, the leadership was from the responsibility of JRC-Ispra and the main research objective was to review the advantages and drawbacks of the two types of experimental facilities for seismic testing (shaking tables and reaction walls) and the circumstances under which the corresponding results can be compared. For this purpose a benchmark study was developed and a particular structure was designed to illustrate the drawbacks of both methodologies and to validate countermeasures leading to enhancements.

Very specific experimental programs were defined to illustrate the complementary of both testing approaches. The experimental procedures, boundary conditions and input excitation signals were thoroughly documented.

The Continuous Pseudodynamic (CPsD) testing method or Shaking Table testing method is currently applied in all the large structural testing facilities in Europe and especially in the scope of the European Commission ECOEST2/ECOLEADER programs. The results of Task 2 mainly profit such research Networks, who include most of Europe’s earthquake engineering specialists.

The purpose of benchmarking studies is to design a single degree of freedom specimen that exhibits a certain flexibility, to be used in different facilities for a better comparison between shaking table and reaction wall tests. The material used in the model should be steel, because it allows good flexibility and easy design of the connection details. In the benchmark studies the specimen must satisfy some requirements in order to optimize its design and to obtain the best modularity to be used in the different experiments (shaking table and pseudo-dynamic test) performed in the laboratories of the consortium. In the following the main requirements that should be fulfilled are presented:

1 Specimens size should be in accordance with the properties of the shaking tables and reaction walls to be suitable for both experiments;

2 The total mass should not exceed the maximum payload capacity of the smallest shaking table involved in the benchmark studies, in this case 10ton which corresponds to the maximum payload for the Athens shaking table;
3 The slab, constituted by sheet metal and concrete properly connected, should be designed to achieve the requested mass, not blocking the connections with the frame and allowing future slabs adding to increase the number of the degrees of freedom;
4 The braces with K and X shapes must allow the work with a structure having a range of natural frequencies of interest for shaking table and pseudo-dynamic tests. The braces are the elements responsible for reducing the maximum displacements observed during the tests, as a good compromise between flexibility and mass requirement;
5 The braces should also be designed to allow the placement of passive-control devices.

2. Earthquake testing facilities involved in NEFOREEE – Task 2

2.1. JRC-Ispra

The ELSA (European Laboratory for Structural Assessment) Laboratory is a structural mechanics laboratory based on a strong reaction wall/floor system, with dimensions and load capacity unique in the European Union. It was built in the period 1990-1992 at the Ispra site (Italy) of the Joint Research Centre (JRC) of the European Commission and it was enlarged in 1995. The ELSA laboratory is based on a 16m high reaction-wall and a 25 m x 21 m + 15 m x 13 m strong-floor system. Such a system provides the strength and rigidity necessary to resist the loads that are applied to the test structures using servo-hydraulic actuators (Table 1). The platform added in 1995 enables to use both sides of the reaction wall. [2]

Table 1: Characteristics of the ELSA Reaction Wall Laboratory [2].

LOAD CAPACITY	**REACTION WALL**	**Bending moment** **Base shear**	200 MN-m 20 MN
	REACTION FLOOR	**Bending moment**	240 MN-m
	ANCHOR LOAD	**Axial Force**	500 kN
HYDRAULIC CHARACTERISTICS	**FLOW**		1500 l/min
	PRESSURE		210 bar
	ACTUATORS	**Load** **Stroke**	(0.5 - 3.0) MN +/- (0.25 - 1.0) m

The actuators are equipped with load cells to measure the applied forces and digital transducers based on optical systems are used to monitor the deformation of the structure. The reaction wall infrastructure allows static, cyclic and pseudo-dynamic testing of large-scale and full-scale models of structures, such as for instance a full-scale 5-storey building or a large bridge. [2]

A particularly original feature of the ELSA reaction wall infrastructure is the possibility to simulate, through the so called pseudo-dynamic test (PDT) method, the response of large and heavy structures to severe dynamic loading, such as induced, for instance, by an earthquake. In the PDT method the test structure is subjected to a displacement history which is calculated on-line by a computer and applied to the "lumped mass" points of the structure via the actuators. In the configuration developed at ELSA, each

actuator has its own digital control system and all the controllers are connected via a local area network to a central computer (Figure 1). Overall, the digital control system, which has been developed in-house, has opened up the possibility of developing state-of-the-art control feedback algorithms, such as the continuous PDT, where the test time scale is reduced up to ten times the time required by classical PDT implementations [2].

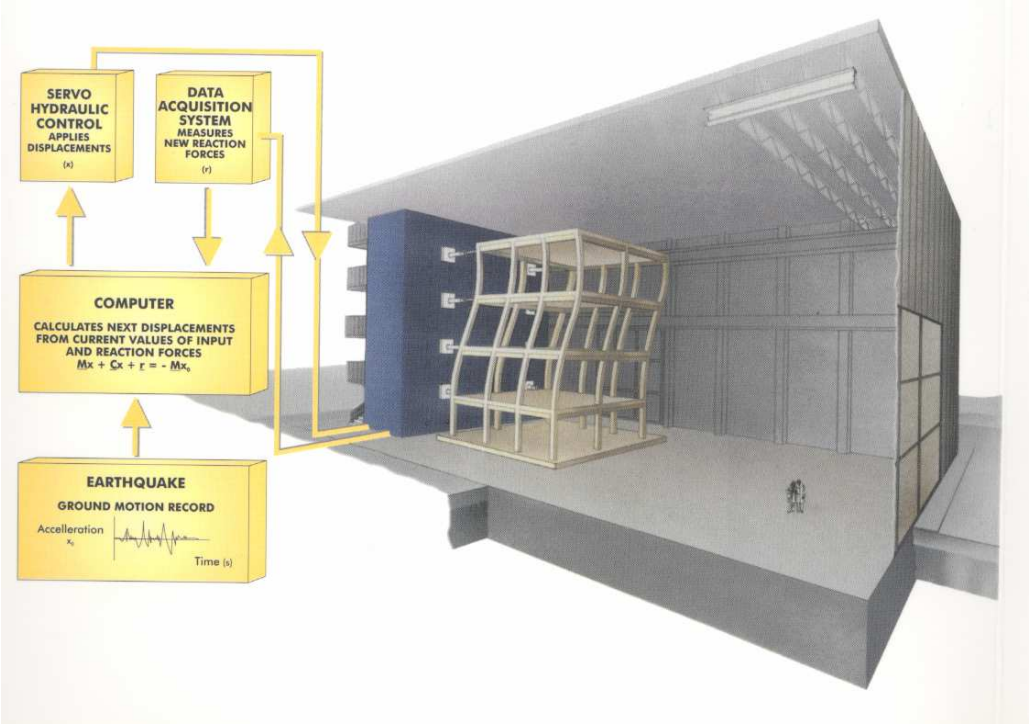

Figure 1: Implementation of the PDT method at ELSA [2].

Another major feature of the reaction wall testing facility is the possibility of using sub-structuring techniques. With this procedure the most interesting part of a structure is tested experimentally, whilst the rest is modeled analytically using, for instance, a finite element computer code. The computer then accounts for the interactions between the two parts of the structure in calculating the displacements to impose on the tested part. Thus, structures much larger than the laboratory itself, such as the bridge shown on Figure 2, can be tested. In this case, by assuming elastic behavior of the bridge deck, the computer accounts for the effects of its behavior and calculates the displacements to be imposed at the top of a physical model of the piers where severe damage is expected during testing. Several experiments of this type have already been successfully performed at ELSA since 1994. [2]

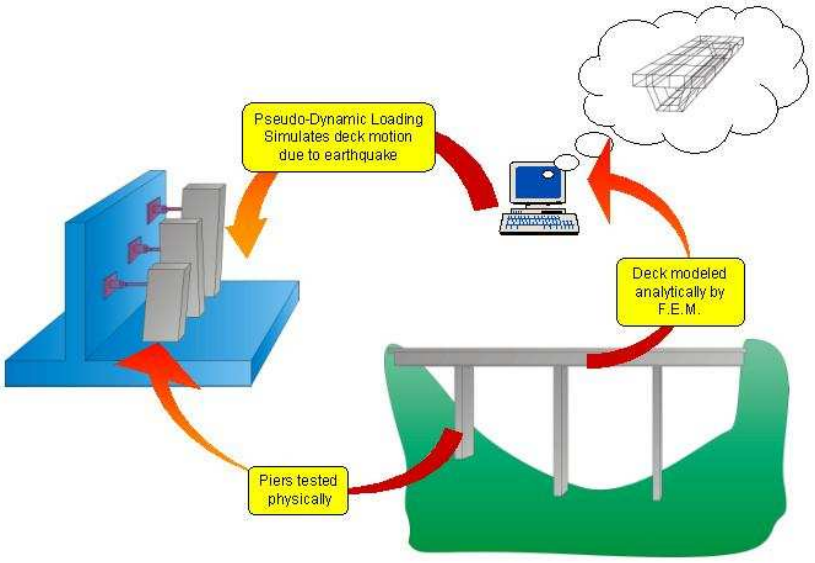

Figure 2: Sub-structuring PDT technique applied to full-scale bridge piers [2].

The ELSA laboratory was the first Laboratory in the world to perform large-scale seismic tests on bridges using the sub-structuring technique. Other tests successfully performed at ELSA using the sub-structuring technique include the testing of full-scale base isolation devices in conjunction with analytical models of the protected structure. [2]

2.2. NTUA – Athens

It is well known that Greece suffers from destructive earthquakes. The best way to mitigate the effects of earthquakes is to improve the knowledge on the subjects and to compile the necessary regulations for the aseismic design. [2]

The destructive earthquakes that occurred in the major cities of Greece during the period 1978-1981 gave a “support” for the construction of the shaking simulator at the Laboratory of Earthquake Engineering at National technical University of Athens. This facility was totally funded from national sources. The simulator consists of a rigid platform with dimension 4.00 x 4.00m^2 with 6 degrees of freedom and of a system controlling the input motion and the response of the specimen tested on the platform. [2]

The earthquake simulator was calibrated and became fully operational at the beginning of 1987. The six DOF shaking simulator with its control system is unique in the word, that time. The steel table was constructed in Athens, as well as other minor items of the facility. The weight of the reinforced concrete reaction mass amounts to 25MN. The facility has a full active control along the 6 degrees of freedom. The whole laboratory and the adjacent to it office building was specially designed and constructed to serve the facility under consideration [2]. The NTUA shaking table platform presents the characteristics defined in the following tables

Table 2: Type of Shaking Table (adapted from [2]).

	Transl. X	Transl. Y	Transl. Z	Pitch	Roll	Yaw
Uniaxial	-	-	-	-	-	-
Biaxial	-	-	-	-	-	-
Multiaxial	**YES**	**YES**	**YES**	**YES**	**YES**	**YES**

Type of Actuation **Electrohydraulic**

Table 3: Characteristics of the Actuators (adapted from [2]).

	Manufacturer	Model	Force (kN)	Number of units
Horizontal (X)			**320**	**2**
Horizontal (Y)			**320**	**2**
Vertical			**640**	

Table 4: Characteristics of the Platform.

Material	**Steel**
Size (mxm)	**4×4**
Weight (kN)	**100**

Table 5: Shaking Table Performances

Frequency range (Hz)			**0-100**
Stroke (mm p-p)	Horizontal		**200**
	Vertical		**200**
Max Velocity (m/s)	Horizontal		**1,0**
	Vertical		**1,0**
Max Acceleration at bare table (m/s^2)	Horizontal	harmonic	**20**
		impulse	
	Vertical	harmonic	**40**
		impulse	
Yaw	Rotation degrees (±)		**±4,0**
	Velocity (rad/s)		
Pitch/Roll	Rotation degrees (±)		**±4,0**
	Velocity (rad/s)		
Max Overturning Moment (kNxm)			**200**
Max Specimen Dead Weight (kN)			**100**

The control system of the NTUA facility is constituted by an analogue and a digital units. The first one is a specific analogue unit with which the user has the possibility of independent performance of each degree of freedom. The unit can produce and combine: sinusoidal, quadrangular etc vibrations for each direction simultaneously. External recordings of other receivers can be used to provide input to the analogue unit. The second one corresponds to a PC based digital unit with possibility of exciting the platform with strong motion data stored in the computer, through D/A converters. The six degrees of freedom can be excited simultaneously or independently. Creation of input signals with specified spectra or other characteristics is available. In parallel, to main pc a second control unit is functioning. With this acquisition, it is possible to handle longer input motions (of several minutes duration) to increase the resolution and to accelerate the evaluation of results. [2]

Besides the 6-D shaking table in the NTUA laboratory are also functioning a reaction wall, a shear walls testing apparatus and an elastomeric isolators testing apparatus.

The first one corresponds to an independent reaction wall facility functioning at the backside of the laboratory. Its capacity is 10 MNm, 6m height and two pieces: 4 and 5 m long, 1.1 m width, out of steel. Several jacks may function with independent control, with a new oil pump. The jacks have capacities of 500 kN, 300 kN, 200kN and 100kN. A mobile data acquisition system of 16 channels is supporting this facility. [2]

The second one corresponds to an innovative testing apparatus that is also functioning in the laboratory for testing under recyclic loads horizontally applied, small walls of any dimension (up to 2 m height, 1.5 m long, 1.0 m thickness). The vertical load may be up to 1000 kN and can be kept constant without any variation throughout the tests.

Finally the elastomeric isolators testing apparatus corresponds to an innovative testing device that is also functioning in the laboratory. It corresponds to a strong beam where only vertically sliding supports is bridging the shaking table. The horizontal motion of the ‘bridge’ is restricted. The elastomers are placed between the ‘bridge’ and the surface of the platform and may be tested under the full capacity of the shaking table [2].

2.3. LNEC – Lisbon [3]

The 3D shaking table together with an uniaxial shaking table, are placed in the Earthquake Engineering Research Centre (NESDE), a LNEC division devoted to the research in the area of Earthquake Engineering. The research is being developed in NESDE in the past years addressing subjects from the seismic experimental and analytical modeling of structural systems to the issues of the seismic hazard and risk analysis.

LNEC seismic facility operates since 1996 and has been integrated in the “Large Scale Scientific Installations” of the European Union since its beginning. The equipment is operated by LNEC personnel. Besides the shaking tables and their power stations, this infrastructure includes specifically dedicated rooms devoted to control, data acquisition and processing.

The use of LNEC seismic testing facility by external users has been providing significant information and important outcomes for the improvement of knowledge on the seismic response of different types of structures. The equipment and the methodologies of testing have to be frequently improved, aiming at the continous improvement of the service provided and the increase of the field of application of the facility.

The interest of the studies performed within the use of this facility has been clearly demonstrated by the results of several large experimental studies carried out within the European funded ECOEST and ECOLEADER networks that enabled, in the framework of the Large Scale Facilities and Access to Research Infrastructures sub-programs of TMR and IHP Programs, the access of numerous foreign researchers to the LNEC facility and allowed the study of several key issues in Earthquake Engineering Research.

LNEC international standing has already attracted a widespread of interested scientific groups, clearly demonstrated by the quality of previous users and also by the interest shown by potential future users. It should be mentioned that LNEC 3D shaking table

has unique features, which justify that some experimental research activities can only be performed in this facility.

On the National scale, LNEC holds a leading position in the fields of seismic testing and earthquake risk assessment. NESDE/LNEC has developed important activity in the framework definition of seismic scenarios for the Metropolitan Area of Lisbon (MAL) by the request of the National Civil Protection.

2.3.1. LNEC 3D shaking table

The LNEC3-D shaking table is constituted by three main subgroups: (1) the body (or platform), on which the models or specimens are attached and tested; (2) the guidance system, whose main mission consists of ensuring that the platform only moves according to desired degrees of freedom; and (3) the actuating system, which includes the control systems associates and that has for mission to impose the desired action during the experimental programs (adapted from [4]).

The platform is a structure in welded steel plates with a triangular prism form, with the corresponding useful dimensions of 4,6x5,6 m^2 where are mounted and fixed, the models or specimens to be tested during the experimental programs developed in LNEC. The structure of the platform was conceived in order to present high local and global rigidity in the connection areas with the remaining subgroups of the main structure (as the actuating and guidance systems) [adapted from 4].

Figure 3: Bottom view of the LNEC-3D seismic platform [4].

The guidance system constitutes an innovative element when compared to other seismic platforms. As it was already related, in the seismic tests carried out in LNEC 3D seismic platform the global movement of the body will be result of the combination of three translation movements (two horizontal and a vertical one). These translations correspond to the three of the six degrees of freedom of the body of the platform. In this context, the guidance system will have to eliminate (or, in the reality, adequately to restrict) the possibility of the movement of the body according to these three remaining degrees of freedom, that, as it is known, are constituted by rotations around the three orthogonal (adapted from [4]). The experience achieved with the seismic platform shows that the performance is not away from what was expect in the design.

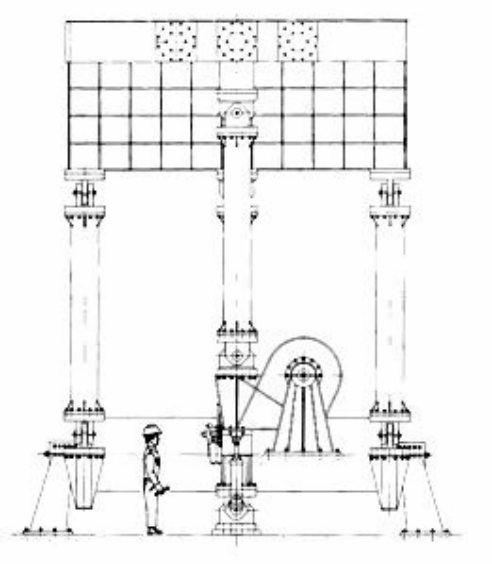

Figure 4: Transverse view [4].

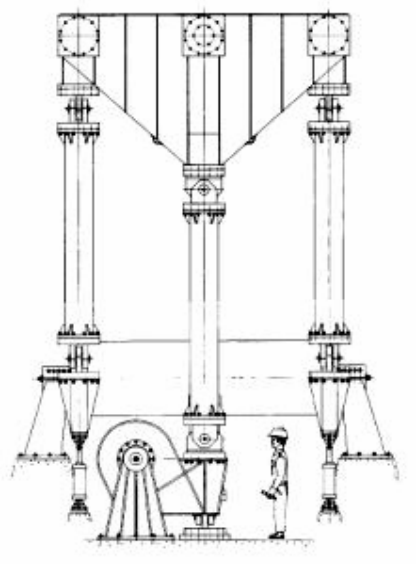

Figure 5: Longitudinal view [4].

The actuating system is essentially constituted by oil-hydromechanical actuators and associated control systems. In a simplified way each actuator is constituted of an hydraulical cylinder of double-effect and pair-connecting rod, one or more servovalves and a set of hydraulical components, responsible for linking, command and security. The oil under pressure (normal pressure of functioning 200 bar) is supplied by a group of hydraulical motion-bombs with a maximum debit of 690 liters/min (adapted from [4]).

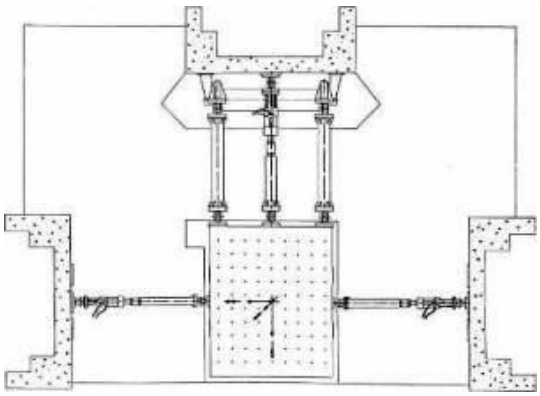

Figure 6: General plan of LNEC-3D shaking table [4].

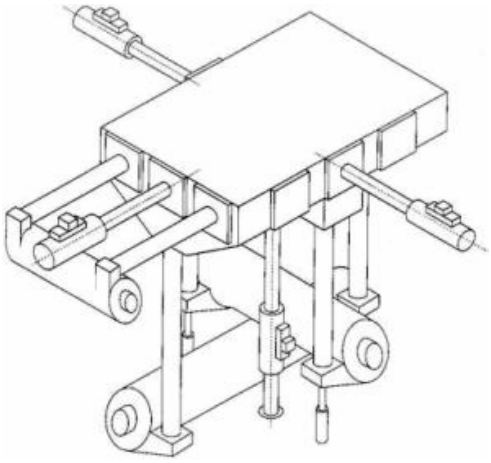

Figure 7: Perspective of LNEC-3D shaking table [4].

In the following tables are resumed the main characteristics of LNEC – 3D shaking table:

Table 6: General Characteristics (adapted from [2]).

General Designation	MESA SÍSMICA TRIAXILAL DO LNEC
Short Designation	LNEC-3G
Design/Construction	LNEC e INSTRON
Year	1995

Table 7: Type of platform (adapted from [2]).

	Longitudinal X	Lateral Y	Vertical Z	Rotation X	Rotation Y	Rotation Z
Uniaxial	-	-	-	-	-	-
Biaxial	-	-	-	-	-	-
Multiaxial	Yes	Yes	Yes	N/A	N/A	N/A

Table 8: Characteristics of the platform (adapted from [2]).

Dimensions (mxm)	4.6x5.6
Weight (kN)	392
Material	Steel

Table 9: Actuators (adapted from [2]).

	Hydraulic actuators		
	Manufacturer	Force (kN)	Units
Longitudinal	INSTRON	1250	1
Lateral	INSTRON	750	2
Vertical	INSTRON	375	1

Table 10: Platform performance (adapted from [2]).

Frequencies			Hz	0.1-40.0
Max efective course	Horizontal		mm_{pp}	290/400
	Vertical		mm_{pp}	290/400
Max velocity (nominal)	Horizontal	Transverse	cm/s	70.1-121.5
		Longitudinal	cm/s	41.9/72.6
	Vertical		cm/s	42.4/73.5
Max acceleration (platform without model)	Horizontal	Transverse	m/s2	18.75
		Longitudinal	m/s2	9.38
	Vertical		m/s2	31.25
Rotations (x, y and z)	Rotation degrees		º	N/A
	Velocity		Rad/s	N/A
Max overturning moment			kNxm	N/A
Max self-weight of the model			kN	392
Max compensated self-weight			kN	392

Table 11: Characteristics of the control system (adapted from [2]).

Type of control	Compound (Analogic/Digital)

Table 12: Characteristics of the analogic control (adapted from [2]).

Manufacturer	INSTRON
Type	Uni-Variable units

Table 13: Characteristics of the digital control (adapted from [2]).

Hardware	Industrial Computer	INSTRON 8580 Control Tower
	Channels D/A	8 ADC channels – 16 bit
	Channels A/D	
Software	Design	INSTRON

In the testing room, where is placed the seismic platform, there are some additional structures that are described in the following tables

Table 14: Hydraulic system (adapted from [2]).

Electric Power (kW)	330
Flow Rate (kN)	690
Pressure (MPa)	20.7

Table 15: Crane system inside the testing room (adapted from [2]).

Number of cranes	2
Maximum capacity (kN)	392
Maximum height (m)	8

Table 16: Access gates (adapted from [2]).

Number of gates	2
Maximum height (m)	4.5

2.3.2. Instrumentation

2.3.2.1. Optical displacement transducers

Optical displacement transducers HAMAMATSU C5949 (comprising F50 mm lens, sensor head and led target) and HAMAMATSU conditioning device PSH Controllers C2399 can be used for measuring the displacements on the vertical/transverse plane. The following figure and table show the type of HAMAMATSUs used in LNEC-3D shaking table experimental programs and their main characteristics.

Table 17: Characteristics of the Optical displacement transducers.

Manufacture	HAMAMATSU PHOTONICS (www.hamamatsu.com)
Model	C2399-00 and C5949
Measurement points	1 to 7
Spectral response	700 to 1150 nm
Sampling frequency	300 Hz
Position detecting error	+/-1
Error due to ligth	+/-1

2.3.2.2. Inductive displacement transducers – LVDTs

RDP Electronics ACT/2000C, ACT4000C and ACT6000 inductive displacement transducers having work strokes of +/-50mm, +/-100mm and +/-150mm, respectively, can be used for measuring vertical and diagonal displacements.

The following tables show some of the main characteristics of the LVDT displacement transducers that can be used during the tests performed in LNEC shaking table.

Table 18: Main characteristics of the LVDT displacement transducers.

Manufacture	RDP ELECTRONICS (www.rdpe.com)
Model	ACT2000, ACT4000 and ACT6000
Stroke	+/-50mm (ACT2000); +/-100mm (ACT4000); +/-150mm (ACT6000)
Sensitivity	15mV/V/mm (ACT6000) to 3030mV/V/mm(ACT2000)
Energising supply	5 Vrms, 5 Hz
Linearity deviation	0.08% (ACT2000) to 0,3% (ACT6000)

Besides the RDP Electronics, and for displacement measurements, are also available in LNEC facility inductive displacement transducers from the type HOTTINGER BALDWIN M. Their main characteristics are presented in the following table.

Table 19: Main characteristics of the Hottinger Baldwin displacement transducers.

Manufacture	HOTTINGER BALDWIN M (www.hbm.com)
Model	WA300 and WA500
Sensitivity	80mV/V
Linear deviation	700 to 1150 nm
Sampling frequency	+/-0.1% to +/-0.2%
Frequency range	5 to 65 Hz

2.3.2.3. Accelerometers

High frequency ENDEVCO, model 7290-A with variable capacitance, CROSSBOW LF series with high precision and PCB Piezotronics, model 337A26, can be used for acceleration measurements in the experimental programs in development in LNEC facility

The following tables show some of the main characteristics of the accelerometers existing in LNEC facility.

Table 20: Characteristics of the high frequency ENDEVCO accelerometers.

Manufacture	ENDEVCO (www.endevco.com)
Model	7290A-2 and 7290A-10
Range [g pk]	+/-2 and +/-10
Sensitivity (at 100Hz) [mV/g]	1000+/-20 and 200+/-10
Amplitude Response +/-5% [Hz]	0 to 15 and 0 to 500
Mounted Ressonance and frequency [Hz]	1300 and 3000
Transverse Sensitivity [% Max]	2
Zero Measurand Output [mV Max]	+/-50
Damping Ratio [-]	4.5 and 0.7

Table 21: Characteristics of the CROSSBOW LF accelerometers.

Manufacture	CROSSBOW (www.xbow.com)
Model	CXL02LF3
Input Range [g pk]	+/-2
Sensitivity [V/g]	1
Transverse Sensitivity [%FS]	+/-5
Non-Linearity [%FS	+/-2
Alignment Error [deg]	+/-2
Noise Density [µg/Hz½]	140
Noise [mg rms]	1
Bandwith [Hz]	DC-50

Table 22: Characteristics of the PCB Piezotronics accelerometers.

Manufacture	PCB PIEZOTRONICS (www.pcb.com)
Model	337A26
Sensitivity [mV/g]	100
Measurement range [g pk]	100
Broadband resolution [g rms]	0.0001
Frequency range [Hz]	0.5 to 5000

3. Description of the specimen

3.1. Design of the main elements of the specimen

The main elements of the specimen were designed through an elastic analysis using the finite element program SAP200NL [5] considering two earthquake time history accelerations: one is an earthquake generated to be in accordance with type 1 of the Eurocode 8 [6] and the other is an El Centro earthquake 1940, both of them with a peak ground acceleration of 0.5g.

The El Centro time history (Figures 8 and 9) is a low frequency shake with most of the corresponding energy in the frequency below 8Hz, hence suitable to test the model at its natural frequency. Moreover the referred earthquake, even if not ideally suited to the role of standard time history, is useful to test the shaking tables to its performance limits. [7]

On the other hand the choice of an earthquake artificially generated in accordance to type 1 of Eurocode8 (Figures 10 and 11) is also justified by the will of exciting the model with the maximum force at its natural frequency of about 8Hz. [7]

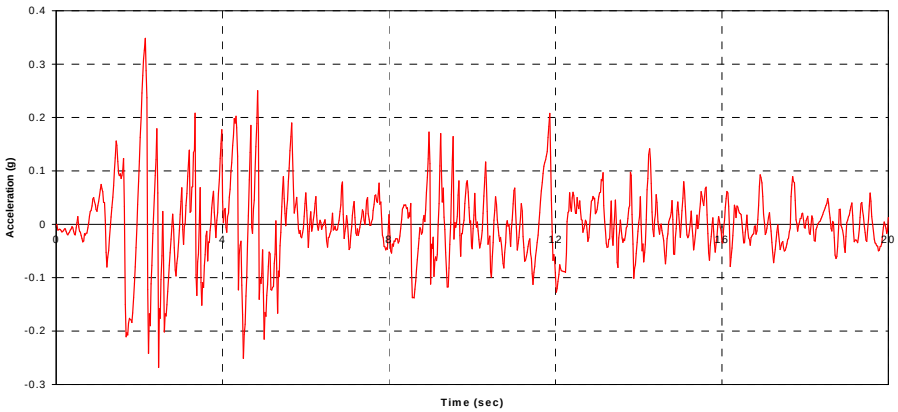

Figure 8: Original El Centro earthquake (1940) time history acceleration [adapted from 7].

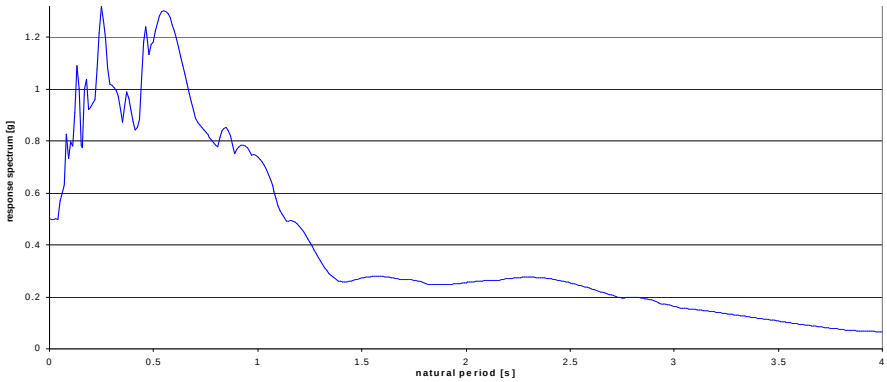

Figure 9: Response spectrum for El Centro earthquake (1940) [adapted from 7].

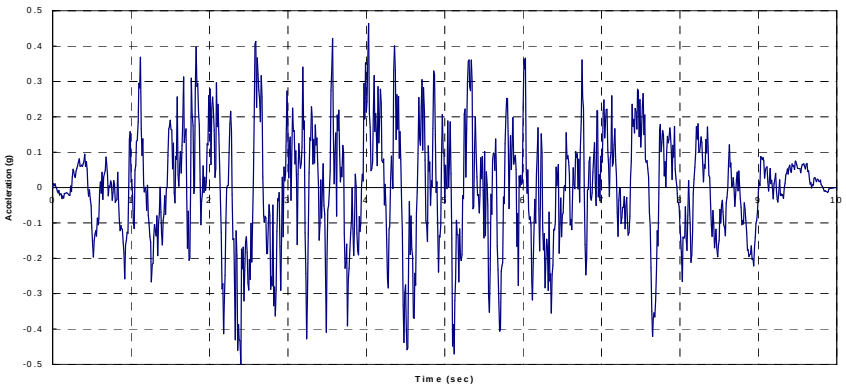

Figure 10: Time history acceleration of simulated earthquake according to type 1 of Eurocode8 [adapted from 7].

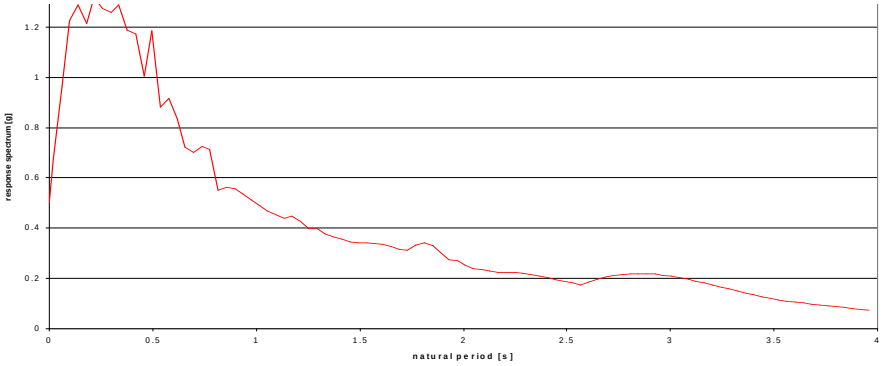

Figure 11: Response spectrum for simulated earthquake according to type 1 of Eurocode 8 (adapted from [7]).

According to the design requirements the frame should present a longitudinal size of 300 cm; a transversal size of 275 cm; a column height of 450 cm; and an interstorey distance of 300 cm. The longitudinal and transversal dimensions were chosen according to the specimen limit for shaking table tests. In what regards the height of the column and the inter-storey distance, the slabs could be spaced with 3m, allow another steel-concrete composite slab to be added at a height of 6m and consequently a second degree of freedom can be obtained simply through the use of elements with the same characteristics and details of the basic structure. [7]

The choice of the steel to be used in the steel sections was based on the compromise between flexibility and maximum admissible displacements during the tests without damage. The connections between braces and bracing joints as well as bracing joints and beam and column elements are achieved with the same construction details, in order to prefabricate easily the structure. Sections and shapes of braces are chosen to allow: the crossing of the braces; the location of passive energy dissipation devices; and to grant the resistance to external forces. The beams and the columns were chosen to be made with HEB 100 and HEB 180 steel sections, the inverted V and X braces with HEB 100 and UPN 100 sections, in the latter case the choice is imposed to allow the crossing of the braces in the central position. The inverted V braces with dampers in the upper position are located in the longitudinal direction; while X braces are chosen to grant stiffness to the frame in the transversal direction. The steel selected is of grade S355. [8] All selected steel sections satisfy Eurocode 3 checks [10].

After choosing of main element steel sections, the frame was verified through an elastic analysis assuming the passive device with high yield strength and hence unable to dissipate energy. The weight of the upper concrete slab, 8250 kg, was then chosen to make the total weight of the model close to 10 tons, which corresponds to the nominal capacity of the smallest shaking table facility involved [NTUA). The composite slab and the shear connectors satisfy Eurocode 4 checks [11].

A one degree-of-freedom full-scale shear type K-braced steel frame, easily transportable from lab to lab, was conceived at the University of Trento. The structure was designed to allow two types of dissipation devices to be inserted: a shear panel device (Dorka) and the Jarret device. The model without the energy dissipation devices included presented a very linear behavior with a very low damping. This should certainly put in evidence the alteration introduced by the testing methods such as control delays in the PsD method or spurious rocking on the shaking table. With non-linear dissipator devices, those deficiencies may be hidden by the large damping

developed at the specimen, but an appropriate strain-rate effect compensation technique is necessary within the PsD method. In a similar way, that non linearity may impose limitations as well on the compensation techniques based on linear filtering of the reference signal and traditionally used at the shaking tables. [8]

For the experimental program, and in accordance with the details of the University of Trento, two twin full-scale steel structures were constructed at the JRC Ispra. One structure was kept to be tested using the pseudo-dynamic method on the Ispra reaction wall. The second structure was sent by NTUA, in Athens, where it was dynamically tested on the shaking table. The structure was afterwards dismounted and sent to the LNEC, in Lisbon, in order to repeat the same tests as in the NTUA campaign. [9] The specimens were equipped with two types of energy dissipation devices in the longitudinal direction. The first one corresponds, as referred before, to a steel shear panel device engineered by Schmidt and Dorka [12] and which is inserted into a square steel tube and dissipates energy by means of elastic-plastic shearing. The second one is the Jarret's energy dissipative device which relies heavily on the compression of a viscous-elastic silicone fluid. [9] Details on both dampers are drawn in the following subsection of this report.

The main characteristics of the specimen and a corresponding global view can be easily observed in Figures 12 and 13, respectively.

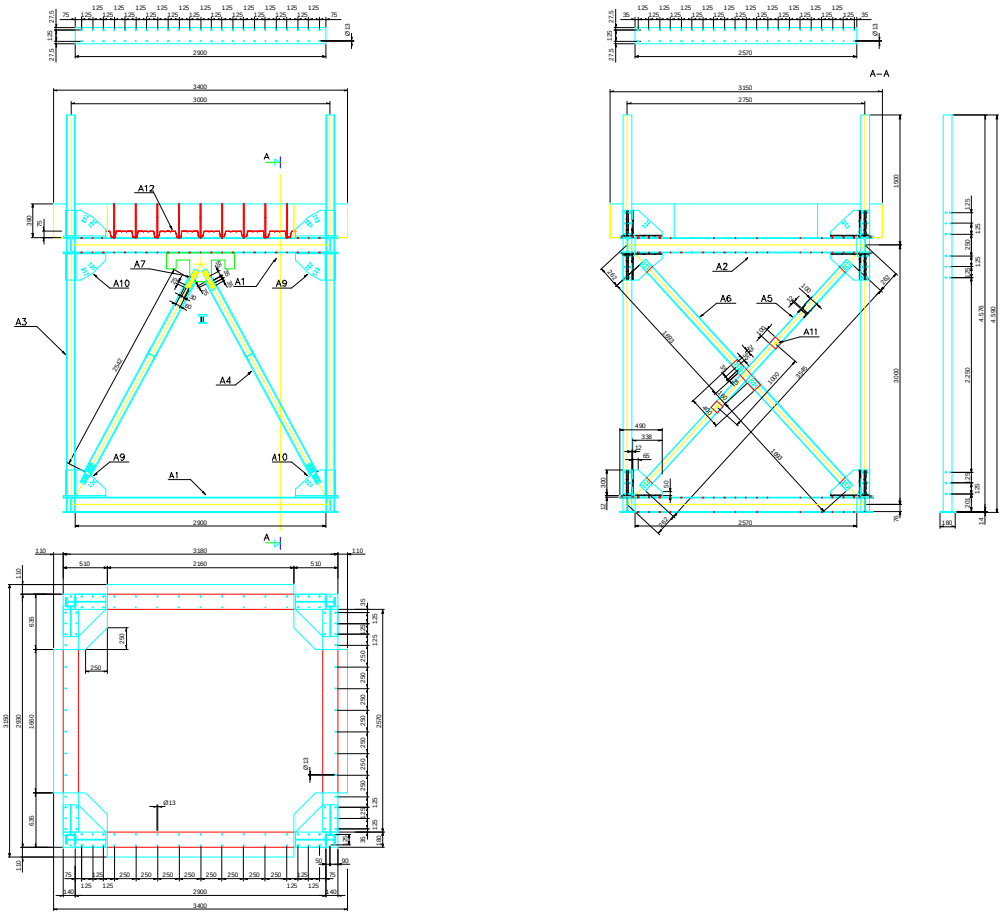

Figure 12: Main characteristics of the single degree of freedom specimen, plant, longitudinal and transversal profiles [adapted from 7].

Figure 13: General overview of the specimen.

3.2. Design of the dissipation devices

The structure is equipped with energy dissipation devices in the longitudinal direction. In particular, two dampers have been designed.

3.2.1. Dorka devices

The first one is a steel shear panel device which was engineered by Schmidt and Dorka [12]; it is inserted into a square steel tube and dissipates energy by means of elastic-plastic shearing. Details of the damper are drawn in Figure 14 while the relevant specimen is shown in Figure 15. [9]

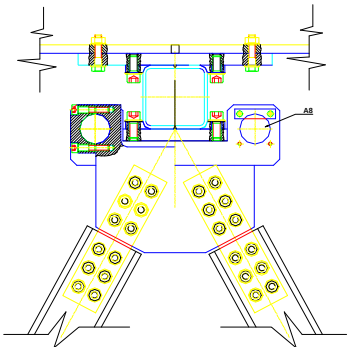

Figure 14: Dorka shear panel, adapted from [7].

Figure 15: View of Dorka shear panel devices.

The steel shear panel is inserted into a square tubular, that dissipates the energy imposed by the earthquake with its elastic-plastic behavior; the device is easily replaceable and the stress-strain relationship can be reproduced through a Bouc-Wen model [13]. The choice of the optimized model's parameters is made in order to reach the best correspondence to the experimental tests of the device developed in ELSA Laboratory [7].

3.2.2. Jarret devices

The second type of device tested was the Jarret's energy dissipative which relies on the compression of a viscous-elastic silicone fluid. These devices are applied to the specimen to dissipate a large part of the kinetic energy generated in a seismic event [7]. Extensive applications of this damper in braced structures have been made by Sorace and Terenzi [14]. The details of the damper are drawn in Figure 16 while a view of the devices is reported in Figure 17.

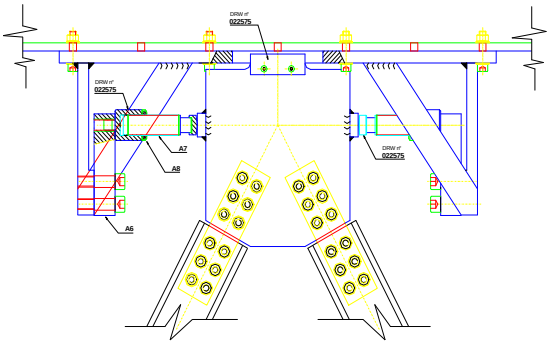

Figure 16: Jarret's viscous fluid damper, adapted from [7].

Figure 17: View of Jarret's viscous fluid damper.

3.3. Numerical analysis of the model and the devices

The specimen and the dampers (Dorka and Jarret) were modeled and analyzed through the Sap2000NL computer program [5]. There were performed preliminary simulations and the corresponding natural frequencies of the model were determined for the different configurations of passive energy dissipation devices. In detail, the natural frequencies of the specimen are summarized in Table 23. It is important to refer that three structures have been considered: i) Unbraced structure, ii) Braced structure with Dorka devices, iii) Braced structure with Jarret devices. During the experimental programs these structures will be labeled as Specimen I, II and III, respectively. [9]

Table 23: Dynamic properties of the model obtained from the numerical analysis (adapted from [9]).

Specimen	Mass [kg]	Damper	1st mode	2nd mode	3rd mode	4th mode
I	9030	None	2.3	17.7	29.9	48.5
II	9943	Dorka	7.8	18.4	25.6	39.7
III	9943	Jarret (initial/inelastic stiffness)	(8.4/3.4)	37.2	70.0	79.9

Simulations of Specimen II and III were performed under sine sweeps and earthquakes of different amplitudes in order to highlight the behavior of the Structures endowed with different dampers [9] In the following figures is showed the behavior of the dampers when subjected to the El Centro records and to the artificial EC8 accelerograms.

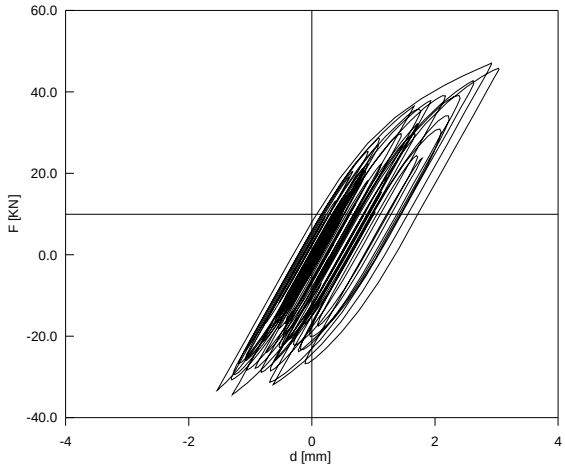

Figure 18: Numerically simulated hysteretic loops of steel damper subjected to the NS component of El Centro accelerogram with a 0.5g PGA, adapted from [9].

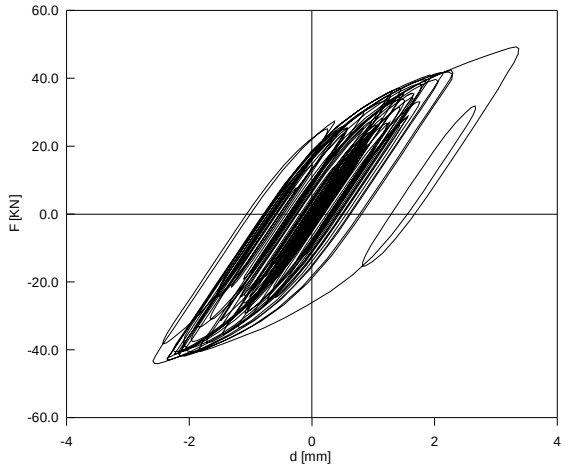

Figure 19: Numerically simulated hysteretic loops of steel damper subjected to the EC-8 artificial accelerogram with a 0.5g PGA, adapted from [9].

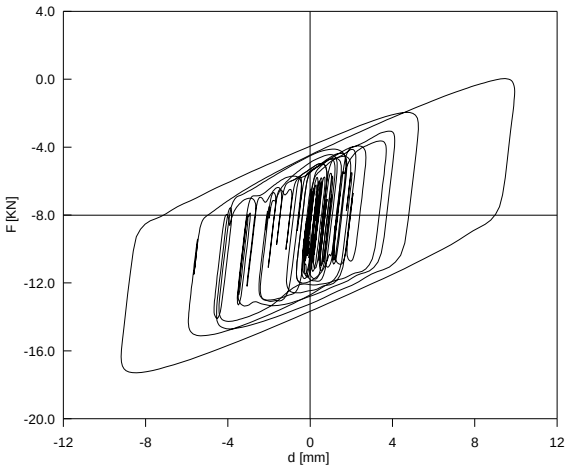

Figure 20: Numerically simulated hysteretic loops of Jarret's damper subjected to the NS component of El Centro accelerogram with a 0.5g PGA, adapted from [9].

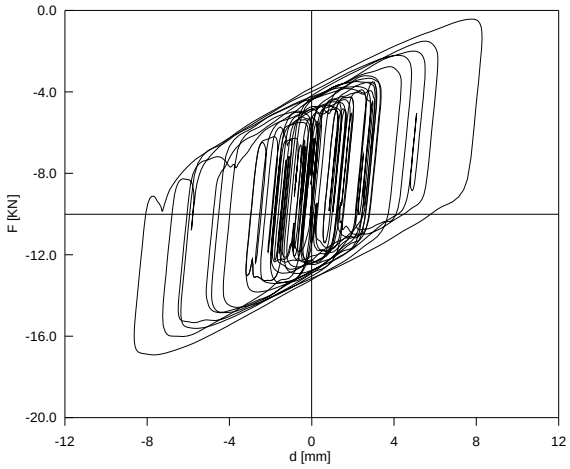

Figure 21: Numerically simulated hysteretic loops of Jarret's damper subjected to the EC-8 artificial accelerogram with a 0.5g PGA, adapted from [9].

As expected, these simulations show clearly that the EC-8 artificial earthquake is more severe in terms of hysteretic cycles than the El Centro accelerogram at the same PGA. level. Therefore, the former accelerogram will be employed for the inelastic testing of dampers. [9]

4. Instrumentation

The instrumentation set-up that was used to measure the response of each specimen to earthquake tests on the shaking table is shown in Figure 22. In the instrumentation of the specimen were used accelerometers, inductive displacement transducers (LVDTs) and optical displacement transducers (Hamamatsu) from the types referred in section 2 of the present report.

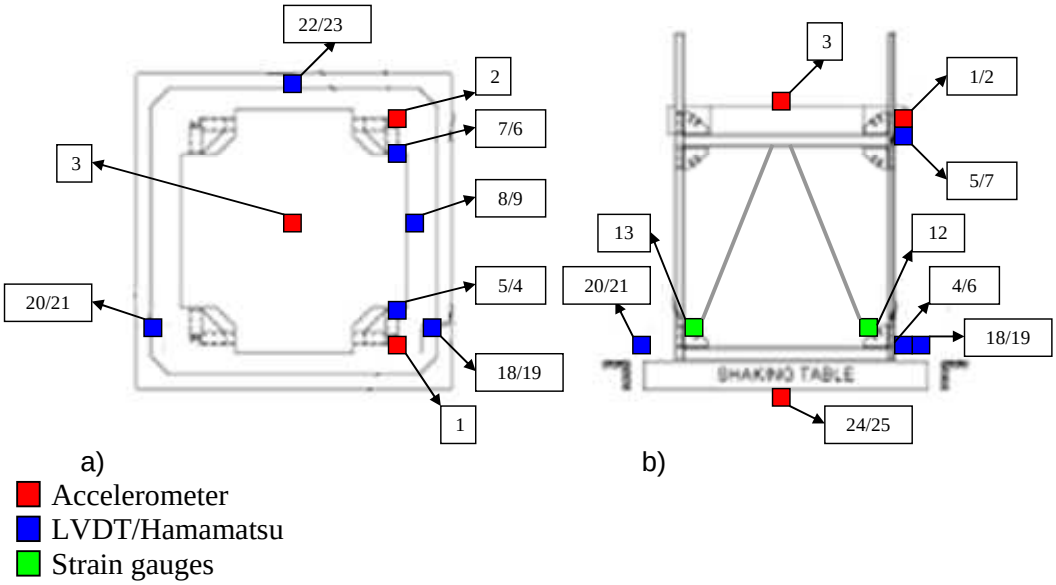

Figure 22: Instrumentation set-up of the SPECIMEN I at LNEC shaking table: a) Plan View and b) elevation.

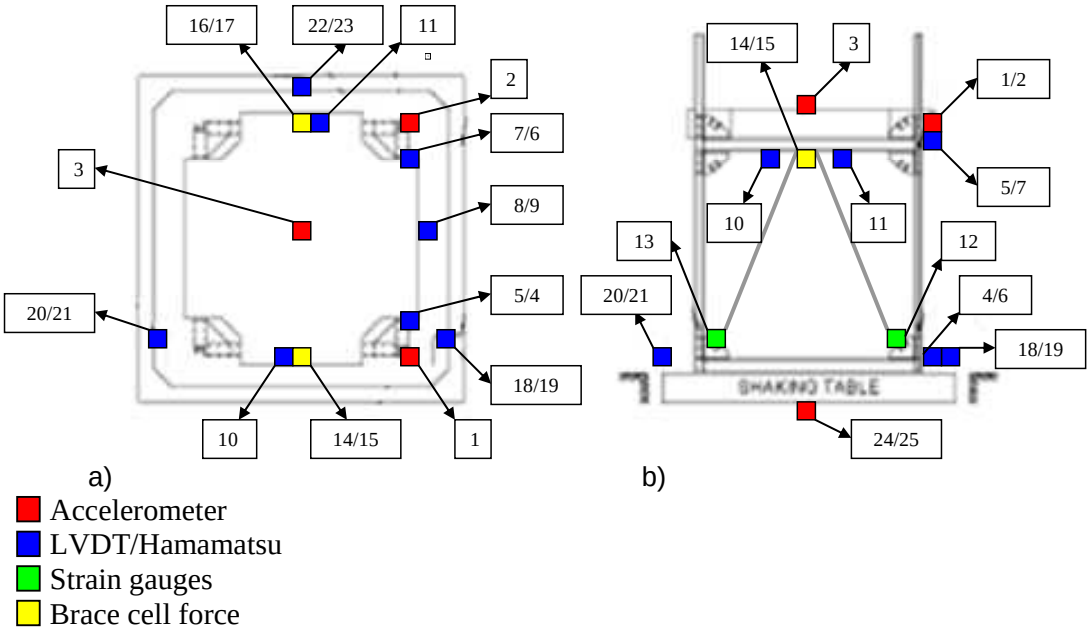

Figure 23: Instrumentation set-up of the SPECIMEN II and III at LNEC shaking table: a) Plan View and b) elevation.

Three accelerometers (A1X, A2X, A3X) were fixed on the top of the specimen in order to measure in and out-of-plane accelerations. Absolute displacements at the top (D3, D4) and at the bottom (D1, D2) level of each specimen were measured with respect to a stiff frame, which was fixed outside the shaking platform. Strain gauges (SG1, SG2) were also used in order to check the strain level at the end of steel columns. For the tests performed on SPECIMEN II and III the shear force was measured directly on dissipation devices (LC), while two additional displacement transducers were mounted at the devices as well (Figure 23)

5. Experimental Program

5.1. Input signal

The tests included in the LNEC experimental program comprised the called Stage tests and the called Characterisation tests. The Stage tests corresponded to main earthquake series with increasing intensities from 0.2 to 1.0g.

The main earthquake series used corresponded to uniaxial earthquake tests on the specimens performed using two different time histories in the main direction (X). These time histories were, as referred in subsection 3.1, a modified component of El Centro earthquake (1940) and an artificial time history, which was generated to match the elastic response spectrum Type 1 of Eurocode8 [6] with corresponding peak ground acceleration of 0.5g, damping at 5% and subsoil category A.

The characterisation tests comprised the so called sin-sweep test and the cat tests. The first one corresponded to the performance of a complementary a Ramp sinusoidal excitation with test frequency 100% and 80% of natural frequency of the specimen in order to achieve each specimen resonant response. This way just before the

earthquake tests, the specimen was tested under sine logarithmic sweep excitation along X direction for the determination of its natural frequencies and their damping. The sine logarithmic sweep signal that has been applied is in a frequency range of 1-35 Hz at a rate of one octave per minute. The tests were executed along global X axis with an amplitude vibration of 0.05g.Since sine sweep rate is one octave per minute and the start frequency is 1 Hz, the exciting frequency versus time is given by the following expression [9]:

$$f(Hz) = 1.0 \times 2^{\frac{Time(s)}{60}} \quad (1)$$

These sine sweep tests were performed to evaluate the natural frequencies and the damping of each specimen. It were also performed the so called Cat tests which precede every Stage.
Series and corresponded to low amplitude, broadband base signals with the objective of estimating the specimen's dynamic characteristics and their evolution during the experimental tests.

In the following figures are presented some examples of the time histories used in LNEC facility for the earthquake tests and the corresponding spectra.
In Annex are presented all the input signals used in LNEC experimental program.

5.2. Loading sequence

In the following tables (24 to 26) are presented the tests performed in each specimen during the experimental program developed in LNEC.

Table 24: Tests performed on the SPECIMEN I (Bare Frame).

Test	Description
1	Cat00 along EW direction, Table acceleration 0.05g
2	El Centro earthquake along EW direction, Table Acceleration 0.20g
3	Cat01 along EW direction, Table acceleration 0.05g

Table 25: Tests performed on the SPECIMEN II (Frame with Dorka devices).

Test	Description
4	Cat02 along EW direction, Table acceleration 0.05g
5	El Centro along EW direction, Table acceleration 0.20g
6	Sinusoidal 10.28 Hz, Table acceleration 0.05g
7	Artificial EC8 time history along EW direction, Table acceleration 0.20g
8	Sinusoidal 8.22 Hz, Table acceleration 0.05g
9	Cat03 along EW direction, Table acceleration 0.05g
10	Artificial EC8 time history along EW direction, Table acceleration 0.60g
11	Cat04 along EW direction, Table acceleration 0.05g
12	Artificial EC8 time history along EW direction, Table acceleration 0.80g
13	Cat05 along EW direction, Table acceleration 0.05g
14	Artificial EC8 time history along EW direction,Table acceleration 1.0g
15	Cat06 along EW direction, Table acceleration 0.05g

Table 26: Tests performed on the SPECIMEN III (Frame with Jarret devices).

Test	Description
16	Cat07 along EW direction, Table acceleration 0.05g
17	El Centro along EW direction, Table acceleration 0.20g
18	Sinusoidal 9.48 Hz, Table acceleration 0.05g
19	Artificial EC8 time history along EW direction, Table acceleration 0.20g
20	Sinusoidal 7.58 Hz, Table acceleration 0.05g
21	Cat09 along EW direction, Table acceleration 0.05g
22	Artificial EC8 time history along EW direction, Table acceleration 0.60g
23	Cat10 along EW direction, Table acceleration 0.05g
24	Artificial EC8 time history along EW direction, Table acceleration 0.80g
25	Cat11 along EW direction, Table acceleration 0.05g
26	Artificial EC8 time history along EW direction, Table acceleration 1.0g

6. Data acquisition

The instrumentation of the SPECIMENS was the previously referred. The corresponding physical units used all along the present Report are g and mm, respectively.
The different sensors were connected to 4 posts corresponding, respectively to: Post 1 – accelerometers, Post 2 – inductive displacement transducers, Post 3 – strain gauges and Post 4 – Optical displacement transducers.
In the following tables are presented the list of channels with the corresponding identification numbers and simplified description of the measurement parameters:

Table 27: List of channels used during the tests on SPECIMEN I.

Channel	Description
1	Top Beam transverse acceleration (NW) – A1X
2	Top Beam transverse acceleration (SW) – A2X
3	Mass center vertical acceleration – A3X
4	NW Base transverse displacement
5	NW Top column transverse displacement
6	SW Base transverse displacement
7	SW Top column transverse displacement
8	Longitudinal mass displacement (West beam)
9	Vertical mass displacement (West beam)
12	Strain gauge E1
13	Strain gauge E2
18	Transverse table displacement (NW corner)
19	Vertical table displacement (NW corner)
20	Transverse table displacement (NE corner)
21	Vertical table displacement (NE corner)
22	Longitudinal table displacement (S)
23	Vertical table displacement (S)
24	EW Table acceleration
25	NS Table acceleration

Table 28: List of channels used during the tests on SPECIMEN II and III.

Channel	Description
1	Top Beam transverse acceleration (NW) – A1X
2	Top Beam transverse acceleration (SW) – A2X
3	Mass center vertical acceleration – A3X
4	NW Base transverse displacement
5	NW Top column transverse displacement
6	SW Base transverse displacement
7	SW Top column transverse displacement
8	Longitudinal mass displacement (West beam)
9	Vertical mass displacement (West beam)
10	Brace Displacement North Side (LVDT)
11	Brace Displacement South Side (LVDT)
12	Strain gauge E1
13	Strain gauge E2
14	Brace Cell Force South Side (NW)
15	Brace Cell Force South Side (NE)
16	Brace Cell Force South Side (SW)
17	Brace Cell Force South Side (SE)
18	Transverse table displacement (NW corner)
19	Vertical table displacement (NW corner)
20	Transverse table displacement (NE corner)
21	Vertical table displacement (NE corner)
22	Longitudinal table displacement (S)
23	Vertical table displacement (S)
24	EW Table acceleration
25	NS Table acceleration

7. Tests results and other analysis

The modal frequencies were identified using frequency response functions estimations and the peak picking method. It was identified one translational single mode as a result of the dynamic action imposed for each characterization (cat) series. The evolution of the modal frequencies during the experimental program is presented in Figure 24.

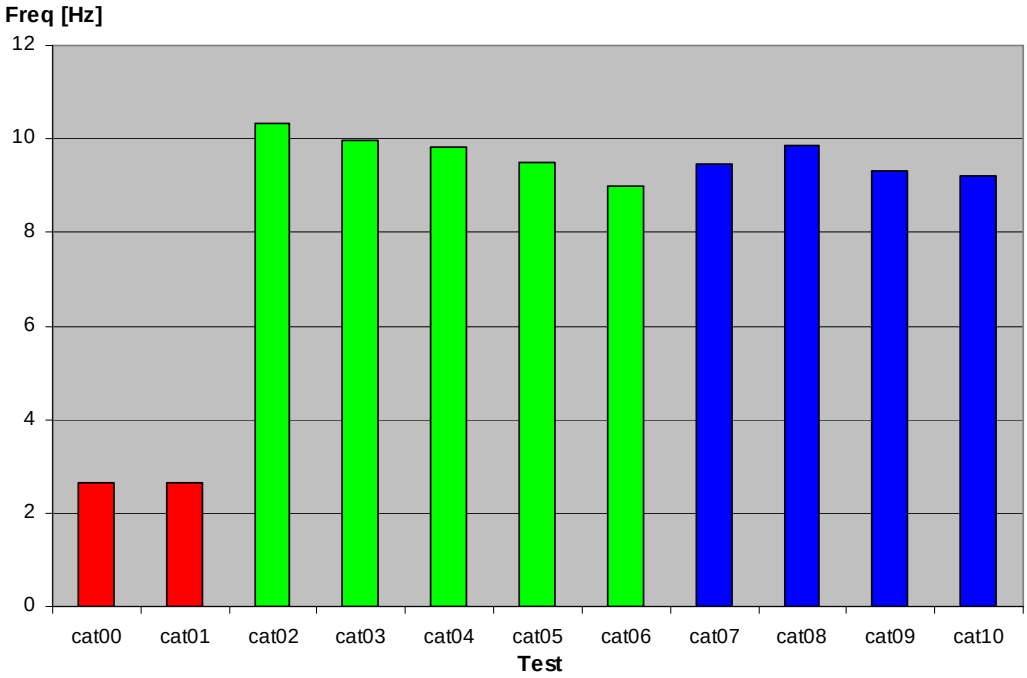

Figure 24: Experimental modal frequencies.

An example of the identified frequency response functions obtained during the experimental program is presented in Figures 25 and 26 for the cases of the Dorka devices and Jarrett devices (viscous fluid damper), respectively, and after an artificial EC8 input with a shaking table peak acceleration of 0.8g.

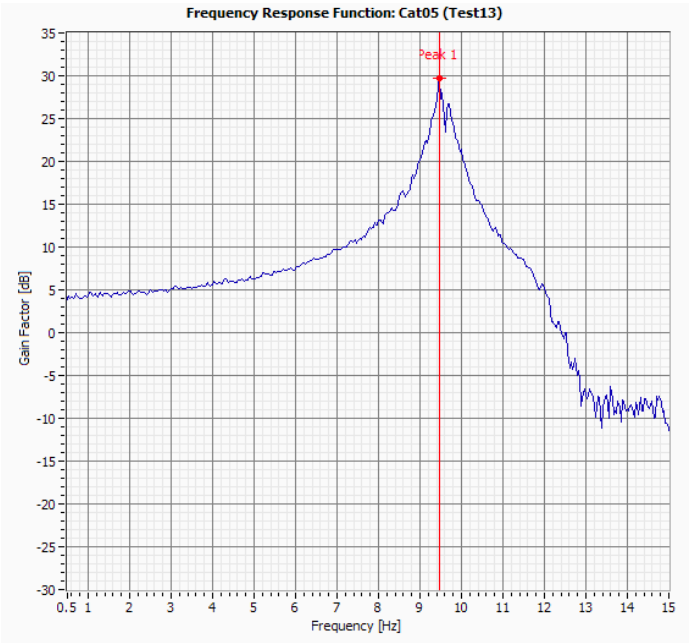

Figure 25: FRF peak picking for SPECIMEN II – cat5 (Test13).

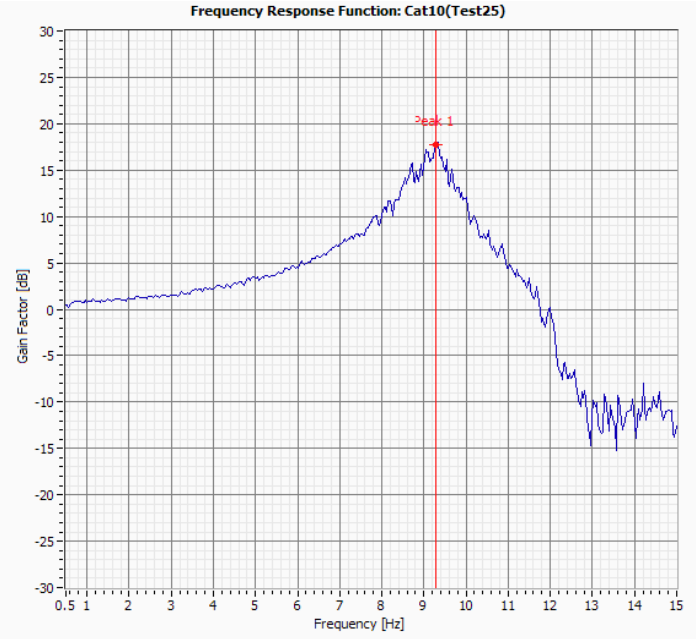

Figure 26: FRF peak picking for SPECIMEN III – cat10 (Test25).

The damping was estimated for all the specimens, being obtained approximated values of 1.5%, 3% and 7.5% for SPECIMEN I, II and III, respectively. All the FRFs, obtained during the analysis of the results, as well as the corresponding damping values are presented in Annex III.

During the experimental program all the channels identified in Table 27 and 28 were recorded (Annex IV).

Figures 27 and 28 show some of the results obtained for the NW top transverse acceleration and the NW top column displacement during the ElCentro 0.2g input, corresponding to Test2, Test5 and Test17. In these figures Plot 0 corresponds to the results obtained for SPECIMEN I, plot 1 for SPECIMEN II and plot 2 for SPECIMEN III.

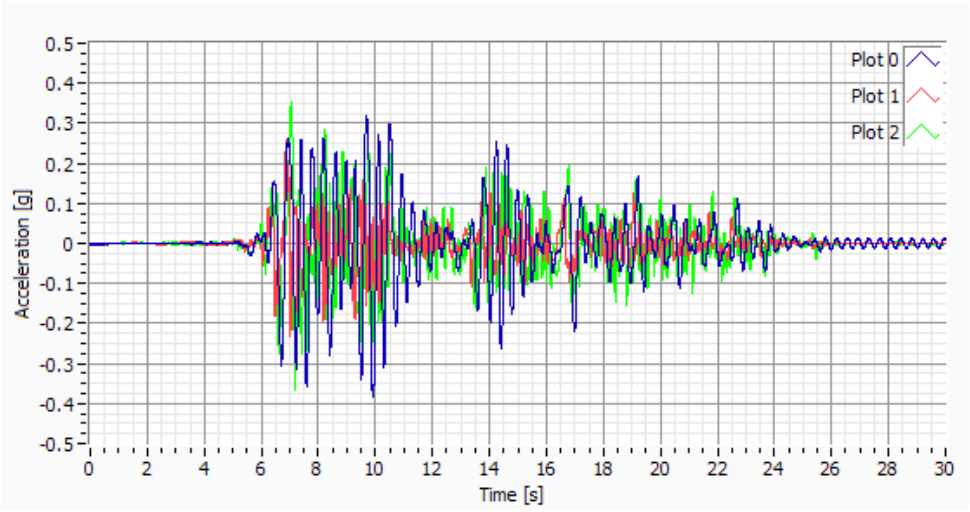

Figure 27: Comparison of NW top mass transverse acceleration.

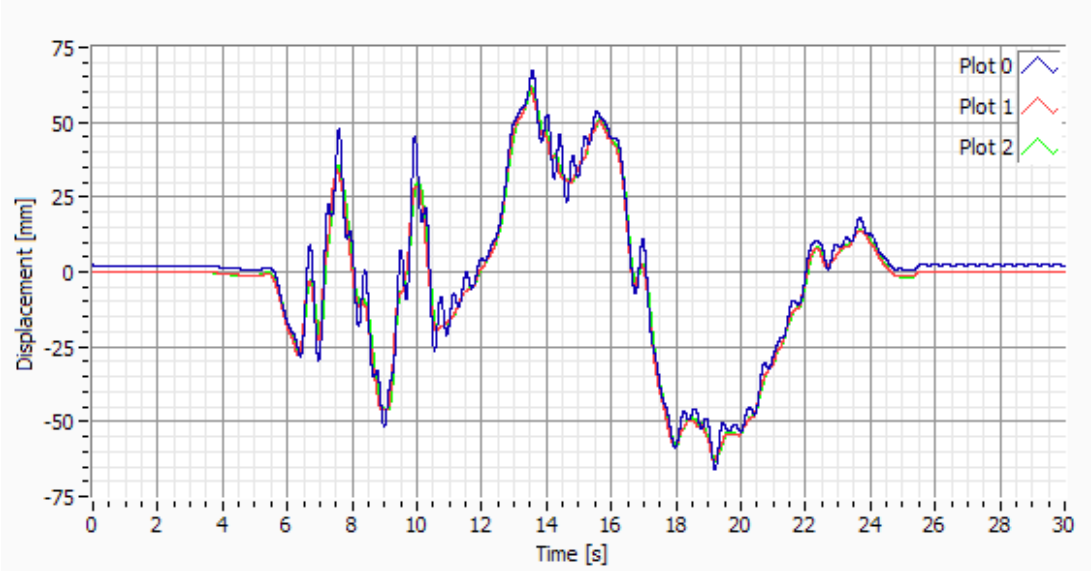

Figure 28: Comparison of NW top column transverse displacement.

From the observation of these results it can be concluded that concerning accelerations, the SPECIMEN II was the one which has presented the lowest values at the top mass level. Concerning displacements, all the SPECIMENS have presented a similar behaviour.

Tables 29 and 30 present the main results obtained for the specimens with dissipation devices. The maxima values recorded at the most representative channels are shown.

Table 29: Maxima values for the tests performed on SPECIMEN II.

	ElCentro 0.2g	EC8 0.2g	EC8 0.6g	EC8 0.8g	EC8 1g
NW top accel trans [g]	0.26	0.32	1.02	1.16	1.39
SW top accel trans [g]	0.27	0.37	1.11	1.25	1.51
Vert mass accel (CM) [g]	0.014	0.020	0.47	1.18	1.26
NW top column displ [mm]	63.34	26.23	78.92	104.40	110.20
SW top column displ [mm]	63.45	26.49	80.57	106.69	133.85
FNorth [kN]	10.49	14.47	42.87	49.43	56.98
FSouth [kN]	12.59	17.47	47.41	58.22	60.12
Displ North [mm]	0.27	0.40	1.03	1.75	4.02
Displ South [mm]	0.38	0.36	1.26	2.51	5.49

Table 30: Maxima values for the tests performed on SPECIMEN III

	ElCentro 0.2g	EC8 0.2g	EC8 0.6g	EC8 0.8g	EC8 1g
NW top accel trans [g]	0.37	0.27	0.89	1.50	1.70
SW top accel trans [g]	0.33	0.30	0.87	1.58	1.74
Vert mass accel (CM) [g]	0.007	0.009	0.05	0.09	0.13
NW top column displ [mm]	63.04	28.27	85.57	107.12	102.23
SW top column displ [mm]	63.35	28.65	86.30	114.06	133.63
FNorth [kN]	6.30	8.21	20.89	35.63	50.54
FSouth [kN]	6.76	8.63	21.63	39.48	54.81
Displ North [mm]	1.96	1.99	10.61	11.71	12.55
Displ South [mm]	1.95	1.89	10.33	12.00	12.48

In what concerns the top accelerations (NW and SW) the values obtained were similar for low and medium intensities while for the two highest levels bigger values for the Jarrett device were achieved. This can be explained by the specific characteristics of the materials used in this device (viscous fluid).

The clearly higher values of vertical mass acceleration obtained for the Dorka devices are due to the plastic behaviour of the steel cubes allowing vertical deformations for all levels of PGA intensity.

In spite of the different behaviour observed for the devices the values of maxima top displacements recorded at both columns were very similar due to the high rigidity of the common V (K) bracing system adopted for both specimens.

The forces recorded in the two pairs of devices achieved approximately the same values in the final tests despite the differences observed in the beginning. For the low to medium intensity tests (ElCentro 0.2g, EC8 0.2g and EC8 0.6g) the measured forces were approximately two times in the Dorka devices which corresponds to a high concentration of stress. In the final steps, corresponding to high intensity tests, the values installed in each pair of devices were approximately the same.

For the maxima displacements in the devices the Jarret type presented higher displacement values varying from six times to three times the corresponding displacement in the Dorka device, from low to high intensity tests. This corresponds to high ductility characteristic of the Jarrett devices.

Figures 29 and 30 present interaction diagrams of the force-displacement records at the North side Dorka dissipation device (SPECIMEN II), for a medium and the maximum EC8 input accelerations, respectively. The maxima force and displacement values are clearly identified.

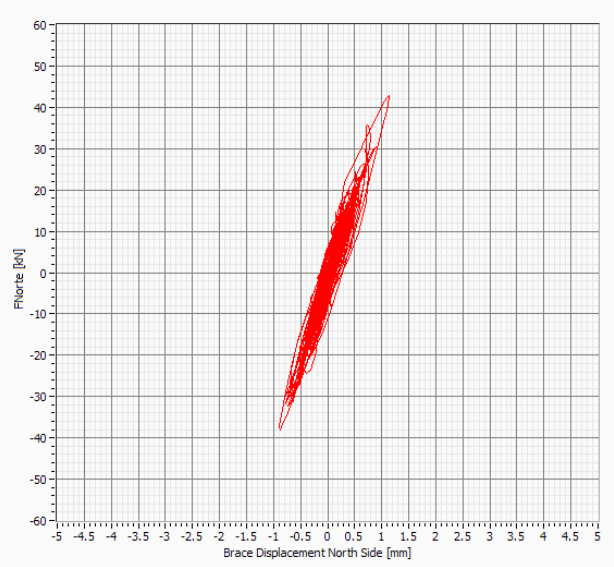

Figure 29: Hysteretic loops SPECIMEN II (EC8 0.6g).

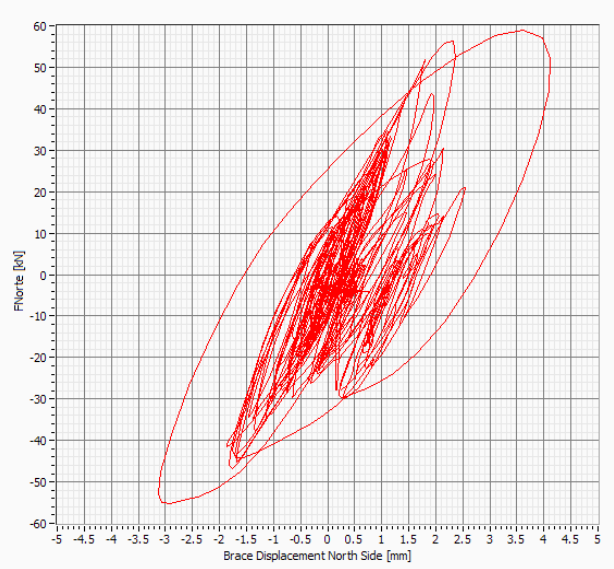

Figure 30: Hysteretic loops SPECIMEN II (EC8 1.0g).

Figures 31 and 32 present identical hysteretic loops for the North side Jarrett dissipation device (SPECIMEN III) for the same medium to high EC8 input accelerations, respectively.

The different behaviour of both the devices is clearly identified from the comparison of the figures.

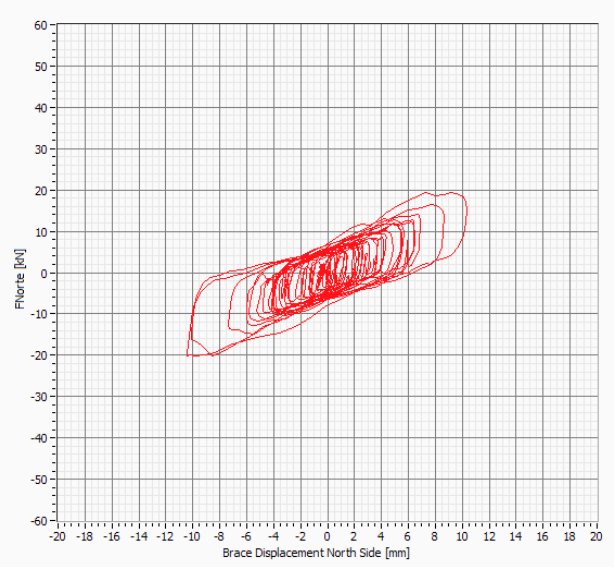

Figure 31: Hysteretic loops SPECIMEN III (EC8 0.6g)

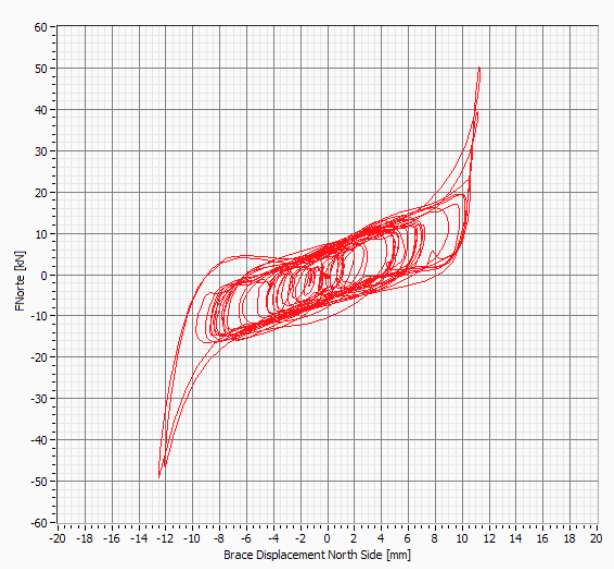

Figure 32: Hysteretic loops SPECIMEN III (EC8 1.0g).

From the observation of the previous figures it can be stated that apparently the Jarrett devices present a better dissipation performance with much higher displacements for the same levels of force when compared with the Dorka cubes.

It is also clear that the Jarrett characteristics are kept up to almost the maximum level of input accelerations achieved as it is presented in Figure 32 where it is shown that the changing of the global hysteretic loop shape appears only through final peaks in both directions.

Concerning the displacements recorded for both devices, for the Dorka the values have increased substantially from medium (0.6g) to high (1.0g) PGA values, while for the Jarrett those values were similar under both conditions. Although this fact, the Jarrett deformations were always extremely bigger thus proving their high capability. On the

other hand when comparing the hysteretic loops for the Dorka devices from medium to high intensities there is a clear improvement due to the shear behaviour of the steel membrane used.

The tests at NTUA and LNEC for the bare frame, braced frame with Dorka device and braced frame with Jarret device have been performed successfully in accordance with the program defined for the purpose. The frequencies obtained for all the experimental programs developed in each of the mentioned laboratories are the following presented.

Table 31: Comparison between frequencies obtained from the different experimental programs and the analytical frequencies.

Specimen	f_{exp} NTUA	Damping [%]	f_{exp} LNEC	Damping [%]	F_{anal}
I	2.6	3.02	2.65	1.60	2.3
II	8.6	5.3	8.99	2.98	7.8
III	8	17	9.21	7.63	8.4

It is also important to refer that for the comparison between PsD tests with the corresponding earthquakes used in NTUA and LNEC shaking-tables the measured displacements at the PsD test were compared with the measured values from the shaking table tests after a conversion to motions relative to the base by subtracting from them the displacement of the table itself. Then, the average of the two top displacements was used for the comparison.

The comparison of the final results will be object of future publications.

8. Conclusions

Within the NEFOREEE project, the activities on benchmark testing on shaking tables and reaction walls have successfully allowed to design a structural steel frame model with an upper reinforced concrete block according to which two identical specimens have been constructed.

The first one of these specimens has been dedicated to the tests on the shaking table facilities, while the second one was dedicated to the reaction-wall experiments. The shear-type benchmark structure was designed to exhibit a certain flexibility to be used in different laboratories for the comparison between the capabilities of shaking table and reaction wall tests. The material used is steel, because it allows specimens with good flexibility and easy connection details to be designed and to obtain the best modularity in order to be used in different laboratories. The adopted design allows working within a range of natural frequencies of interest for PsD and shaking table tests, reducing the maximum displacements during the tests as a good compromise between flexibility and mass requirement. The design of the model allowed for at least three interesting configurations: one as an unprotected frame without bracing and the other two with two different hysteretic dissipator devices connected to the frame through K braces. Tests have been performed of these configurations and for two specified accelerograms, apart from some other tests that helped to characterize the specimens [8].

The benchmark structure and related tests campaign are very specific to illustrate the complementarity of the different testing approaches. The whole benchmark testing

campaign allowed the comparison between experimental results from the dynamic tests performed in the two shaking tables (NTUA and LNEC) and the results obtained from a reaction wall performing PsD tests (ELSA-JRC). [8]

From the shaking table tests performed in LNEC it can be stated that the frequencies obtained were a little higher than the expected.

Some important studies on the control performance on shaking tables had already been conducted in the previous network projects. From the first comparison analysis of the tests results of the unprotected specimen, very useful information is being obtained about some previously disregarded aspects such us the spurious pitching on shaking tables, that may introduce an additional apparent damping in the response. Other useful information is expected to come when comparing results for the tests with the dissipator devices where the strain-rate effects may have introduced special difficulties for the PsD tests while those effects are non-existent for the real-time tests on the shaking tables or using the substructured approach. [8]

9. Acknowledgements

The studies described in the present paper were financed by the European Union (contract HPRI-CT-2001-50023) under the NEFOREEE Project (New Fields of Research in Earthquake Engineering Experimentation) in the aim of the “Specific Research and Technological Development Programme” of the “Human Research Potential and Socio-Economic Knowledge Base”. The cooperation of LNEC personnel, namely Engº Paulo Morais, Engº Luís Mendes, Artur Santos, Ana Marques, Paulo Semedo and Dulcina Marecos, during the preparation and the performance of the shaking table tests, was deeply appreciated.

The helpful contribution of Ana Marques during the preparation of this report is also deeply acknowledged.

References

[1] New Fields of Research in Earthquake Engineering Experimentation (NEFOREEE) – Third Annual Report on RTD CONTRACT HPRI – CT – 2001 – 50023

[2] R. Bairrão, M.J. Falcão Silva, 2007, “Experiences under ECOLEADER – “European Consortium of Laboratories for Earthquake and Dynamic Experimental Research”, Rogério Bairrão and Roy Severn (Editors), LNEC, Chapter 5, pp. 133-176, ISBN 972-49-1972-2

[3] Coelho, E., Campos Costa, A., 2005, Experimental Earthquake Engineering Research in LNEC, LNEC divulgation brochure.

[4] Emílio, F.T., Duarte, R.T., Carvalhal, F.J., Costa, C.O., Vaz, C.T., Corrrêa, M.R., The new LNEC shaking table for earthquake resistance testing, Memoire LNEC 757, 1989.

[5] SAP200NL Release 7.8.0., Structural Analysis Program, Computers and Structures Inc., Berkeley, CA, 2000.

[6] prEN 1998-1, Eurocode 8: Design of structures for earthquake resistance. Part 1: general rules, seismic actions and rules for buildings, CEN, European Committee for Standardization, Brussels, Belgium, 2002.

[7] University of Trento, Industrial application of shaking tables and reaction walls, NEFOREEE Project, 2004

[8] Molina, F.J., Bairrão, R., Blakeborough, T., Bursi, O., Tirelli, D., Magonette, G., Mouzakis, H., Williams, M.S., Testing performance benchmark for shaking tables and reaction walls within the NEFOREEE Project, 1ECEES, Paper 303, Geneve, Switzerland, September, 2006.

[9] Bairrao, R., Bursi, O., Carydis, P., Magonette, G., Mouzakis, H., Tirelli, D., Williams, M., Benchmark testing and performance comparison of shaking tables and reaction walls, Proceedings of 13WCEE, Paper N. 441, Vancouver, Canada, August, 2004

[10] prEN 1993-1. “Eurocode 3: Design of steel structures. Part 1: General rules for buildings”, CEN, 2003.

[11] prEN 1994-1, “Eurocode 4: Design of composite steel and concrete structures. Part 1: General rules for buildings”. CEN, 2003.

[12] Schmidt K., Dorka U., “Experimental Verification of Hyde-System”, Paper 3163, Proceedings of the 13th World Conference on Earthquake Engineering, Vancouver, Canada, 2004.

[13] Wen Y-K, Method for random vibration of hysteretic systems. J. of Engineering Mechanics, 102(2), 1976, 249-263.

[14] Sorace S., Terenzi G., “Large-scale experimental validation of a design procedure for damped braced steel structures.” Mazzolani F. Editor. Behaviour of steel structures in seismic areas, Lisse:AA Balkema, 2003:657-662.

ANNEX I

Details of the Specimen – Photographic Record

INDEX OF FIGURES

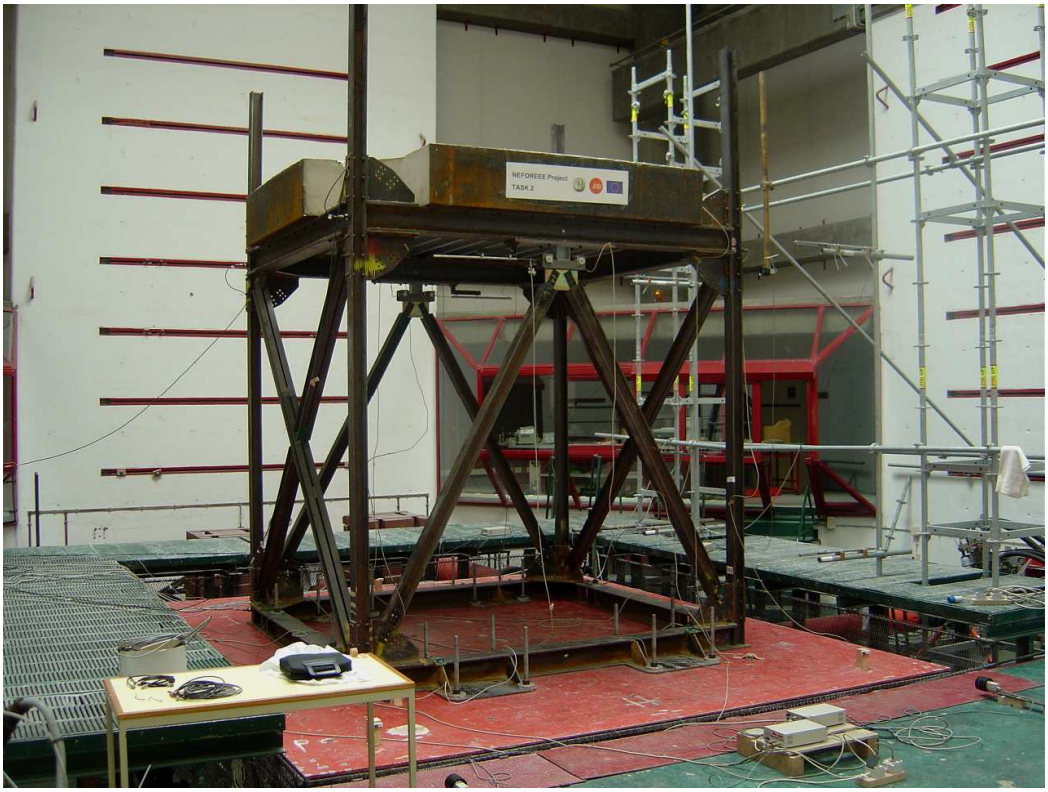

Figure I.1: General view of the model before the 2nd day tests (Dorka devices).

Figure I.2: Detail on the Dorka device (South).

Figure I.3: Bottom view of the Dorka device (North).

Figure I.4: Instrumentation in the top West of the model.

Figure I.5: Instrumentation in the top East side of the model.

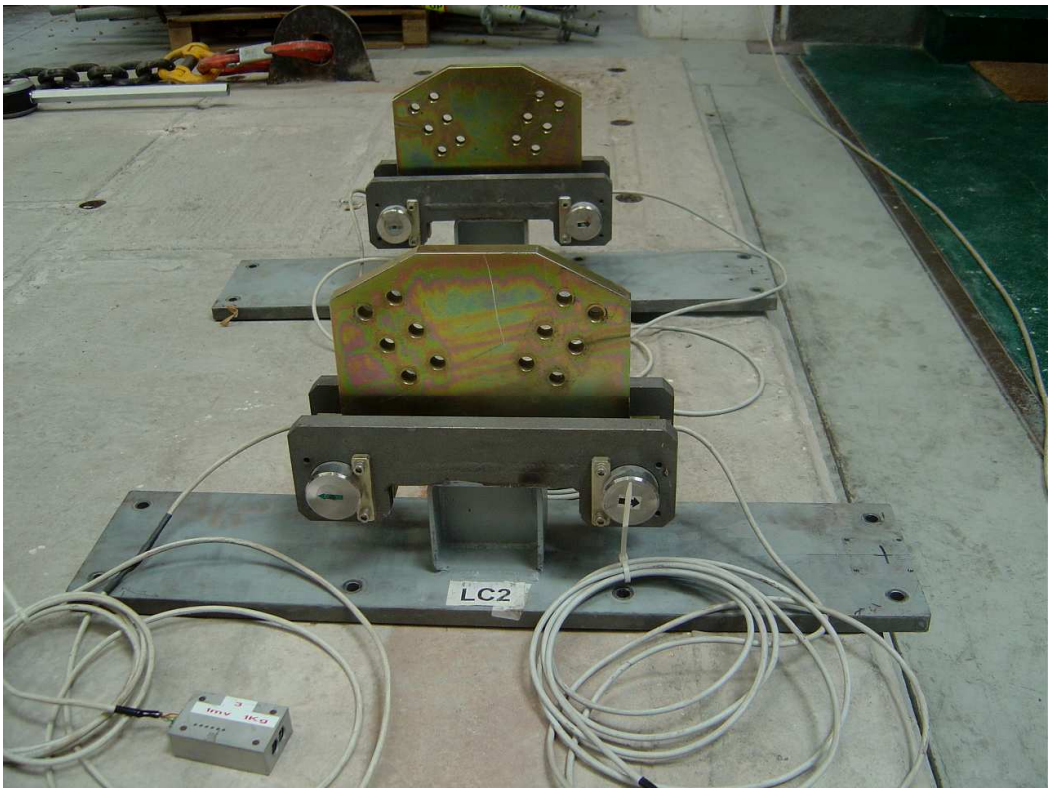

Figure I.6: Detail on the pair of Dorka devices tested.

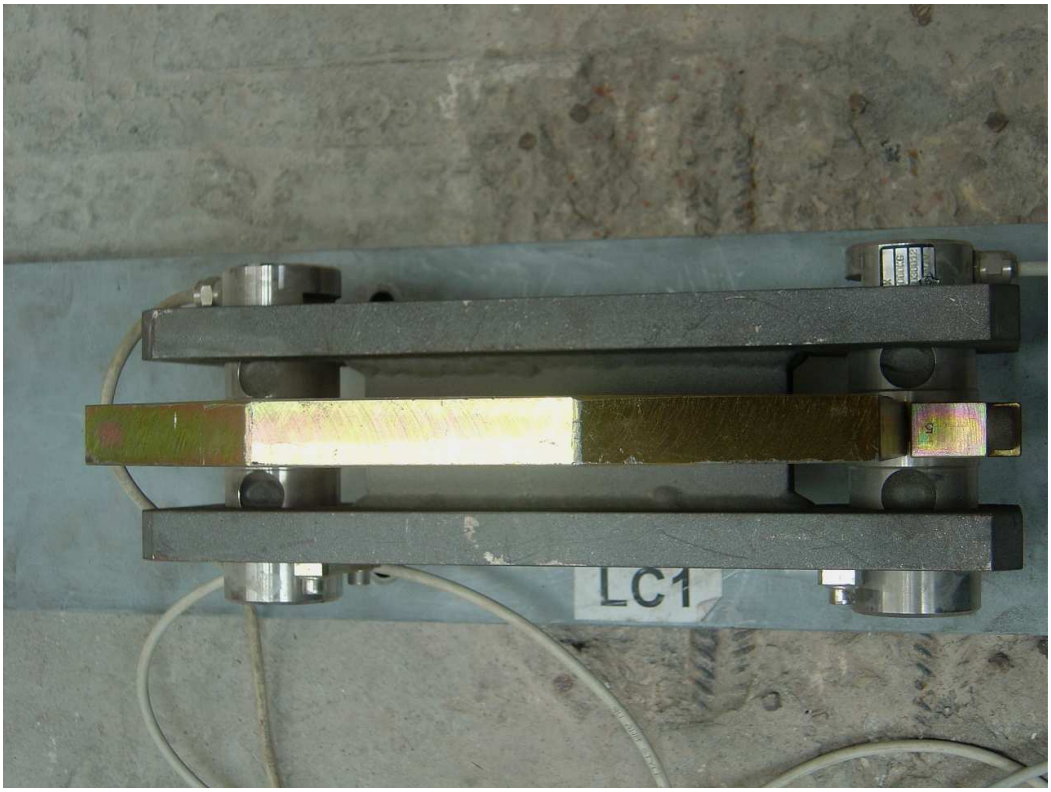

Figure I.7: Top view of a Dorka device.

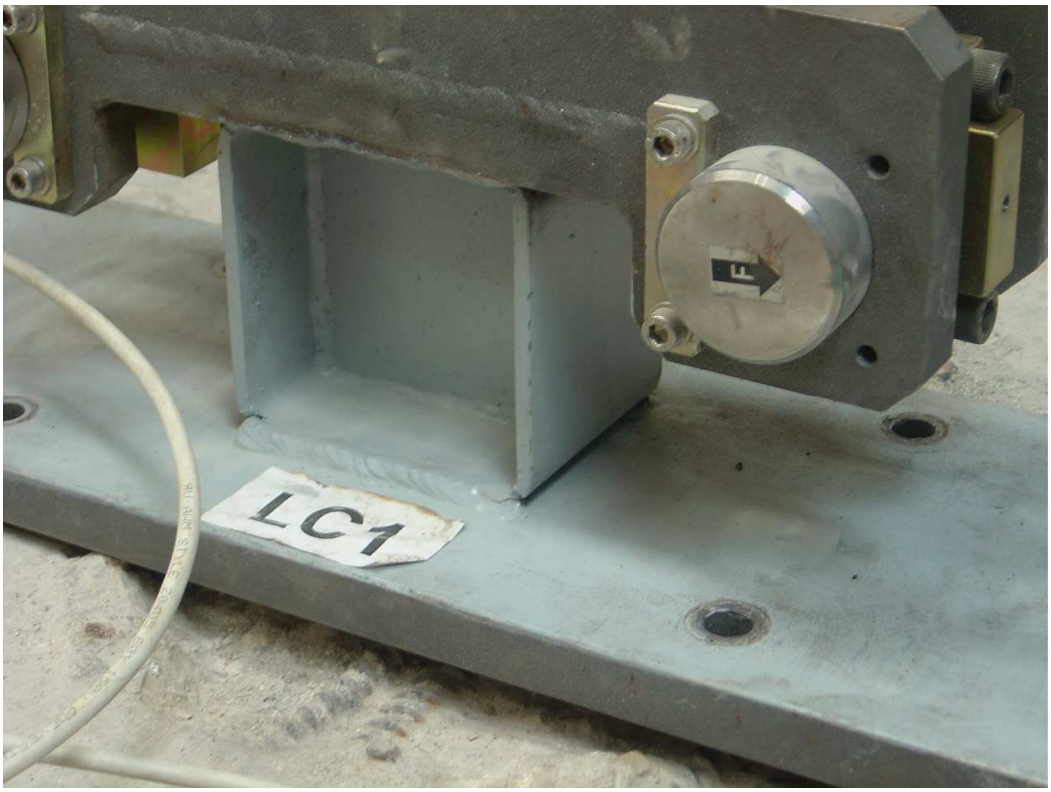

Figure I.8: Detail on the steel tube of the Dorka device.

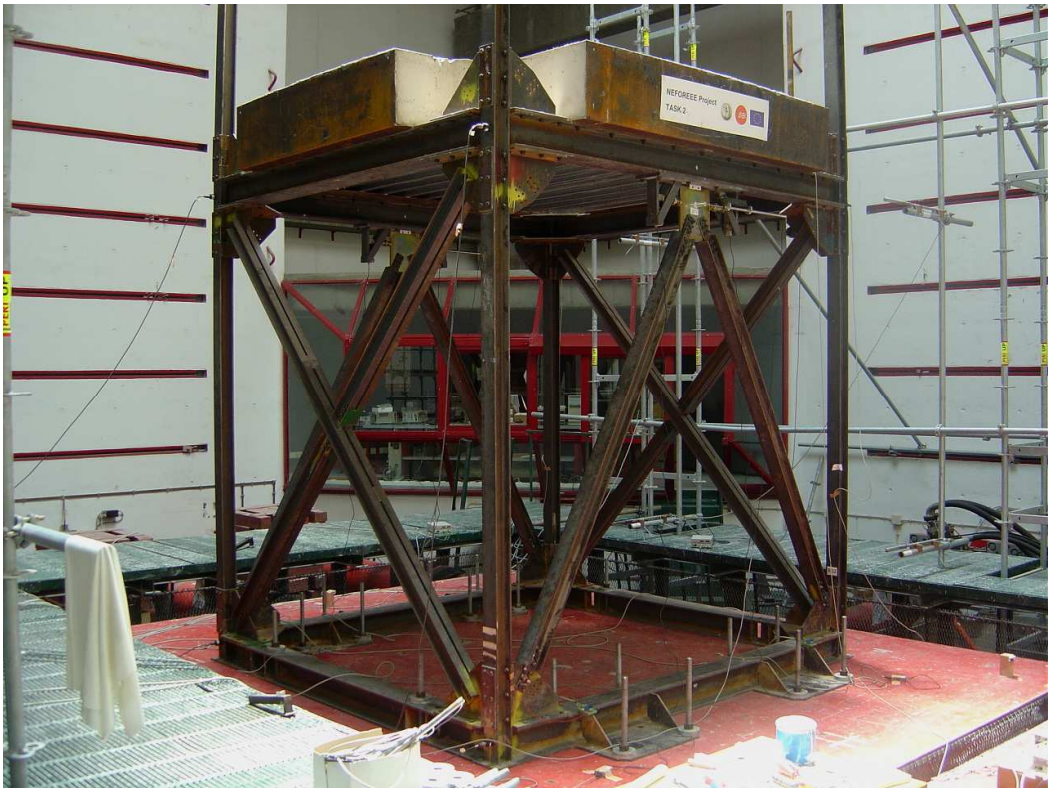

Figure I.9: General view of the model before the 3rd day tests (Jarrett devices).

Figure I.10: Detail on the Jarrett device (North).

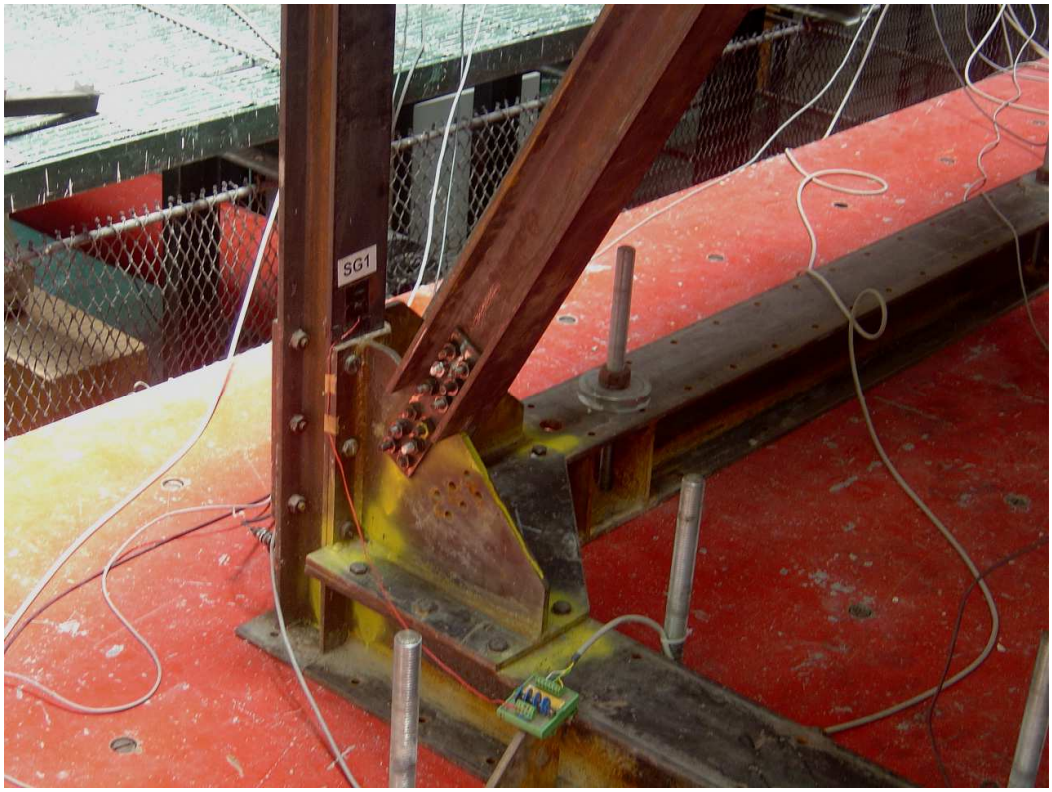

Figure I.11: Detail on the strain gauges (NE base).

Figure I.12: Detail on the Jarrett device (South).

ANNEX II

Earthquake scenario

INDEX OF FIGURES

INDEX OF TABLES

TIME HISTORIES

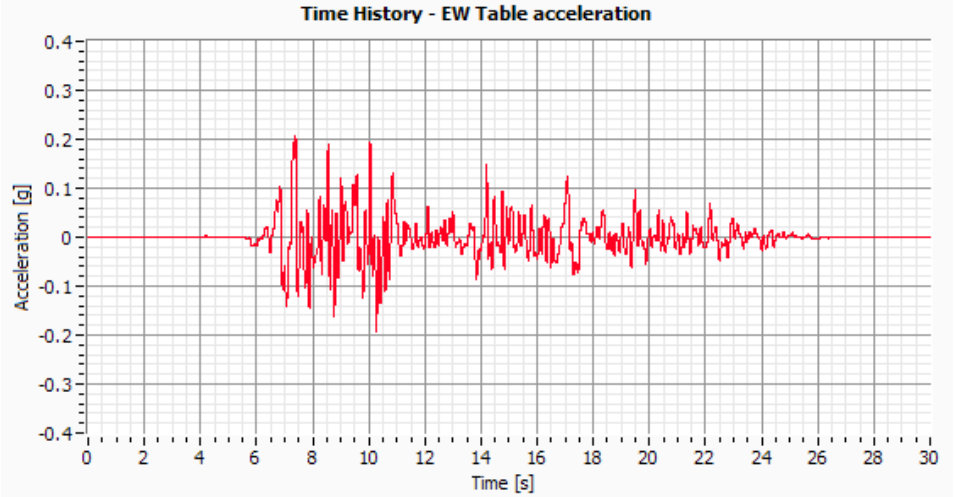

Figure II.1: Base acceleration in transverse direction (Test2).

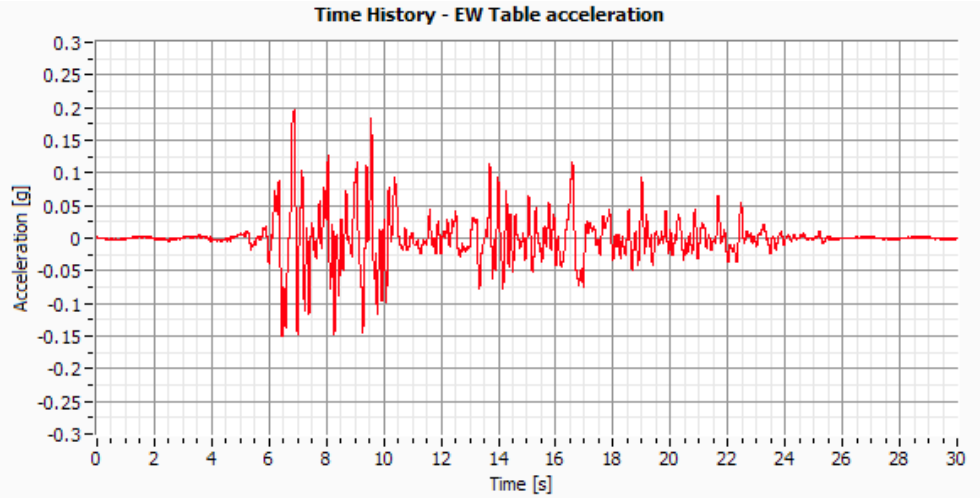

Figure II.2: Base acceleration in transverse direction (Test5).

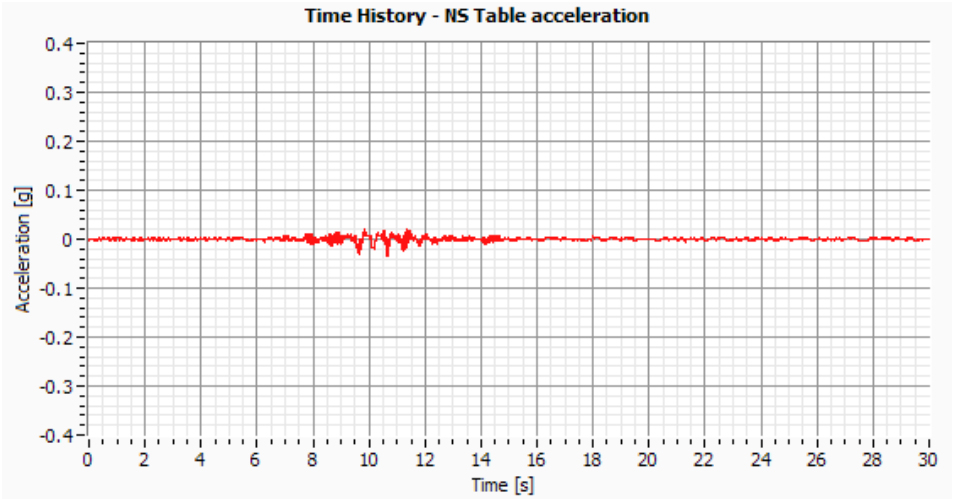

Figure II.3: Base acceleration in transverse direction (Test7).

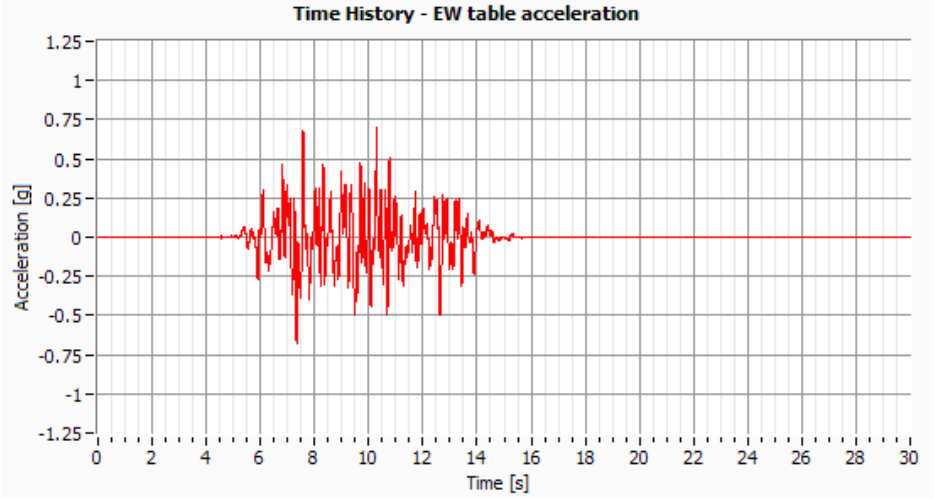

Figure II.4: Base acceleration in transverse direction (Test10).

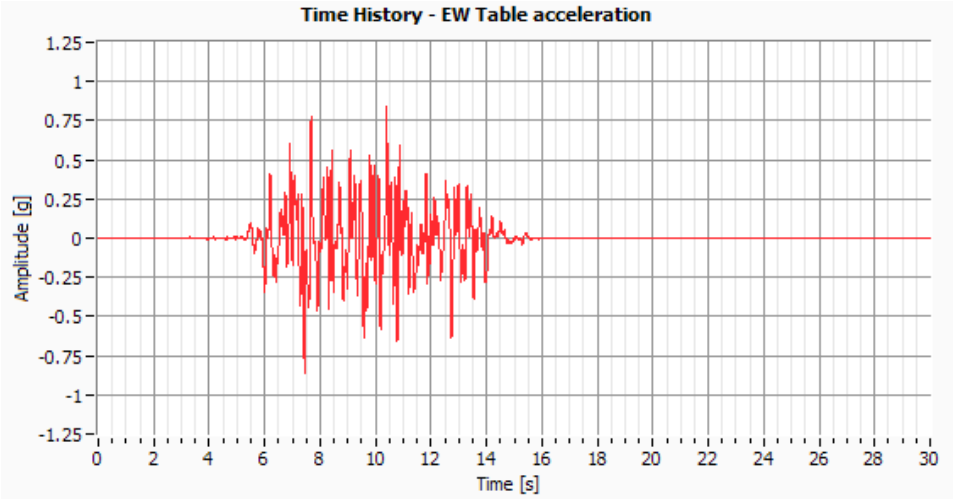

Figure II.5: Base acceleration in transverse direction (Test12).

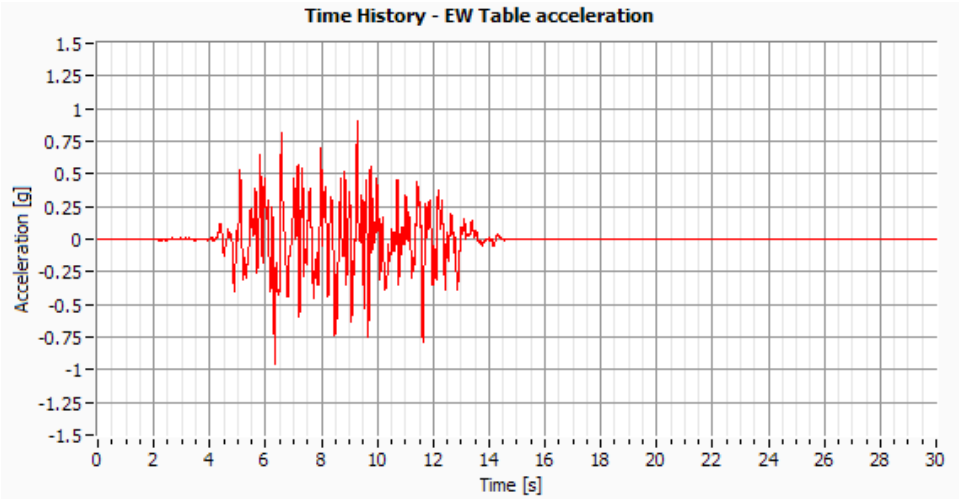

Figure II.6: Base acceleration in transverse direction (Test14).

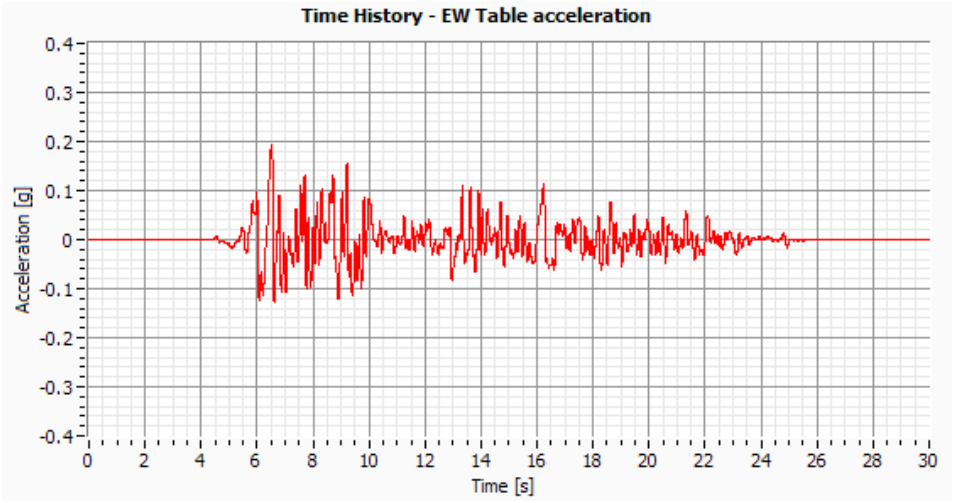

Figure II.7: Base acceleration in transverse direction (Test17).

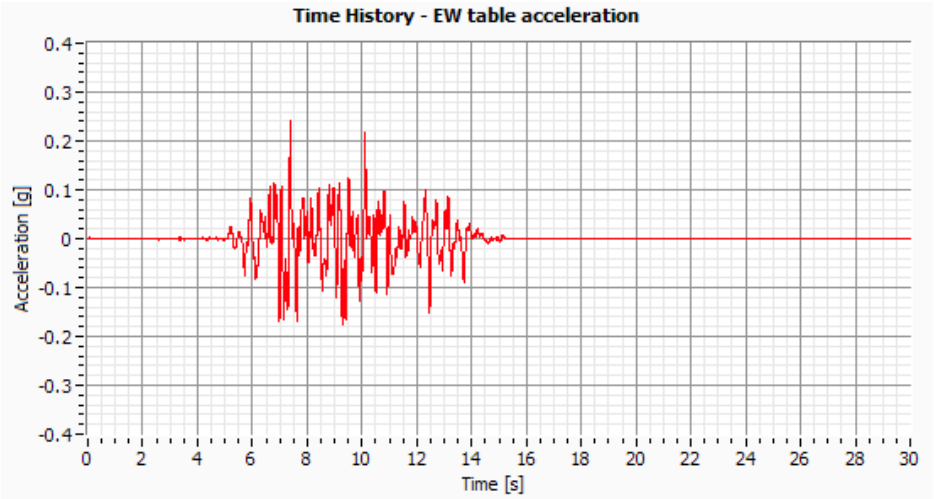

Figure II.8: Base acceleration in transverse direction (Test19).

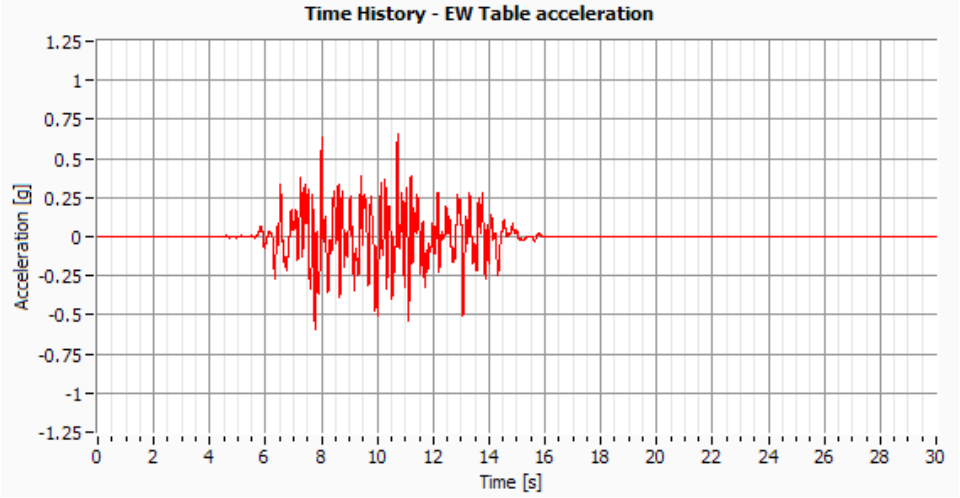

Figure II.9: Base acceleration in transverse direction (Test22).

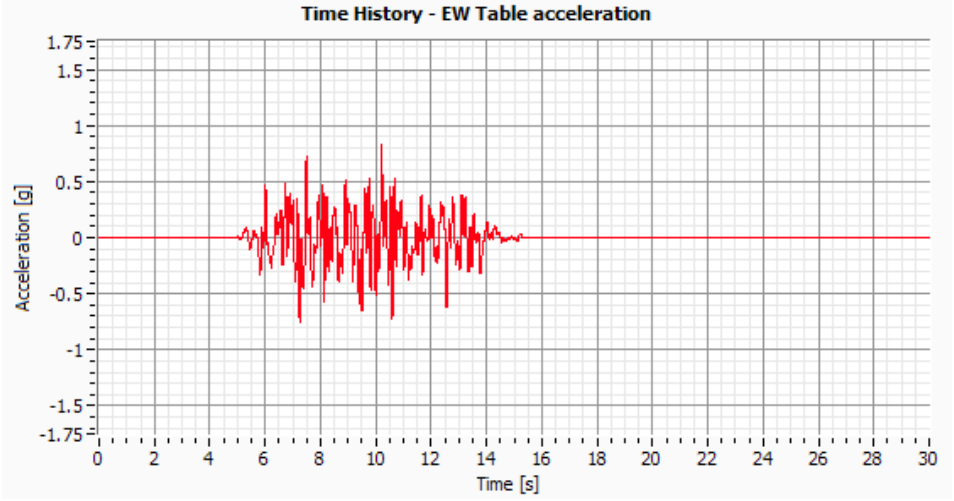

Figure II.10: Base acceleration in transverse direction (Test24).

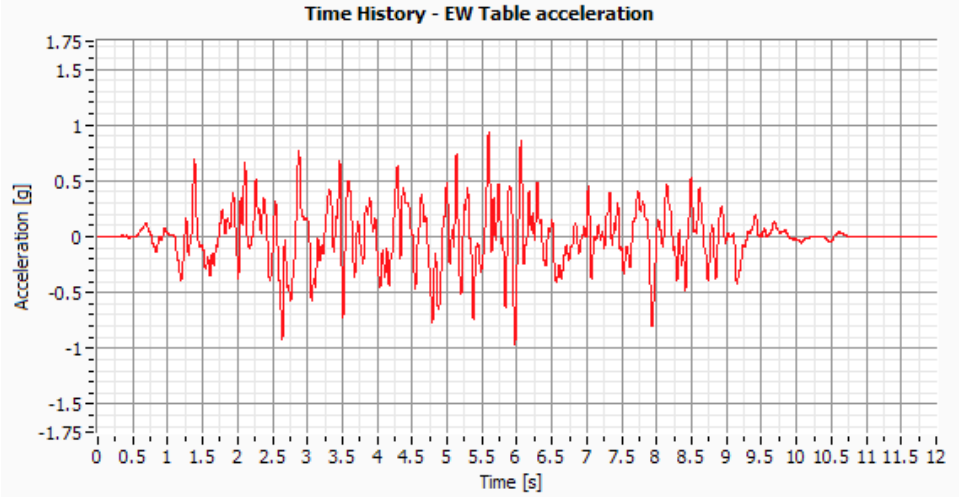

Figure II.11: Base acceleration in transverse direction (Test26).

POWER SPECTRAL DENSITIES

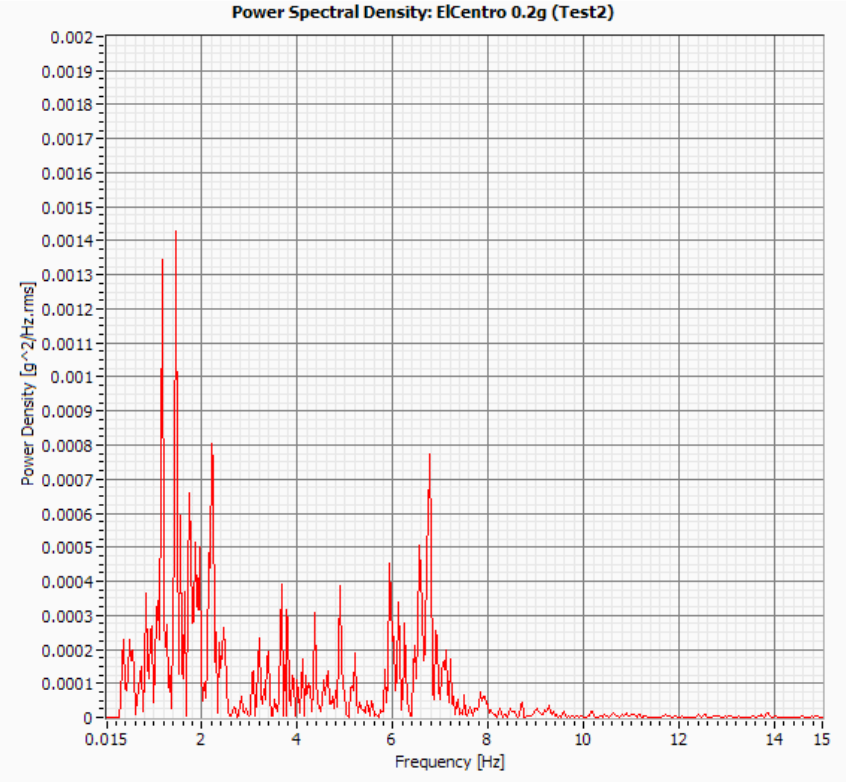

Figure II.12: Power spectral density of base acceleration (Test2).

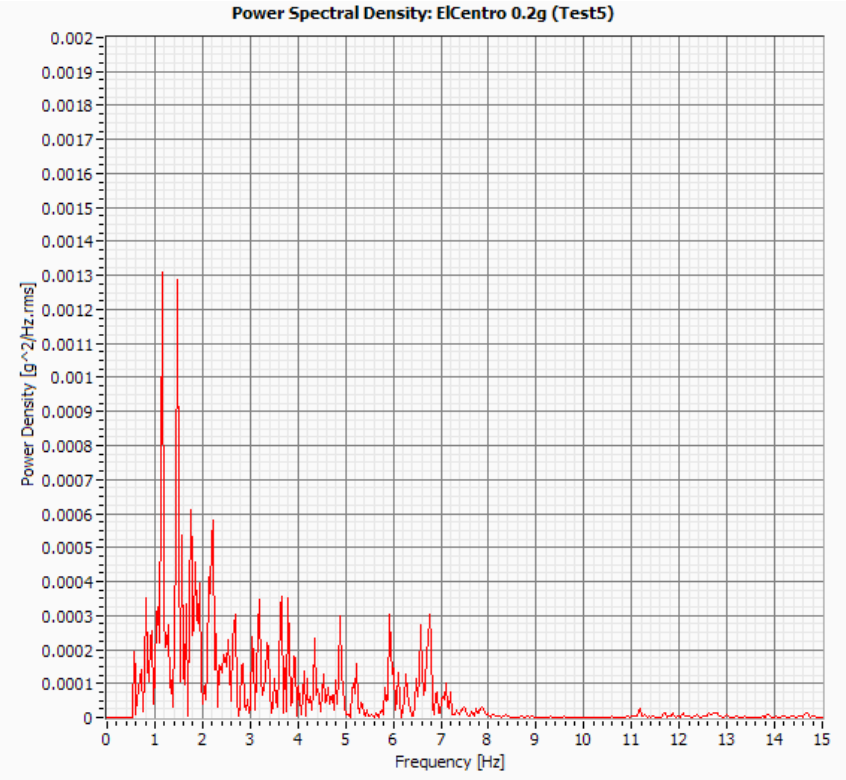

Figure II.13: Power spectral density of base acceleration (Test5).

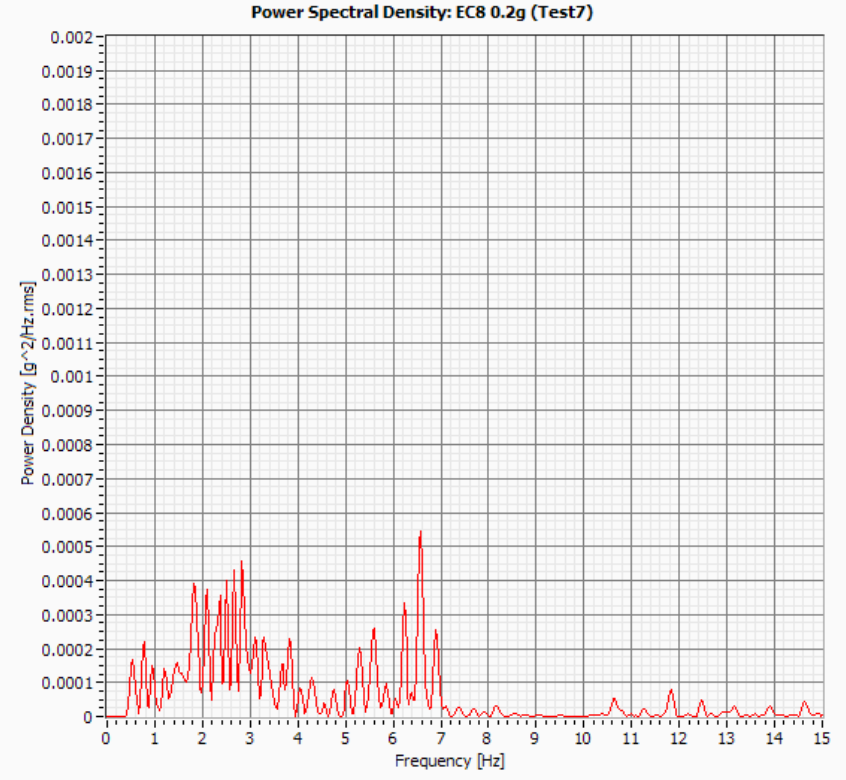

Figure II.14: Power spectral density of base acceleration (Test7).

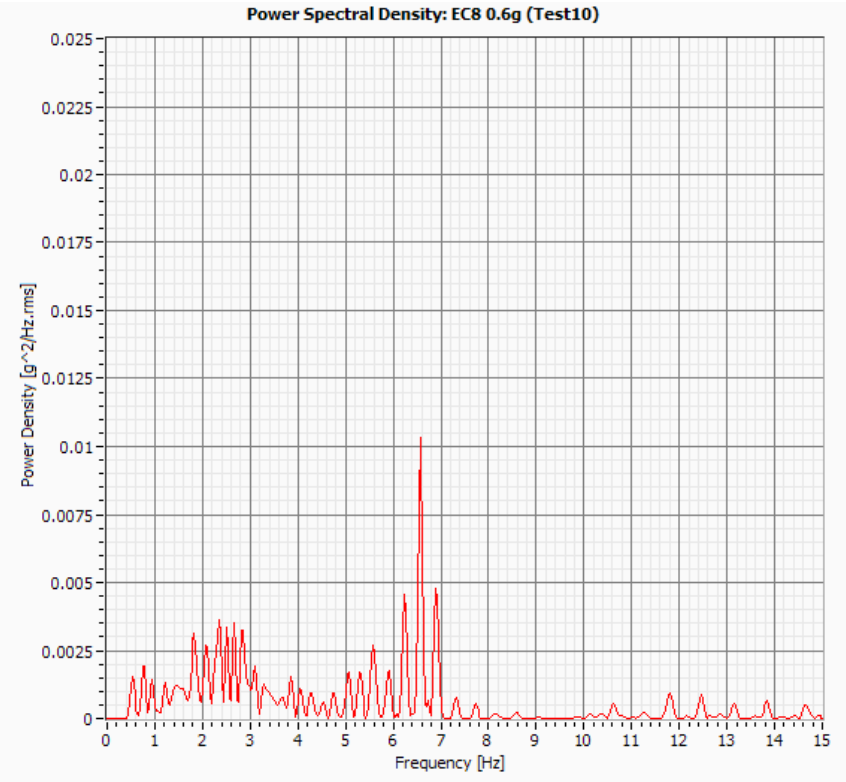

Figure II.15: Power spectral density of base acceleration (Test10).

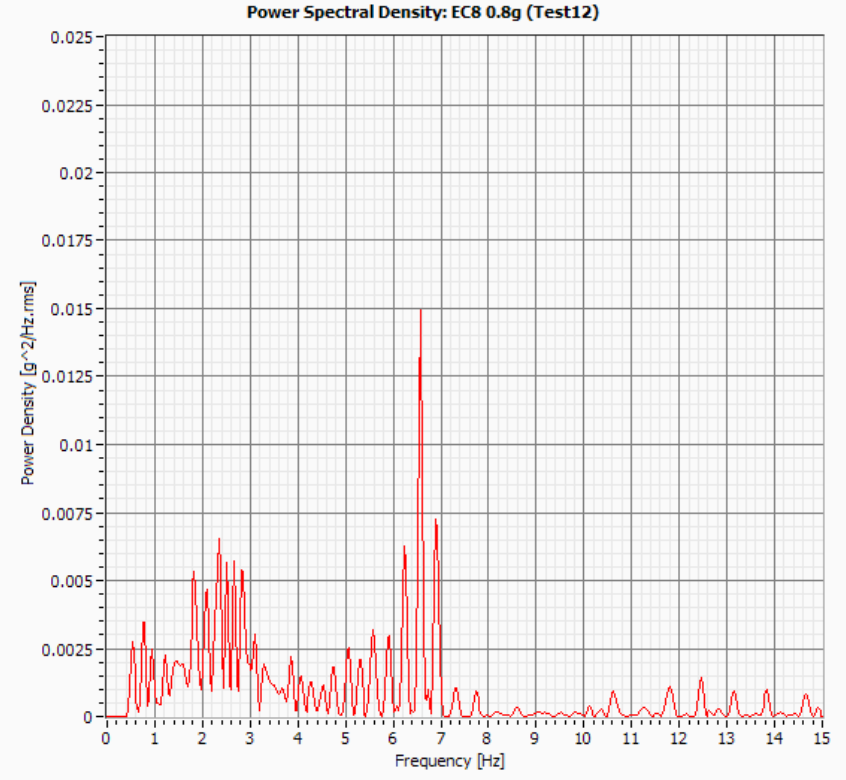

Figure II.16: Power spectral density of base acceleration (Test12).

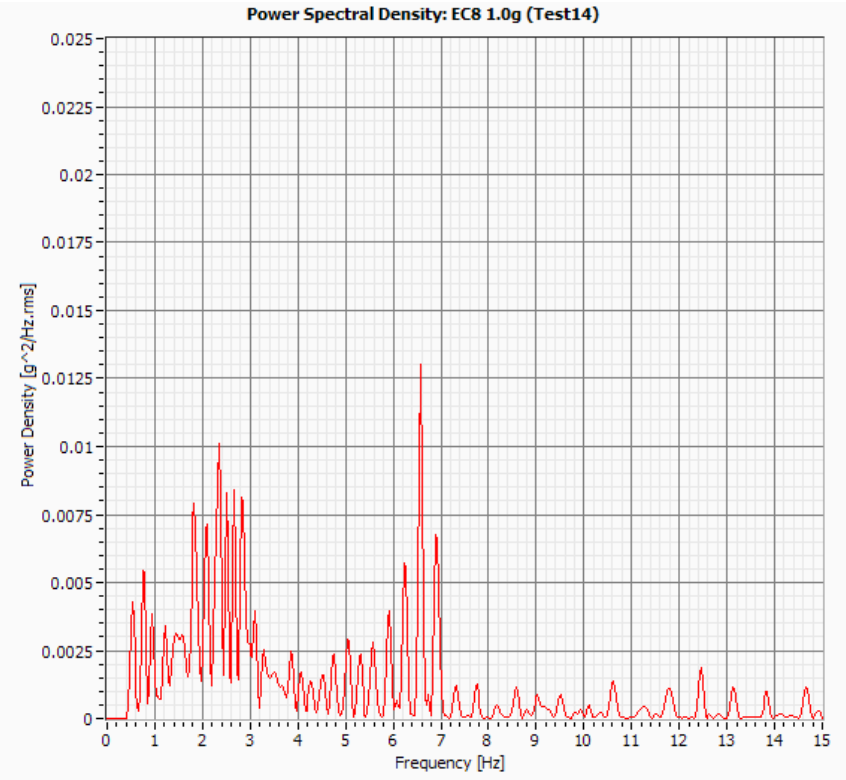

Figure II.17: Power spectral density of base acceleration (Test14).

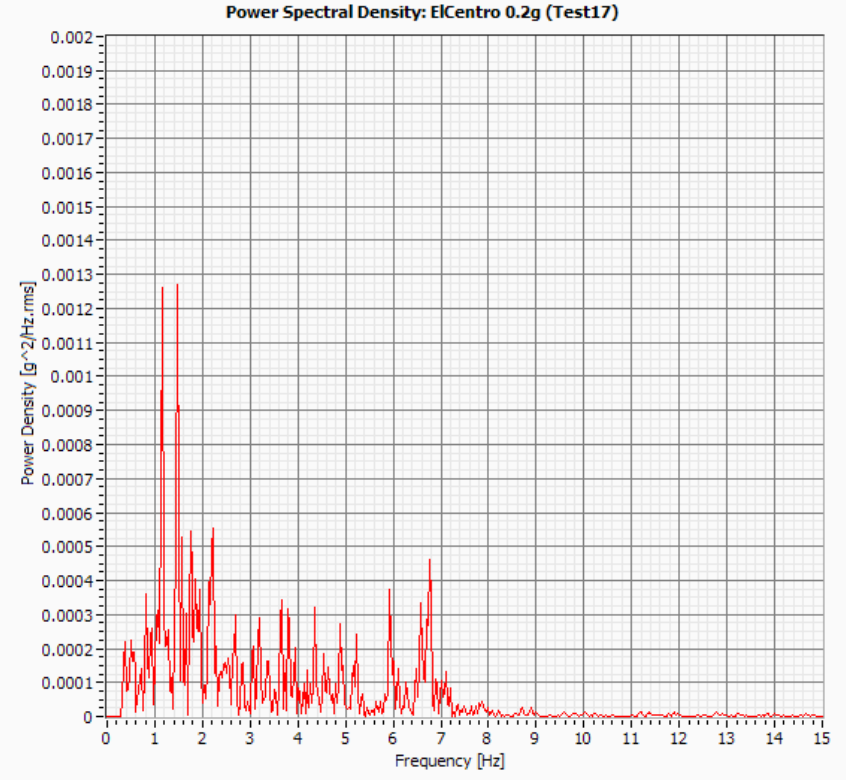

Figure II.18: Power spectral density of base acceleration (Test17).

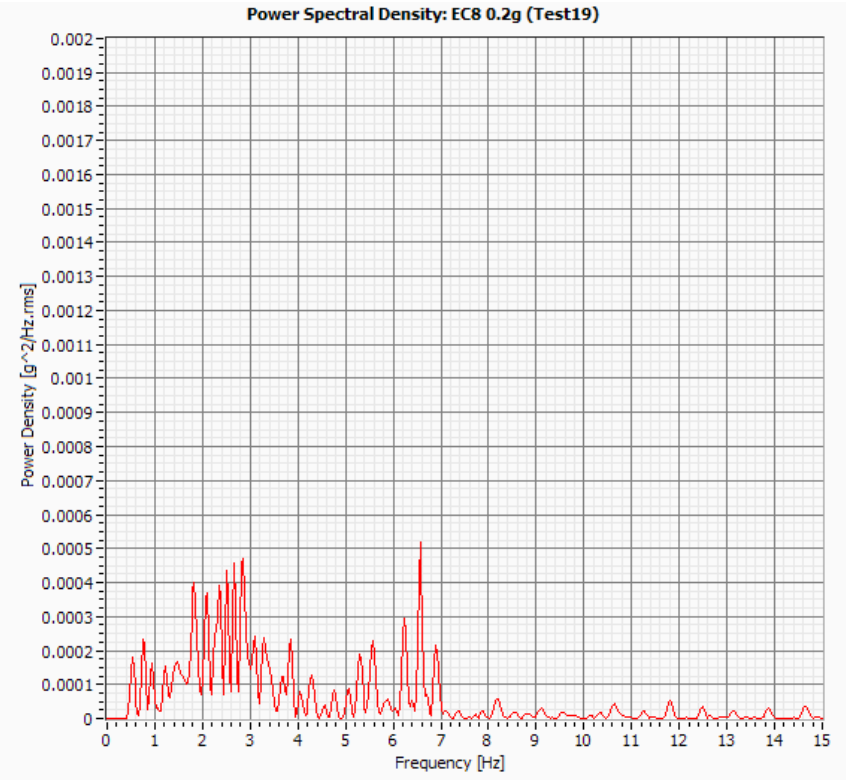

Figure II.19: Power spectral density of base acceleration (Test19).

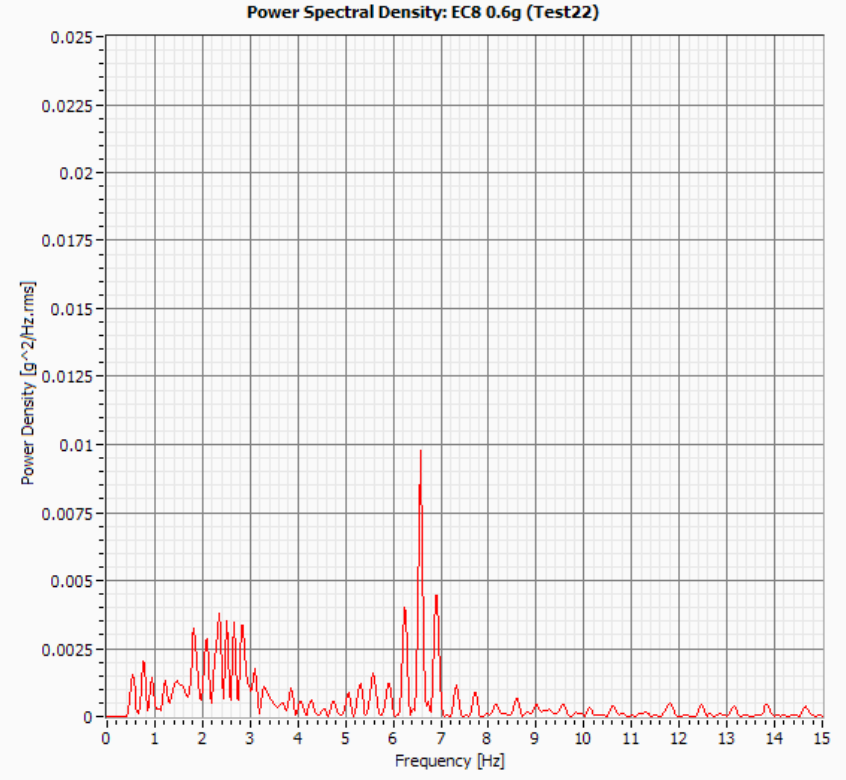

Figure II.20: Power spectral density of base acceleration (Test22).

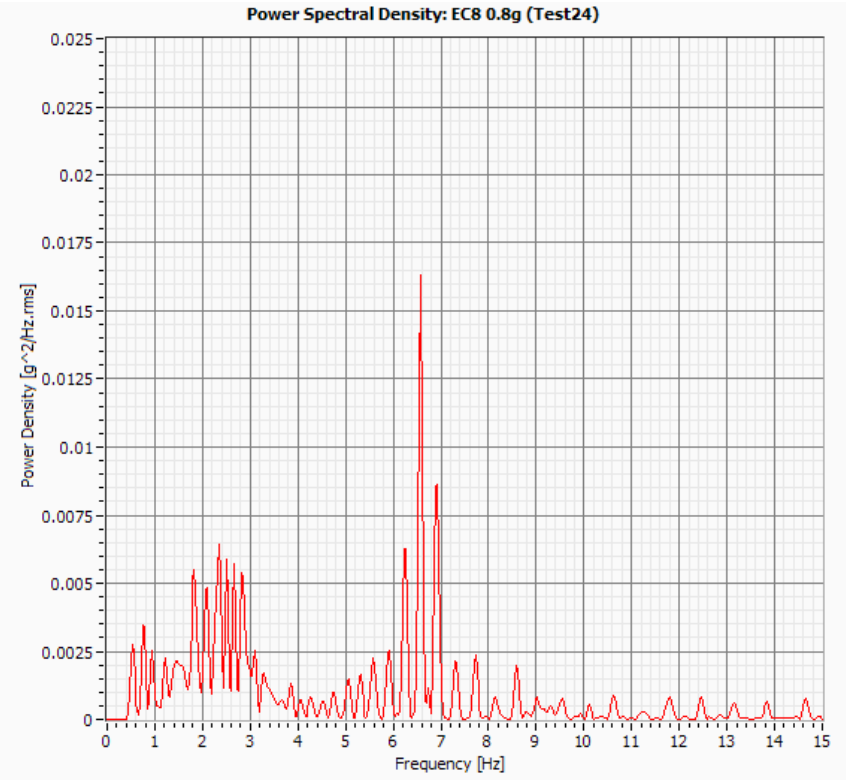

Figure II.21: Power spectral density of base acceleration (Test24).

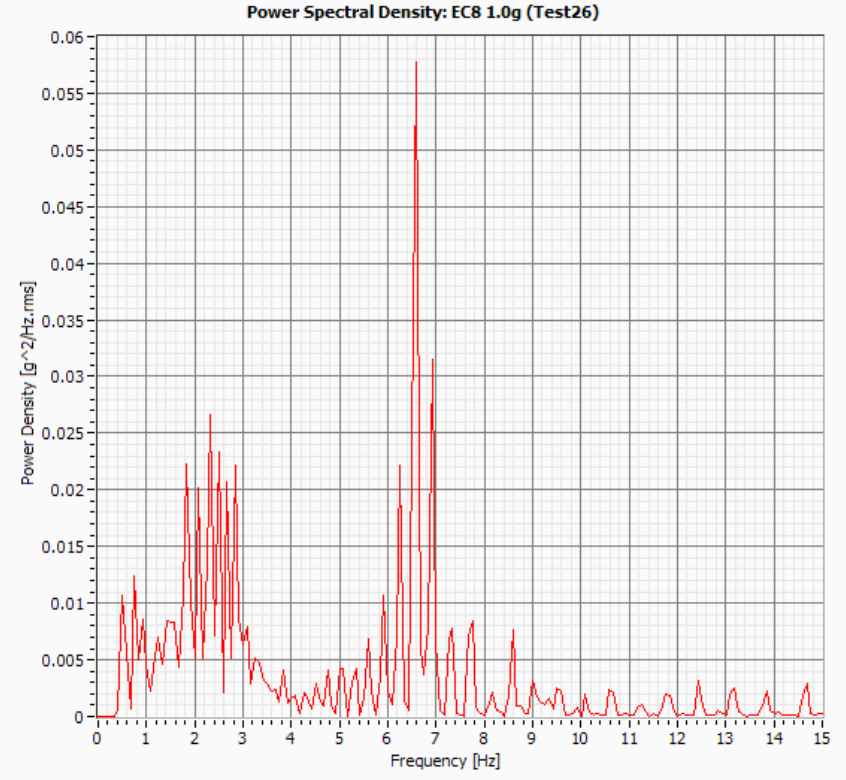

Figure II.22: Power spectral density of base acceleration (Test26).

Ground Motion Parameters and Response Spectra

Considering:

1) Peak Ground acceleration (PGA):

$$PGA = \max|a(t)|$$

2) Peak Ground velocity (PGV):

$$PGV = \max|v(t)|$$

3) Peak Ground displacement (PGD):

$$PGD = \max|d(t)|$$

4) Peak Velocity and Acceleration ratio (v_{max}/a_{max}):

$$v_{\max} / a_{\max} = \frac{\max|v(t)|}{\max|a(t)|}$$

5) Arias Intensity (I_a):

$$I_a = \frac{\pi}{2g}\int [a(t)]^2 dt$$

6) A95 parameter (A95):

The A95 value is the maximum acceleration value which corresponds to 95% of the Arias intensity value.

7) t05 parameter (t05):

The t05 is the time instant where 5% of the Arias intensity is reached.

8) T95 parameter (t95):

The t05 is the time instant where 95% of the Arias intensity is reached.

9) Significant duration (SD):

$$SD = t_{95} - t_{05}$$

10) Characteristic intensity (I_c):

$$I_c = \left(\sqrt{\frac{1}{t_{tot}}\int [a(t)]^2}\right)^{\frac{3}{2}} \cdot \sqrt{t_{tot}}$$

11) Predominant period (Tp):

Corresponds to the period where is reached the maximum spectral accelerations (response spectra with ξ=5%)

12) Mean period (Tm):

$$T_m = \frac{\sum C_i^2 / f_i}{\sum C_i^2}$$

With Ci corresponding to the Fourier amplitudes at fi frequencies between 0.25 and 20 Hz

13) Sustained maximum acceleration (SMA):

Corresponds to the third maximum acceleration measured

14) Sustained maximum velocity (SMV):

Corresponds to the third maximum velocity measured

15) Acceleration Spectrum Intensity (ASI)

$$ASI = \int_{0.1}^{0.5} S_a(\xi = 5\%, T)dT$$

16) Velocity Spectrum Intensity, also known as Housner Intensity (VSI):

$$VSI = \int_{0.1}^{2.5} S_v(\xi = 5\%, T)dT$$

17) Specific Energy Density (SED):

$$SED = \int_{0}^{t_1} [v(t)]^2 \, dt$$

18) Husid plot

Represents the build-up of the Arias Intensity (Ia)

19) Energy Flux plot

Represents the build-up of the Specific Energy Density (SED)

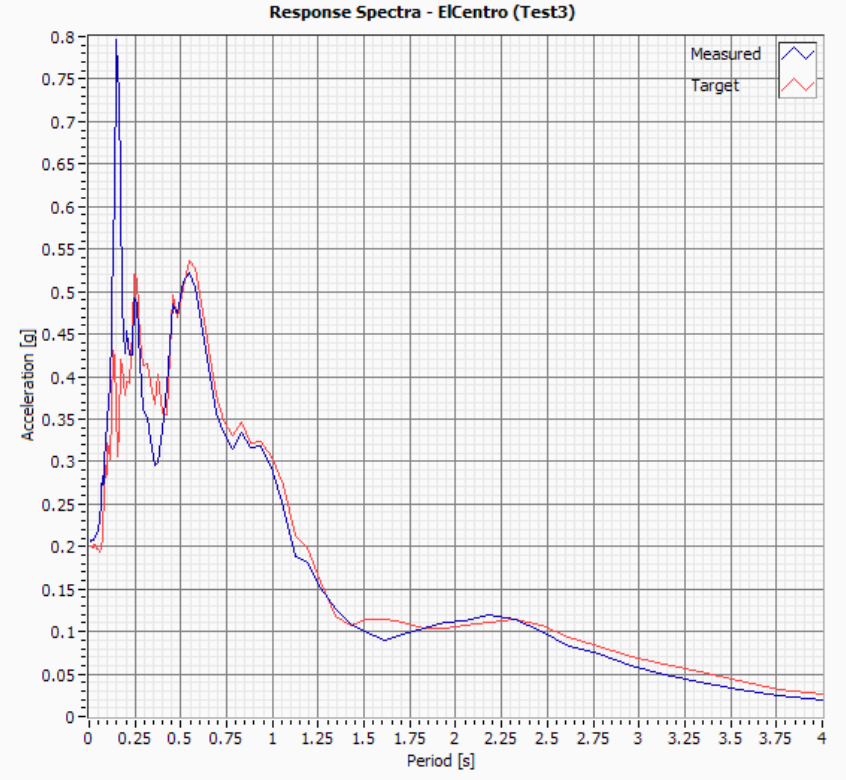

Figure II.23: Response spectra for EW Table acceleration: ElCentro 0.2g (Test2).

Table II.1: Ground Motion Parameters for ElCentro 0.2g (Test2).

Ground Motion Parameters	Test2	Units
Peak Ground Acceleration (PGA)	0.21	g
Peak Ground Velocity (PGV)	18.25	cm/s
Peak Ground Displacement (PGD)	43.06	mm
Peak Velocity and Acceleration ratio	1.67	s
Arias Intensity (Ia)	0.60	m/s
A95 Parameter	0.16	g
t05 (5% of Ia)	6.96	s
t95 (95% of Ia)	19.87	s
Significant duration (t95-t05)	12.91	s
Characteristic Intensity	0.04	-
Predominant Period	0.16	s
Mean Period	0.50	s
Sustained Maximum Acceleration	0.19	g
Sustained Maximum Velocity	15.84	cm/s
Acceleration Spectrum Intensity*	0.18	g
Velocity Spectrum Intensity (Housner Intensity)*	77.75	cm/s
Specific Energy Density (SED)	450.26	cm^2/s

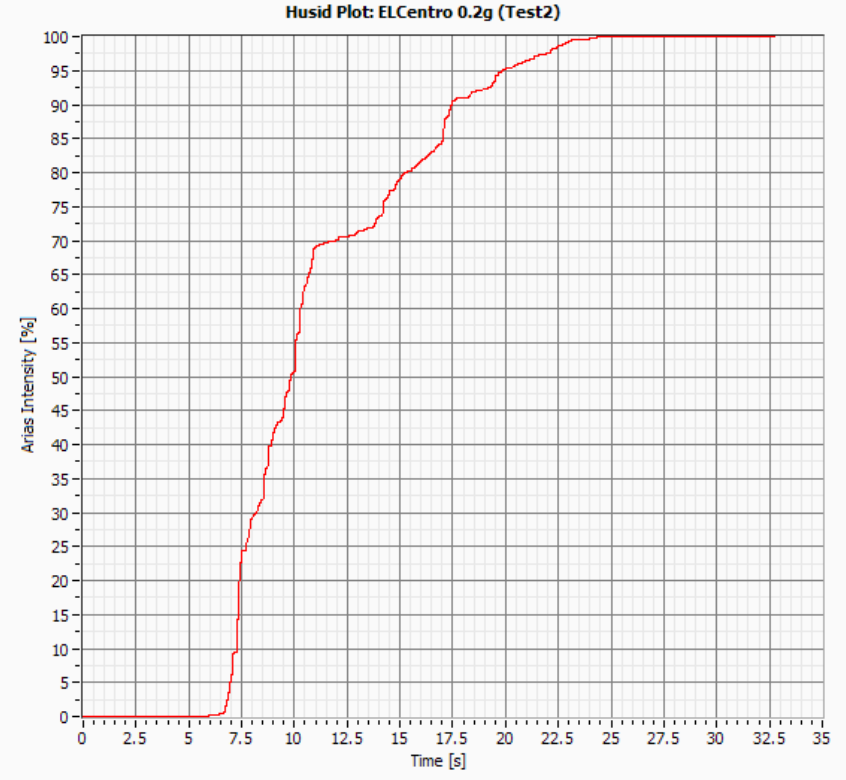

Figure II.24: Arias Intensity (Ia): ElCentro 0.2g (Test2).

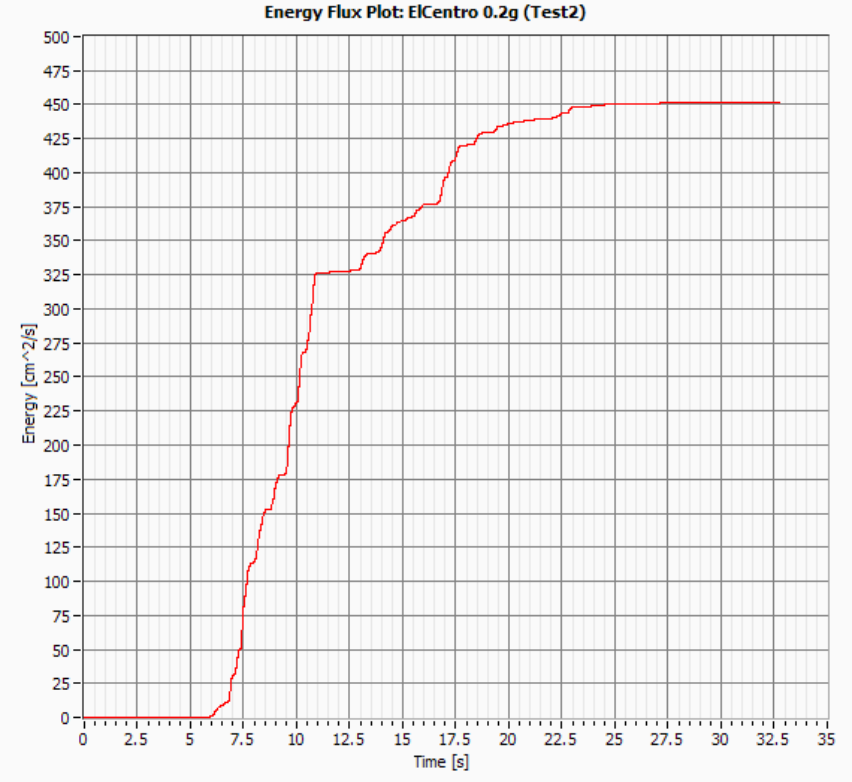

Figure II.25: Specific Energy Density (SED): ElCentro 0.2g (Test2).

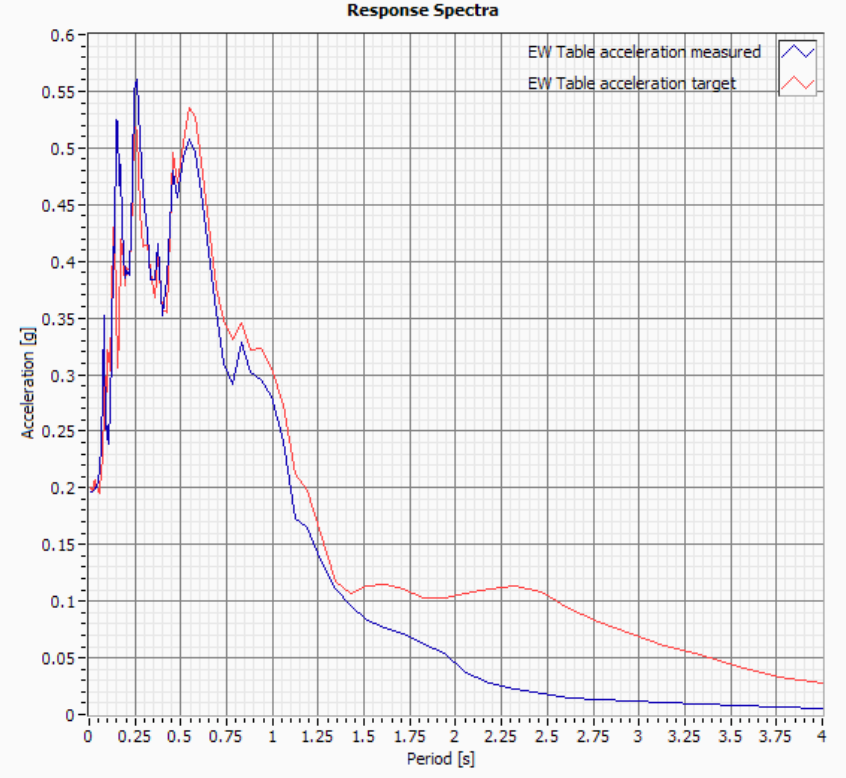

Figure II.26: Response spectra for EW Table acceleration: ElCentro 0.2g (Test5).

Table II.2: Ground Motion Parameters for ElCentro 0.2g (Test5).

Ground Motion Parameters	Test5	Units
Peak Ground Acceleration (PGA)	0.19	g
Peak Ground Velocity (PGV)	15.09	cm/s
Peak Ground Displacement (PGD)	20.45	mm
Peak Velocity and Acceleration ratio	0.20	s
Arias Intensity (Ia)	0.49	m/s
A95 Parameter	0.15	g
t05 (5% of Ia)	6.45	s
t95 (95% of Ia)	19.39	s
Significant duration (t95-t05)	12.94	s
Characteristic Intensity	0.03	-
Predominant Period	0.27	s
Mean Period	0.49	s
Sustained Maximum Acceleration	0.18	g
Sustained Maximum Velocity	11.94	cm/s
Acceleration Spectrum Intensity*	0.17	g
Velocity Spectrum Intensity (Housner Intensity)*	56.11	cm/s
Specific Energy Density (SED)	269.56	cm^2/s

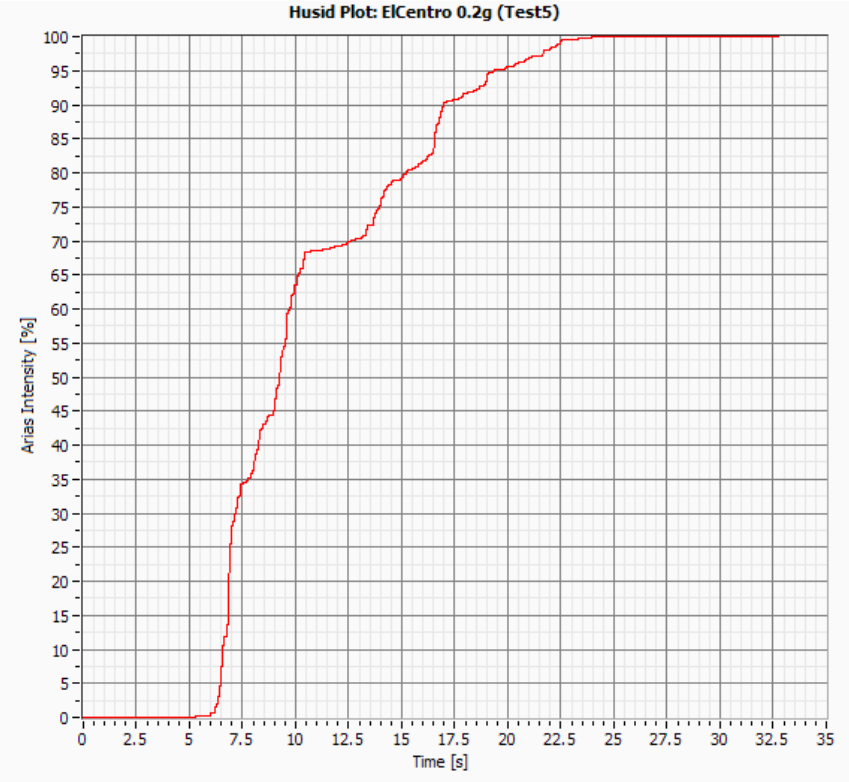

Figure II.27: Arias Intensity (Ia): ElCentro 0.2g (Test5).

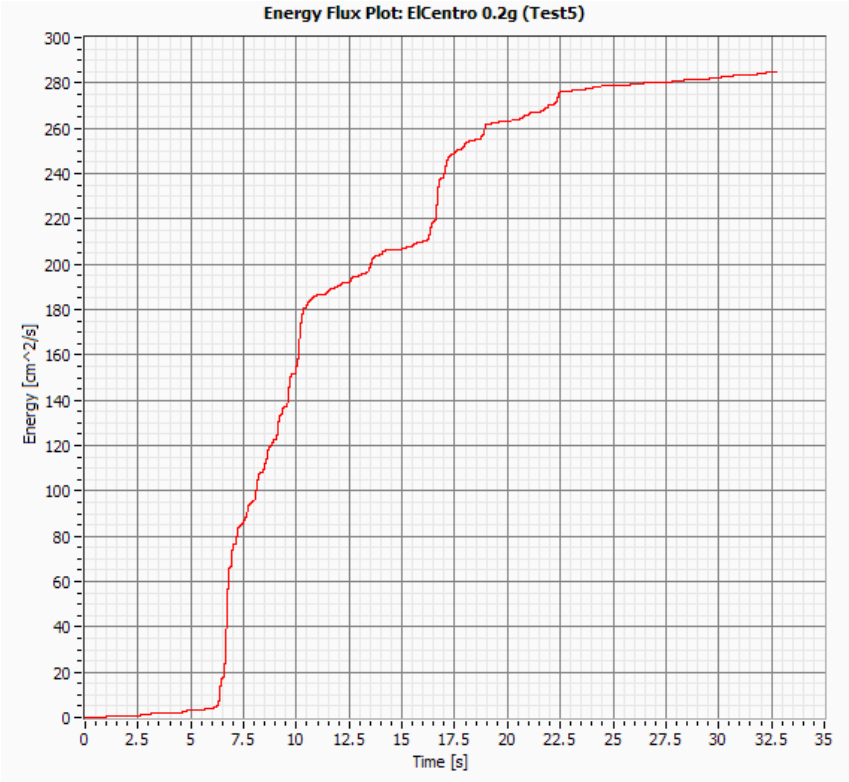

Figure II.28: Specific Energy Density (SED): ElCentro 0.2g (Test5).

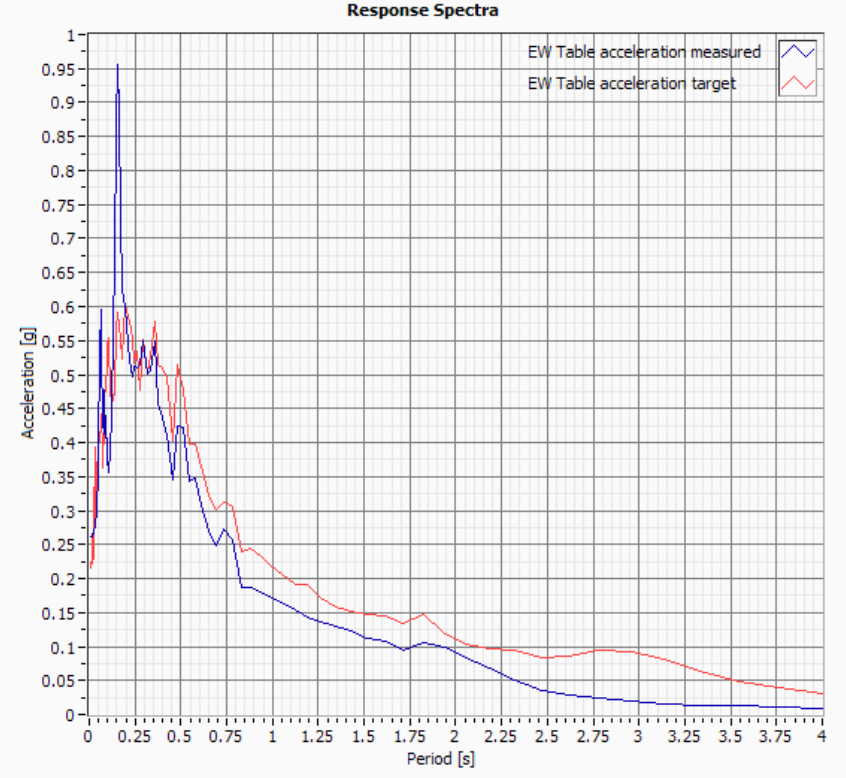

Figure II.29: Response spectra for EW Table acceleration: EC8 0.2g (Test7).

Table II.3: Ground Motion Parameters for EC8 0.2g (Test7).

Ground Motion Parameters	Test7	Units
Peak Ground Acceleration (PGA)	0.26	g
Peak Ground Velocity (PGV)	14.48	cm/s
Peak Ground Displacement (PGD)	23.93	mm
Peak Velocity and Acceleration ratio	3.90	s
Arias Intensity (Ia)	0.50	m/s
A95 Parameter	0.18	g
t05 (5% of Ia)	8.99	s
t95 (95% of Ia)	15.53	s
Significant duration (t95-t05)	6.54	s
Characteristic Intensity	0.03	-
Predominant Period	0.16	s
Mean Period	0.38	s
Sustained Maximum Acceleration	0.23	g
Sustained Maximum Velocity	11.08	cm/s
Acceleration Spectrum Intensity*	0.21	g
Velocity Spectrum Intensity (Housner Intensity)*	60.72	cm/s
Specific Energy Density (SED)	203.89	cm^2/s

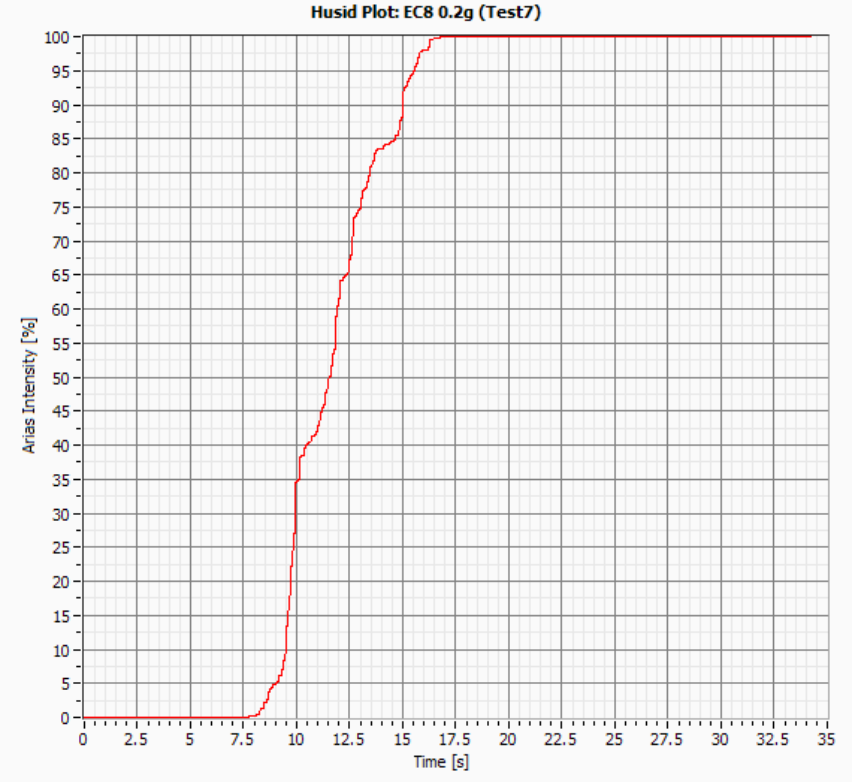

Figure II.30: Arias Intensity (Ia): EC8 0.2g (Test7).

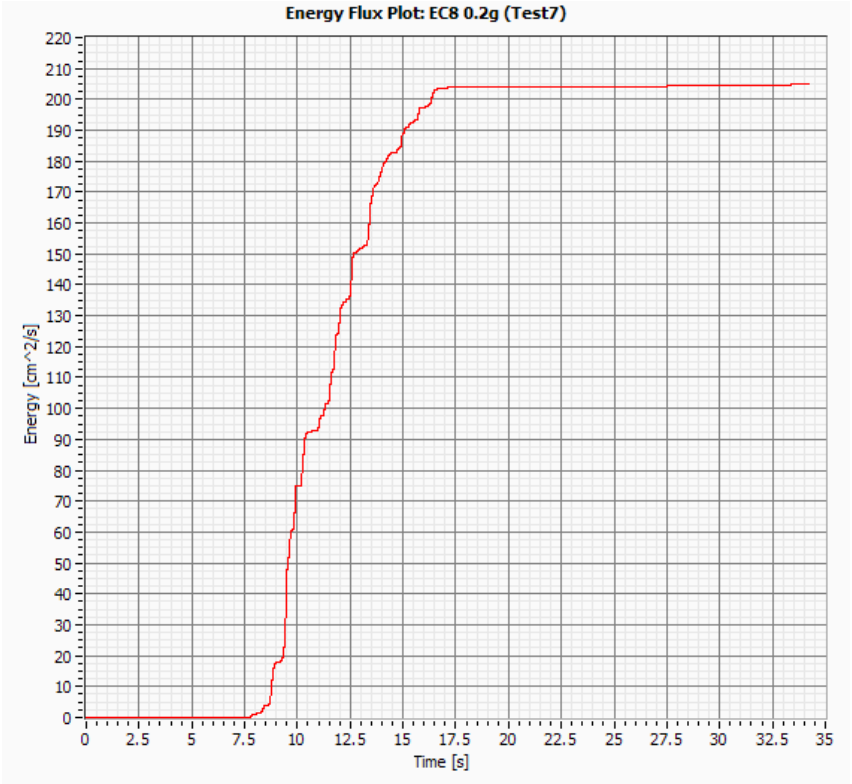

Figure II.31: Specific Energy Density (SED): EC8 0.2g (Test7).

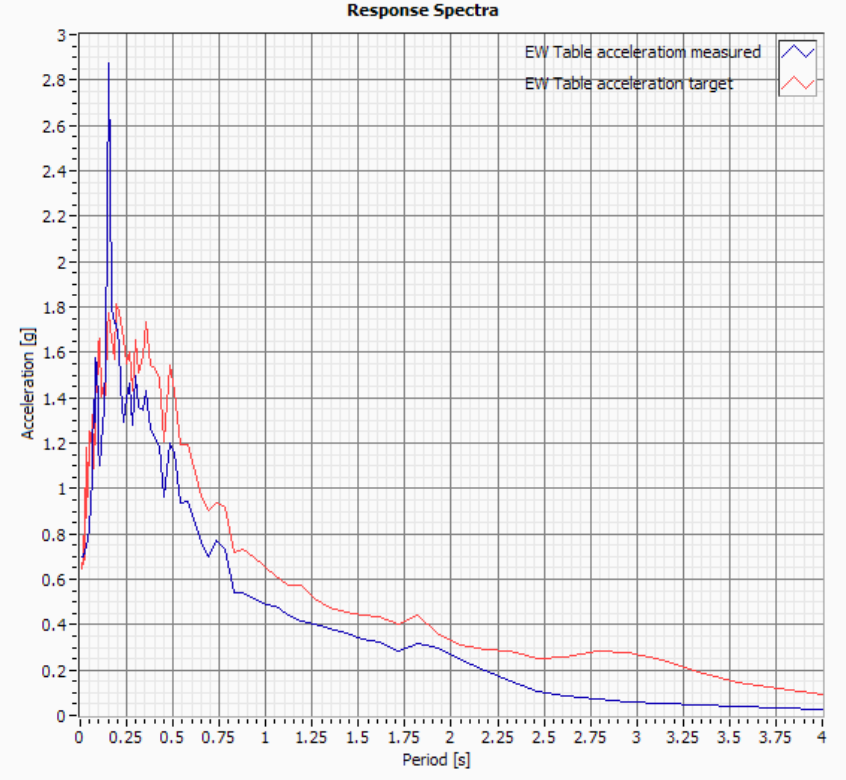

Figure II.32: Response spectra for EW Table acceleration: EC8 0.6g (Test10).

Table II.4: Ground Motion Parameters for EC8 0.6g (Test10).

Ground Motion Parameters	Test10	Units
Peak Ground Acceleration (PGA)	0.70	g
Peak Ground Velocity (PGV)	42.63	cm/s
Peak Ground Displacement (PGD)	72.05	mm
Peak Velocity and Acceleration ratio	0.007	s
Arias Intensity (Ia)	4.70	m/s
A95 Parameter	0.49	g
t05 (5% of Ia)	6.62	s
t95 (95% of Ia)	13.20	s
Significant duration (t95-t05)	6.58	s
Characteristic Intensity	0.17	-
Predominant Period	0.16	s
Mean Period	0.34	s
Sustained Maximum Acceleration	0.68	g
Sustained Maximum Velocity	31.94	cm/s
Acceleration Spectrum Intensity*	0.57	g
Velocity Spectrum Intensity (Housner Intensity)*	175.25	cm/s
Specific Energy Density (SED)	1724.73	cm^2/s

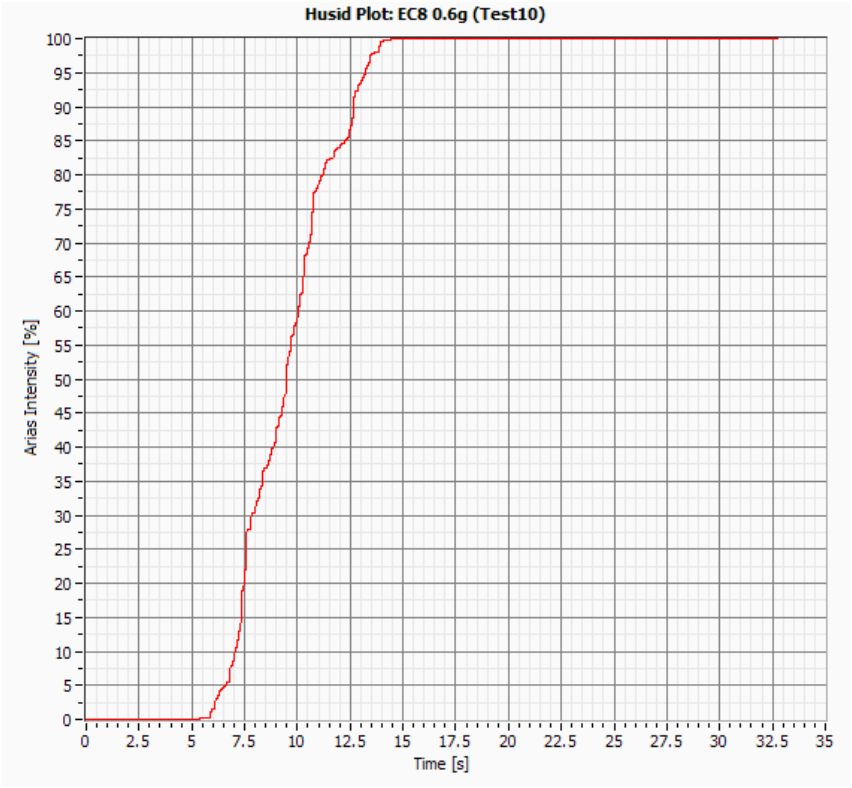

Figure II.33: Arias Intensity (Ia): EC8 0.6g (Test10).

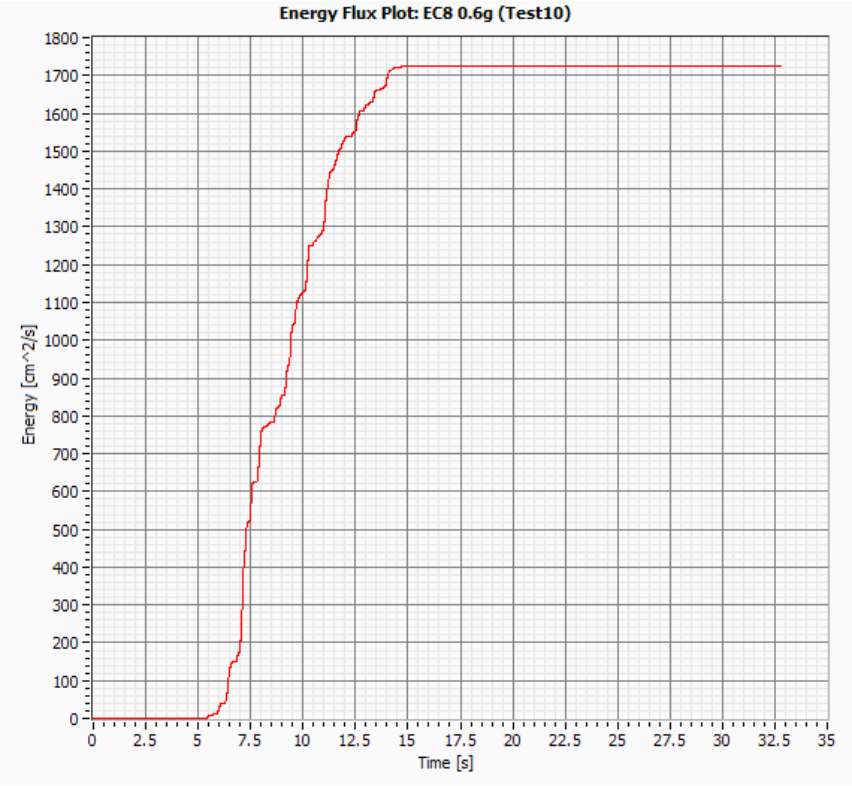

Figure II.34: Specific Energy Density (SED): EC8 0.6g (Test10).

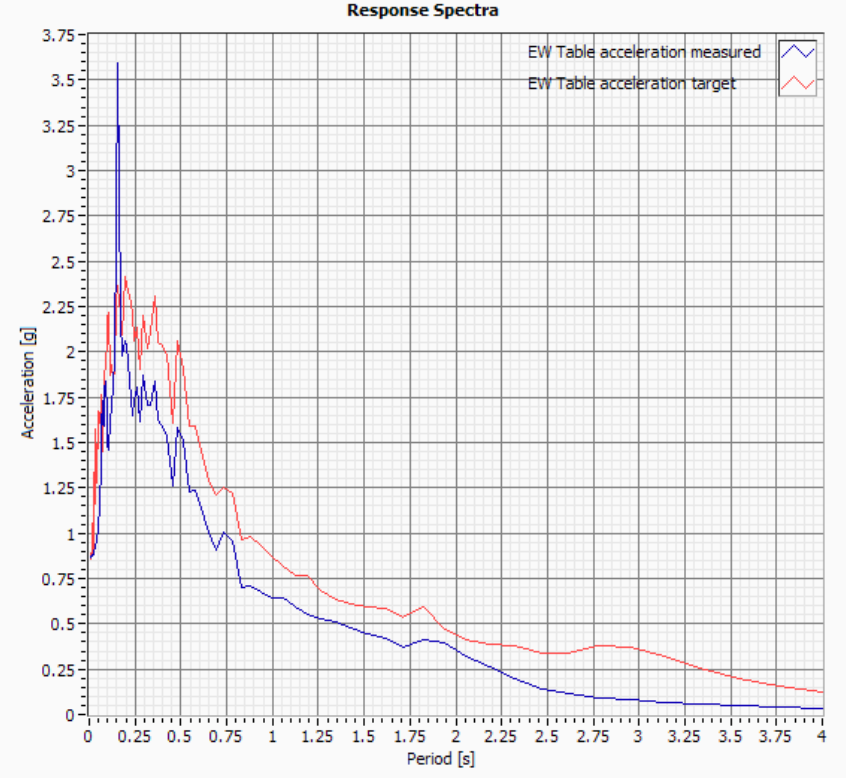

Figure II.35: Response spectra for EW Table acceleration: EC8 0.8g (Test12).

Table II.5: Ground Motion Parameters for EC8 0.8g (Test12).

Ground Motion Parameters	Test12	Units
Peak Ground Acceleration (PGA)	0.87	g
Peak Ground Velocity (PGV)	54.09	cm/s
Peak Ground Displacement (PGD)	99.03	mm
Peak Velocity and Acceleration ratio	0.01	s
Arias Intensity (Ia)	7.41	m/s
A95 Parameter	0.60	g
t05 (5% of Ia)	6.57	s
t95 (95% of Ia)	13.29	s
Significant duration (t95-t05)	6.72	s
Characteristic Intensity	0.24	-
Predominant Period	0.16	s
Mean Period	0.35	s
Sustained Maximum Acceleration	0.78	g
Sustained Maximum Velocity	41.27	cm/s
Acceleration Spectrum Intensity*	0.72	G
Velocity Spectrum Intensity (Housner Intensity)*	230.50	cm/s
Specific Energy Density (SED)	2971.89	cm^2/s

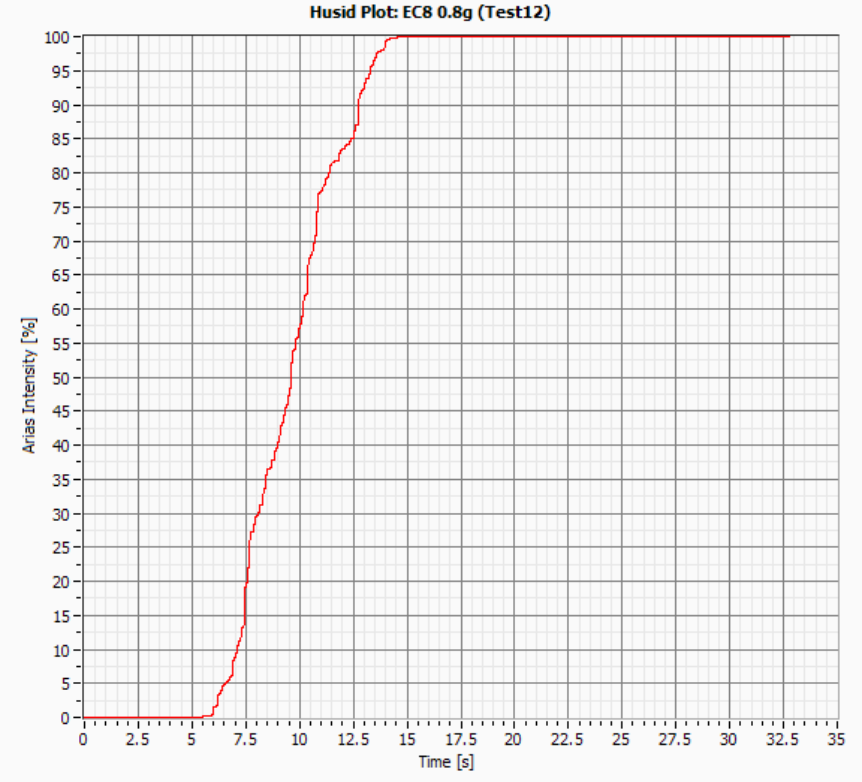

Figure II.36: Arias Intensity (Ia): EC8 0.8g (Test12).

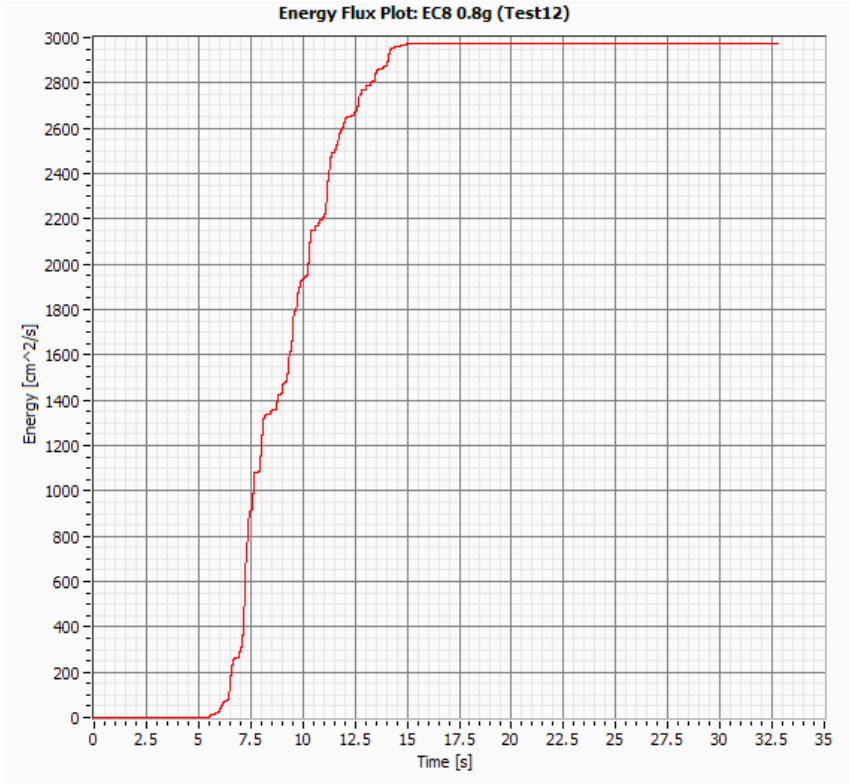

Figure II.37: Specific Energy Density (SED): EC8 0.8g (Test12).

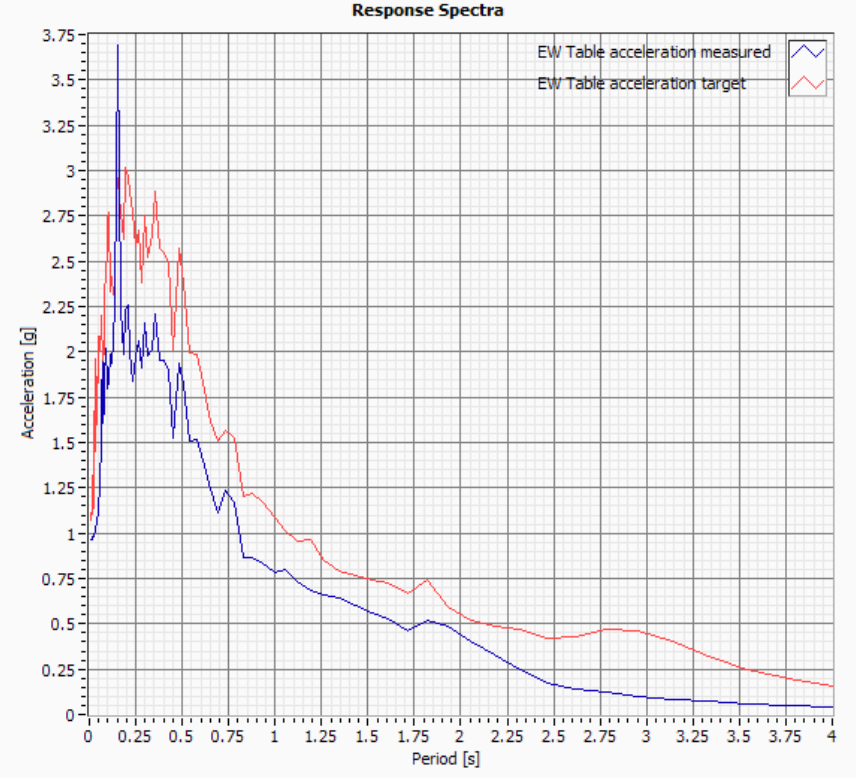

Figure II.38: Response spectra for EW Table acceleration: EC8 1.0g (Test14).

Table II.6: Ground Motion Parameters for EC8 1.0g (Test14).

Ground Motion Parameters	Test14	Units
Peak Ground Acceleration (PGA)	0.96	G
Peak Ground Velocity (PGV)	63.45	cm/s
Peak Ground Displacement (PGD)	124.45	Mm
Peak Velocity and Acceleration ratio	0.06	S
Arias Intensity (Ia)	9.55	m/s
A95 Parameter	0.67	G
t05 (5% of Ia)	5.30	S
t95 (95% of Ia)	12.18	S
Significant duration (t95-t05)	6.89	S
Characteristic Intensity	0.29	-
Predominant Period	0.16	S
Mean Period	0.38	S
Sustained Maximum Acceleration	0.82	G
Sustained Maximum Velocity	49.93	cm/s
Acceleration Spectrum Intensity*	0.83	g
Velocity Spectrum Intensity (Housner Intensity)*	244.00	cm/s
Specific Energy Density (SED)	4485.44	cm^2/s

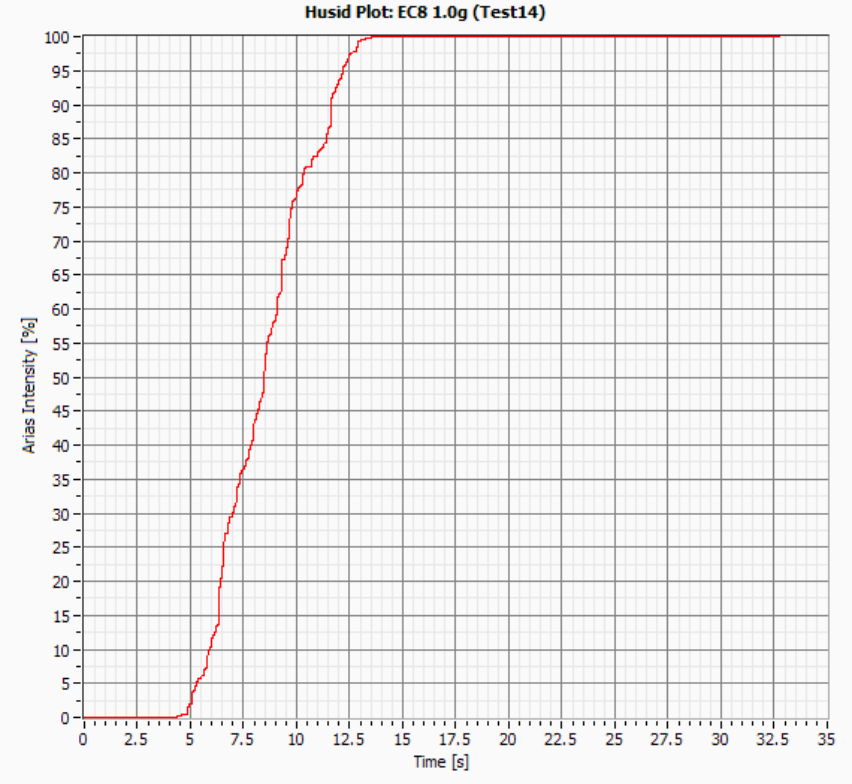

Figure II.39: Arias Intensity (Ia): EC8 1.0g (Test14).

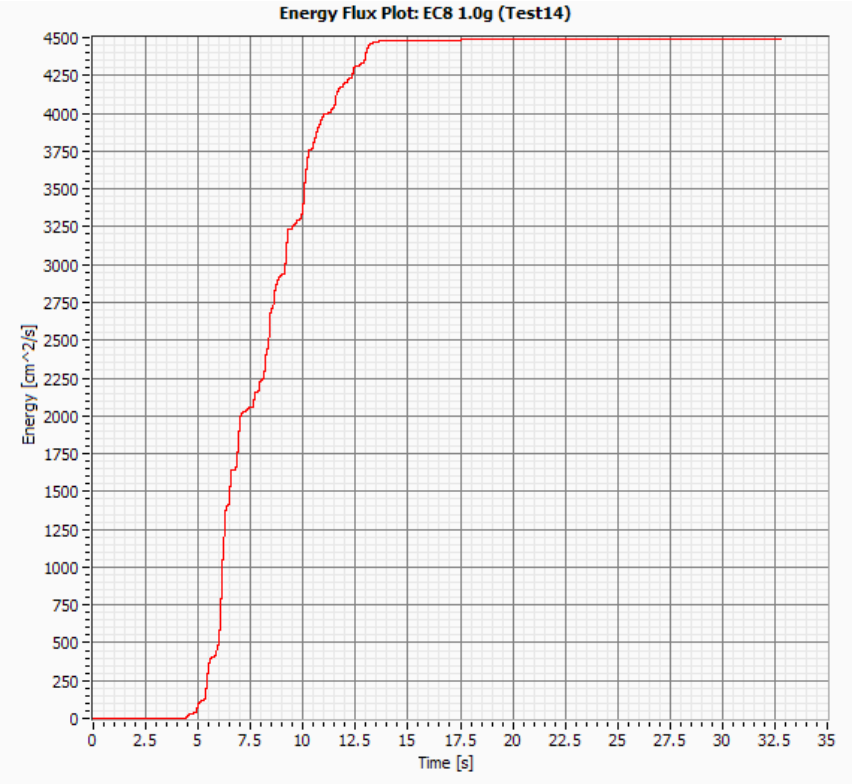

Figure II.40: Specific Energy Density (SED): EC8 1.0g (Test14).

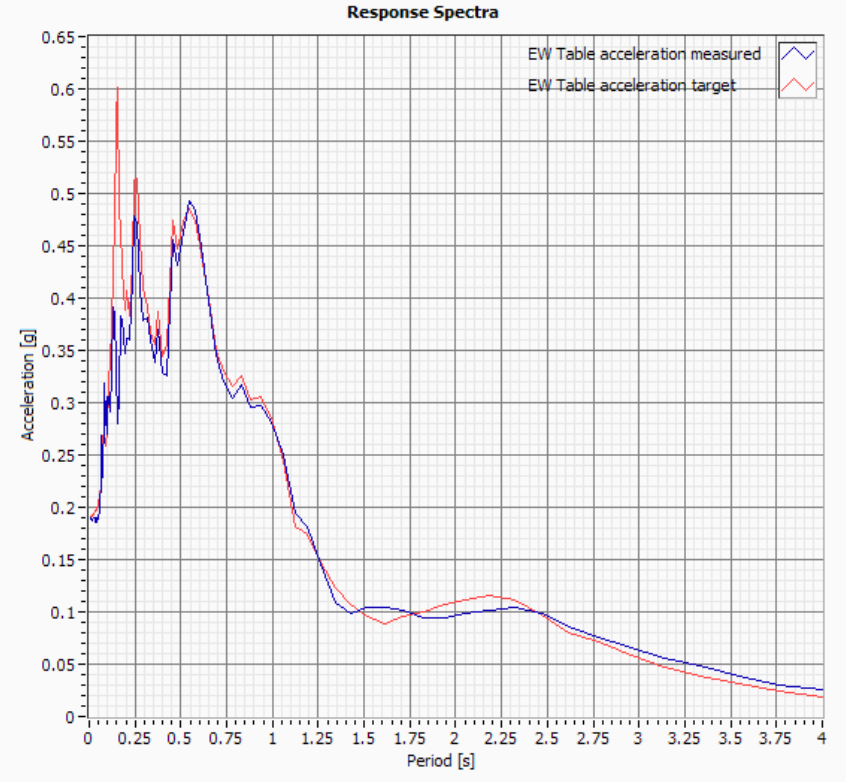

Figure II.41: Response spectra for EW Table acceleration: ElCentro 0.2g (Test17).

Table II.7: Ground Motion Parameters for ElCentro 0.2g (Test17).

Ground Motion Parameters	Test17	Units
Peak Ground Acceleration (PGA)	0.19	g
Peak Ground Velocity (PGV)	17.81	cm/s
Peak Ground Displacement (PGD)	41.91	mm
Peak Velocity and Acceleration ratio	0.07	s
Arias Intensity (Ia)	0.52	m/s
A95 Parameter	0.13	g
t05 (5% of Ia)	6.08	s
t95 (95% of Ia)	19.55	s
Significant duration (t95-t05)	13.47	s
Characteristic Intensity	0.03	-
Predominant Period	0.16	s
Mean Period	0.52	s
Sustained Maximum Acceleration	0.15	g
Sustained Maximum Velocity	15.44	cm/s
Acceleration Spectrum Intensity*	0.17	g
Velocity Spectrum Intensity (Housner Intensity)*	75.83	cm/s
Specific Energy Density (SED)	420.91	cm^2/s

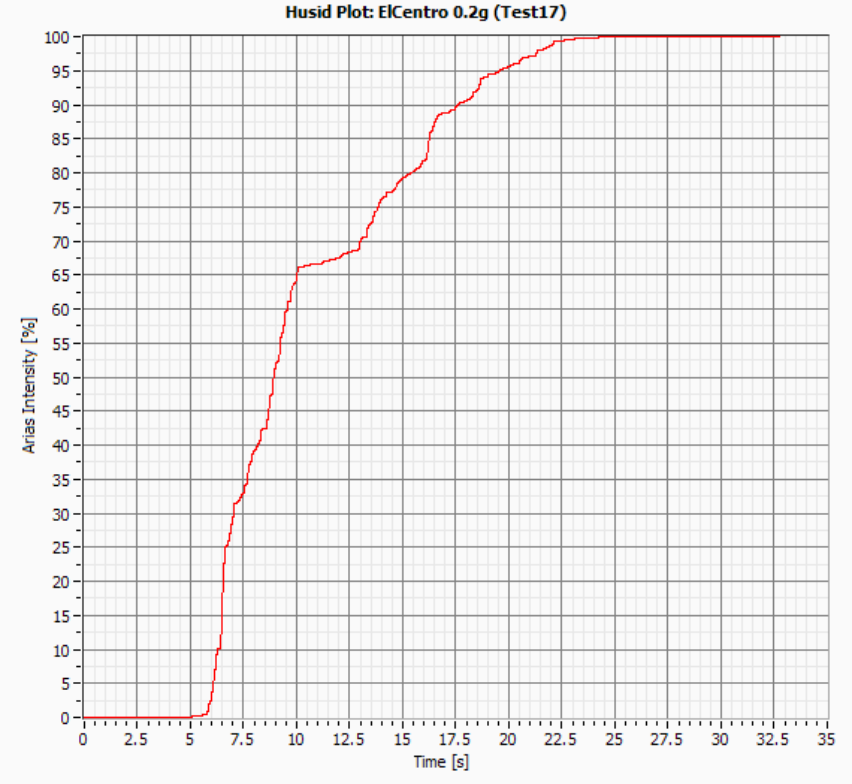

Figure II.42: Arias Intensity (Ia): ElCentro 0.2g (Test17).

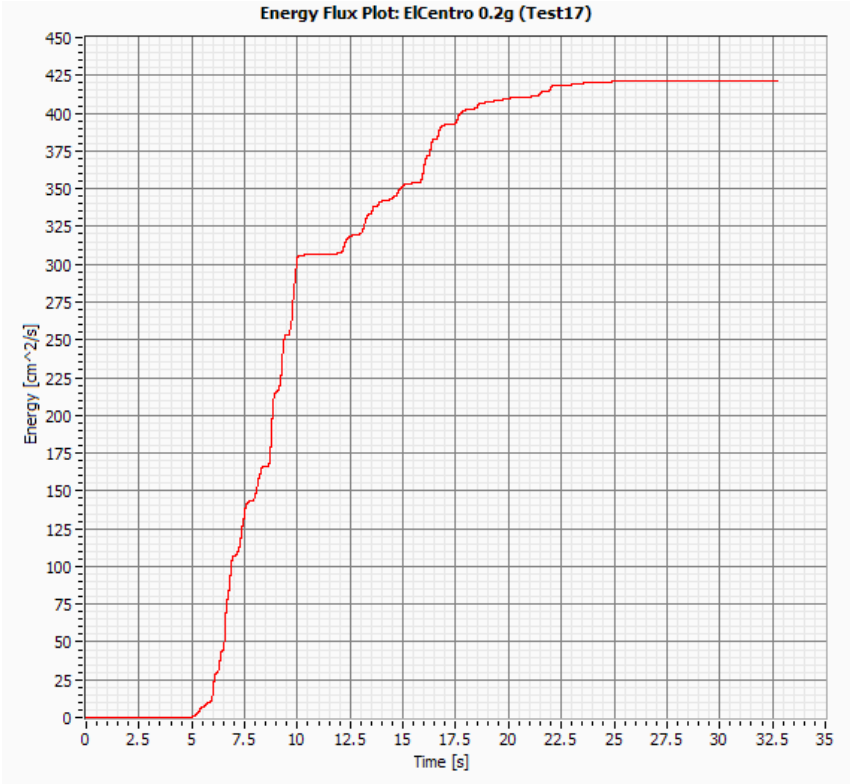

Figure II.43: Specific Energy Density (SED): ElCentro 0.2g (Test17).

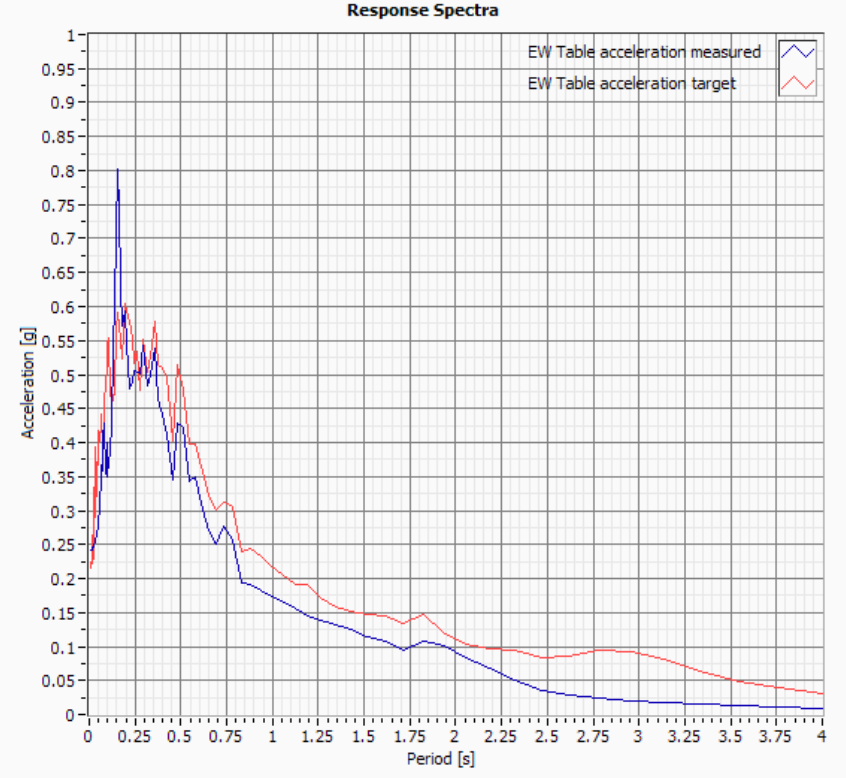

Figure II.44: Response spectra for EW Table acceleration: EC8 0.2g (Test19).

Table II.8: Ground Motion Parameters for EC8 0.2g (Test19).

Ground Motion Parameters	Test19	Units
Peak Ground Acceleration (PGA)	0.24	g
Peak Ground Velocity (PGV)	16.10	cm/s
Peak Ground Displacement (PGD)	25.55	mm
Peak Velocity and Acceleration ratio	0.43	s
Arias Intensity (Ia)	0.46	m/s
A95 Parameter	0.16	g
t05 (5% of Ia)	6.32	s
t95 (95% of Ia)	13.03	s
Significant duration (t95-t05)	6.71	s
Characteristic Intensity	0.03	-
Predominant Period	0.16	s
Mean Period	0.40	s
Sustained Maximum Acceleration	0.18	g
Sustained Maximum Velocity	11.25	cm/s
Acceleration Spectrum Intensity*	0.20	g
Velocity Spectrum Intensity (Housner Intensity)*	60.97	cm/s
Specific Energy Density (SED)	205.63	cm^2/s

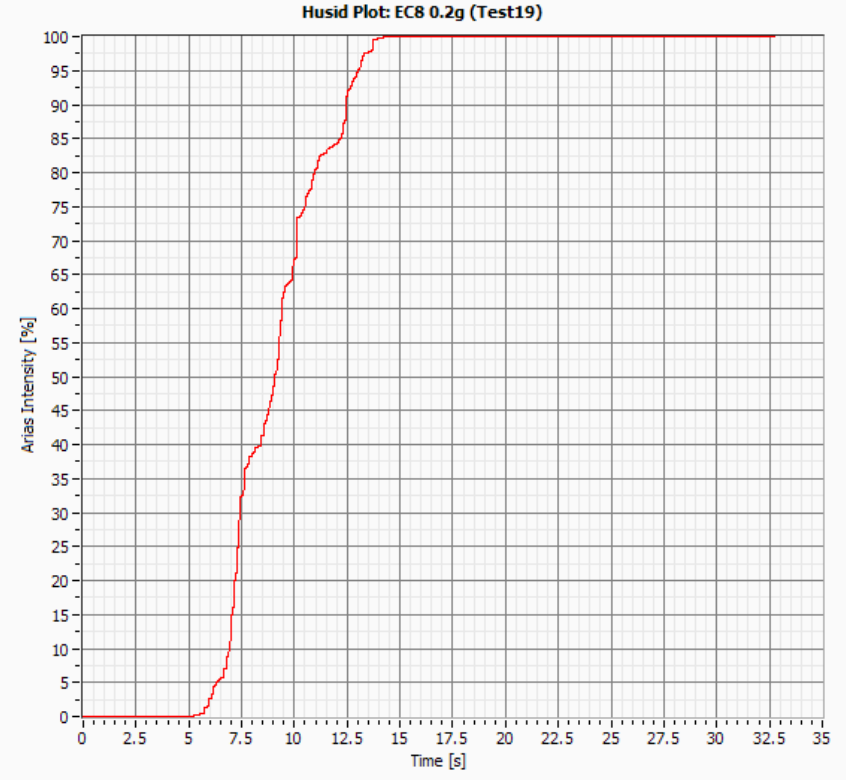

Figure II.45: Arias Intensity (Ia): EC8 0.2g (Test19).

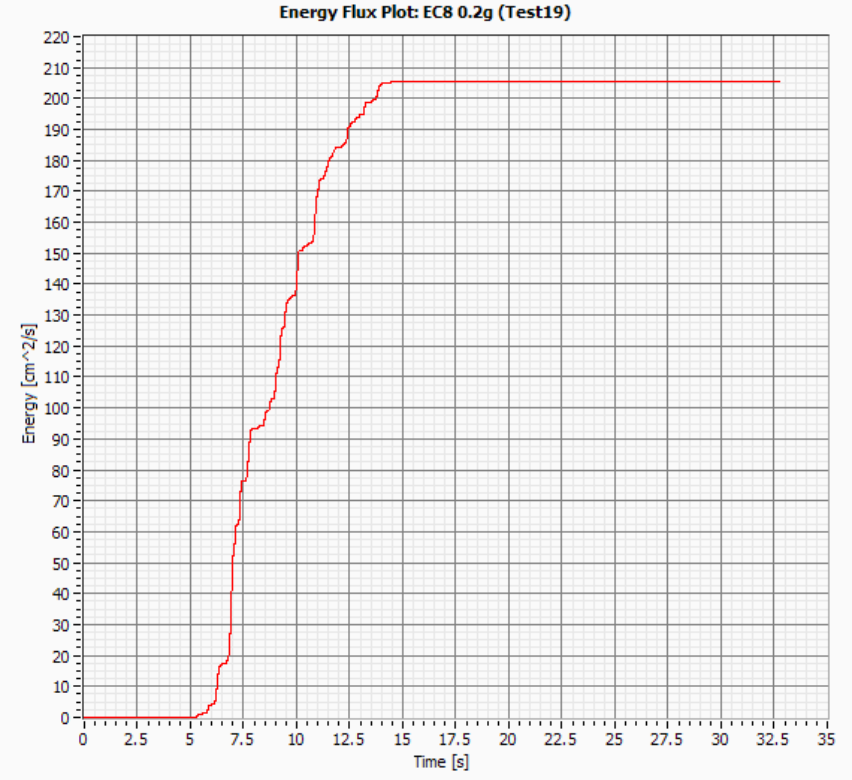

Figure II.46: Specific Energy Density (SED): EC8 0.2g (Test19).

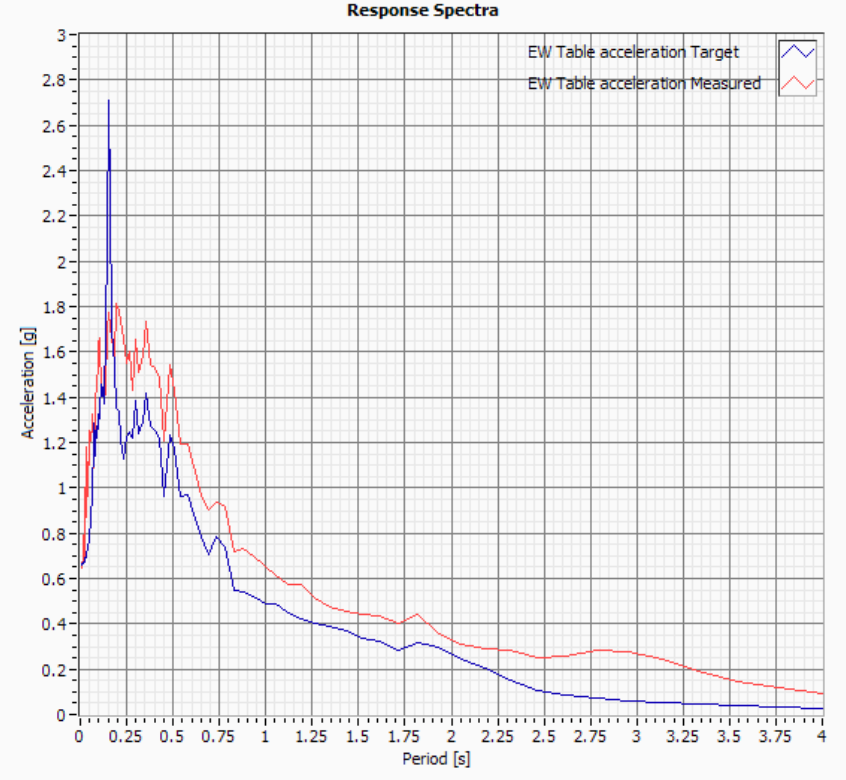

Figure II.47: Response spectra for EW Table acceleration: EC8 0.6g (Test22).

Table II.9: Ground Motion Parameters for EC8 0.6g (Test22).

Ground Motion Parameters	Test22	Units
Peak Ground Acceleration (PGA)	0.66	g
Peak Ground Velocity (PGV)	43.81	cm/s
Peak Ground Displacement (PGD)	73.78	mm
Peak Velocity and Acceleration ratio	0.09	s
Arias Intensity (Ia)	4.41	m/s
A95 Parameter	0.46	g
t05 (5% of Ia)	6.91	s
t95 (95% of Ia)	13.66	s
Significant duration (t95-t05)	6.74	s
Characteristic Intensity	0.16	-
Predominant Period	0.16	s
Mean Period	0.35	s
Sustained Maximum Acceleration	0.59	g
Sustained Maximum Velocity	32.03	cm/s
Acceleration Spectrum Intensity*	0.54	g
Velocity Spectrum Intensity (Housner Intensity)*	175.86	cm/s
Specific Energy Density (SED)	1734.57	cm^2/s

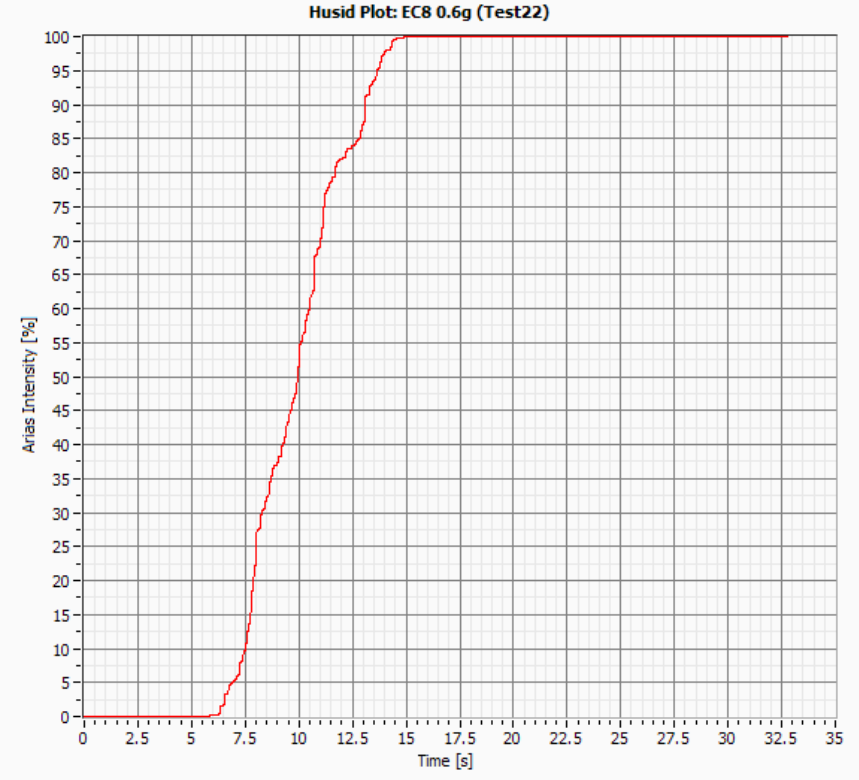

Figure II.48: Arias Intensity (Ia): EC8 0.6g (Test22).

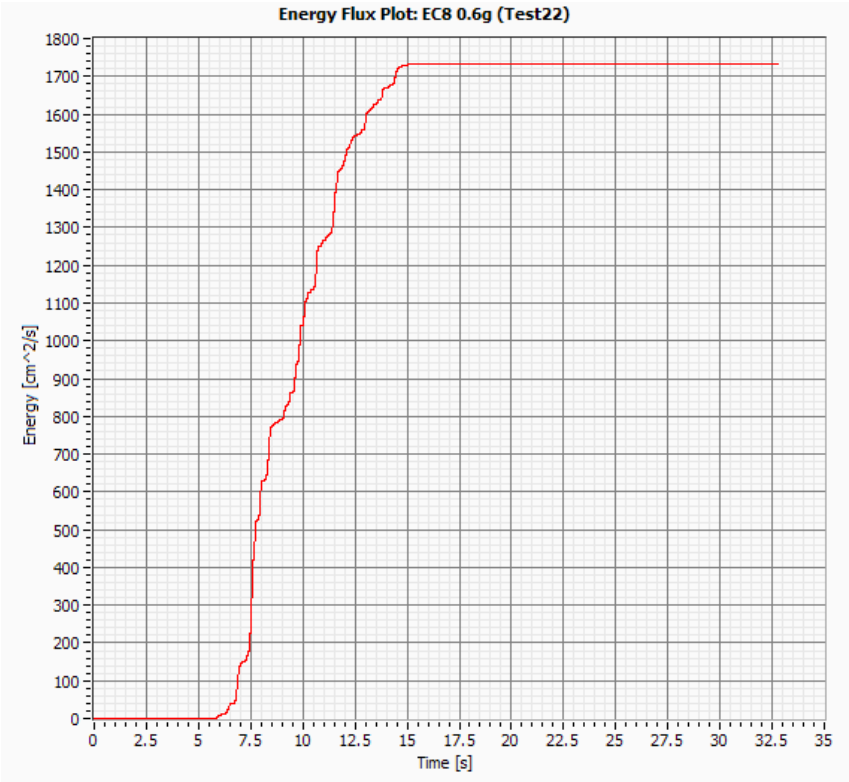

Figure II.49: Specific Energy Density (SED): EC8 0.6g (Test22).

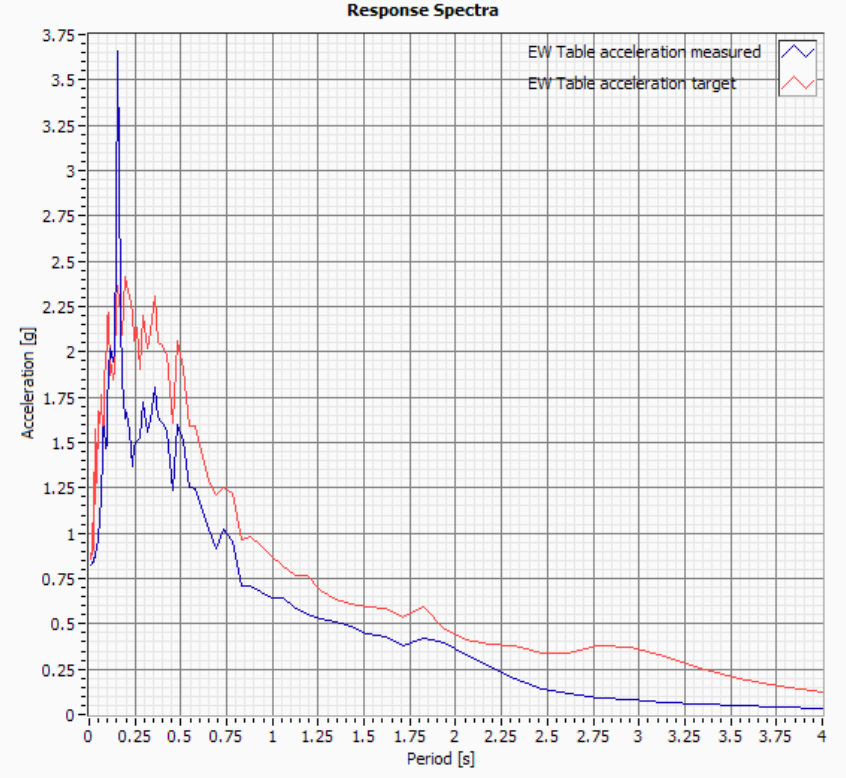

Figure II.50: Response spectra for EW Table acceleration: EC8 0.8g (Test24).

Table II.10: Ground Motion Parameters for EC8 0.8g (Test24).

Ground Motion Parameters	Test24	Units
Peak Ground Acceleration (PGA)	0.82	g
Peak Ground Velocity (PGV)	54.91	cm/s
Peak Ground Displacement (PGD)	97.46	mm
Peak Velocity and Acceleration ratio	0.06	s
Arias Intensity (Ia)	7.43	m/s
A95 Parameter	0.57	g
t05 (5% of Ia)	6.38	s
t95 (95% of Ia)	13.14	s
Significant duration (t95-t05)	6.76	s
Characteristic Intensity	0.24	-
Predominant Period	0.16	s
Mean Period	0.35	s
Sustained Maximum Acceleration	0.73	g
Sustained Maximum Velocity	42.76	cm/s
Acceleration Spectrum Intensity*	0.70	g
Velocity Spectrum Intensity (Housner Intensity)*	230.28	cm/s
Specific Energy Density (SED)	2972.23	cm^2/s

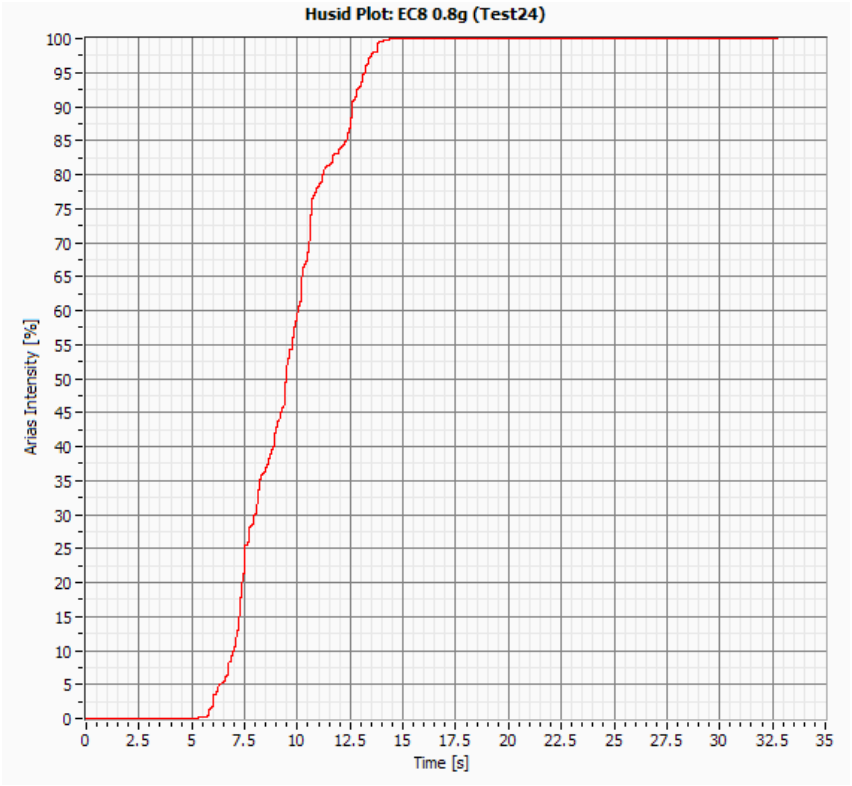

Figure II.51: Arias Intensity (Ia): EC8 0.8g (Test24).

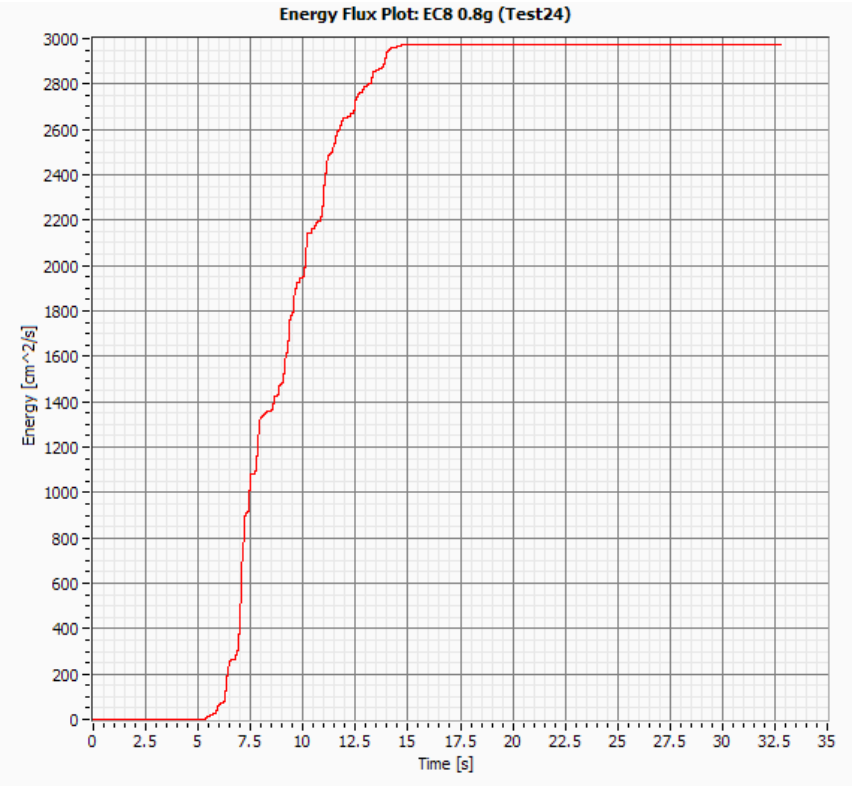

Figure II.52: Specific Energy Density (SED): EC8 0.8g (Test24).

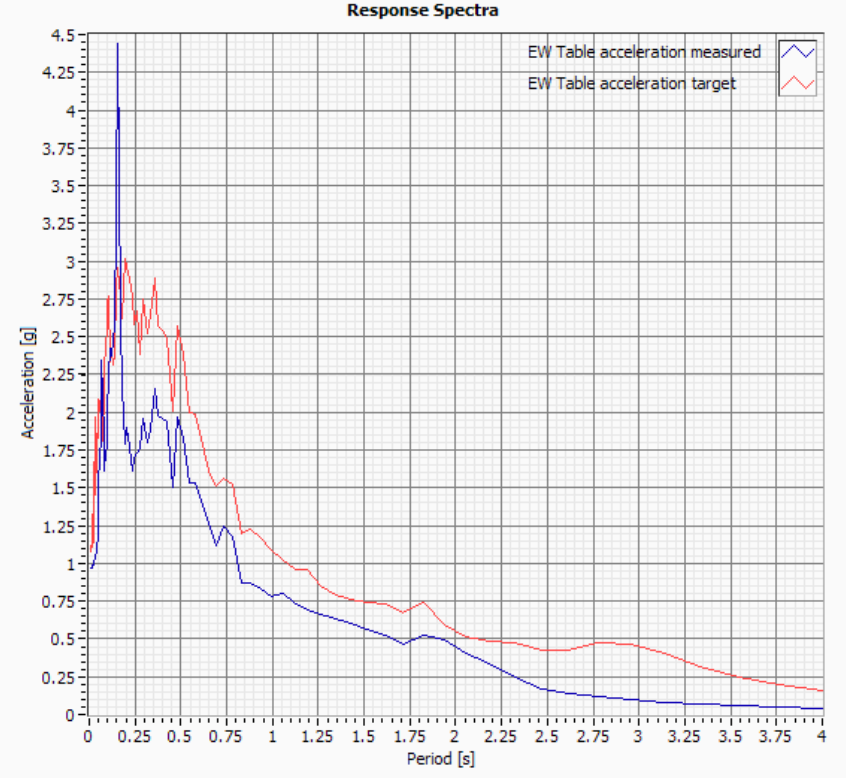

Figure II.53: Response spectra for EW Table acceleration: EC8 1.0g (Test26).

Table II.11: Ground Motion Parameters for EC8 1.0g (Test26).

Ground Motion Parameters	Test26	Units
Peak Ground Acceleration (PGA)	0.96	g
Peak Ground Velocity (PGV)	64.17	cm/s
Peak Ground Displacement (PGD)	123.88	mm
Peak Velocity and Acceleration ratio	0.02	s
Arias Intensity (Ia)	10.85	m/s
A95 Parameter	0.69	g
t05 (5% of Ia)	1.61	s
t95 (95% of Ia)	8.58	s
Significant duration (t95-t05)	6.97	s
Characteristic Intensity	0.41	-
Predominant Period	0.16	s
Mean Period	0.34	s
Sustained Maximum Acceleration	0.92	g
Sustained Maximum Velocity	50.66	cm/s
Acceleration Spectrum Intensity*	0.83	g
Velocity Spectrum Intensity (Housner Intensity)*	284.66	cm/s
Specific Energy Density (SED)	4525.95	cm^2/s

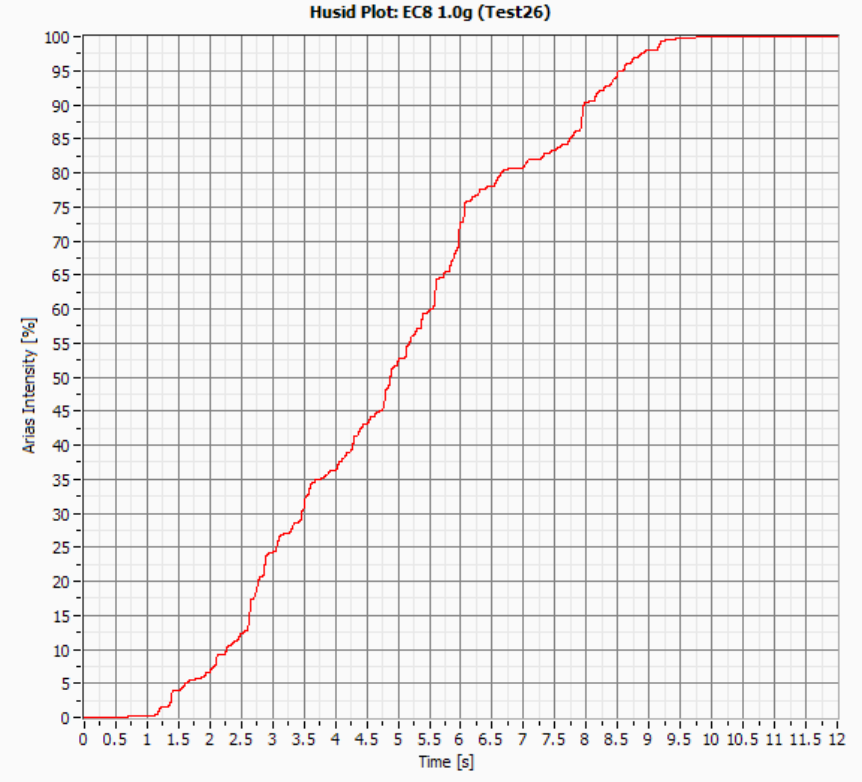

Figure II.54: Arias Intensity (Ia): EC8 1.0g (Test26).

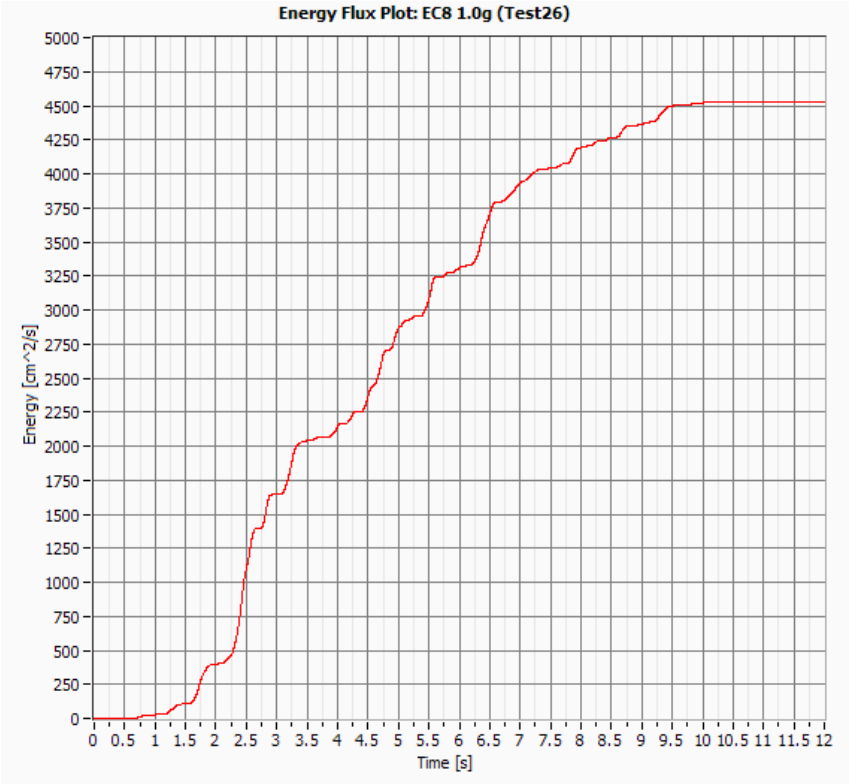

Figure II.55: Specific Energy Density (SED): EC8 1.0g (Test26).

ANNEX III

Experimental Frequencies and Damping

INDEX OF FIGURES

INDEX OF TABLES

Experimental Frequencies

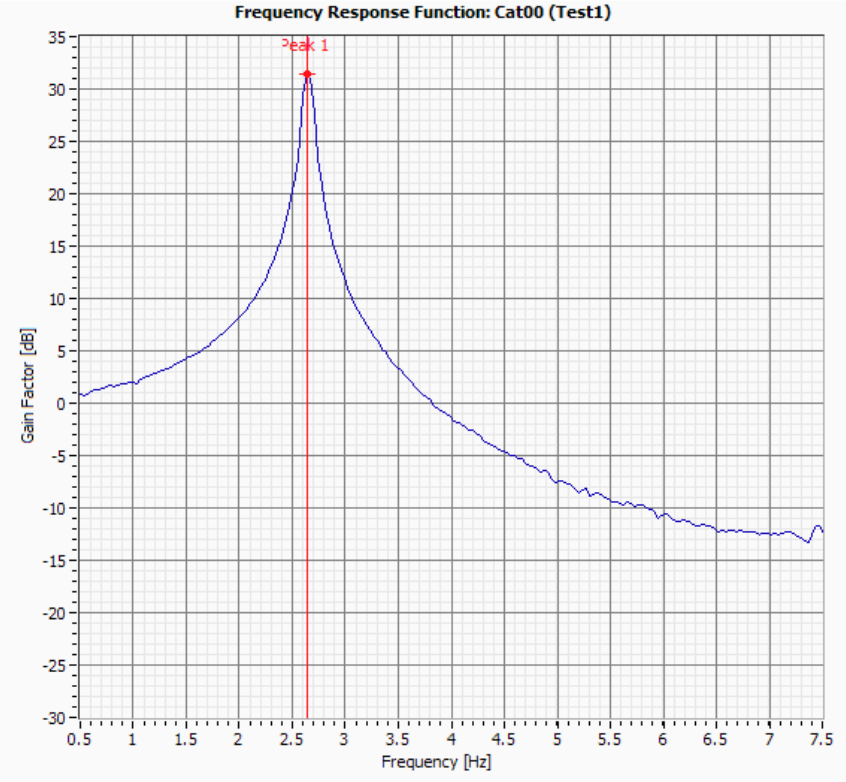

Figure III.1: FRF peak picking – Cat00 (Test1).

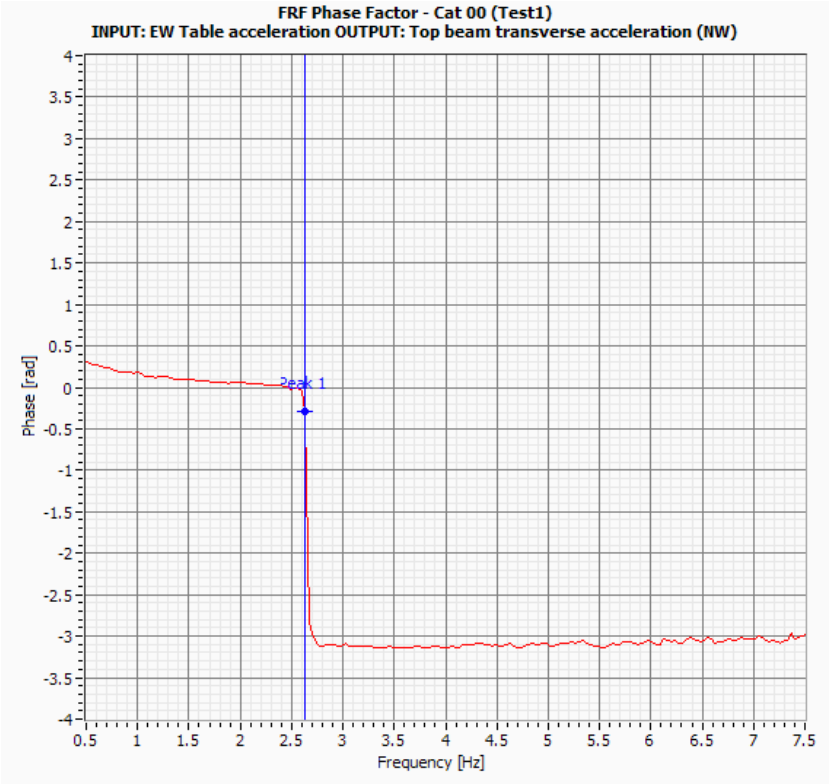

Figure III.2: FRF Phase – Cat00 (Test1).

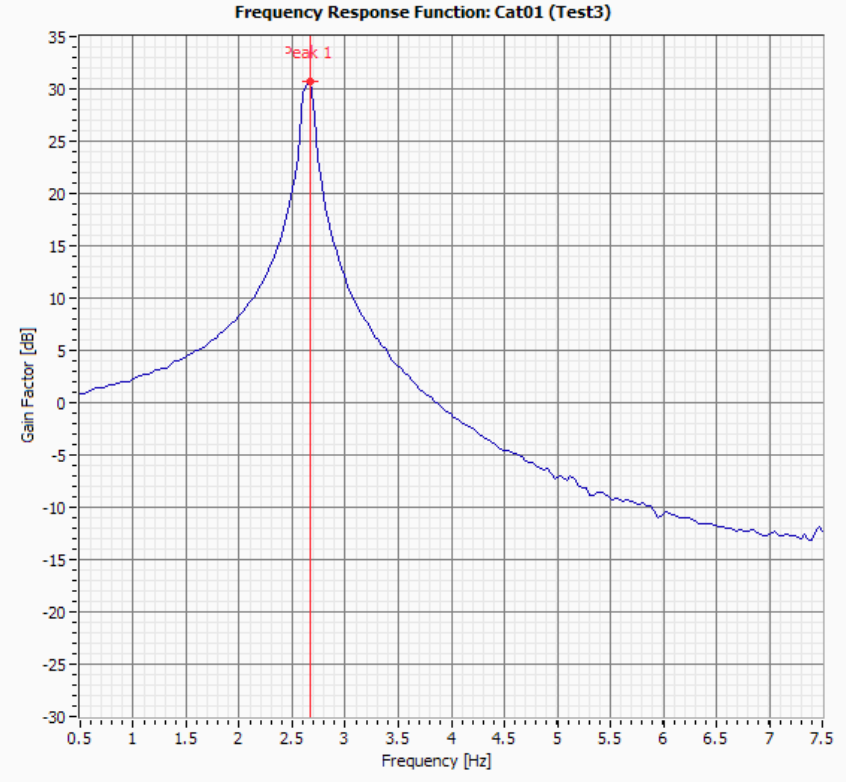

Figure III.3: FRF peak picking – Cat01 (Test3).

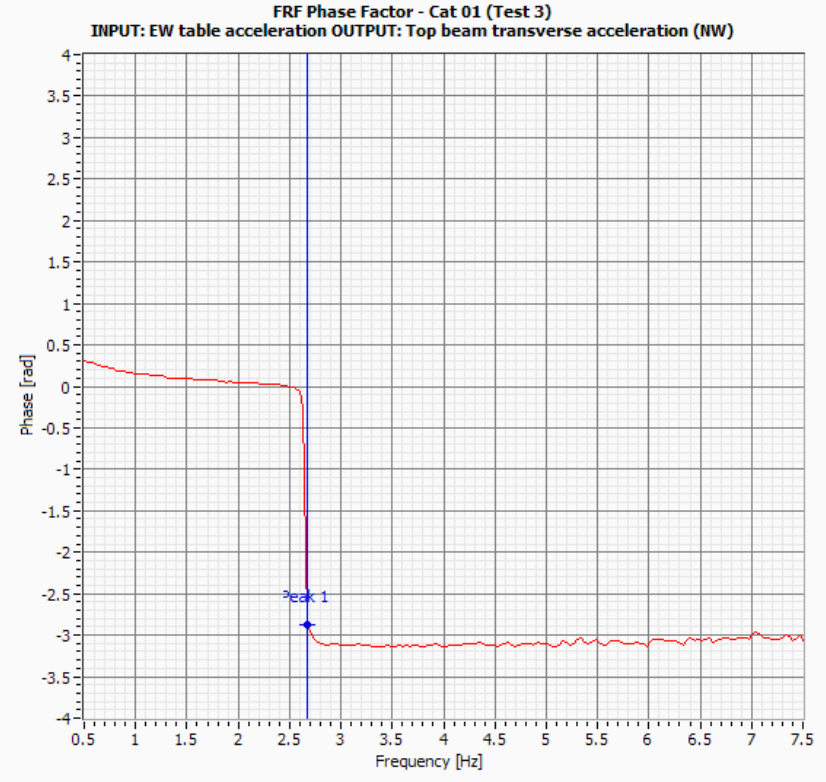

Figure III.4: FRF Phase – Cat01 (Test3).

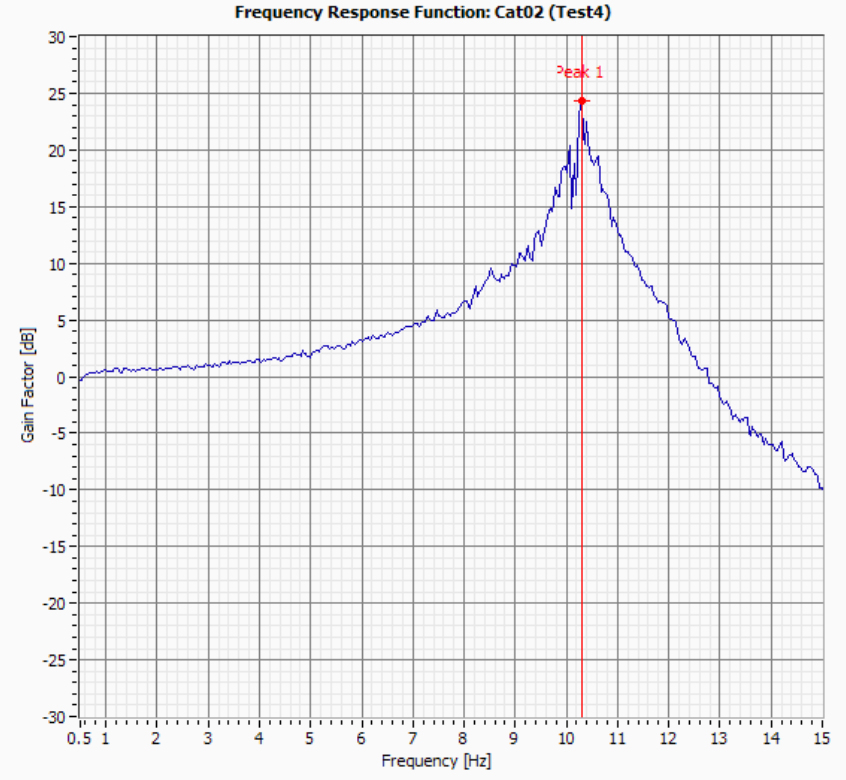

Figure III.5: FRF peak picking – Cat02 (Test4).

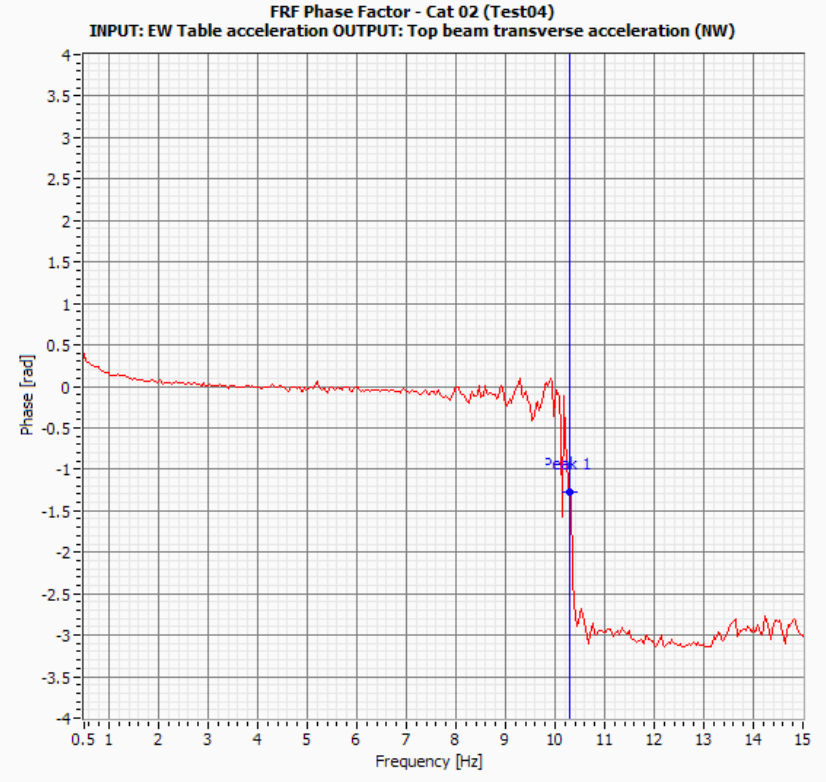

Figure III.6: FRF Phase – Cat02 (Test4).

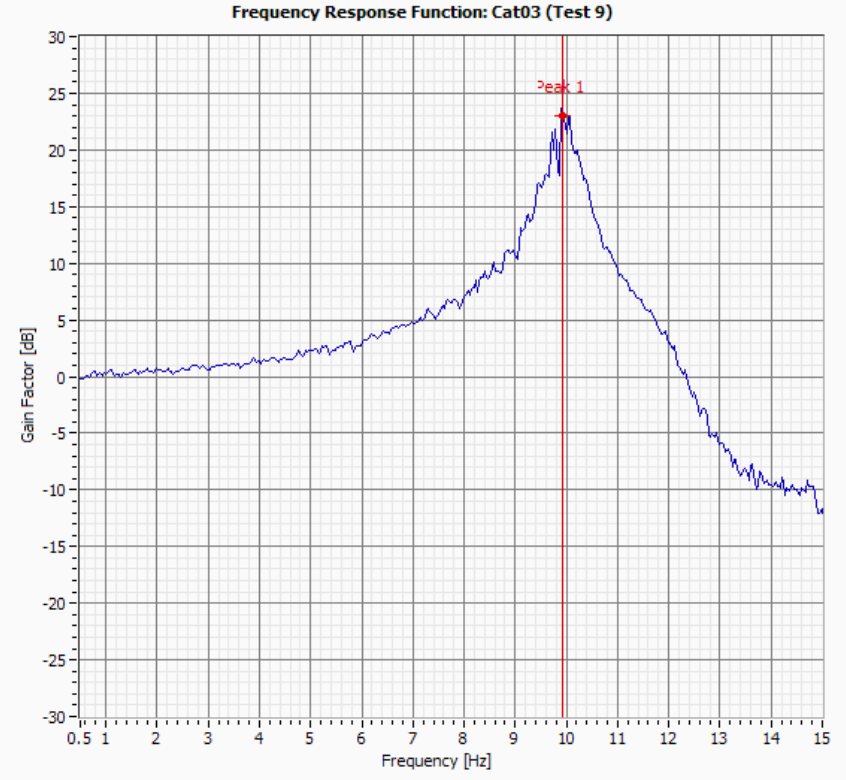

Figure III.7: FRF peak picking – Cat03 (Test9).

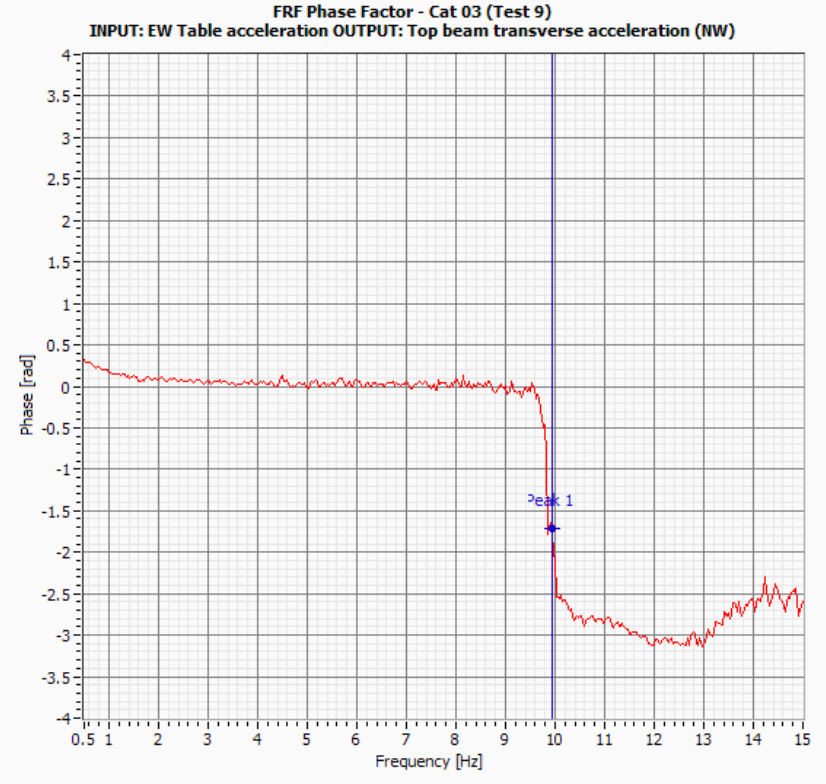

Figure III.8: FRF Phase – Cat03 (Test9).

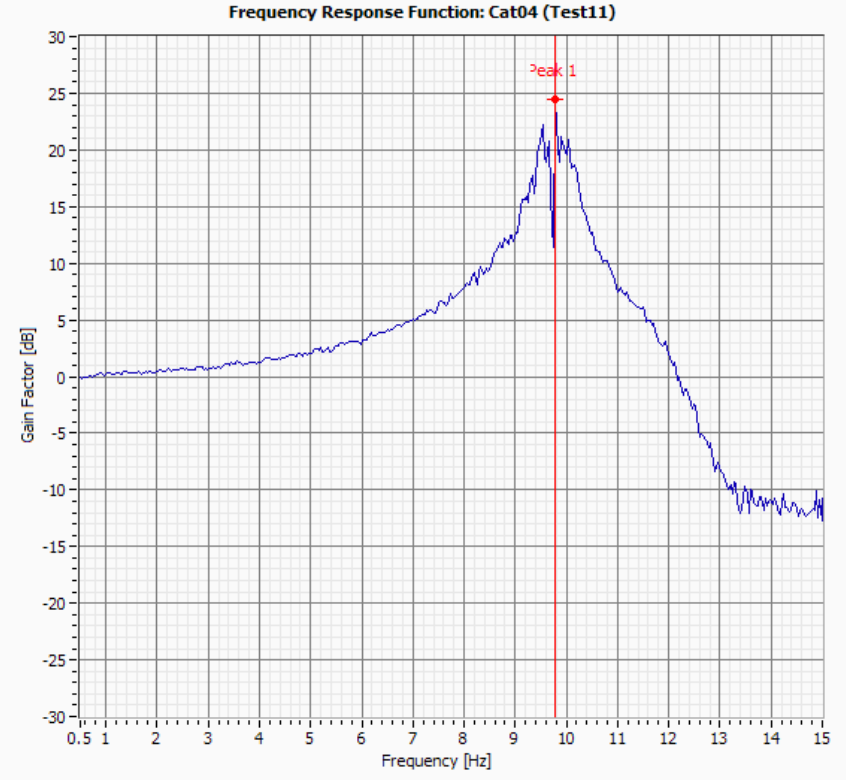

Figure III.9: FRF peak picking – Cat04 (Test11).

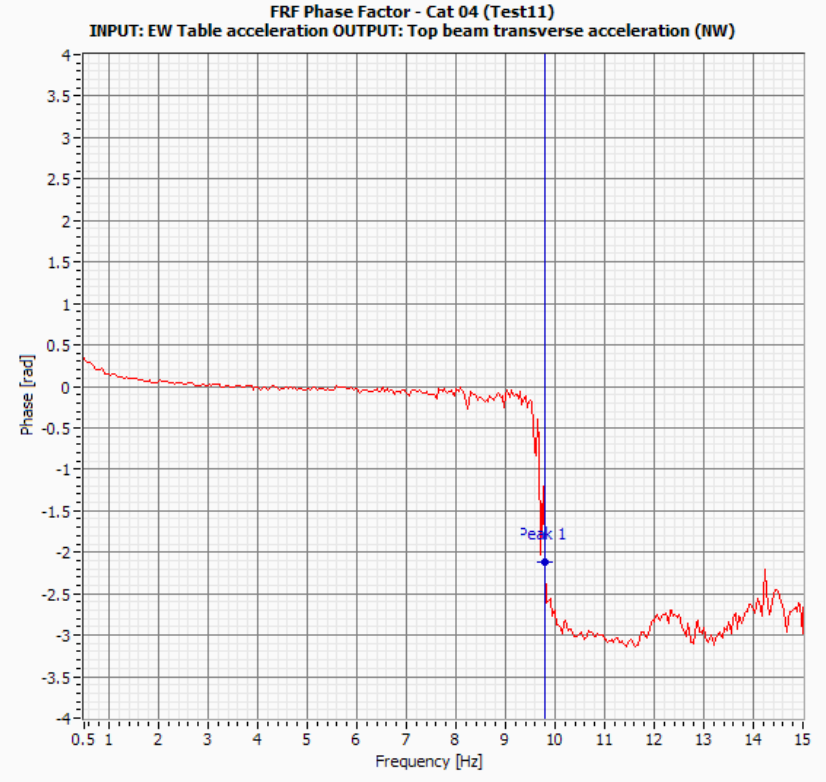

Figure III.10: FRF Phase – Cat04 (Test11).

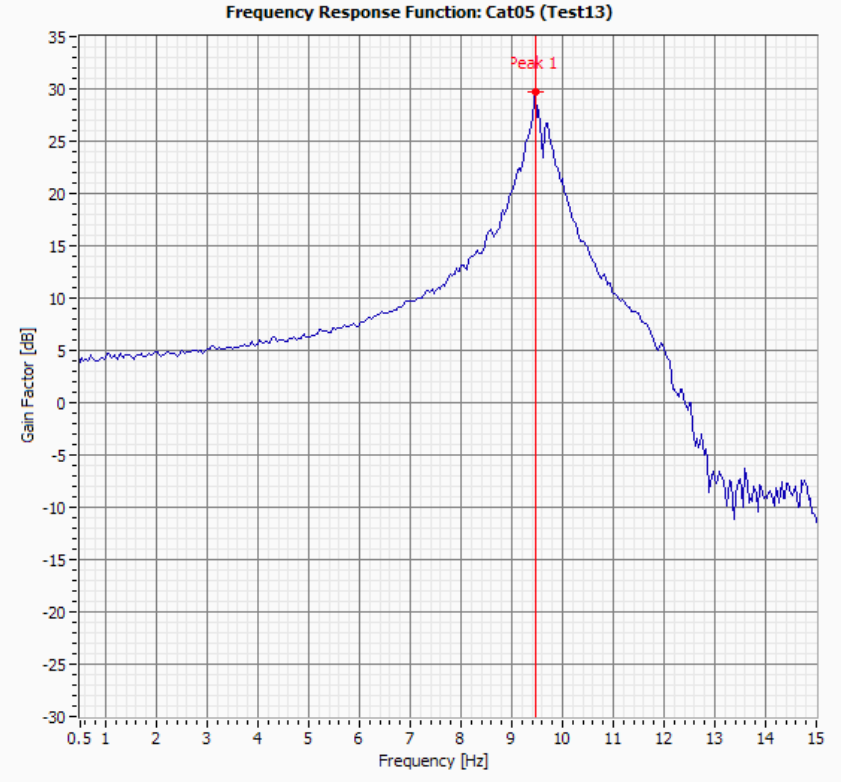

Figure III.11: FRF peak picking – Cat05 (Test13).

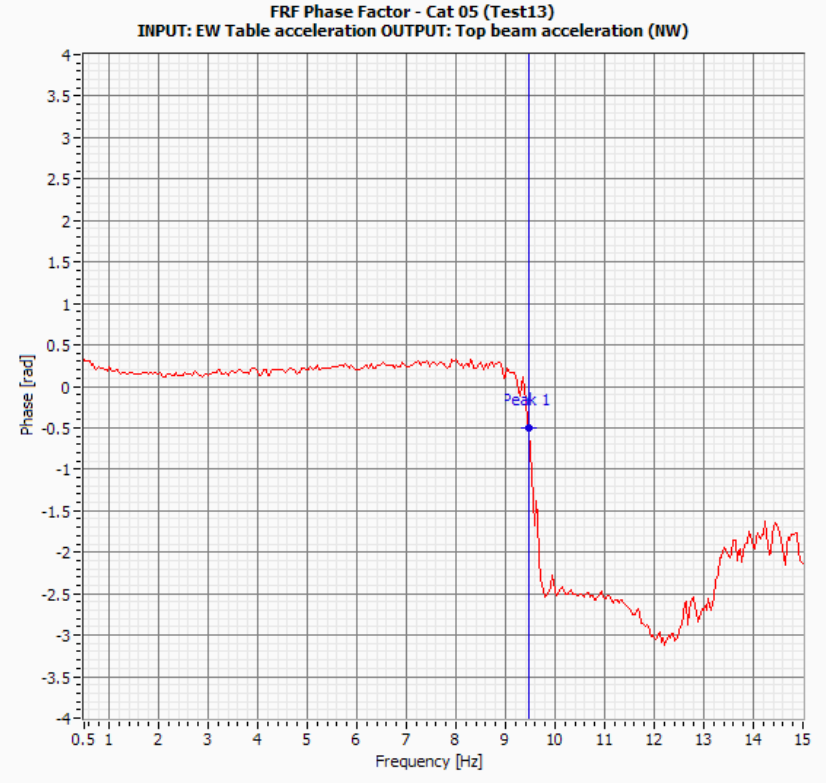

Figure III.12: FRF Phase – Cat05 (Test13).

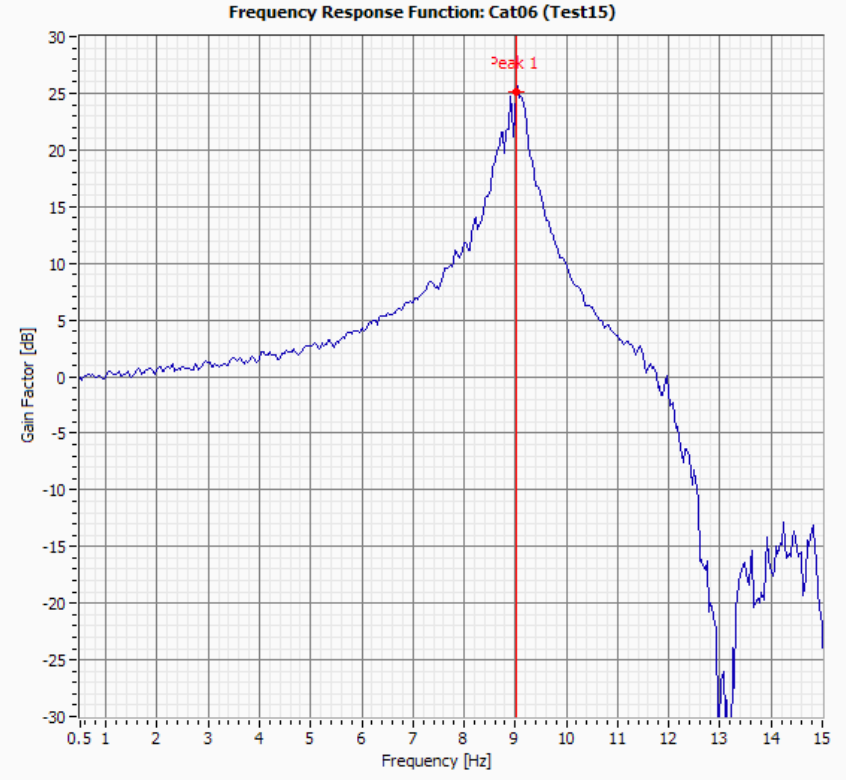

Figure III.13: FRF peak picking – Cat06 (Test15).

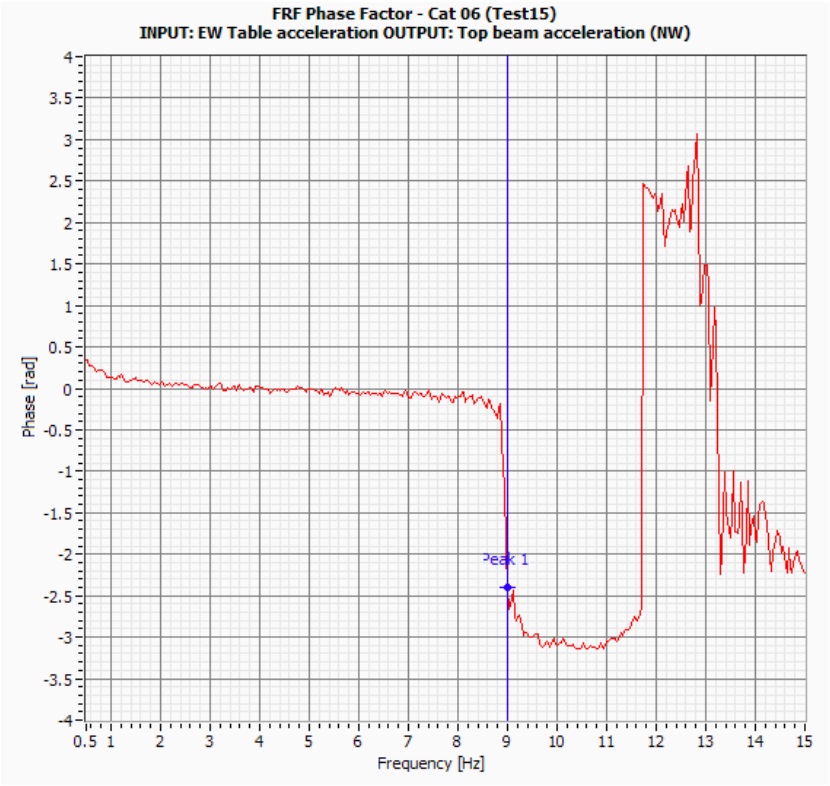

Figure III.14: FRF Phase – Cat06 (Test15).

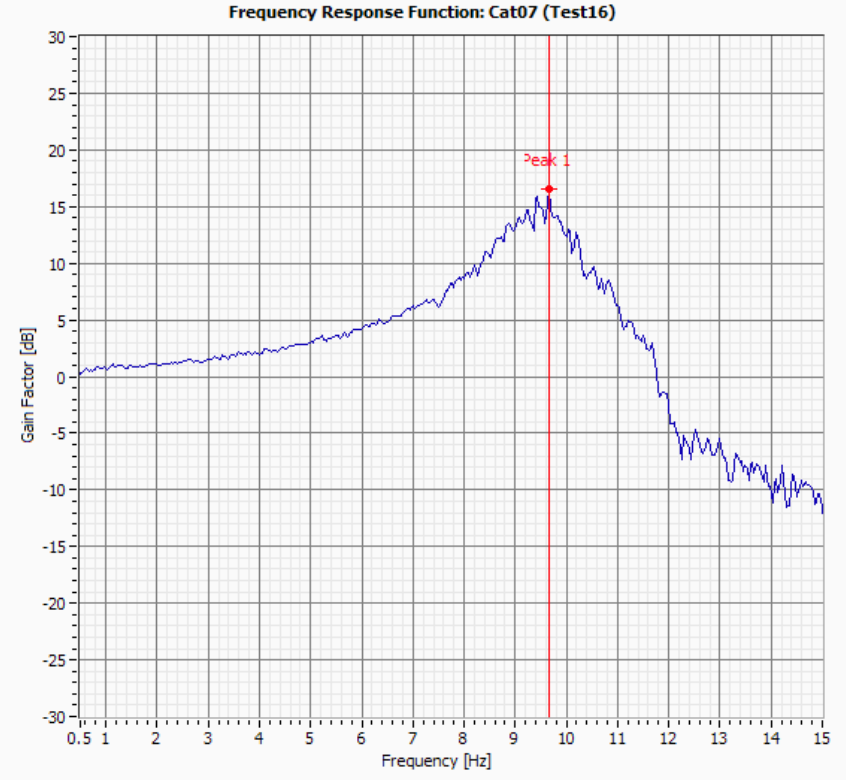

Figure III.15: FRF peak picking – Cat07 (Test16).

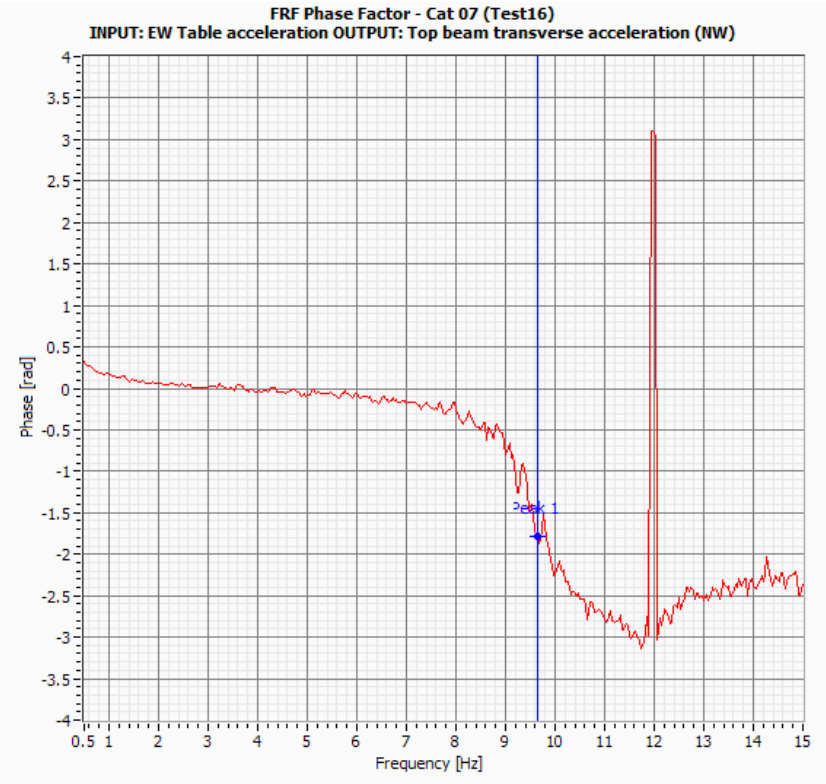

Figure III.16: FRF Phase – Cat07 (Test16).

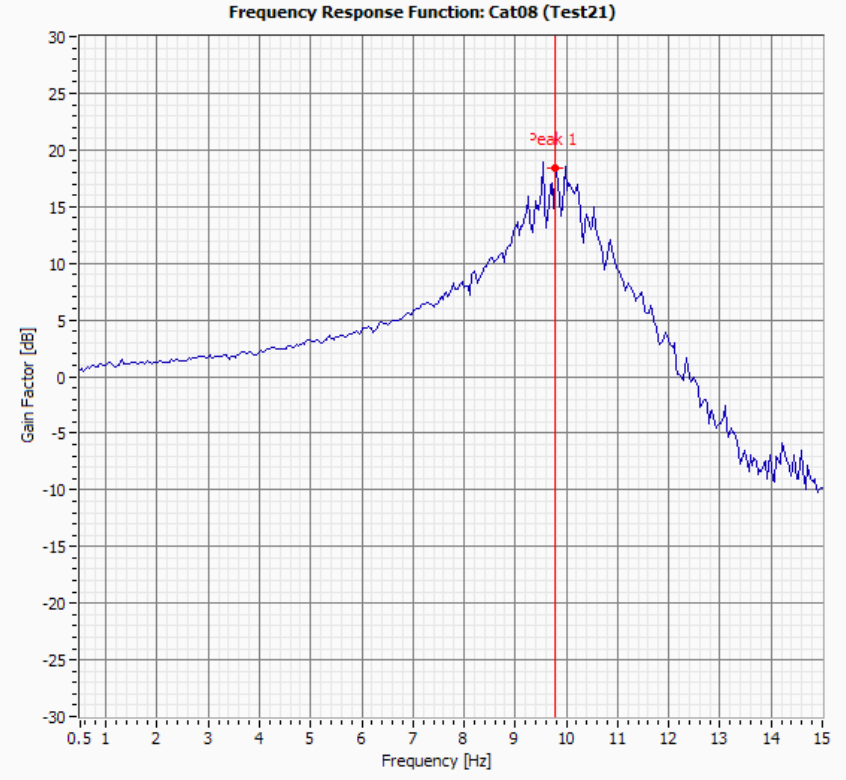

Figure III.17: FRF peak picking – Cat08 (Test21).

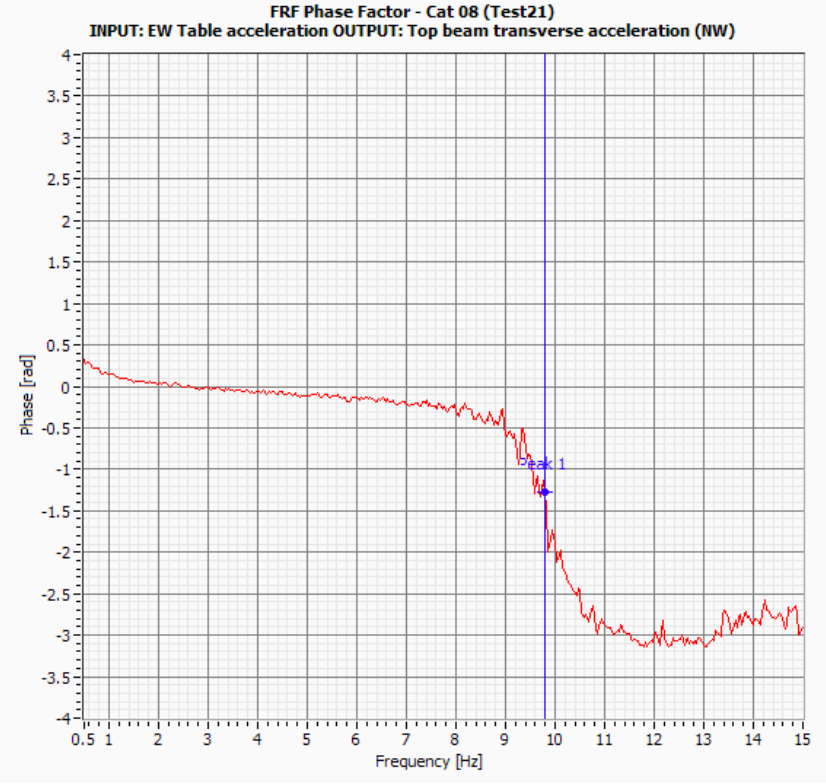

Figure III.18: FRF Phase – Cat08 (Test21).

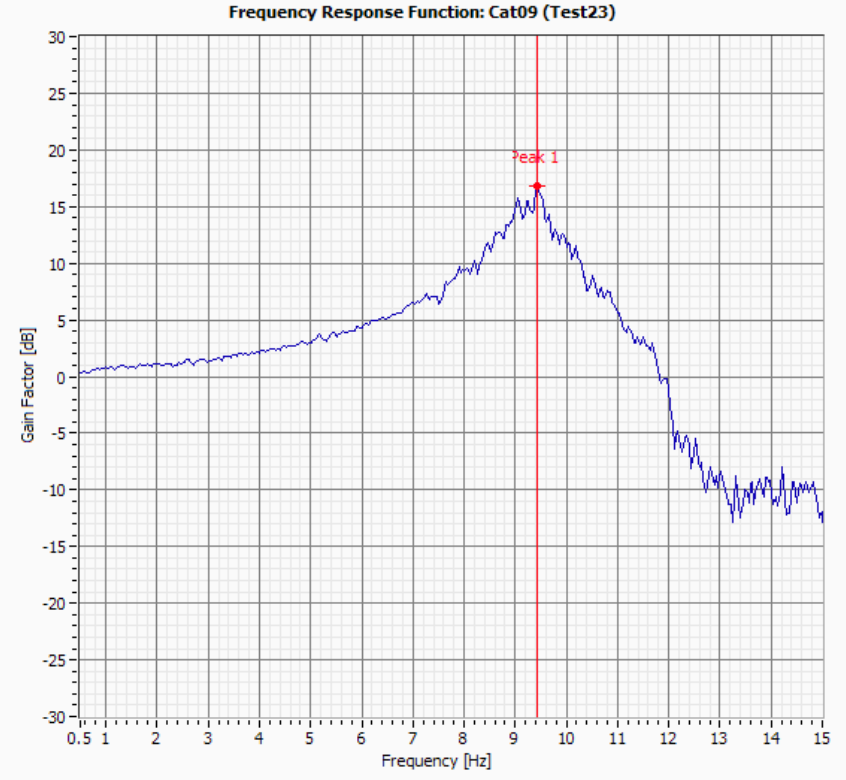

Figure III.19: FRF peak picking – Cat09 (Test23).

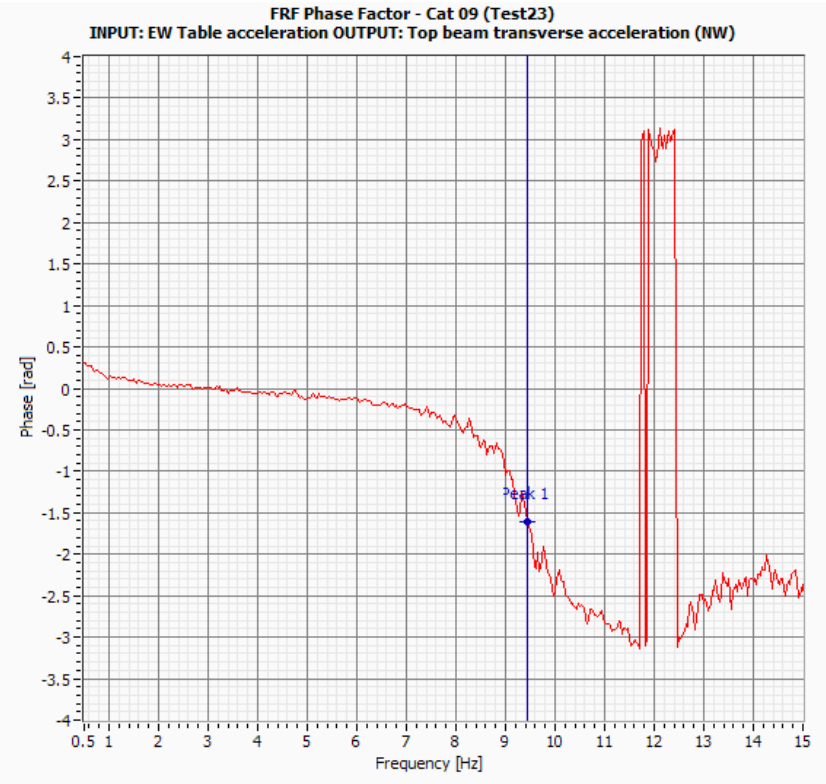

Figure III.20: FRF Phase – Cat09 (Test23).

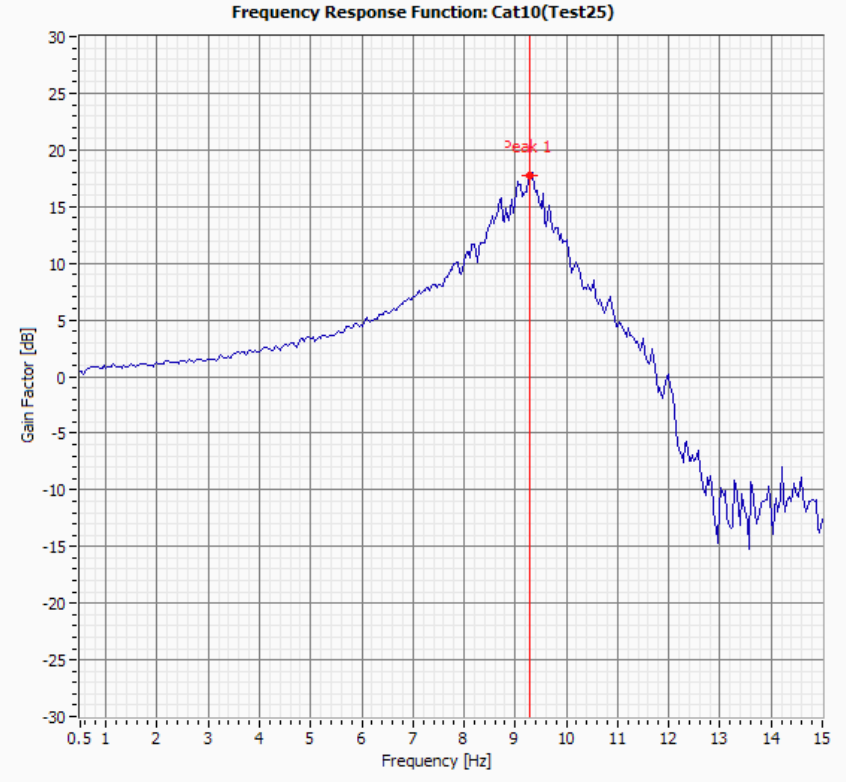

Figure III.21: FRF Phase – Cat10 (Test25).

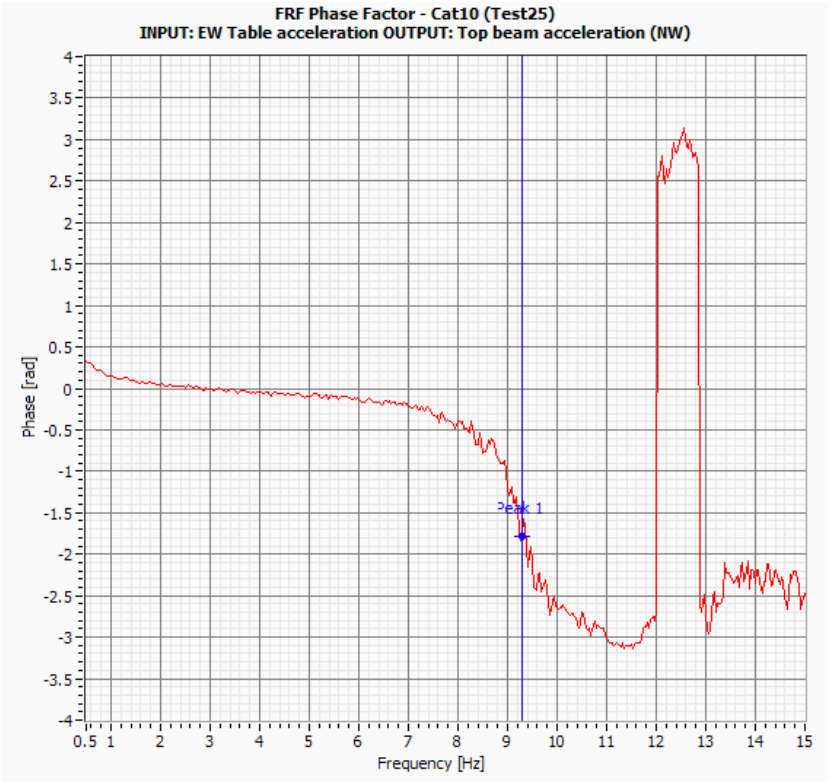

Figure III.22: FRF peak picking – Cat10 (Test25).

Experimental Damping

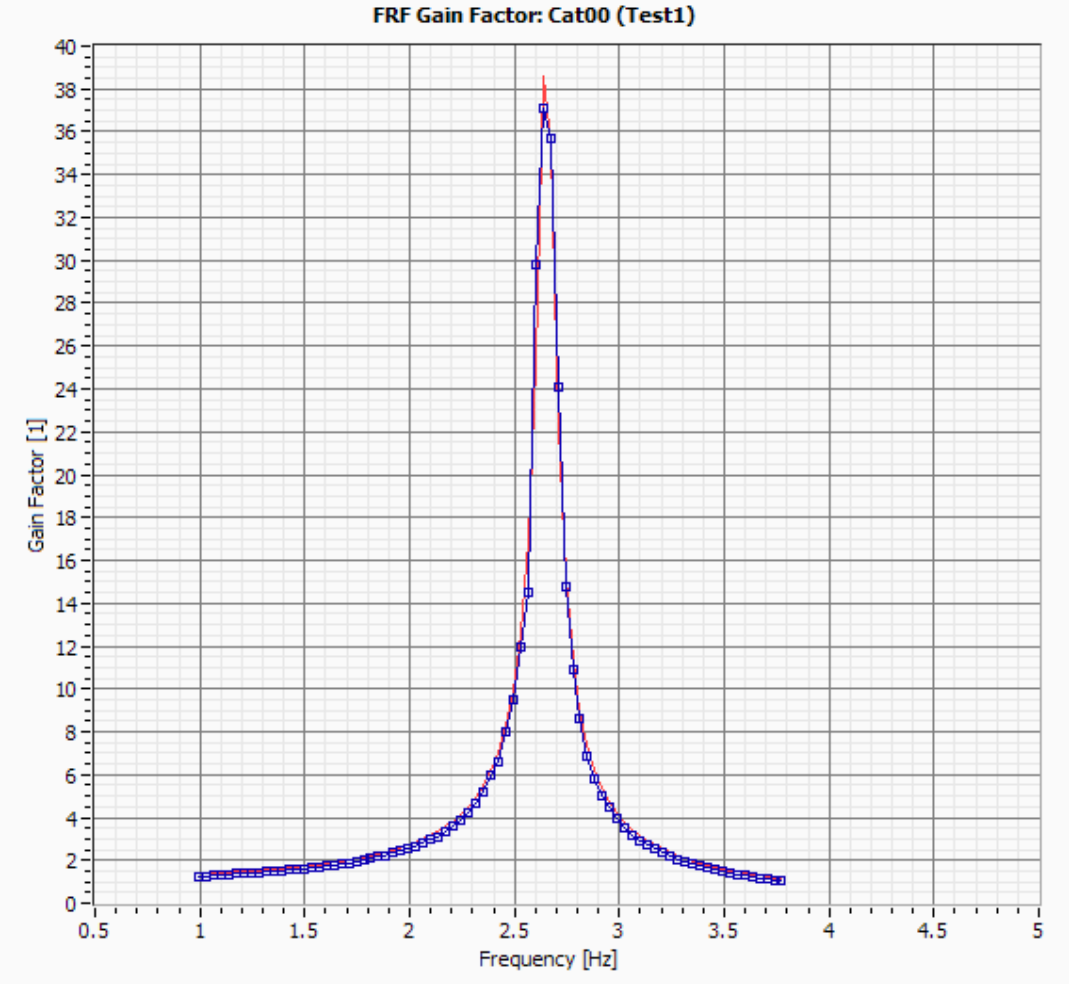

Figure III.23: FRF Gain Factor – Cat00 (Test1).

Table III.1: Experimental Damping for Cat00 (Test1).

Modal Parameter	1.17
Frequency [Hz]	2.65
Damping [%]	1.43

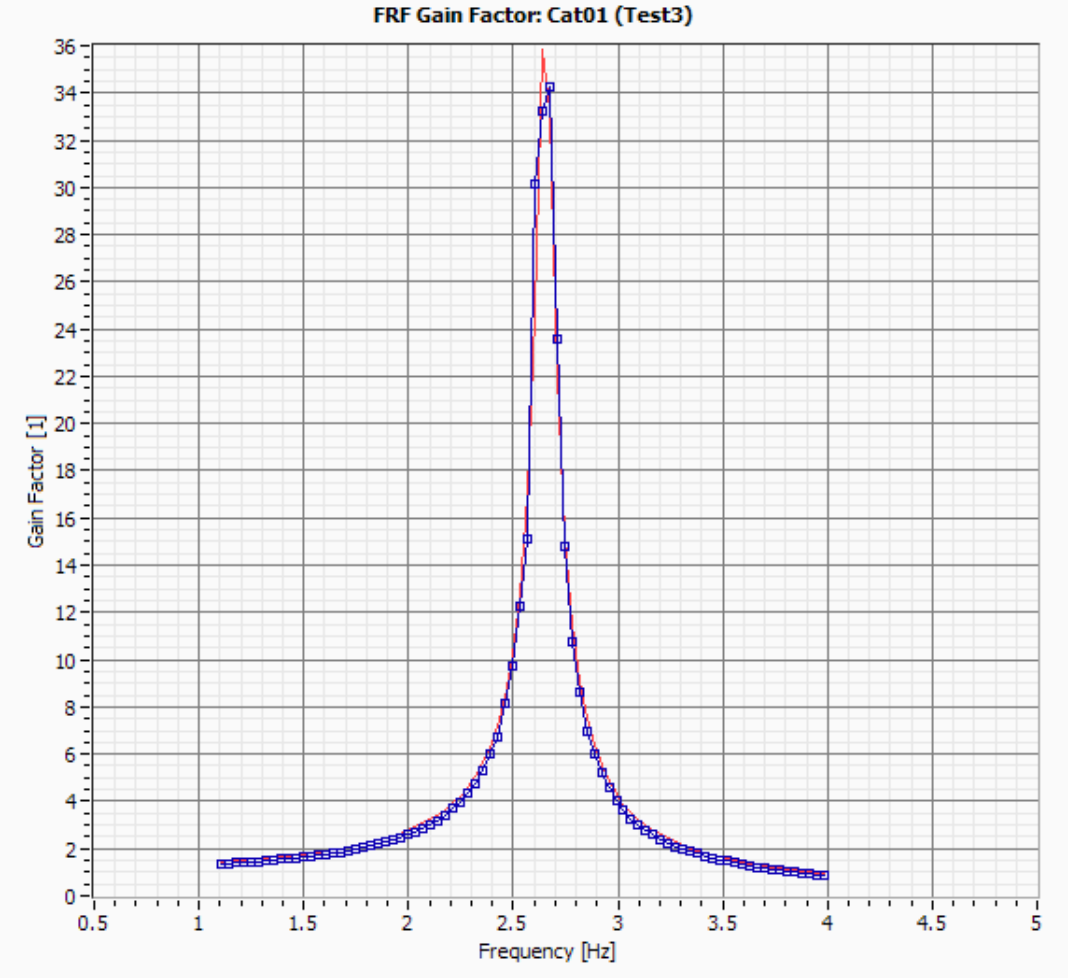

Figure III.24: FRF Gain Factor – Cat01 (Test3).

Table III.2: Experimental Damping for Cat01 (Test3).

Modal Parameter	1.20
Frequency [Hz]	2.65
Damping [%]	1.60

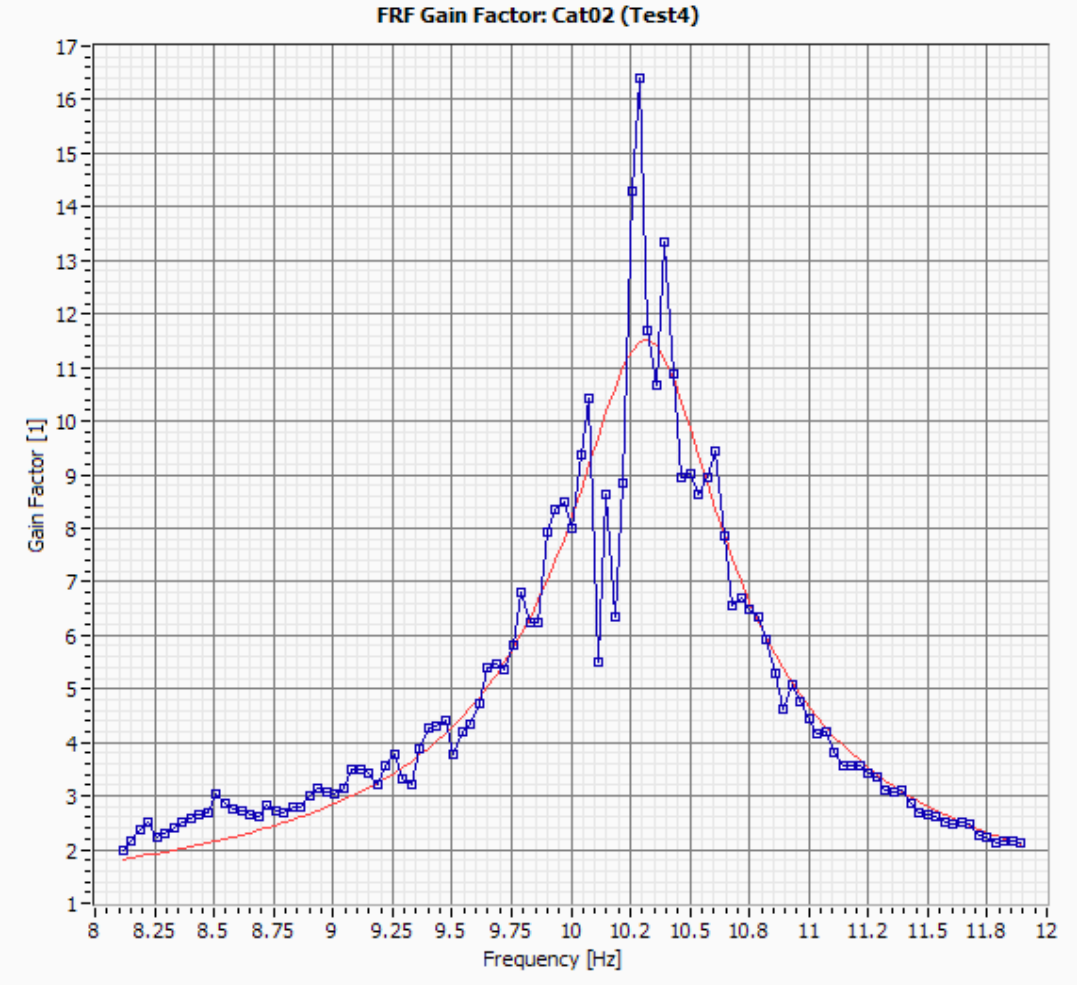

Figure III.25: FRF Gain Factor – Cat02 (Test4).

Table III.3: Experimental Damping for Cat02 (Test4).

Modal Parameter	0.70
Frequency [Hz]	10.33
Damping [%]	3.04

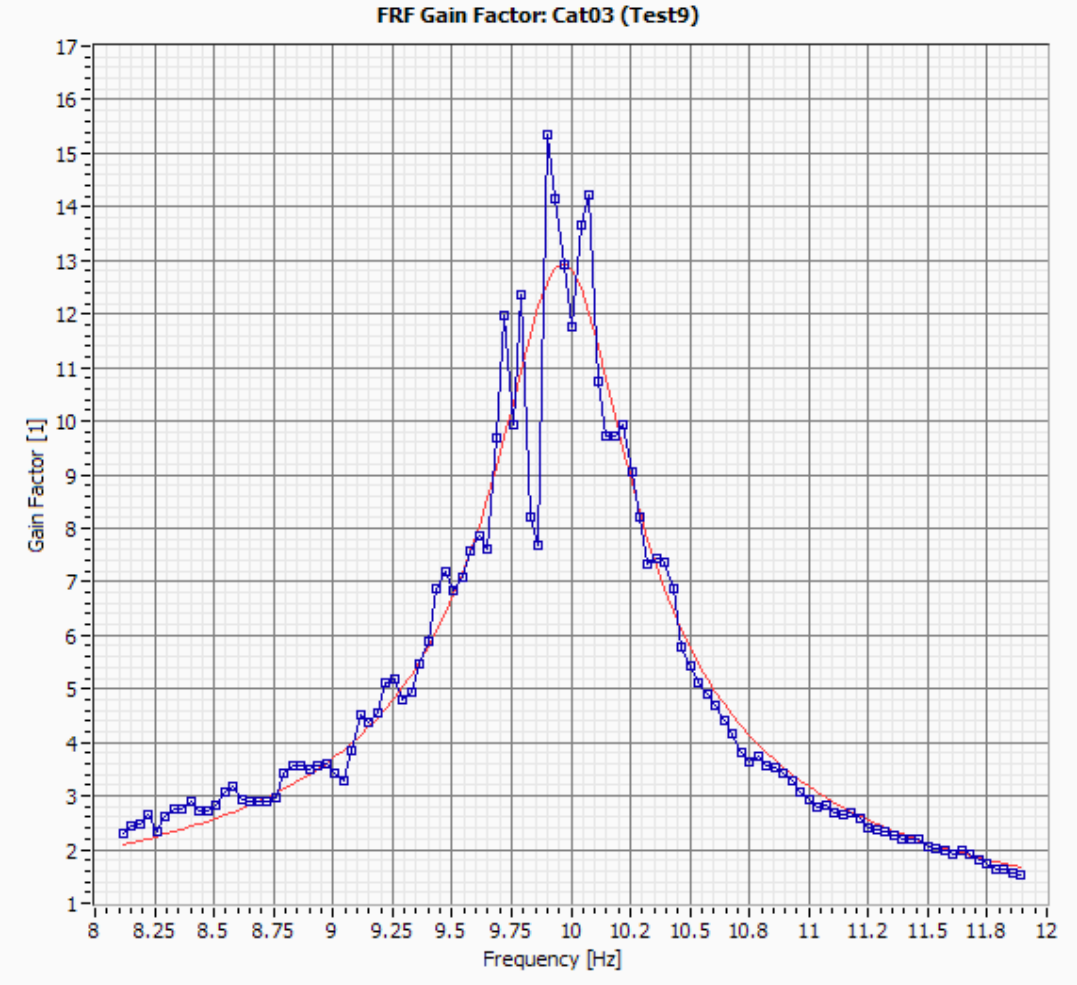

Figure III.26: FRF Gain Factor – Cat03 (Test9).

Table III.4: Experimental Damping for Cat03 (Test9).

Modal Parameter	0.71
Frequency [Hz]	9.97
Damping [%]	2.75

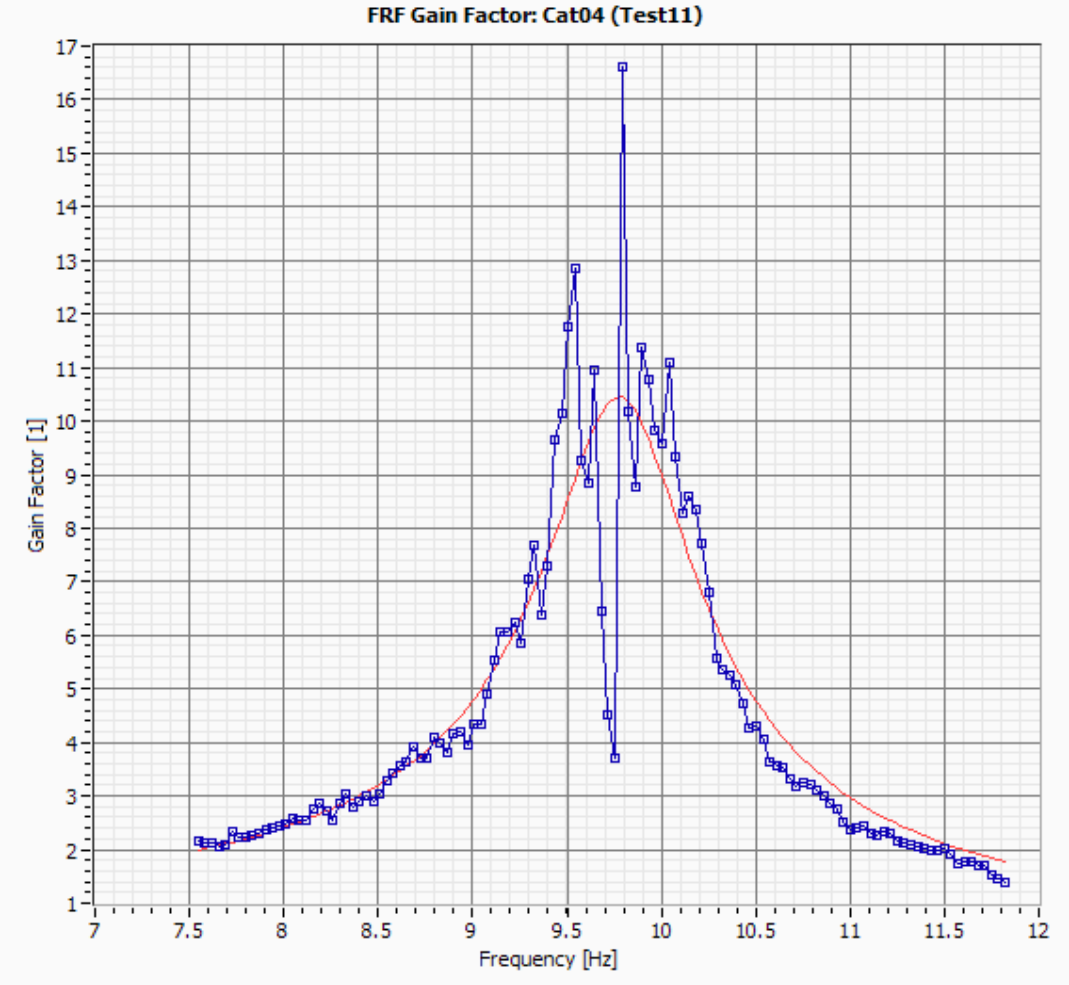

Figure III.27: FRF Gain Factor – Cat04 (Test11).

Table III.5: Experimental Damping for Cat04 (Test11).

Modal Parameter	1.01
Frequency [Hz]	9.82
Damping [%]	2.83

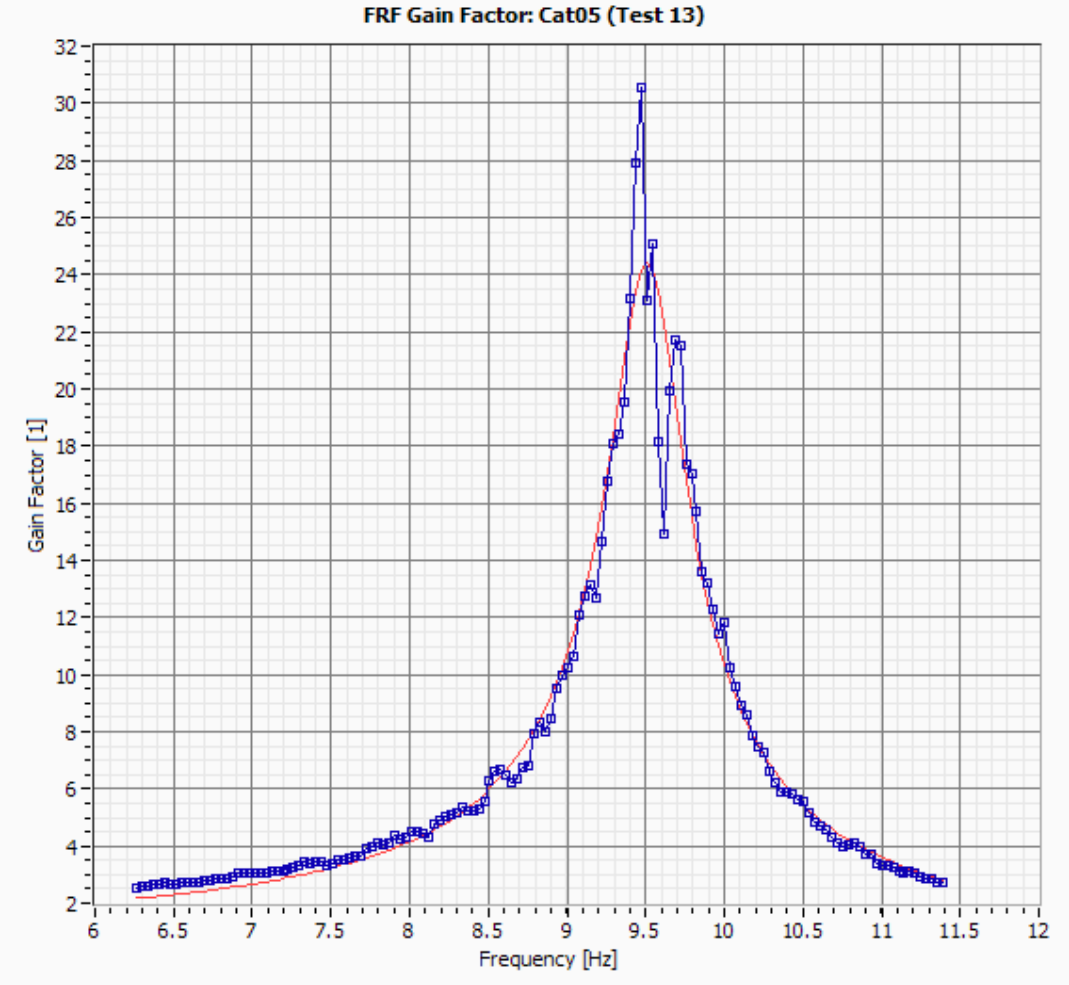

Figure III.28: FRF Gain Factor – Cat05 (Test13).

Table III.6: Experimental Damping for Cat05 (Test13).

Modal Parameter	1
Frequency [Hz]	9.51
Damping [%]	2.93

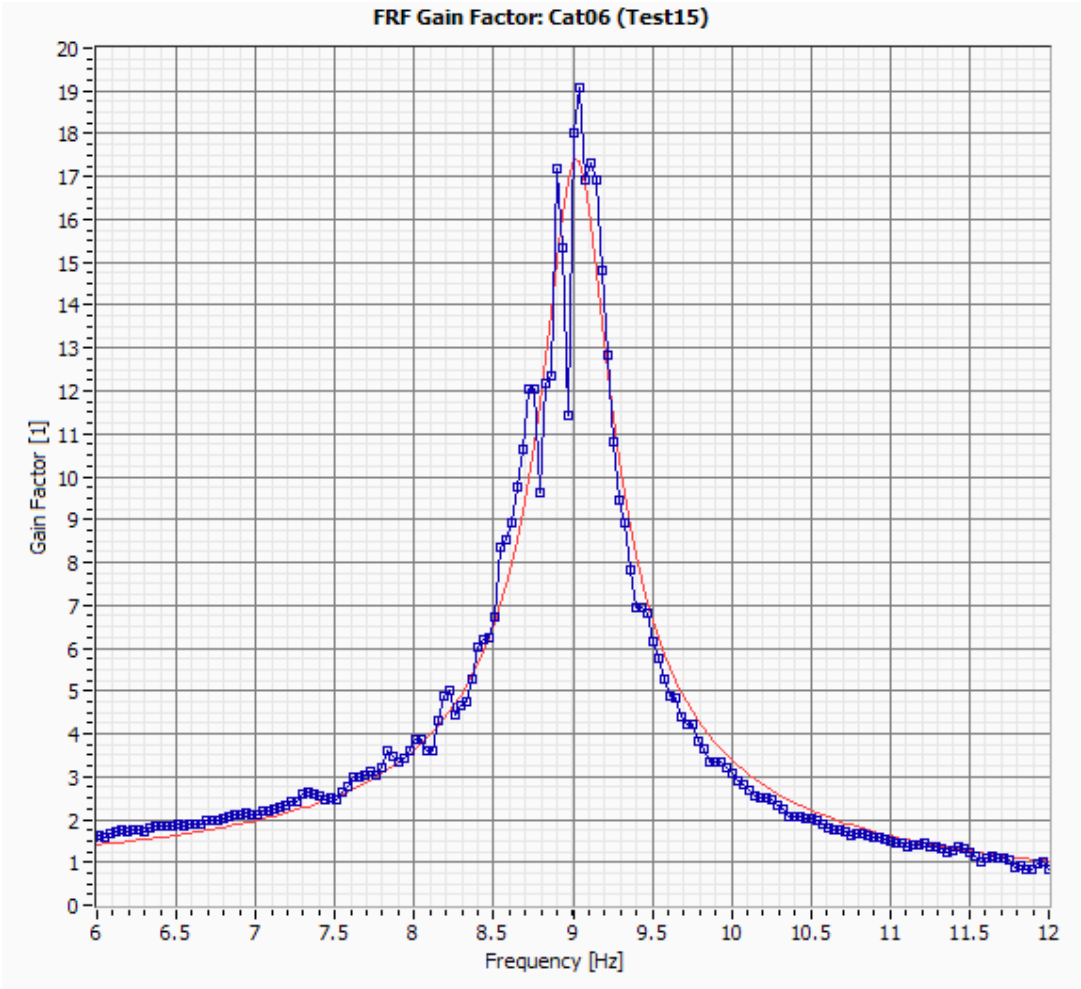

Figure III.29: FRF Gain Factor – Cat06 (Test15).

Table III.7: Experimental Damping for Cat06 (Test15).

Modal Parameter	1.04
Frequency [Hz]	8.99
Damping [%]	2.98

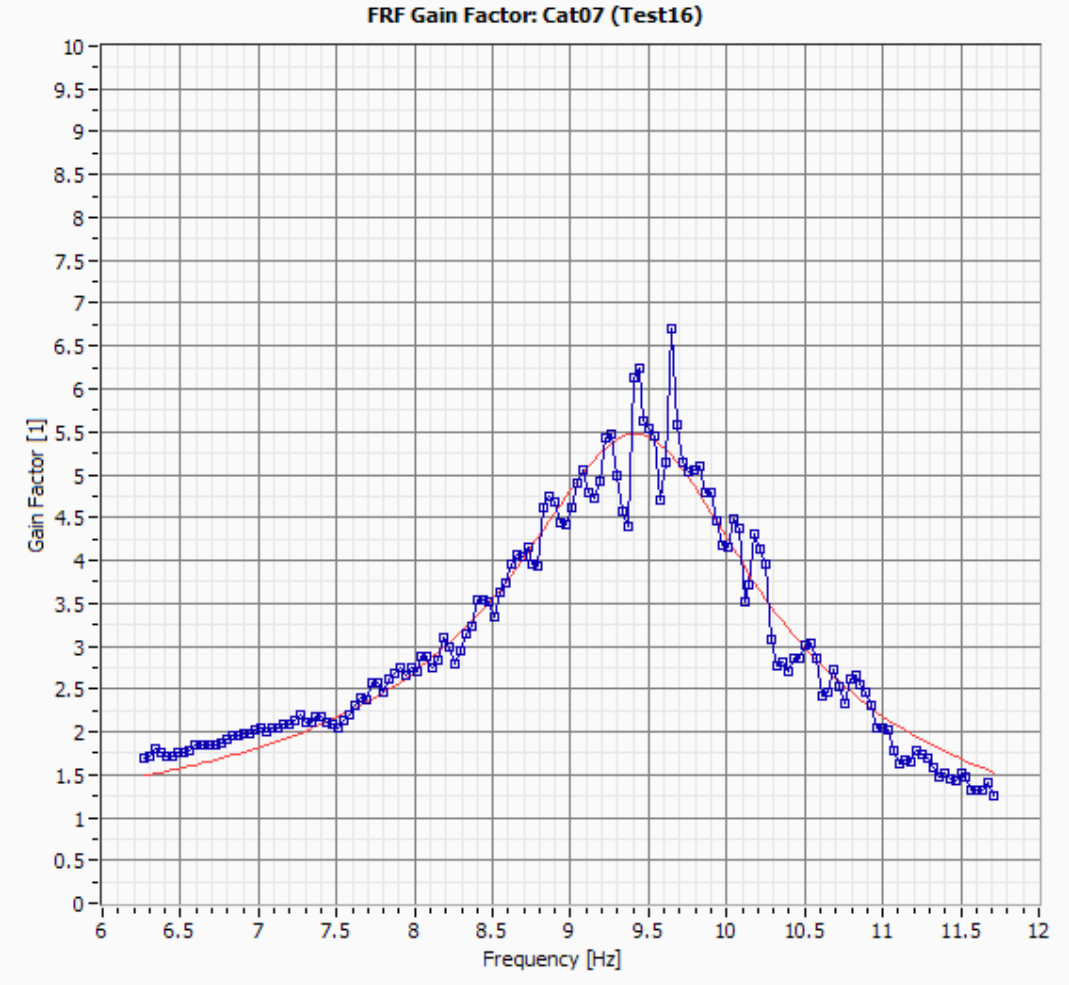

Figure III.30: FRF Gain Factor – Cat07 (Test16).

Table III.8: Experimental Damping for Cat07 (Test16).

Modal Parameter	0.85
Frequency [Hz]	9.47
Damping [%]	7.83

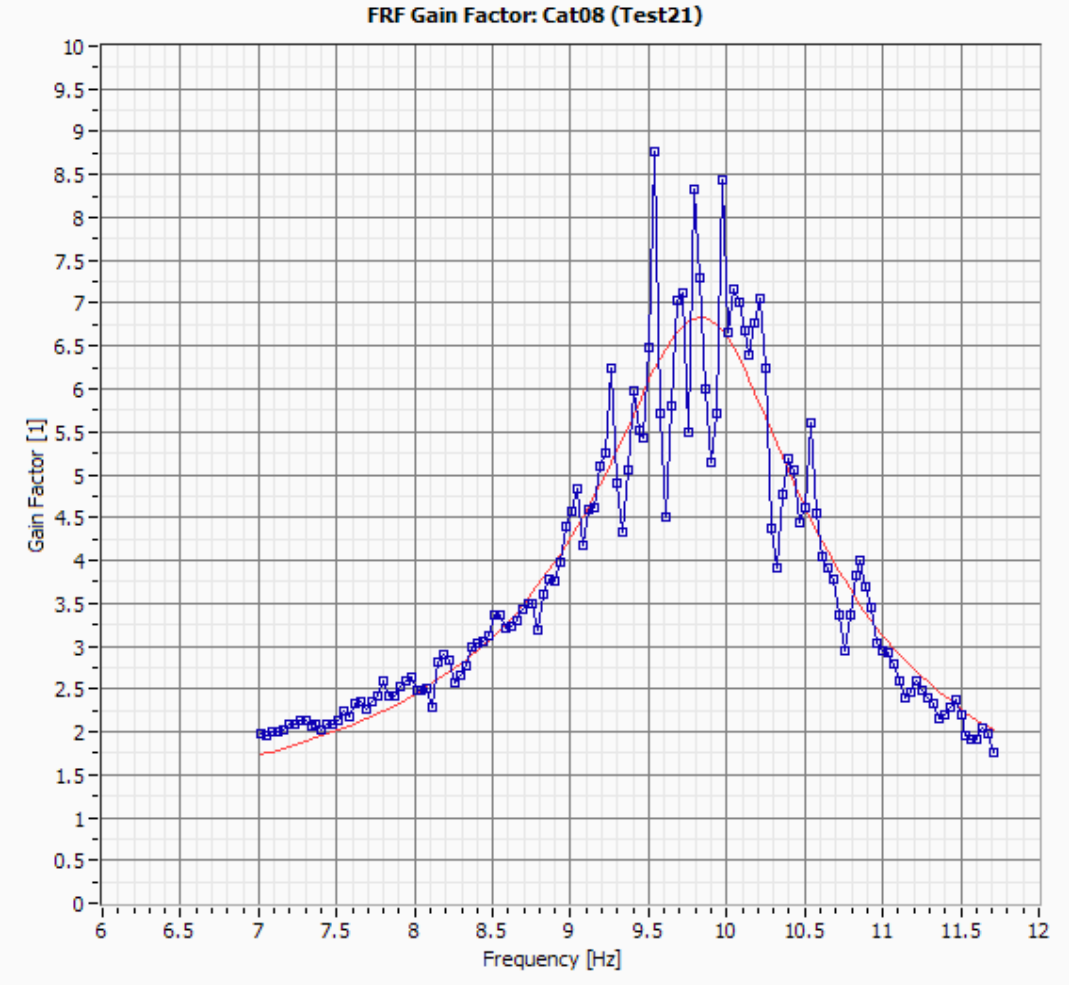

Figure III.31: FRF Gain Factor – Cat08 (Test21).

Table III.9: Experimental Damping for Cat08 (Test21).

Modal Parameter	1
Frequency [Hz]	9.87
Damping [%]	7.56

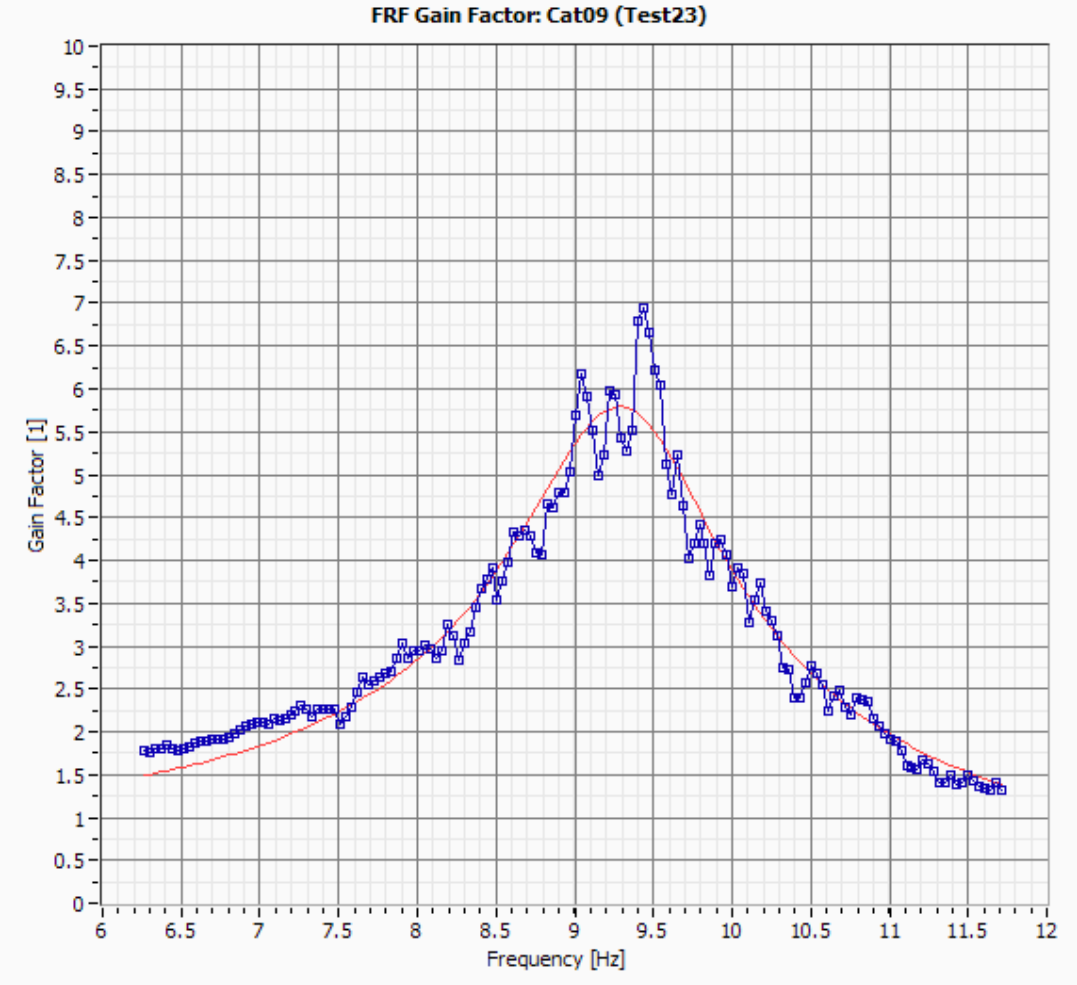

Figure III.32: FRF Gain Factor – Cat09 (Test23).

Table III.10: Experimental Damping for Cat09 (Test23).

Modal Parameter	0.83
Frequency [Hz]	9.33
Damping [%]	7.21

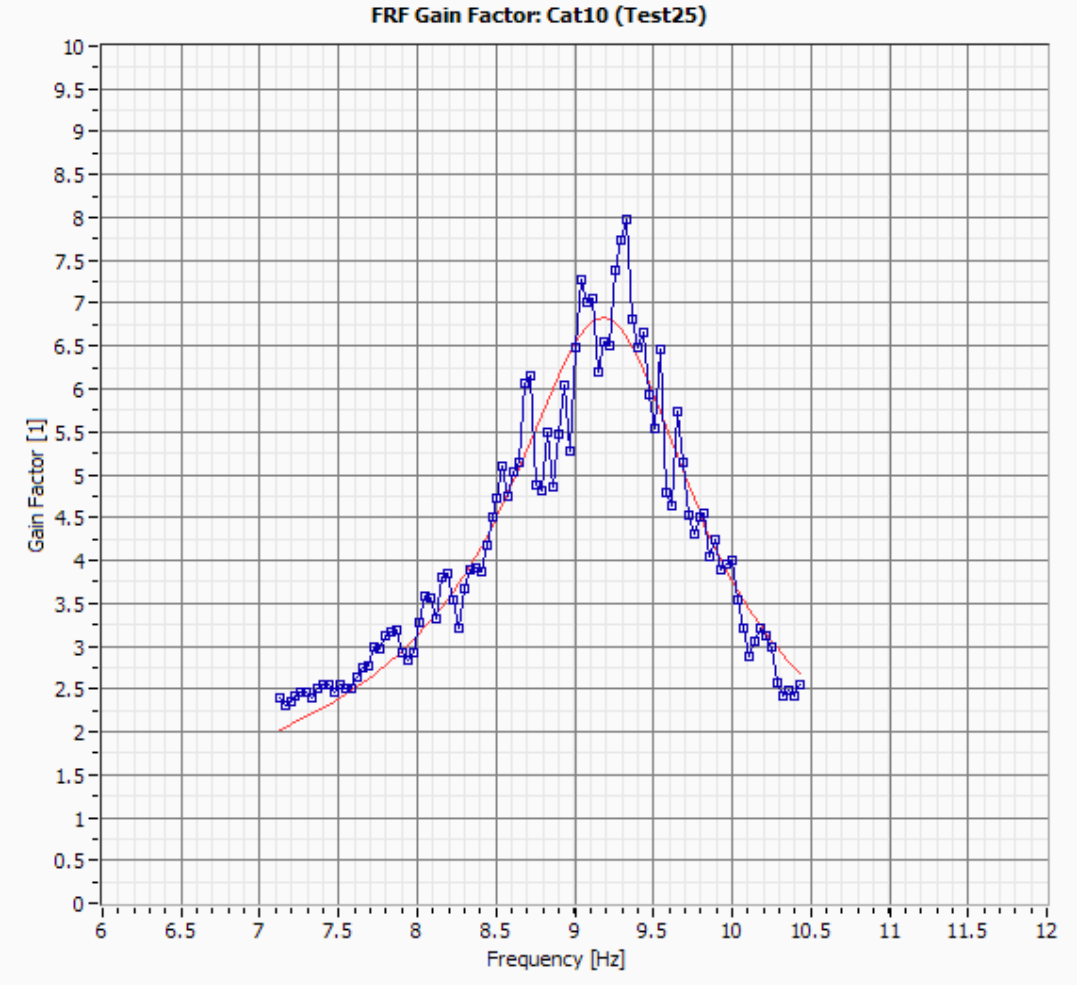

Figure III.33: FRF Gain Factor – Cat010 (Test25).

Table III.11: Experimental Damping for Cat10 (Test25).

Modal Parameter	1.01
Frequency [Hz]	9.21
Damping [%]	7.63

ANNEX IV

Shaking table tests: Graphical presentation of the acquired data

INDEX OF FIGURES

Day 1 – Bare Frame

Test 1 – Cat00 (EW PGA=0.05g)

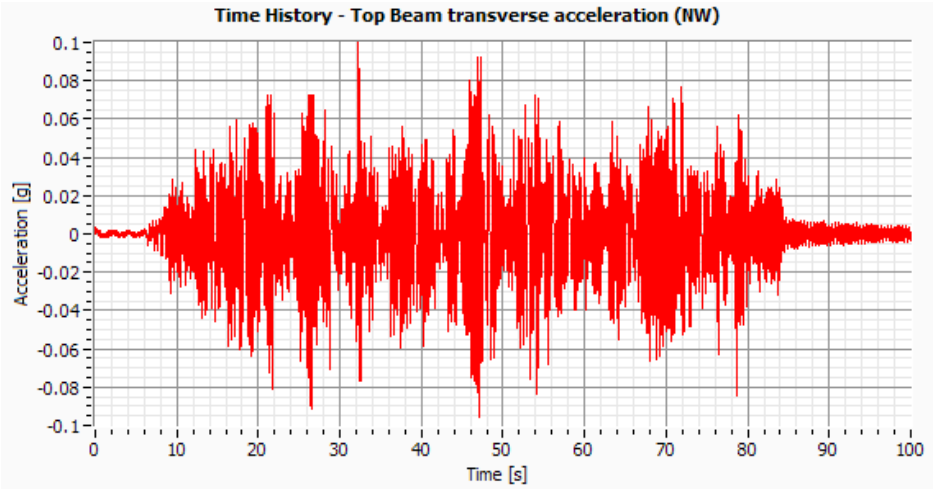

Figure IV.1: NW Top beam transverse acceleration (Channel 1).

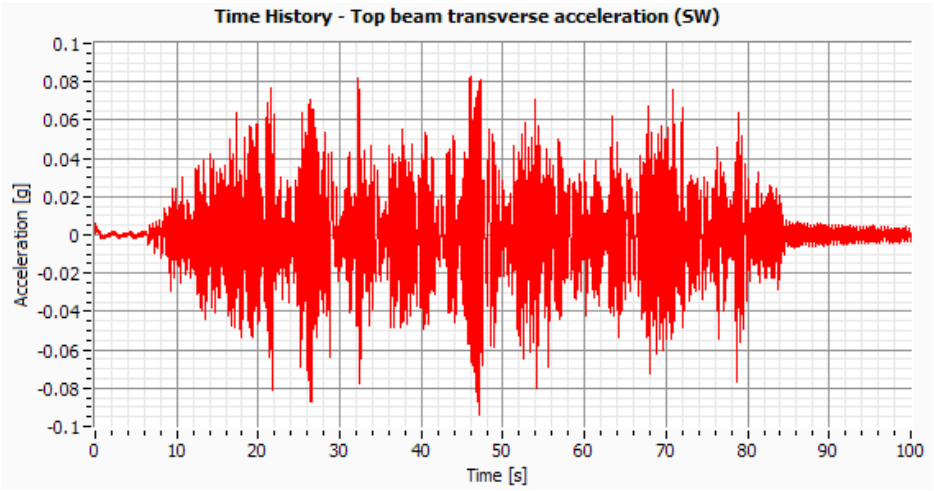

Figure IV.2: SW Top beam transverse acceleration (Channel 2).

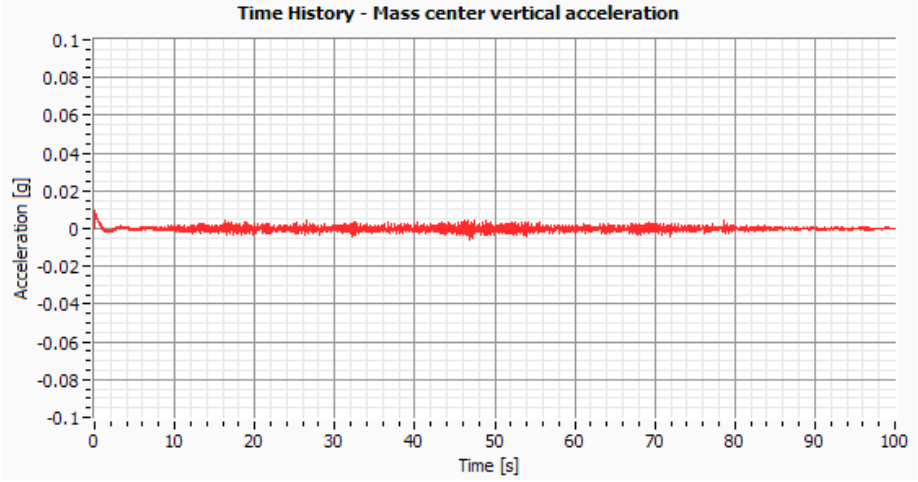

Figure IV.3: Mass center vertical acceleration (Channel 3).

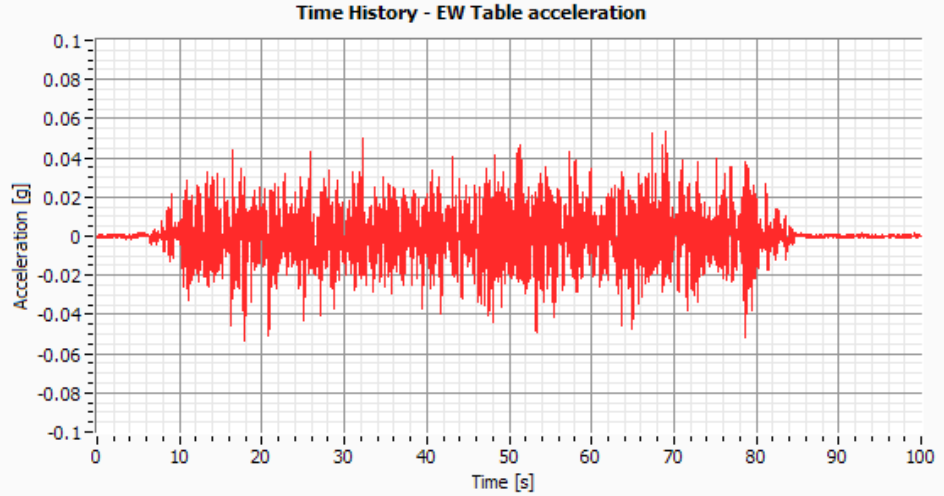

Figure IV.4: EW Table acceleration (Channel 24).

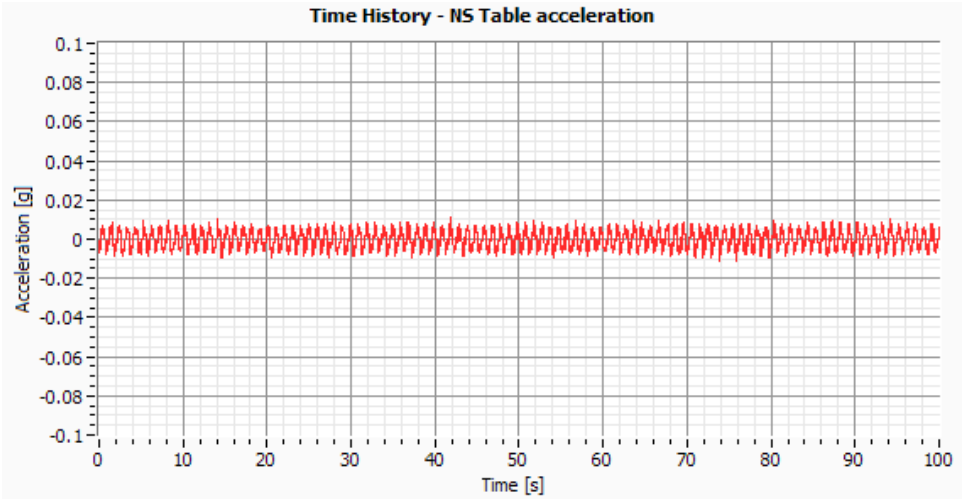

Figure IV.5: NS Table acceleration (Channel 25).

Test 2 – ElCentro (EW PGA=0.20g)

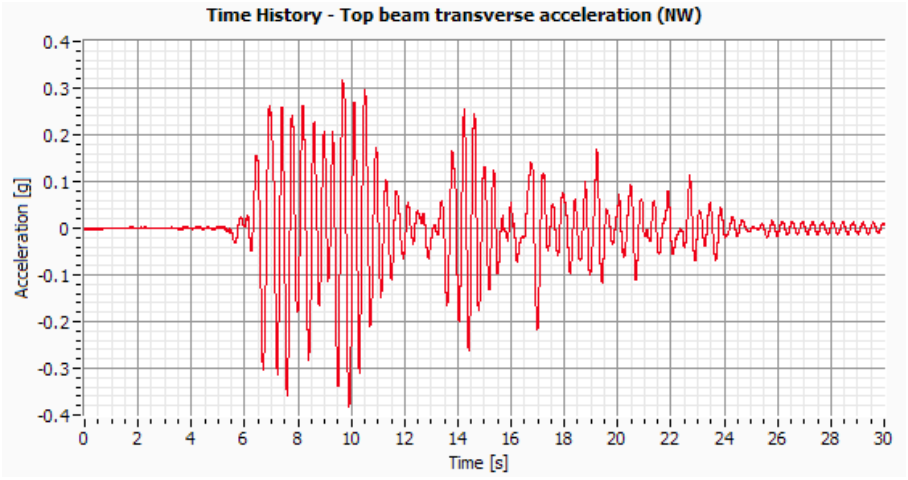

Figure IV.6: NW Top beam acceleration (Channel 1).

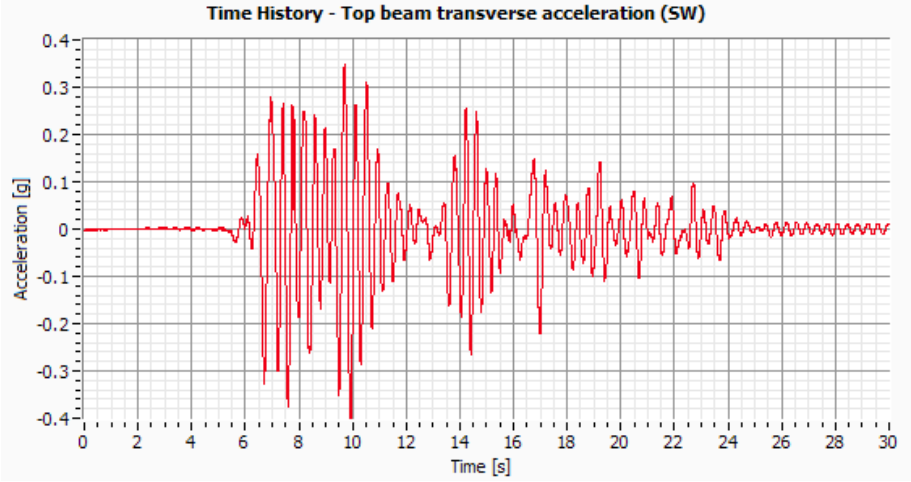

Figure IV.7: SW Top beam acceleration (Channel2).

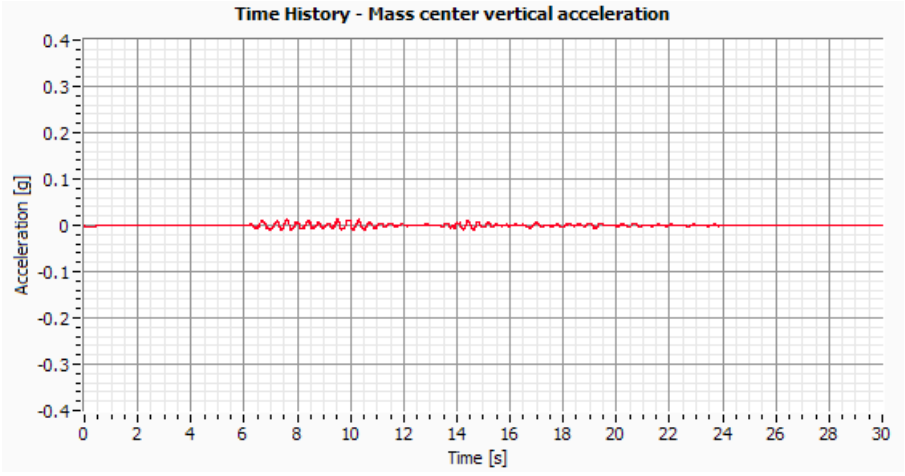

Figure IV.8: Mass center vertical acceleration (Channel 3).

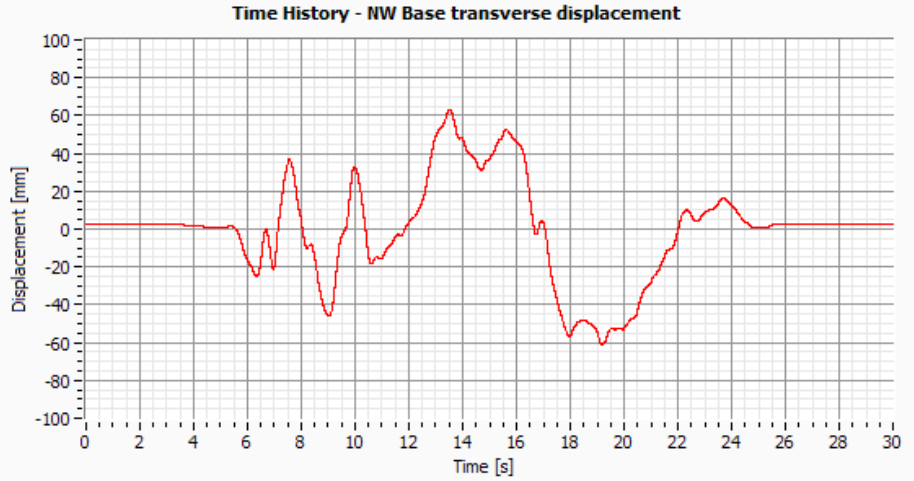

Figure IV.9: NW Base transverse displacement (Channel4).

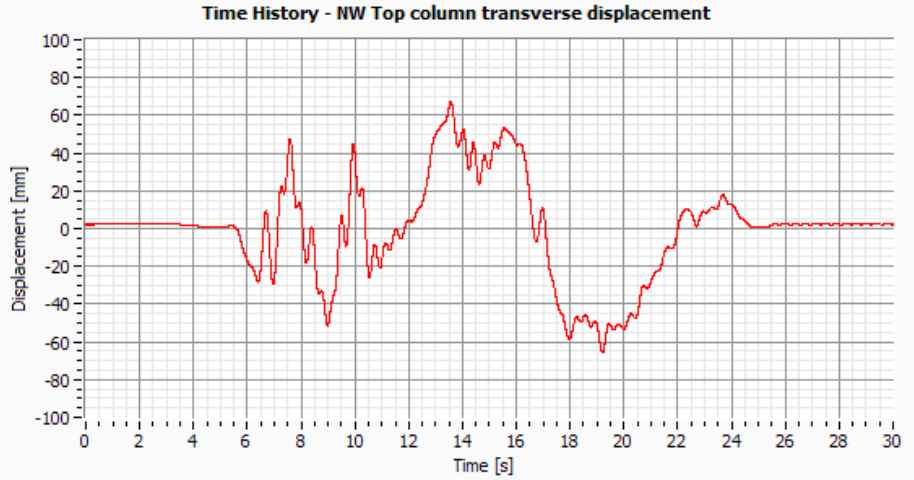

Figure IV.10: NW Top column transverse displacement (Channel5).

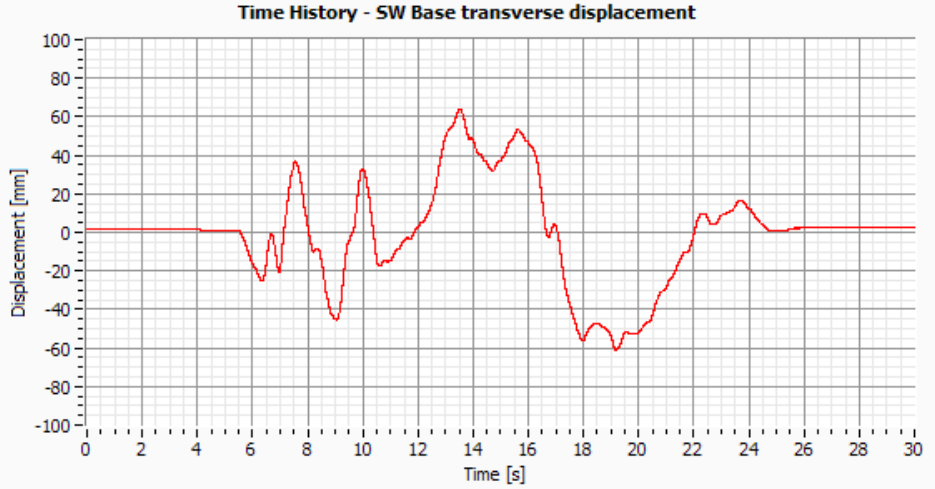

Figure IV.11: SW Base transverse displacement (Channel6).

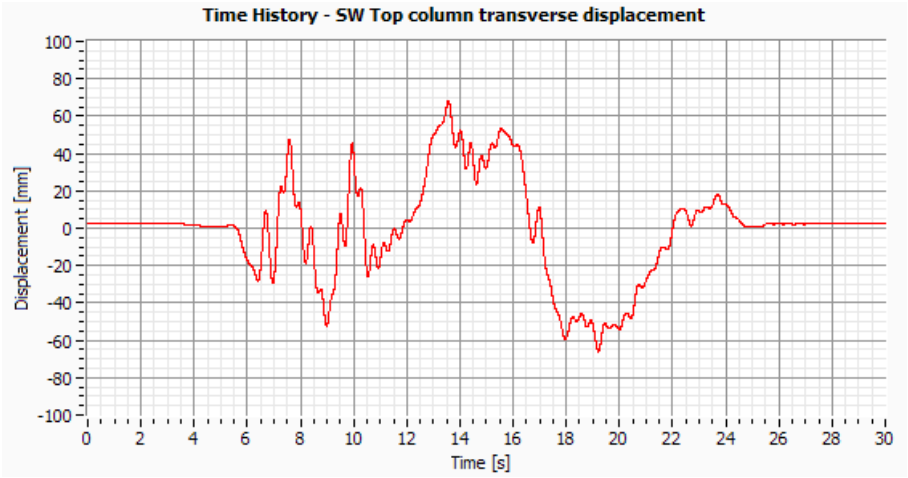

Figure IV.12: SW Top column transverse displacement (Channel7).

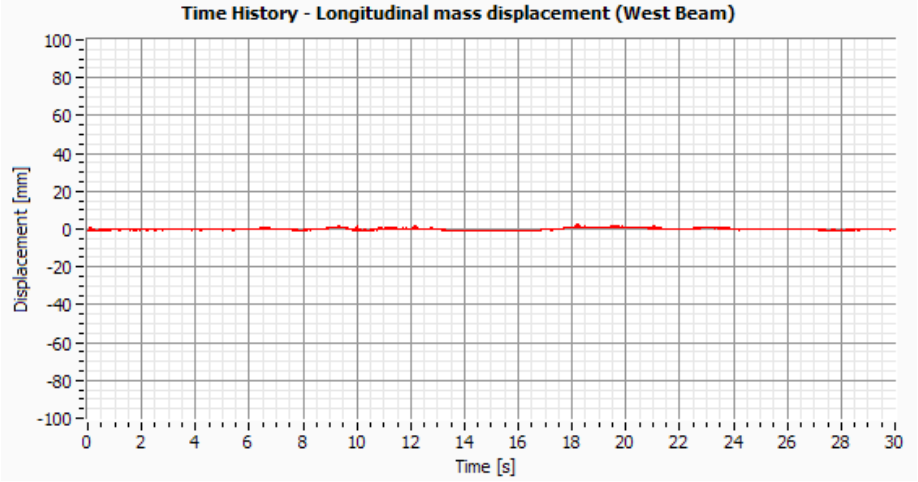

Figure IV.13: Longitudinal mass displacement in the West beam (Channel 8).

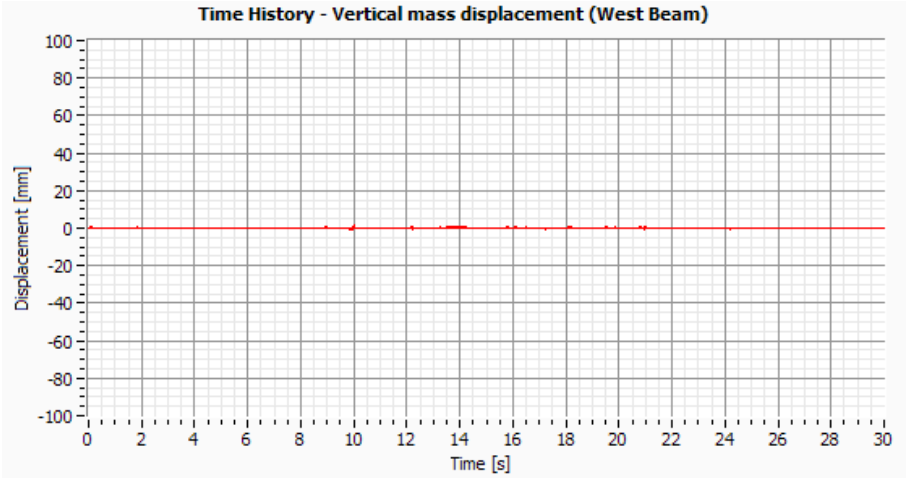

Figure IV.14: Vertical mass displacement in the West beam (Channel9).

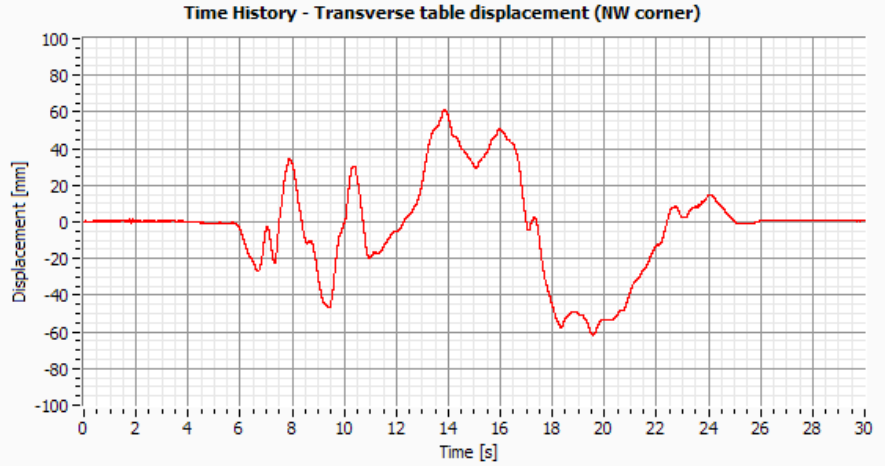

Figure IV.15: Transverse table displacement in the NW corner (Channel18).

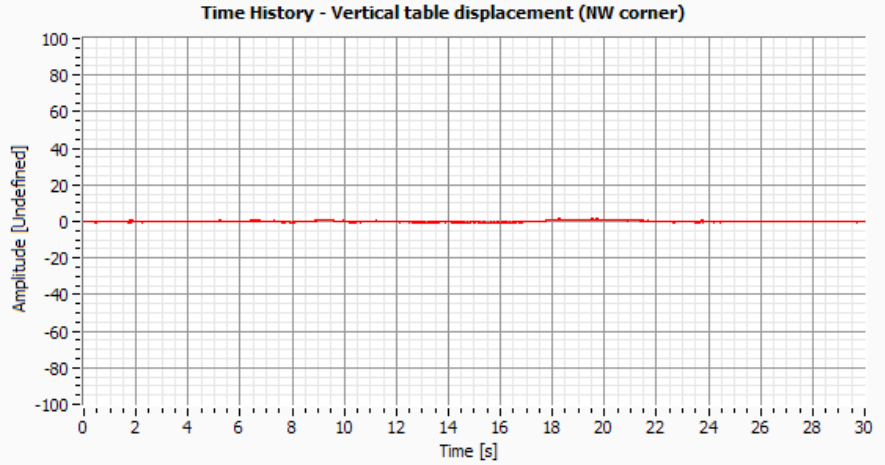

Figure IV.16: Vertical table displacement in the NW corner (Channel19).

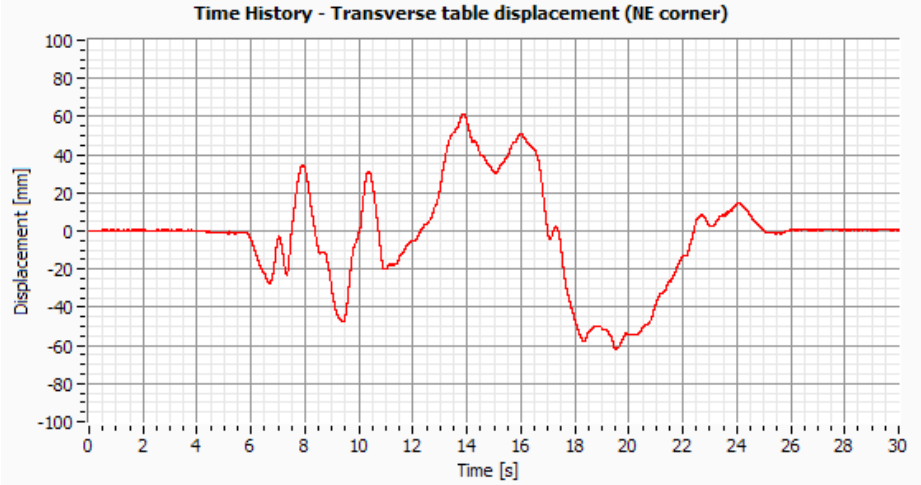

Figure IV.17: Transverse table displacement in the NE corner (Channel 20).

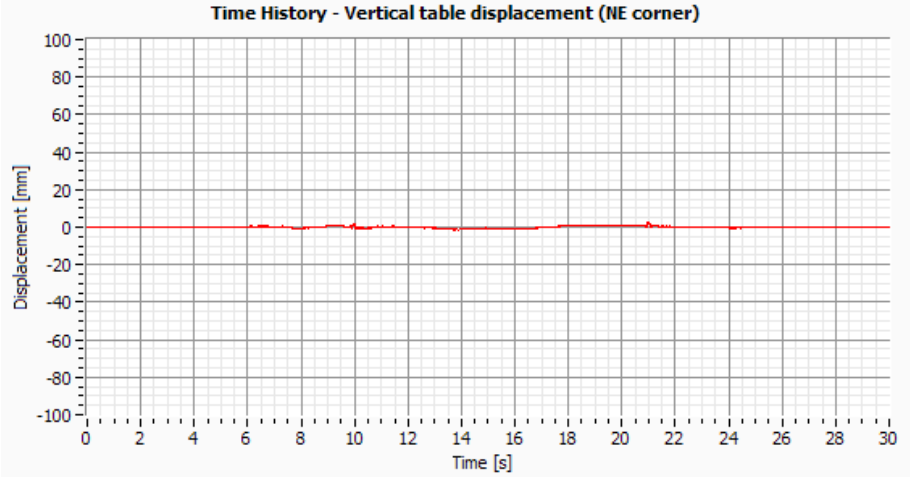

Figure IV.18: Vertical table displacement in the NE corner (Channel 21).

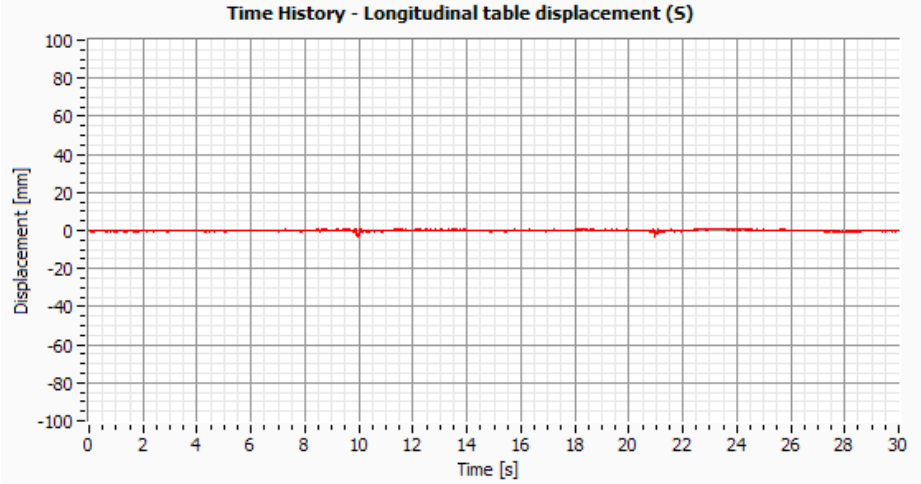

Figure IV.19: Longitudinal table displacement –S (Channel 22).

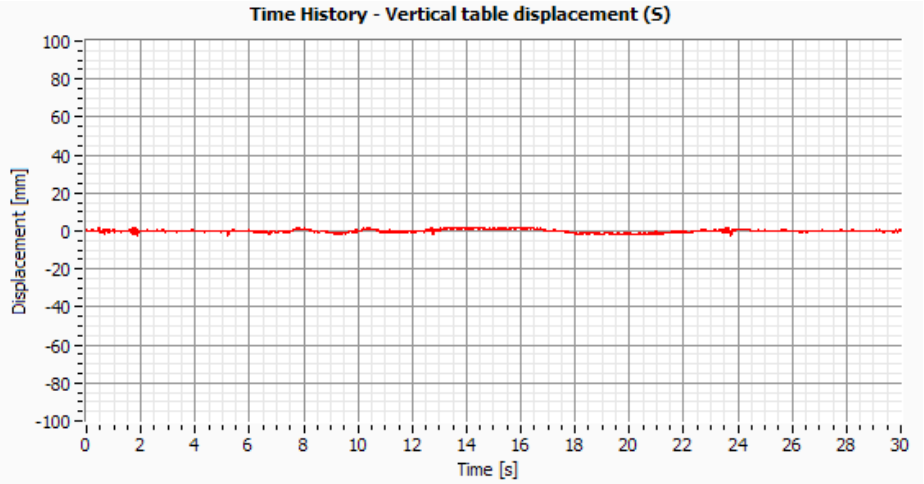

Figure IV.20: Vertical table displacement –S (Channel 23).

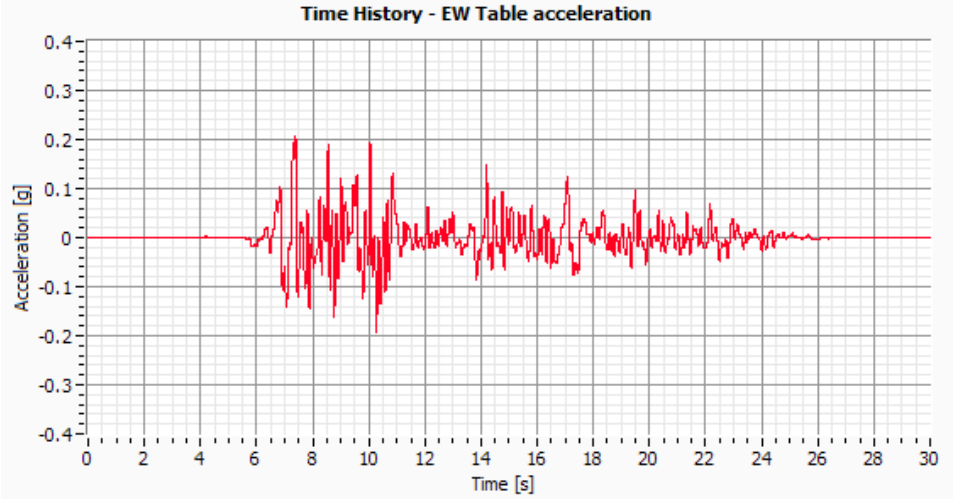

Figure IV.21: EW Table acceleration (Channel 24).

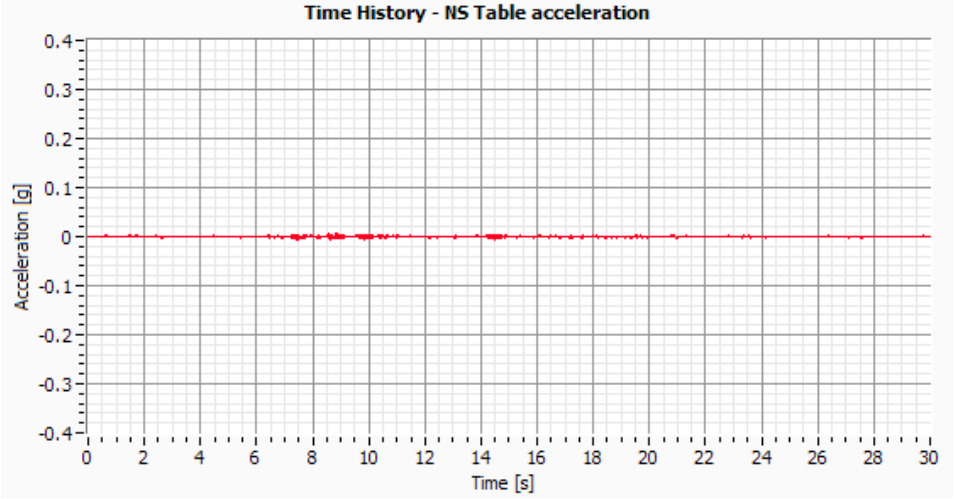

Figure IV.22: NS Table acceleration (Channel 25).

Test 3 – Cat01 (EW PGA=0.05g)

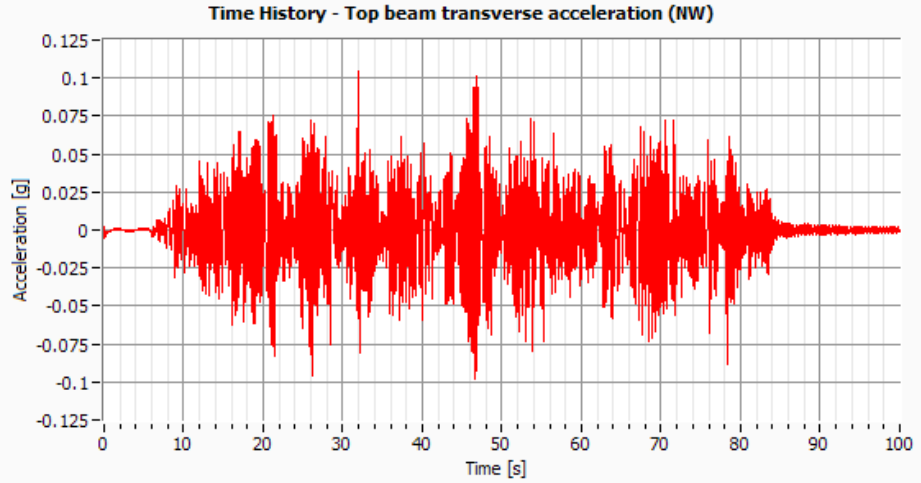

Figure IV.23: NW Top beam transverse acceleration (Channel 1).

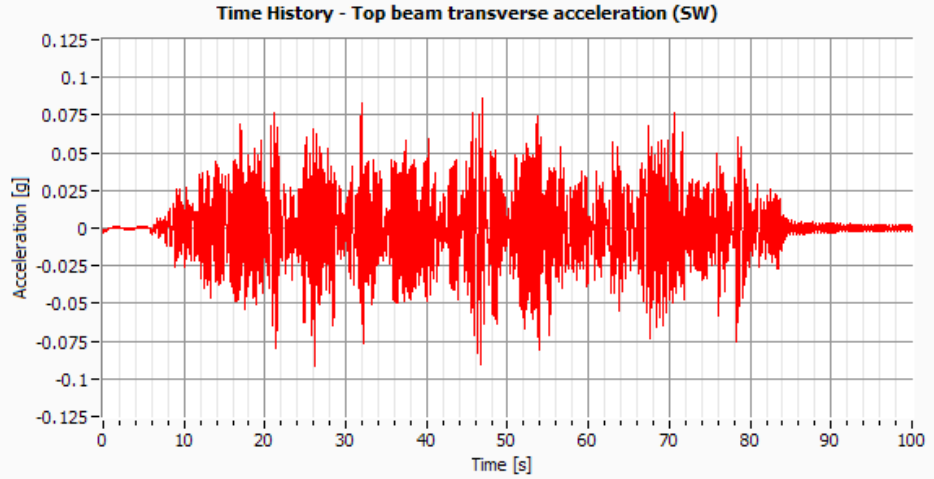

Figure IV.24: SW Top beam transverse acceleration (Channel 2).

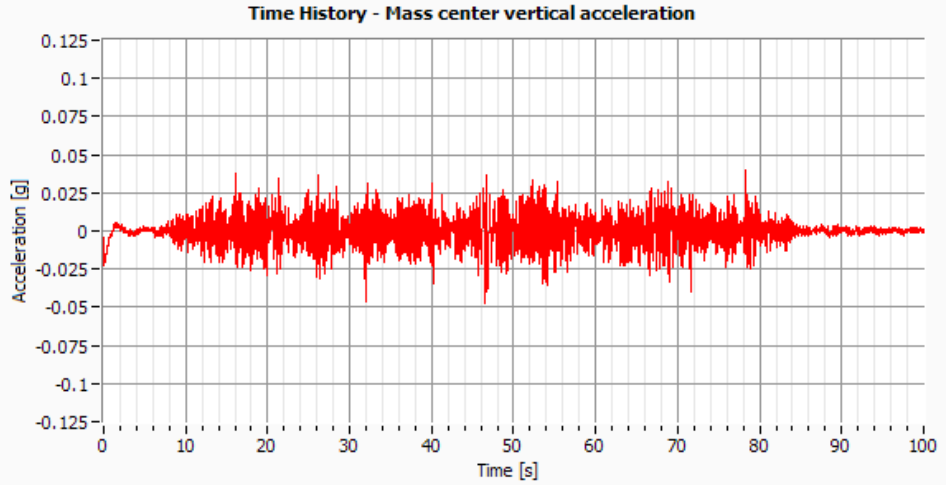

Figure IV.25: Mass center vertical acceleration (Channel 3).

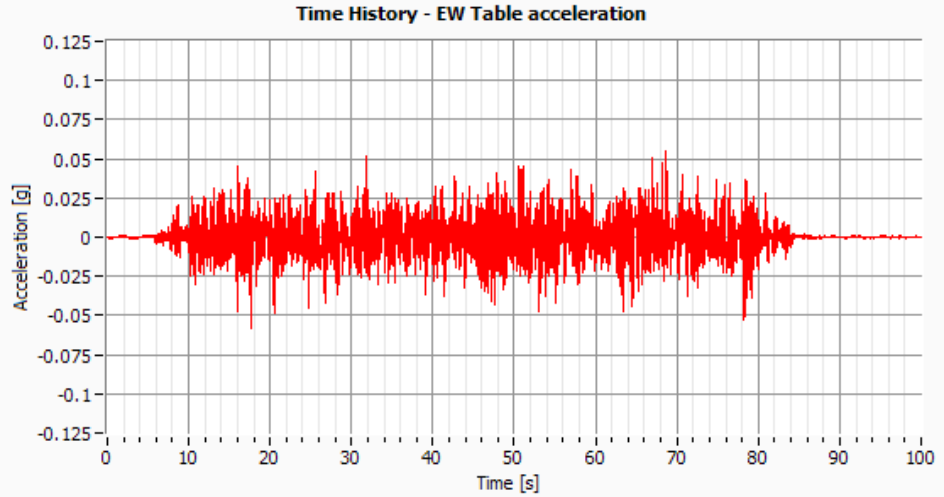

Figure IV.26: EW Table acceleration (Channel 24).

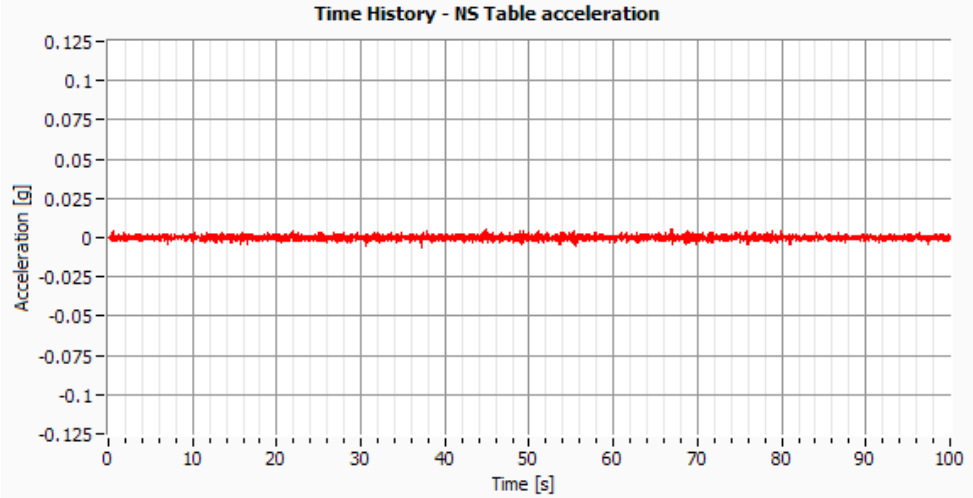

Figure IV.27: NS table acceleration (Channel 25).

Day 2 – Dorka Device

Test 4 – Cat02 (EW PGA=0.05g)

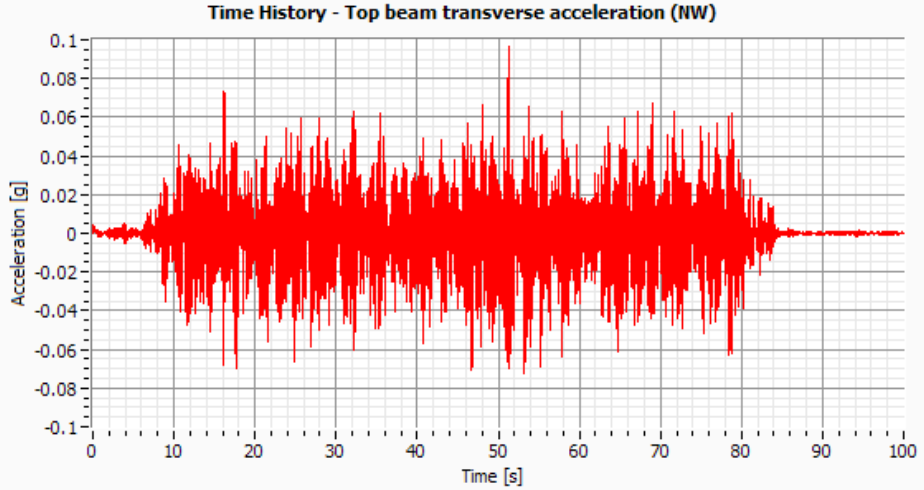

Figure IV.28: NW Top beam transverse acceleration (Channel 1).

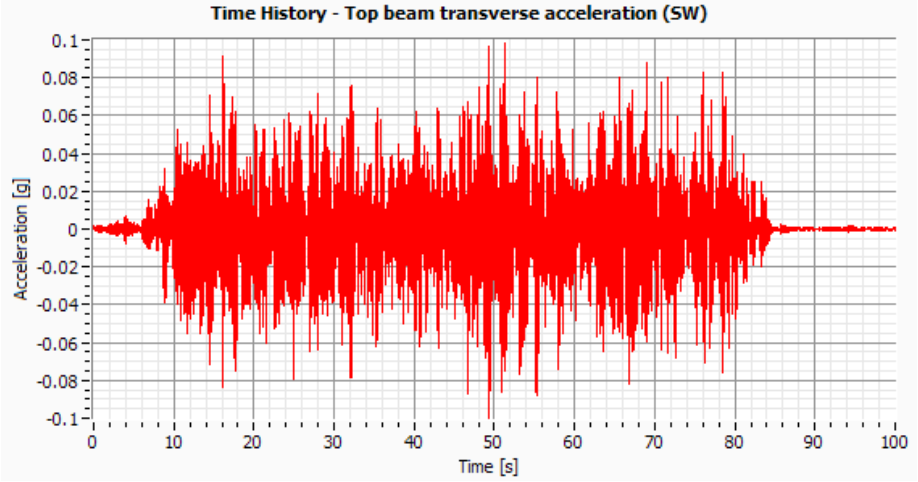

Figure IV.29: SW Top beam transverse acceleration (Channel 2).

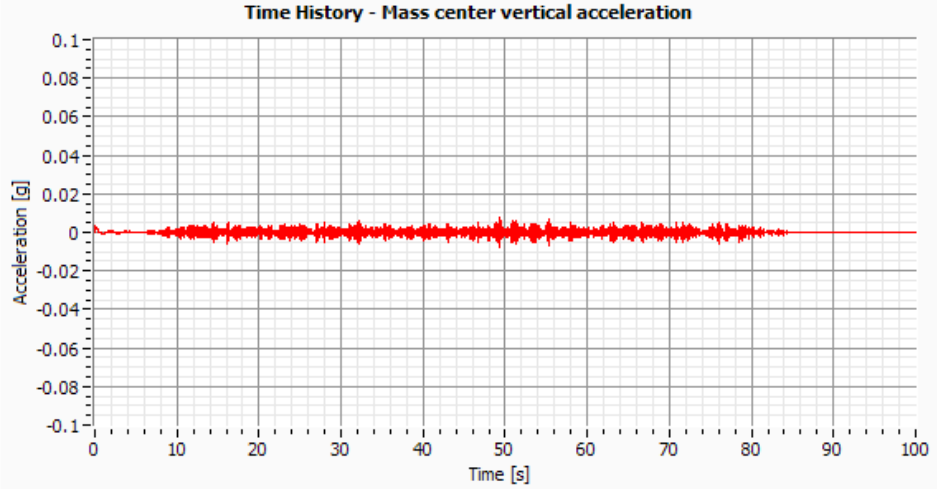

Figure IV.30: Mass center vertical acceleration (Channel 3).

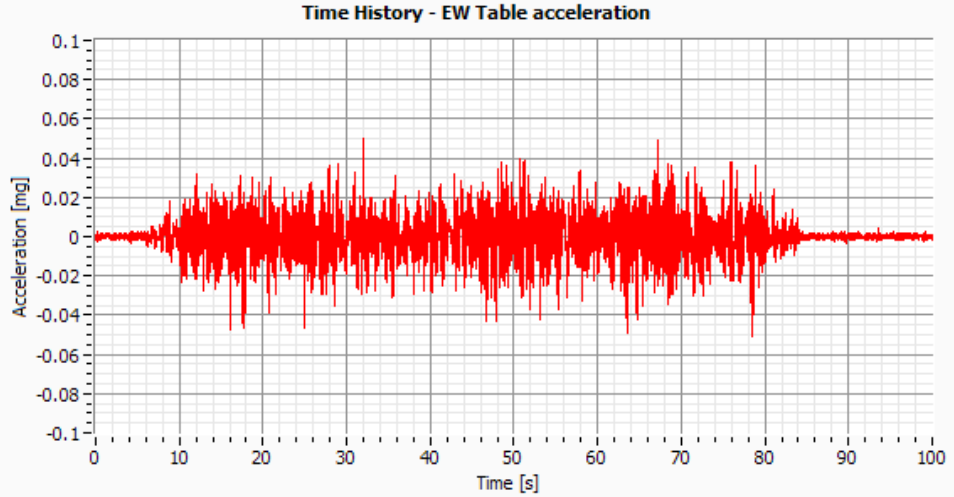

Figure IV.31: EW Table acceleration (Channel 24).

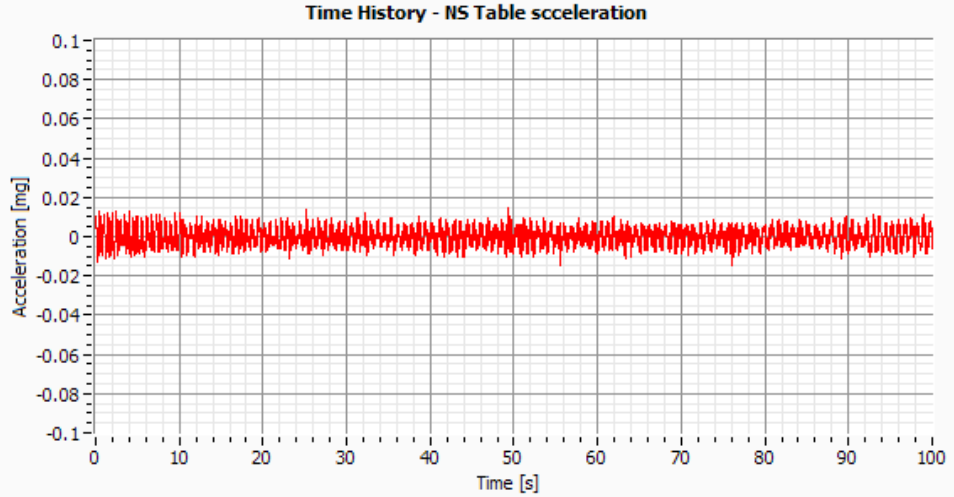

Figure IV.32: NS Table acceleration (Channel 25).

Test 5 – ElCentro (EW PGA=0.20g)

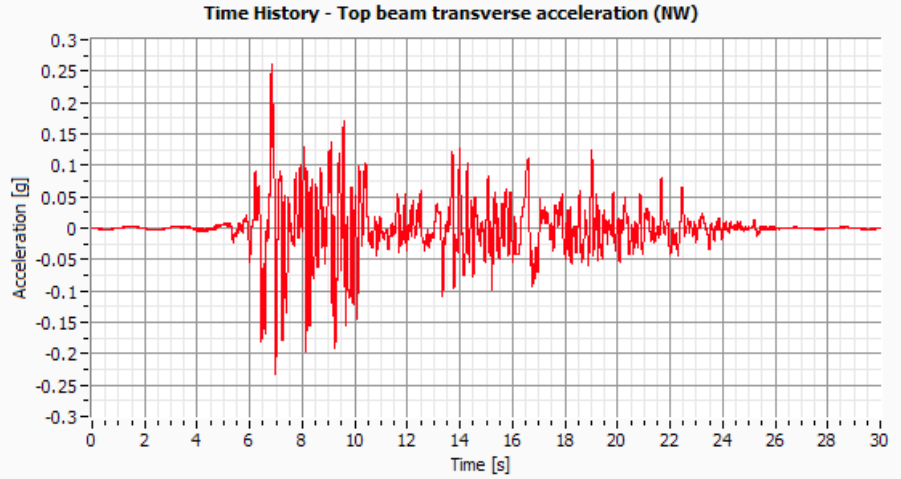

Figure IV.33: NW Top beam acceleration (Channel 1).

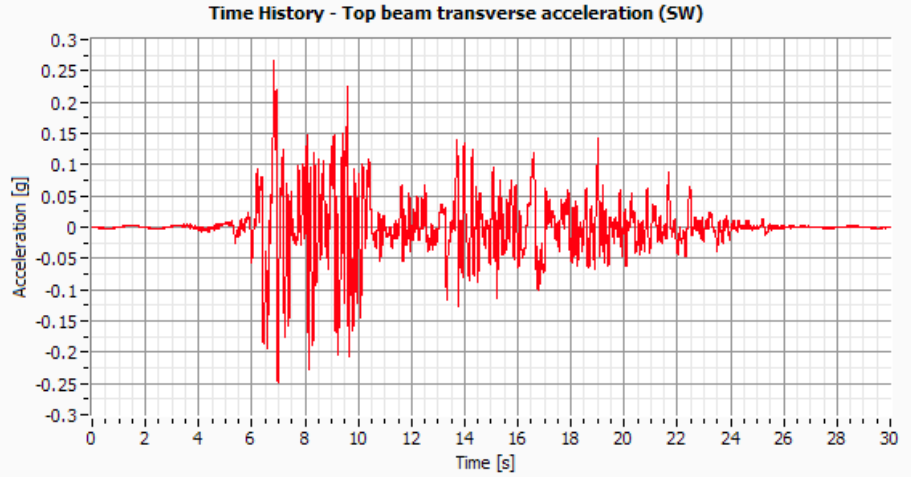

Figure IV.34: SW Top beam acceleration (Channel2).

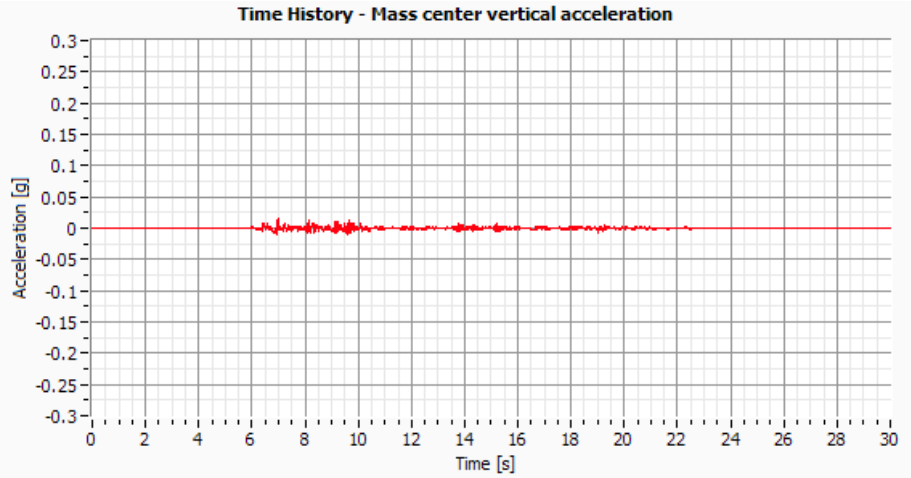

Figure IV.35: Mass center vertical acceleration (Channel 3).

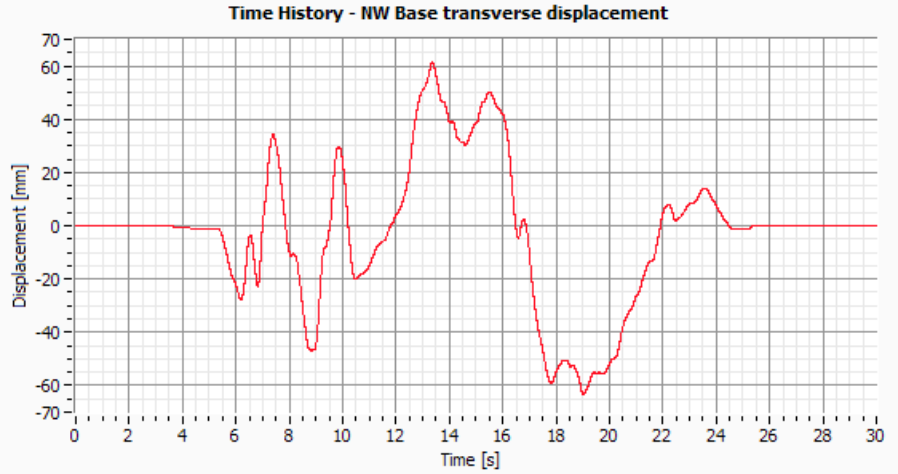

Figure IV.36: NW Base transverse displacement (Channel4).

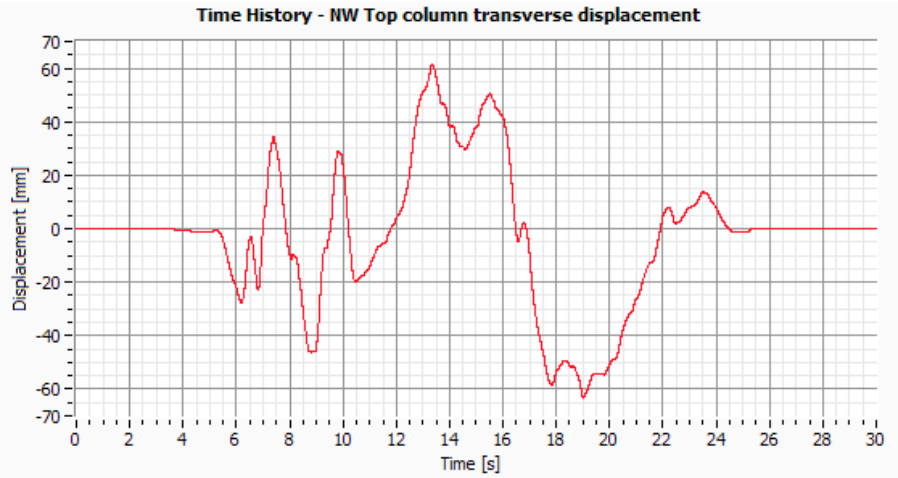

Figure IV.37: NW Top column transverse displacement (Channel5).

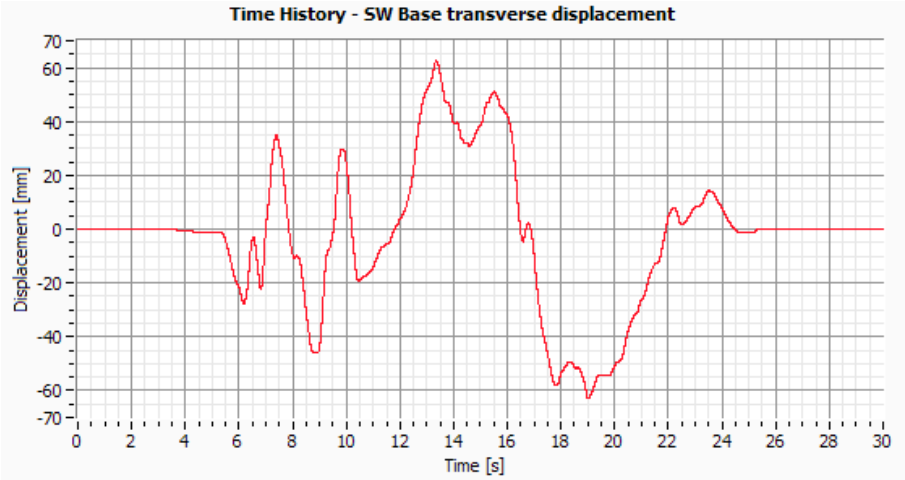

Figure IV.38: SW Base transverse displacement (Channel6).

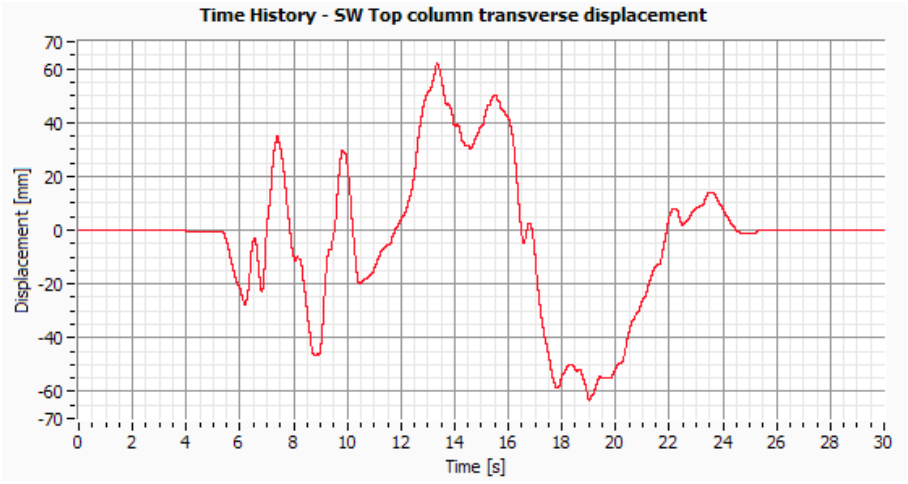

Figure IV.39: SW Top column transverse displacement (Channel7).

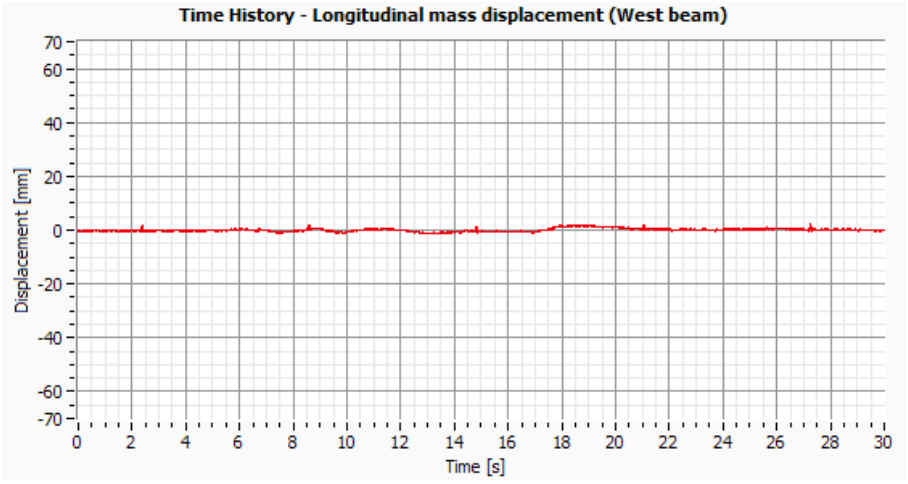

Figure IV.40: Longitudinal mass displacement in the West beam (Channel 8).

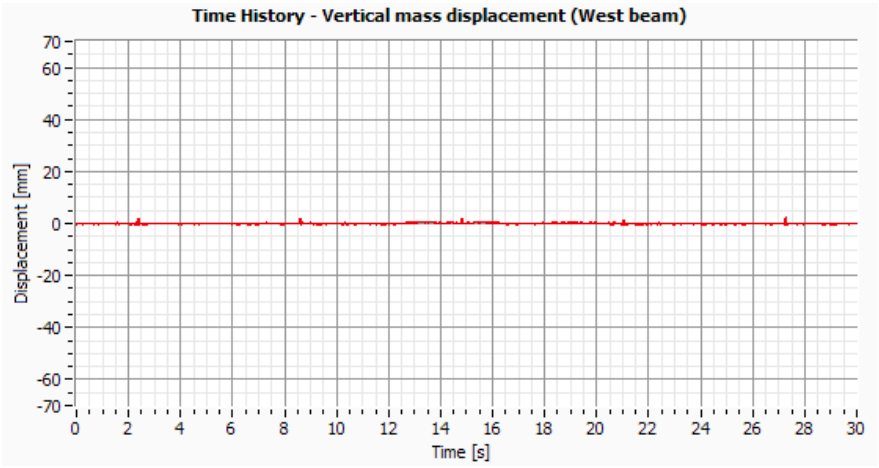

Figure IV.41: Vertical mass displacement in the West beam (Channel9).

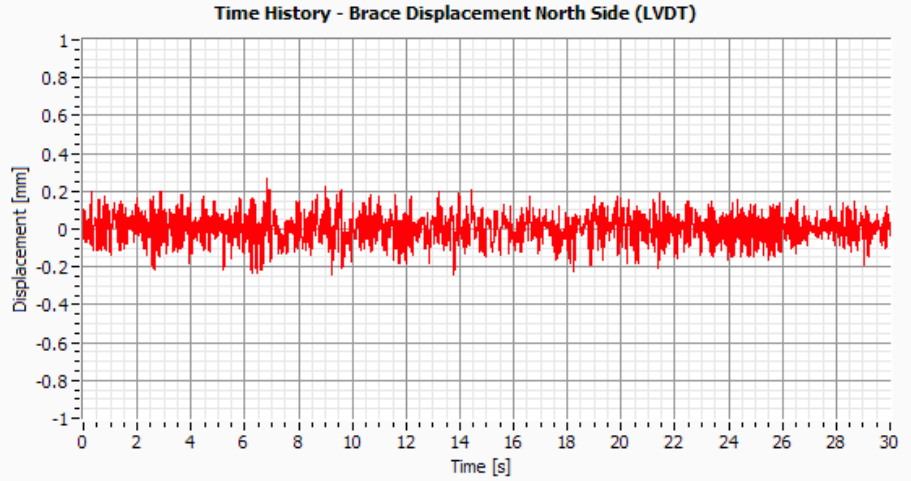

Figure IV.42: Brace displacement North side (Channel10).

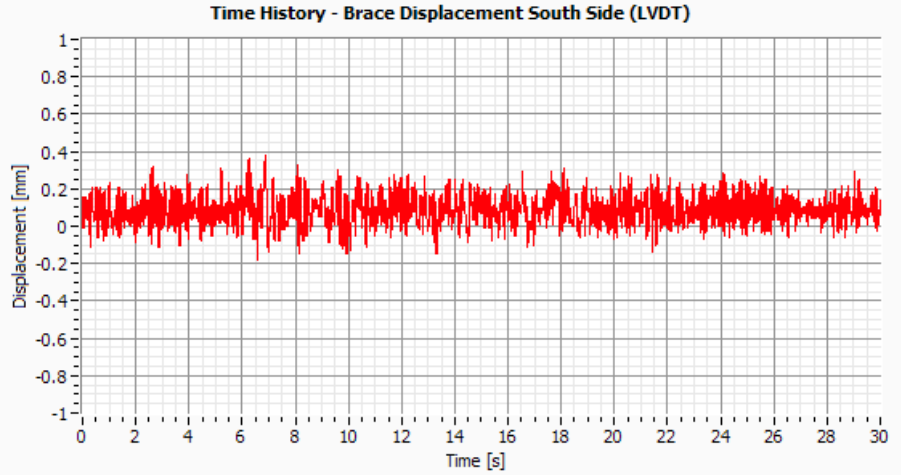

Figure IV.43: Brace displacement South side (Channel11).

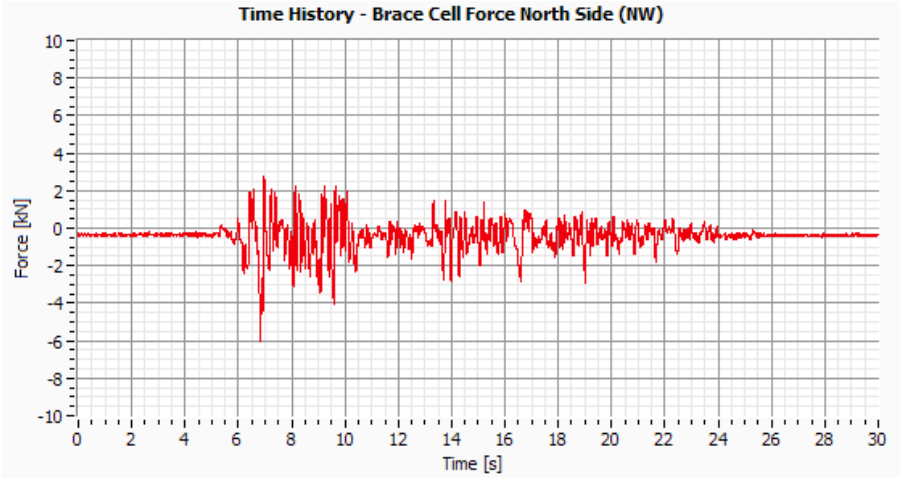

Figure IV.44: Brace cell force North Side – NW (Channel14).

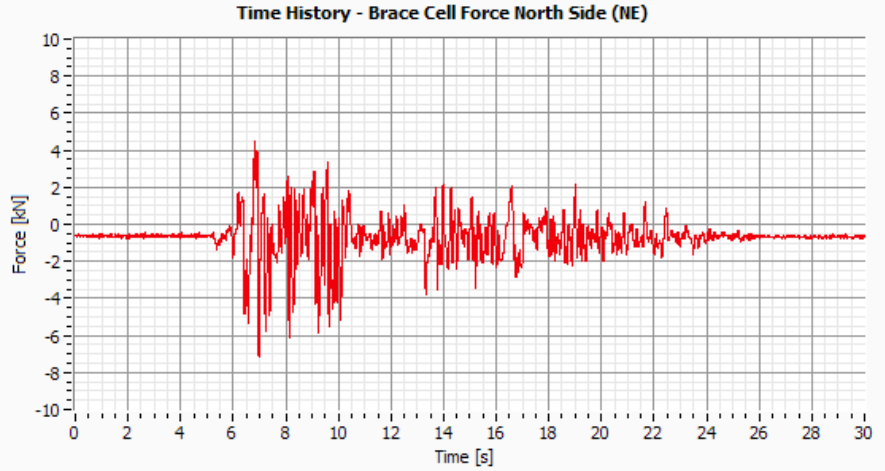

Figure IV.45: Brace cell force North Side – NE (Channel15).

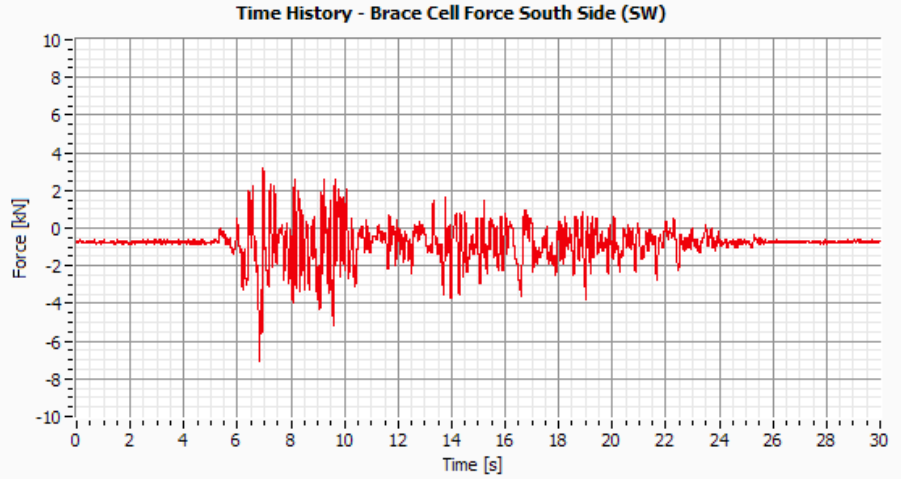

Figure IV.46: Brace cell force South Side – SW (Channel16).

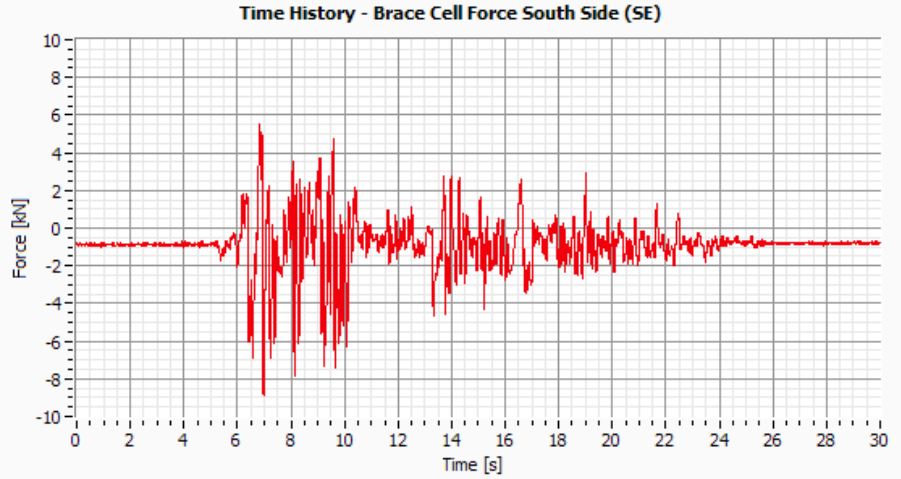

Figure IV.47: Brace cell force South Side – NE (Channel17).

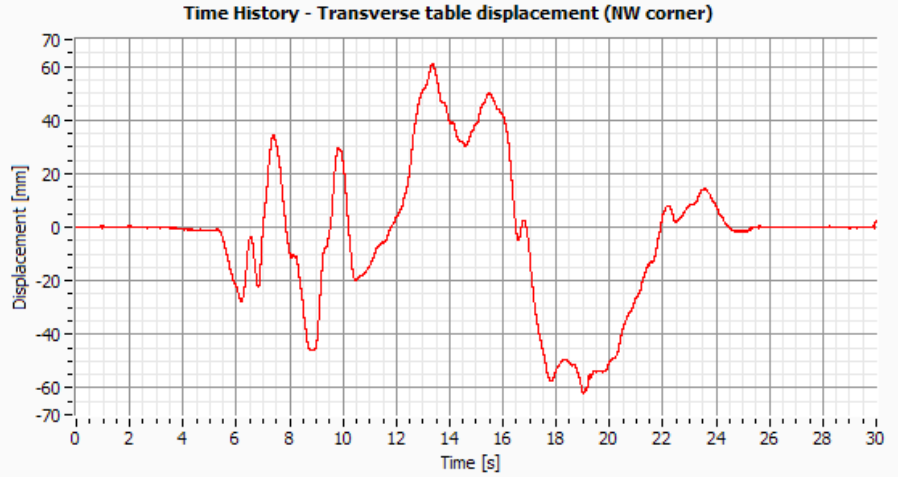

Figure IV.48: Transverse table displacement in the NW corner (Channel18).

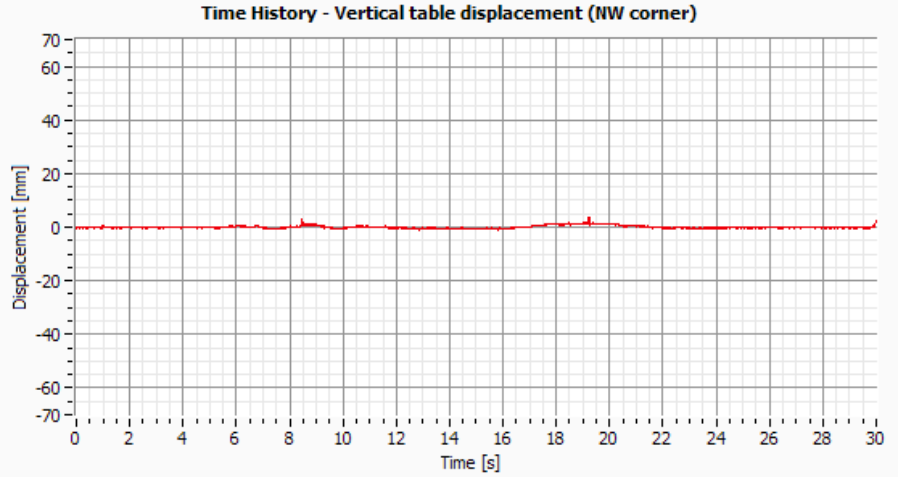

Figure IV.49: Vertical table displacement in the NW corner (Channel19).

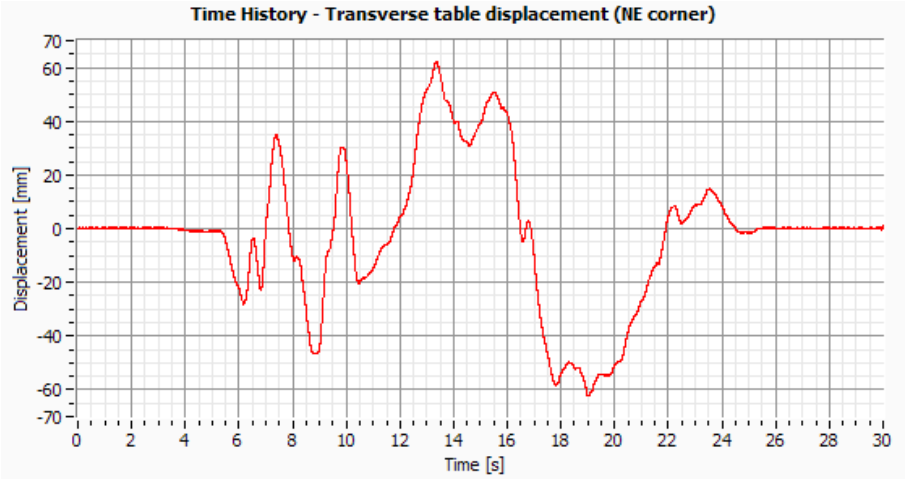

Figure IV.50: Transverse table displacement in the NE corner (Channel 20).

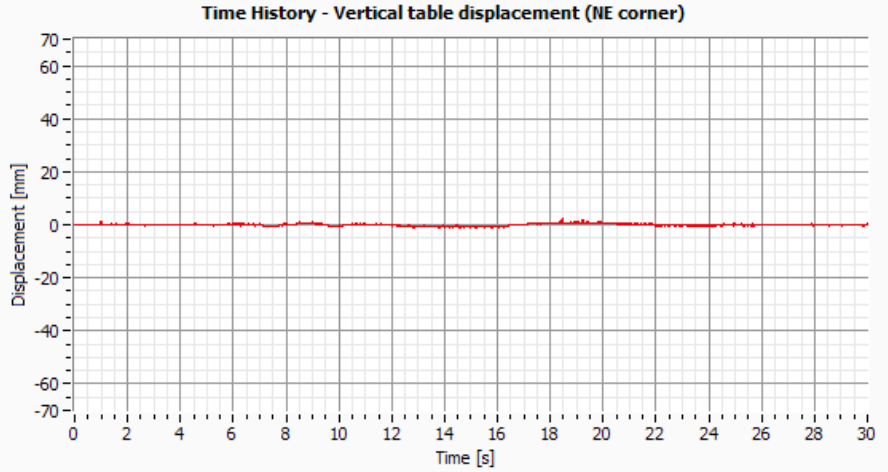

Figure IV.51: Vertical table displacement in the NE corner (Channel 21).

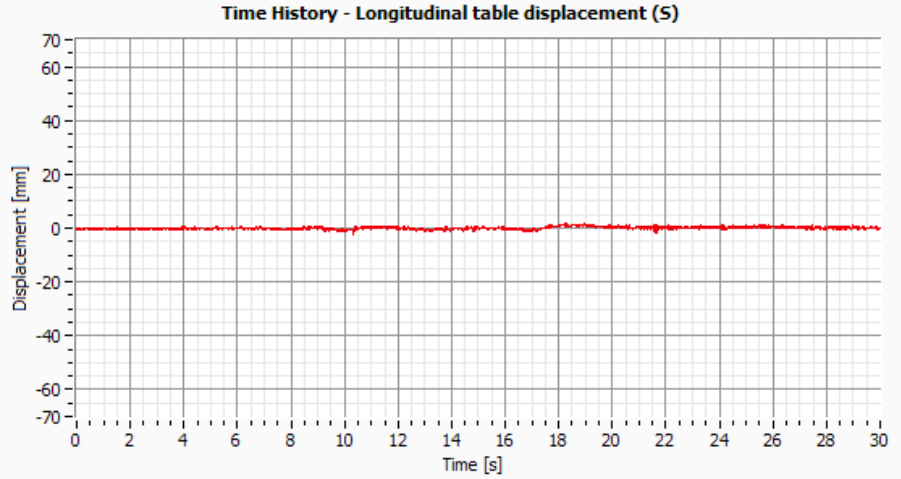

Figure IV.52: Longitudinal table displacement –S (Channel 22).

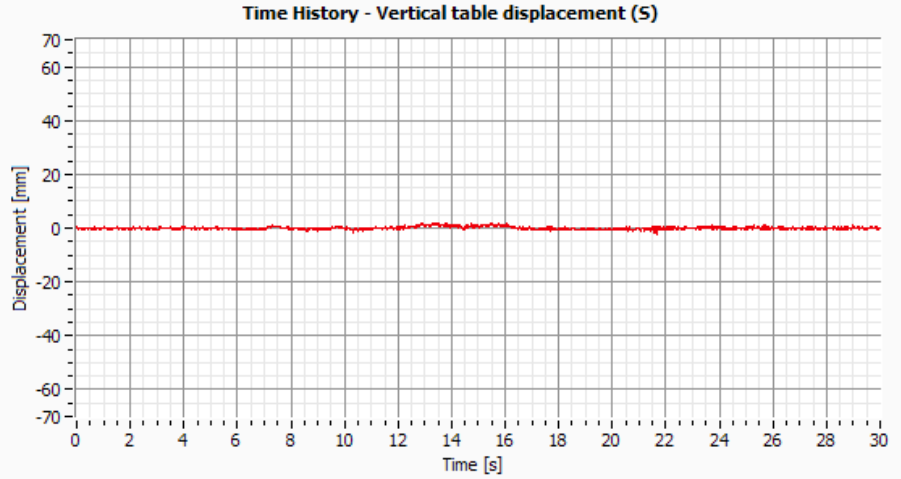

Figure IV.53: Vertical table displacement –S (Channel 23).

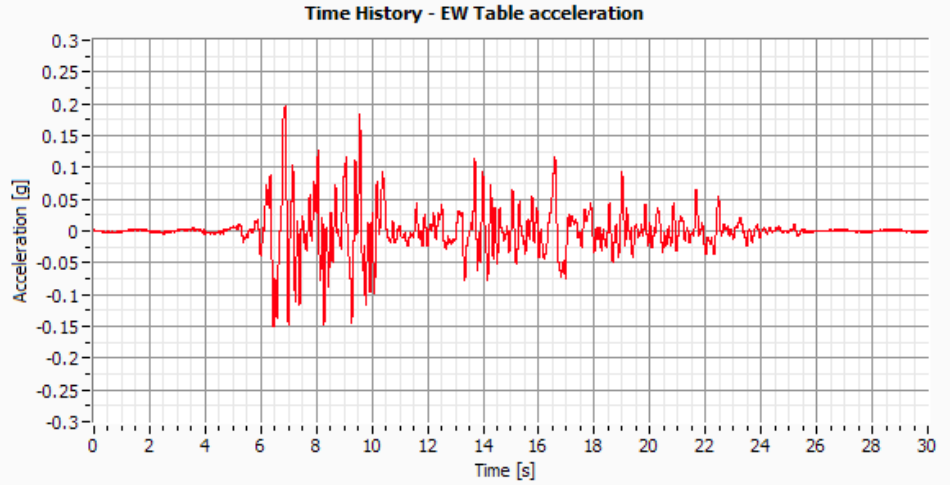

Figure IV.54: EW Table acceleration (Channel 24).

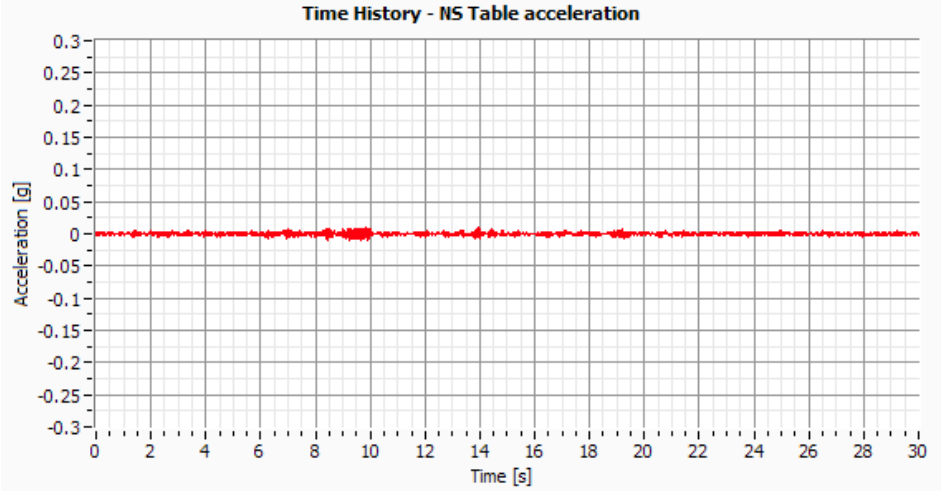

Figure IV.55: NS Table acceleration (Channel 25).

Test 6 – Sen 10.28Hz (EW PGA=0.05g)

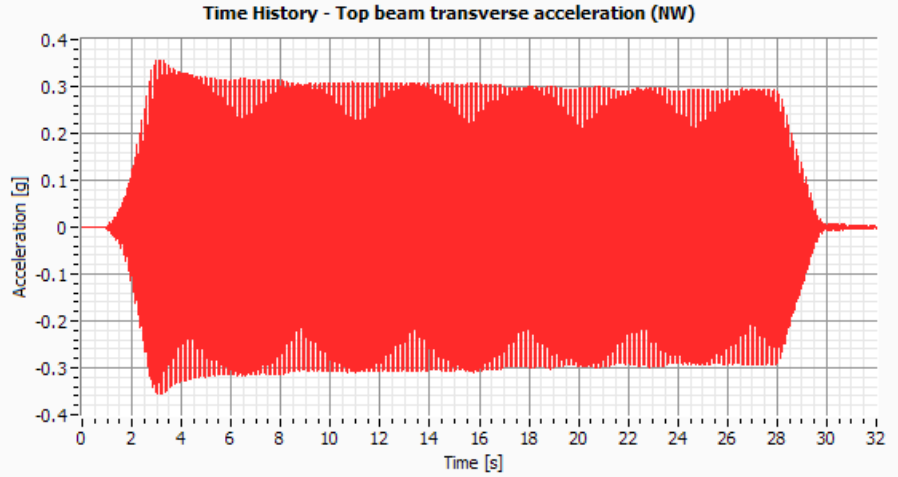

Figure IV.56: NW Top beam acceleration (Channel 1).

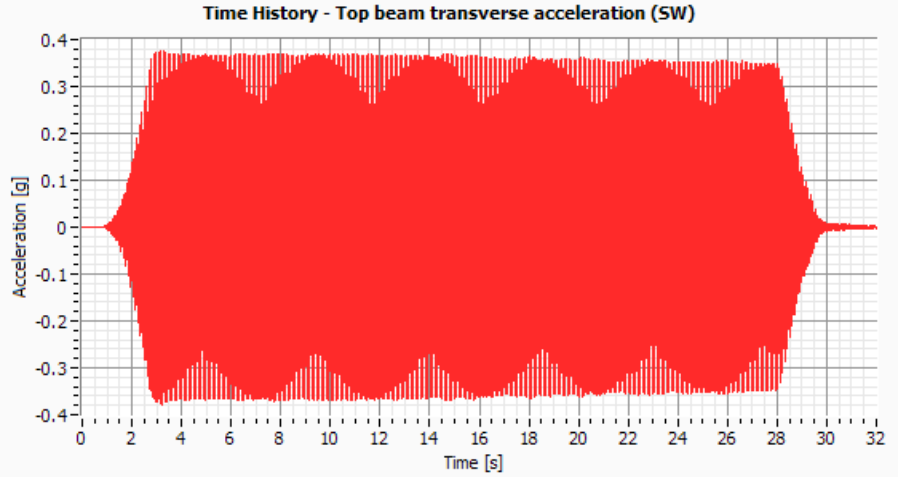

Figure IV.57: SW Top beam acceleration (Channel2).

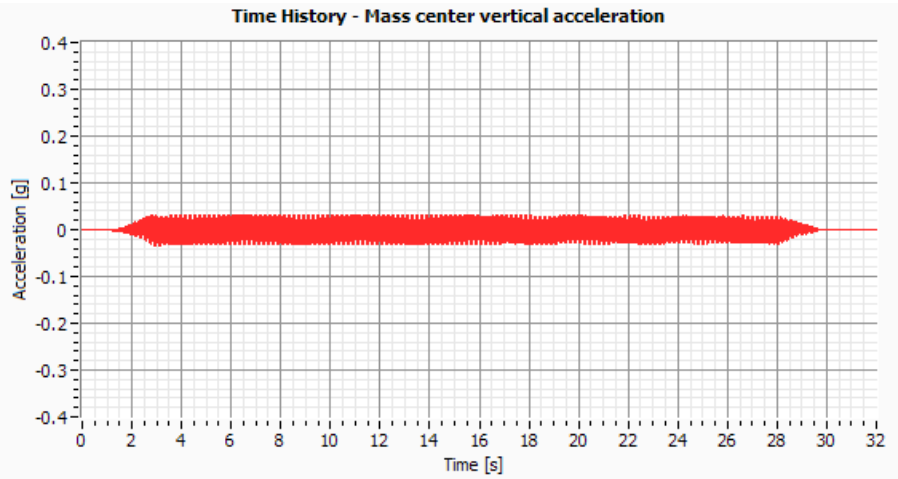

Figure IV.58: Mass center vertical acceleration (Channel 3).

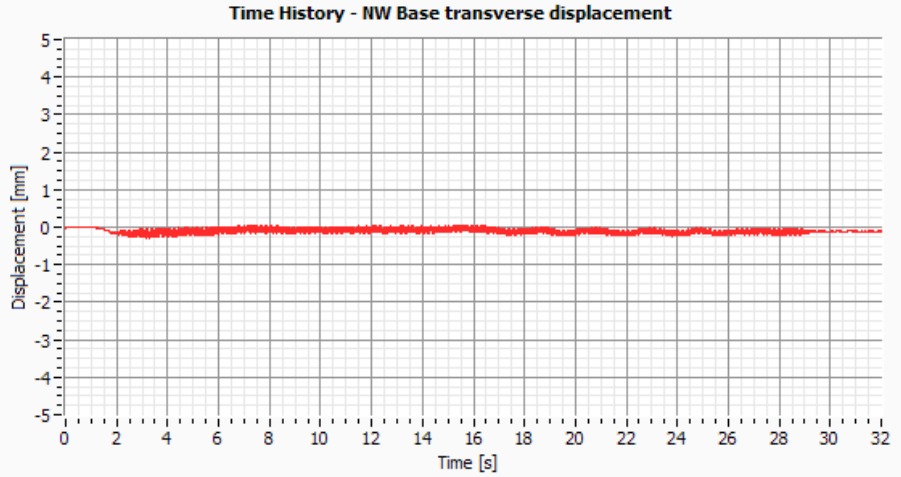

Figure IV.59: NW Base transverse displacement (Channel4).

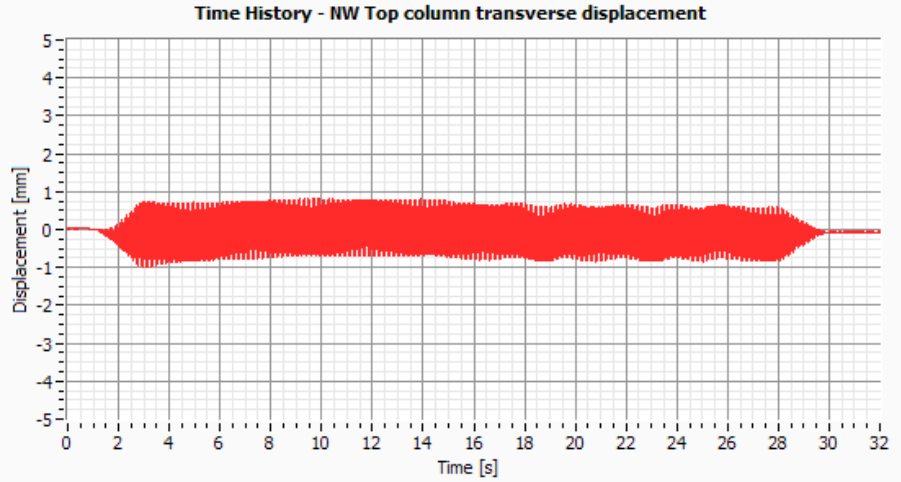

Figure IV.60: NW Top column transverse displacement (Channel5).

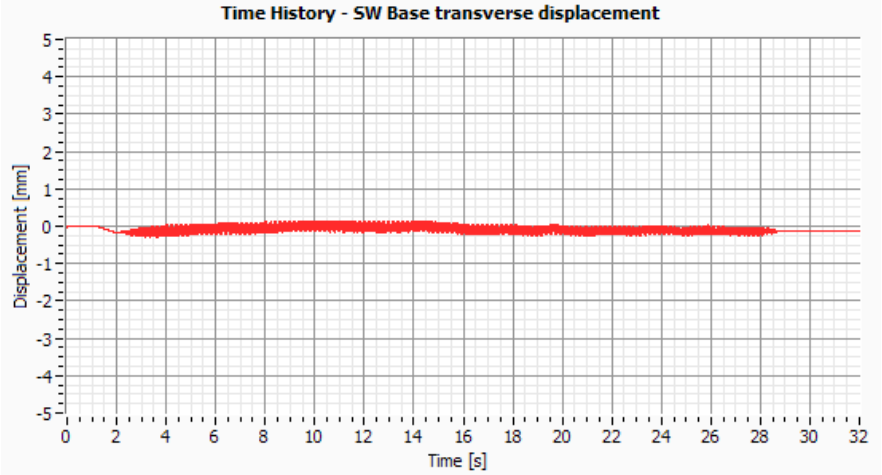

Figure IV.61: SW Base transverse displacement (Channel6).

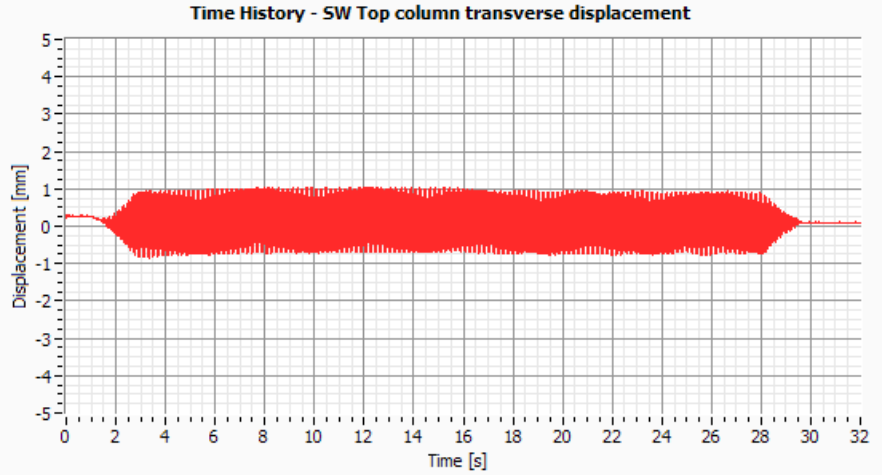

Figure IV.62: SW Top column transverse displacement (Channel7).

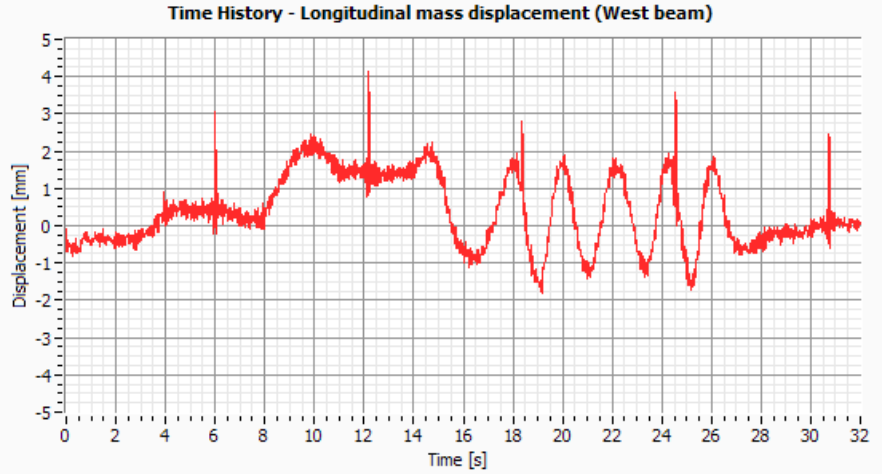

Figure IV.63: Longitudinal mass displacement in the West beam (Channel 8).

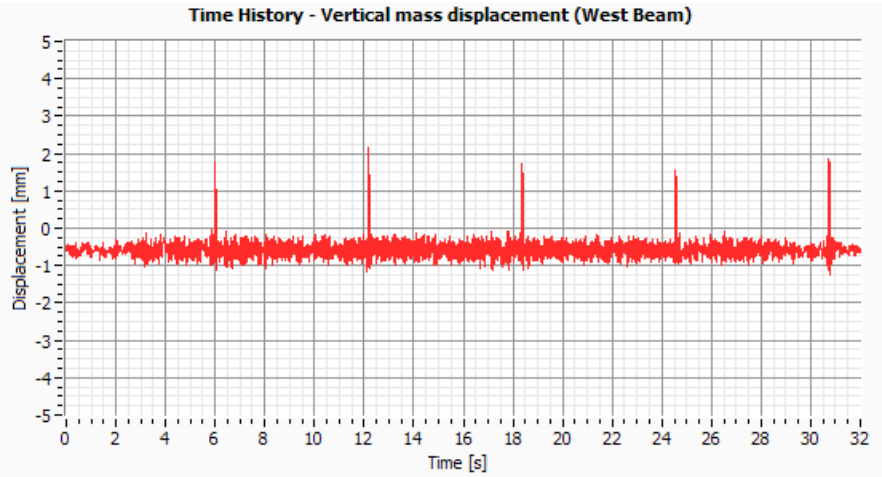

Figure IV.64: Vertical mass displacement in the West beam (Channel9).

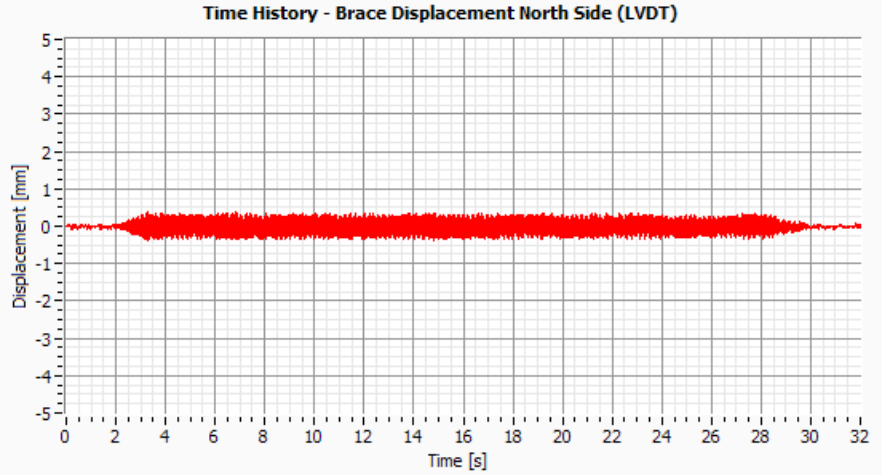

Figure IV.65: Brace displacement North side (Channel10).

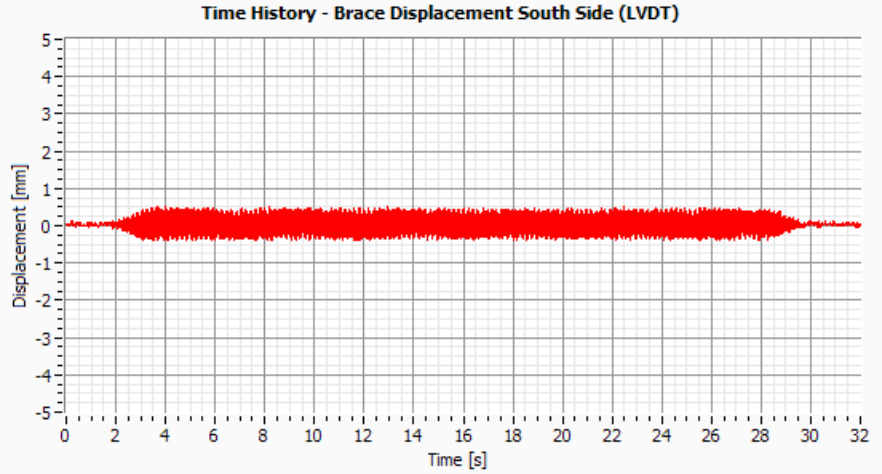

Figure IV.66: Brace displacement South side (Channel11).

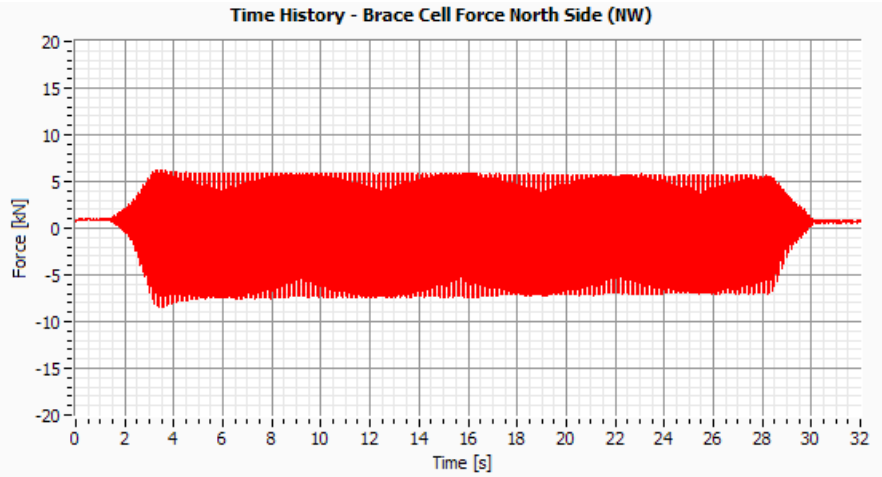

Figure IV.67: Brace cell force North Side – NW (Channel14).

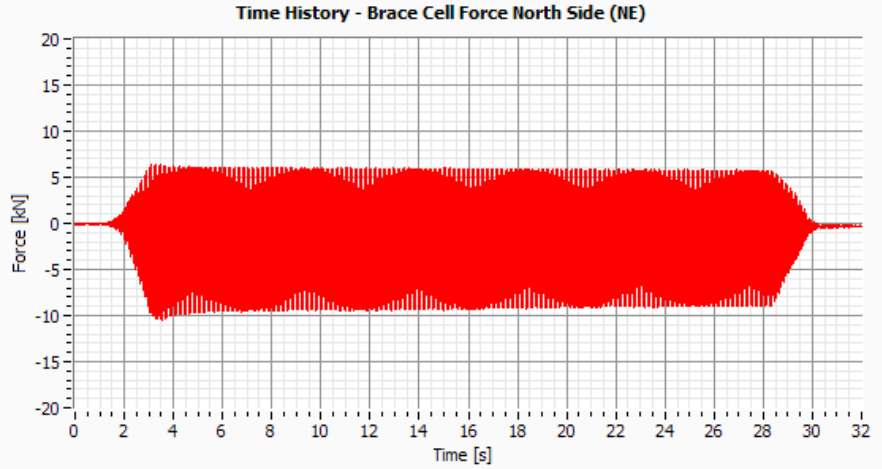

Figure IV.68: Brace cell force North Side – NE (Channel15).

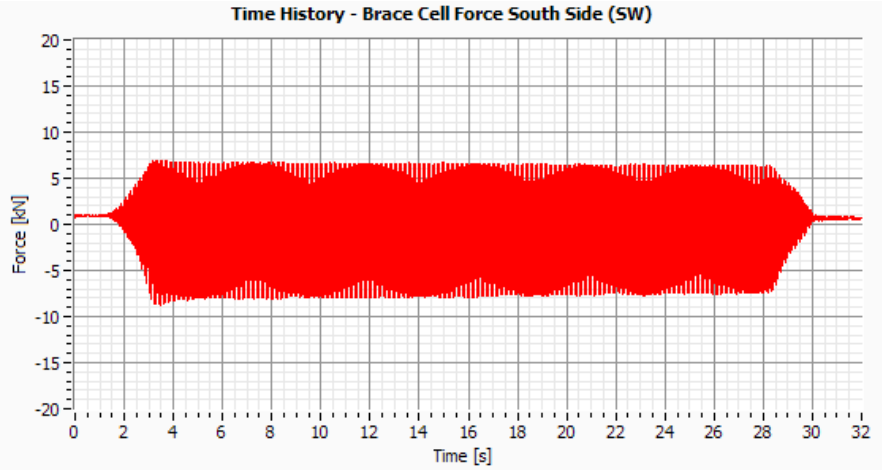

Figure IV.69: Brace cell force South Side – SW (Channel16).

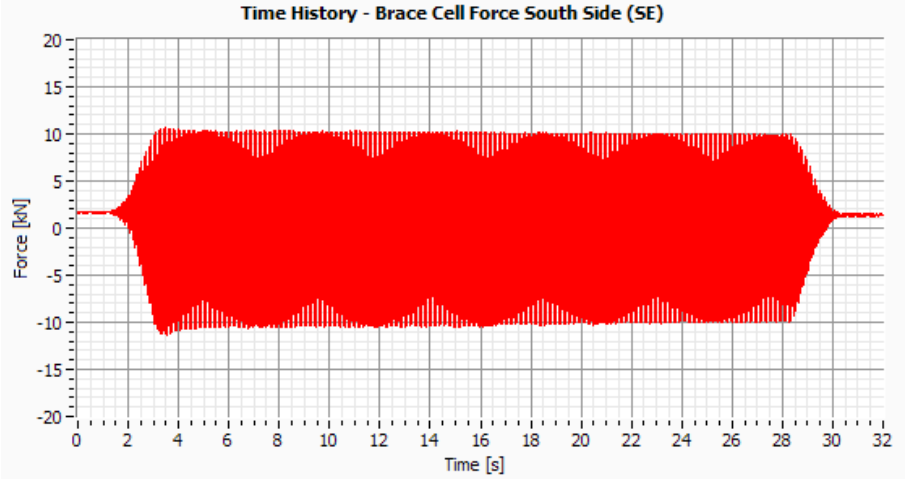

Figure IV.70: Brace cell force South Side – NE (Channel17).

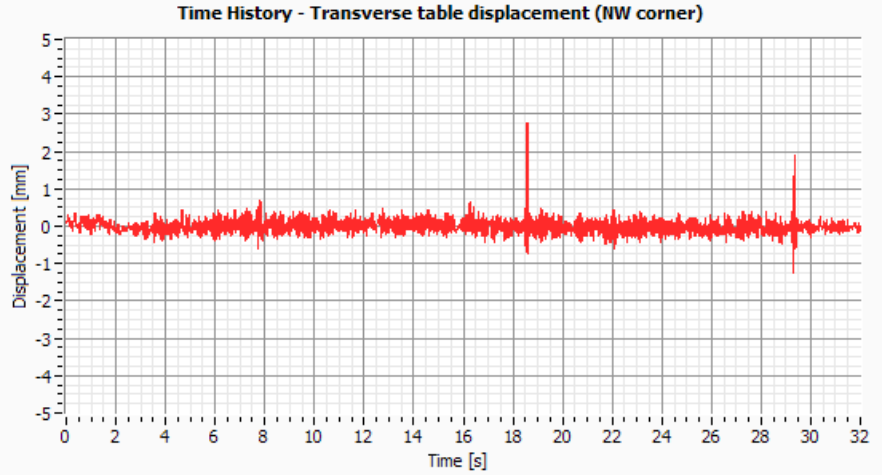

Figure IV.71: Transverse table displacement in the NW corner (Channel18).

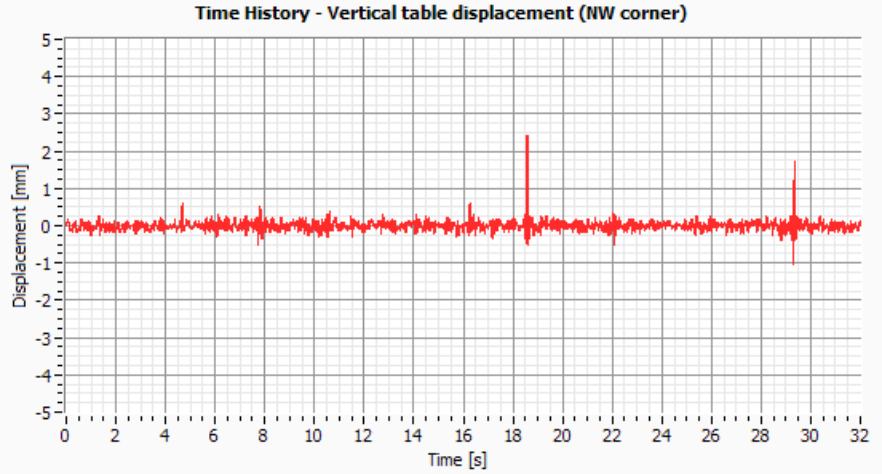

Figure IV.72: Vertical table displacement in the NW corner (Channel19).

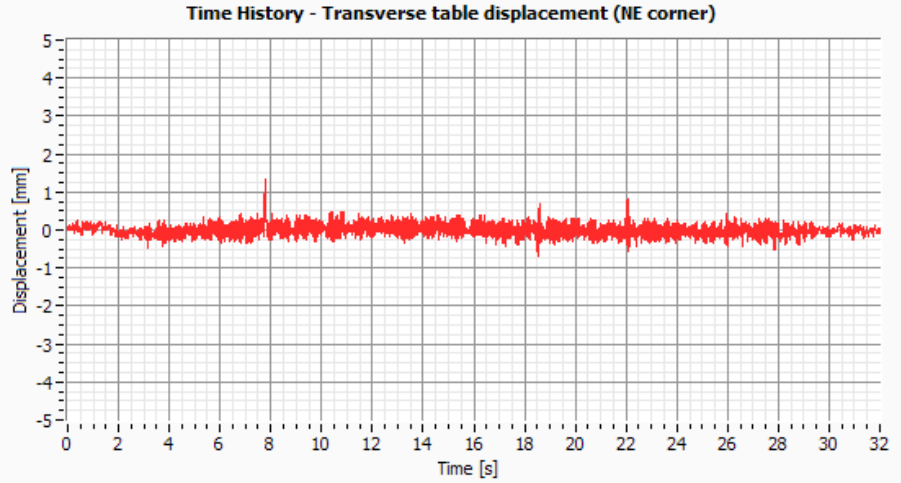

Figure IV.73: Transverse table displacement in the NE corner (Channel 20).

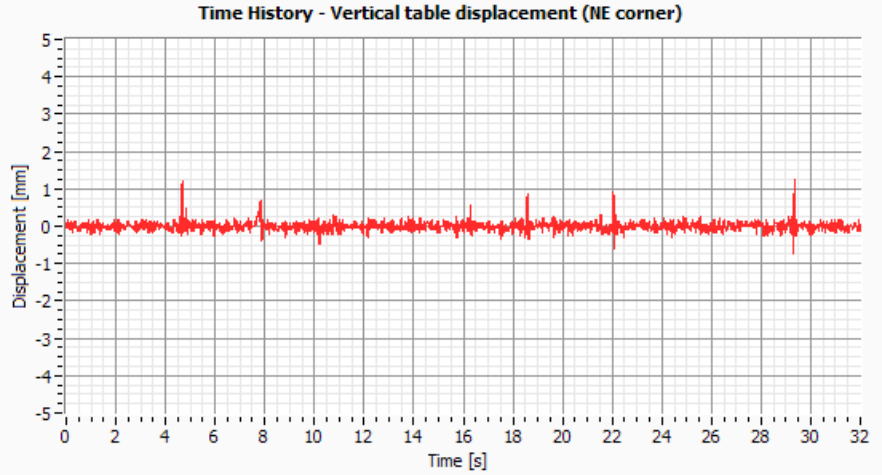

Figure IV.74: Vertical table displacement in the NE corner (Channel 21).

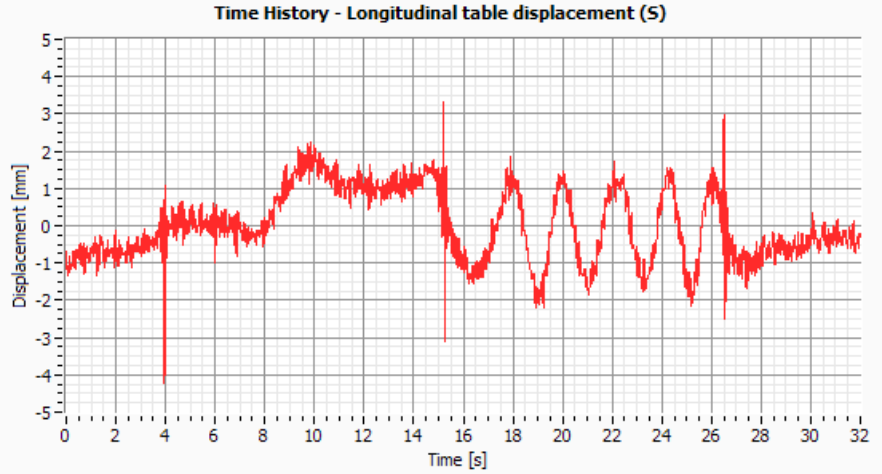

Figure IV.75: Longitudinal table displacement –S (Channel 22).

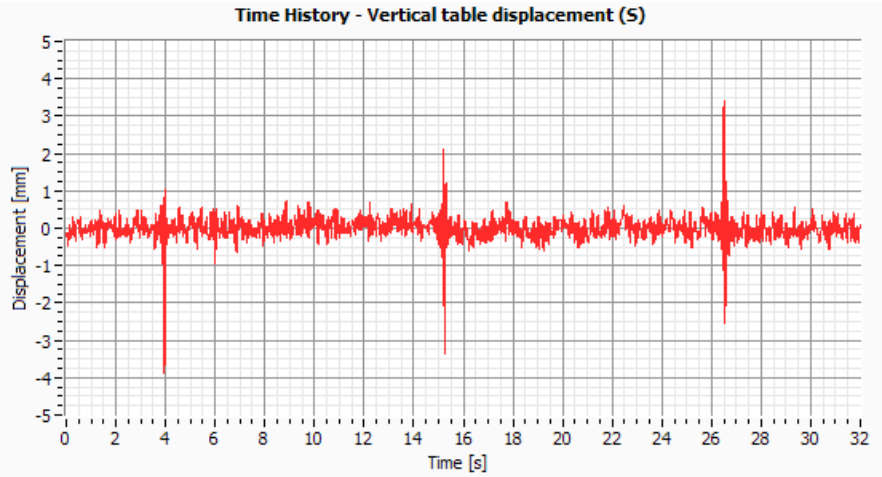

Figure IV.76: Vertical table displacement –S (Channel 23).

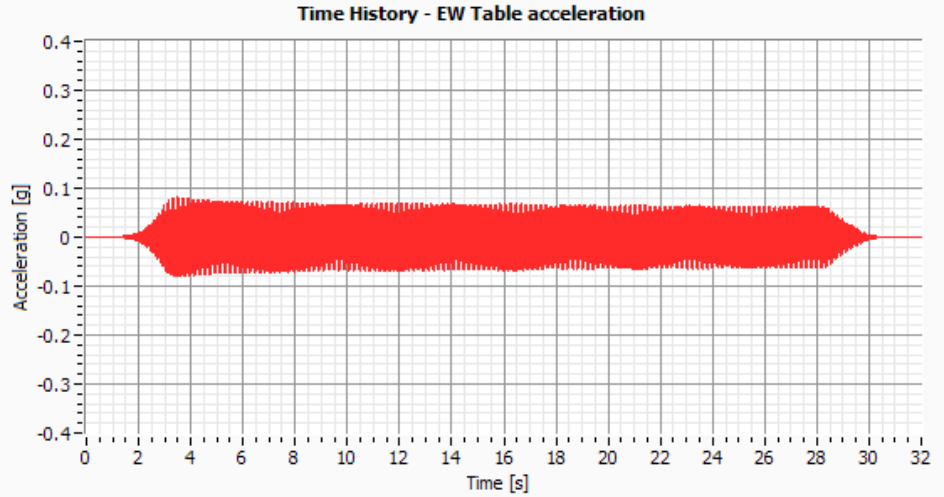

Figure IV.77: EW Table acceleration (Channel 24).

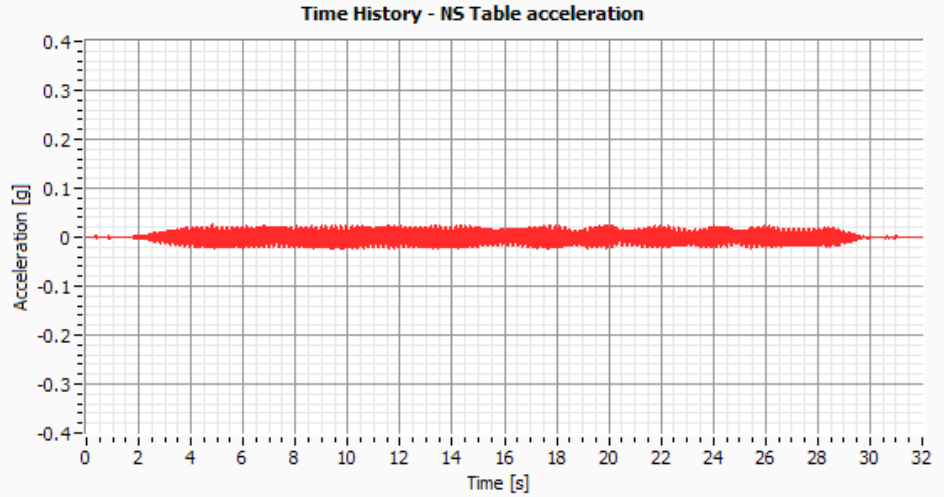

Figure IV.78: NS Table acceleration (Channel 25).

Test 7 – Artificial EC8 (EW PGA=0.20g)

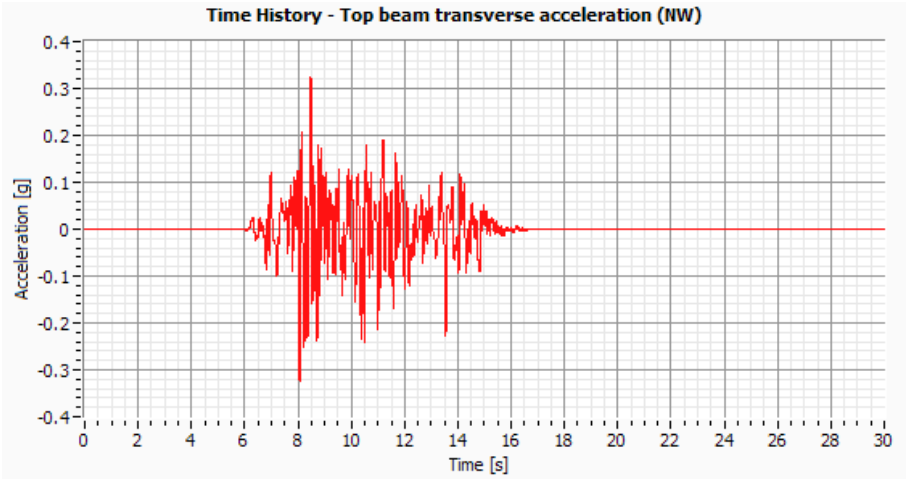

Figure IV.79: NW Top beam acceleration (Channel 1).

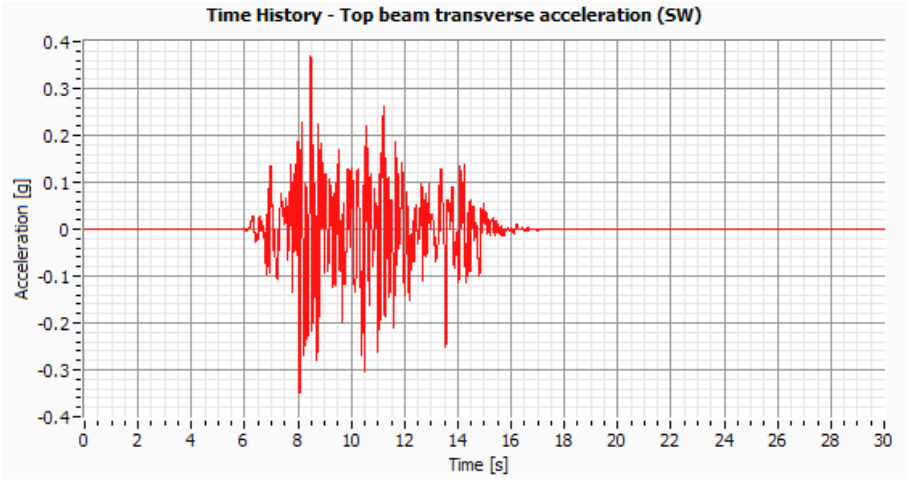

Figure IV.80: SW Top beam acceleration (Channel2).

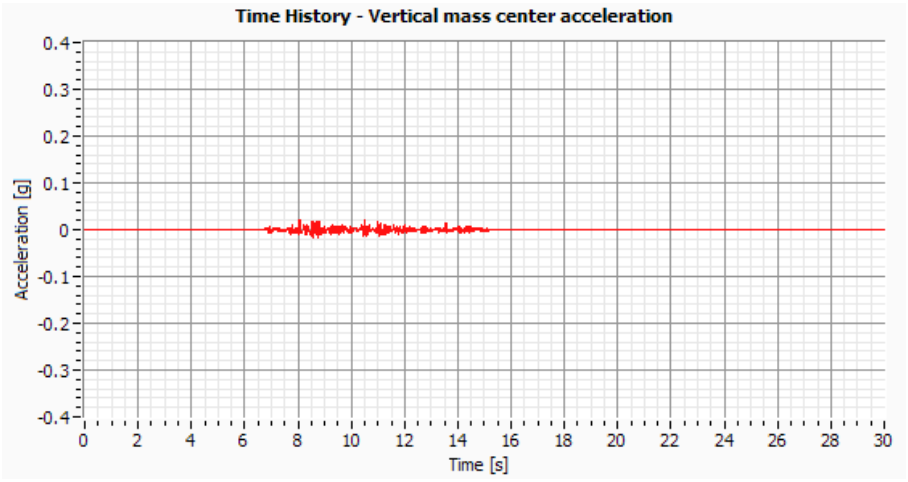

Figure IV.81: Mass center vertical acceleration (Channel 3).

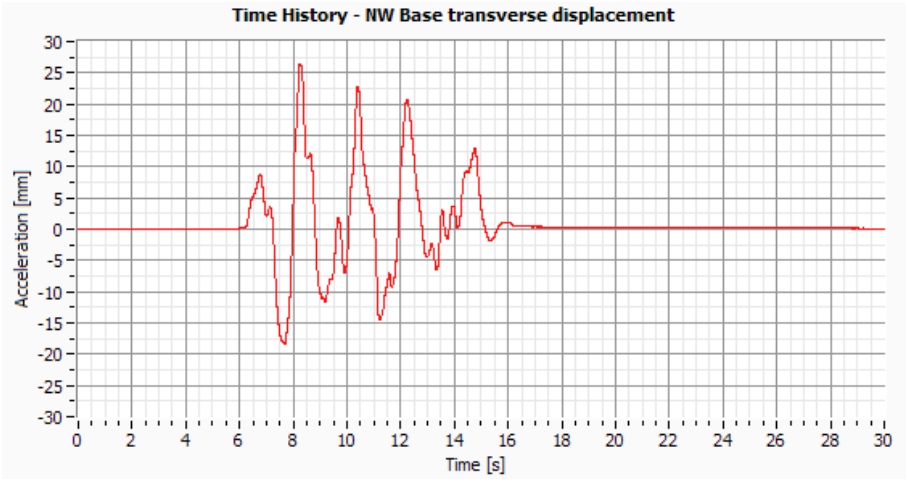

Figure IV.82: NW Base transverse displacement (Channel4).

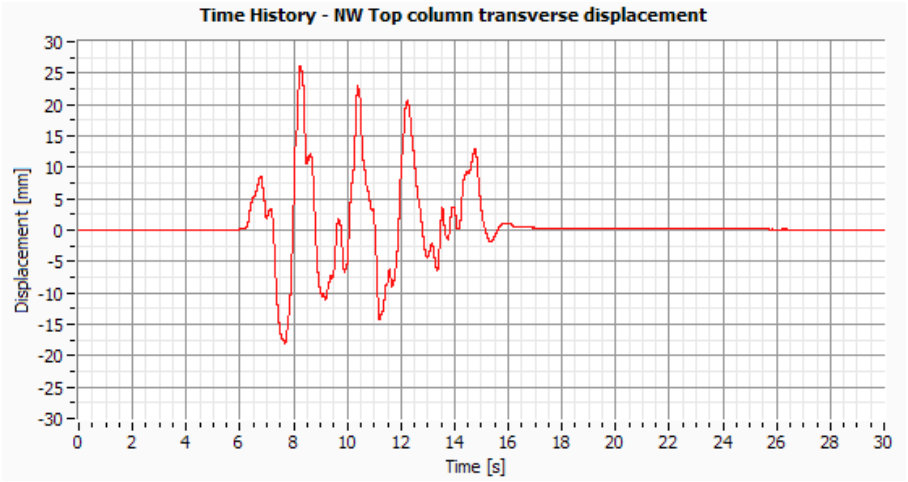

Figure IV.83: NW Top column transverse displacement (Channel5).

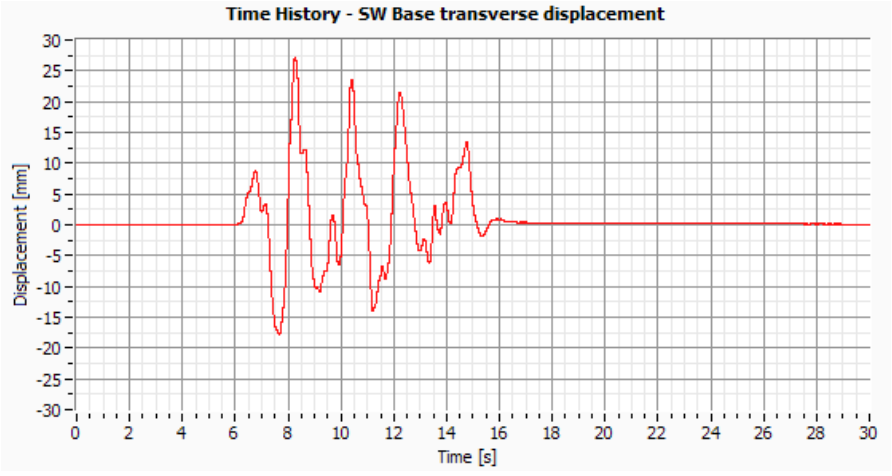

Figure IV.84: SW Base transverse displacement (Channel6).

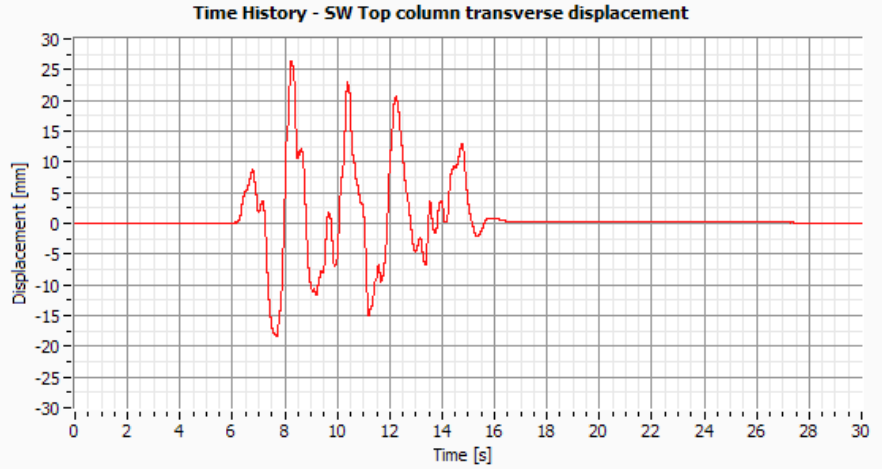

Figure IV.85: SW Top column transverse displacement (Channel7).

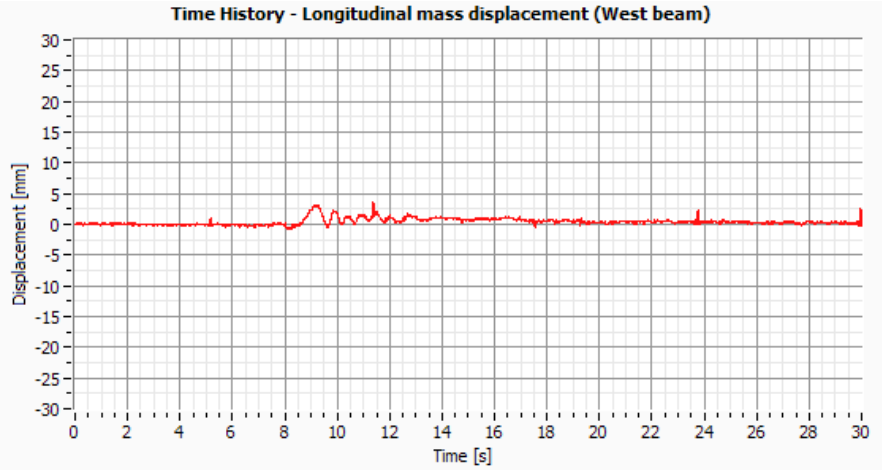

Figure IV.86: Longitudinal mass displacement in the West beam (Channel 8).

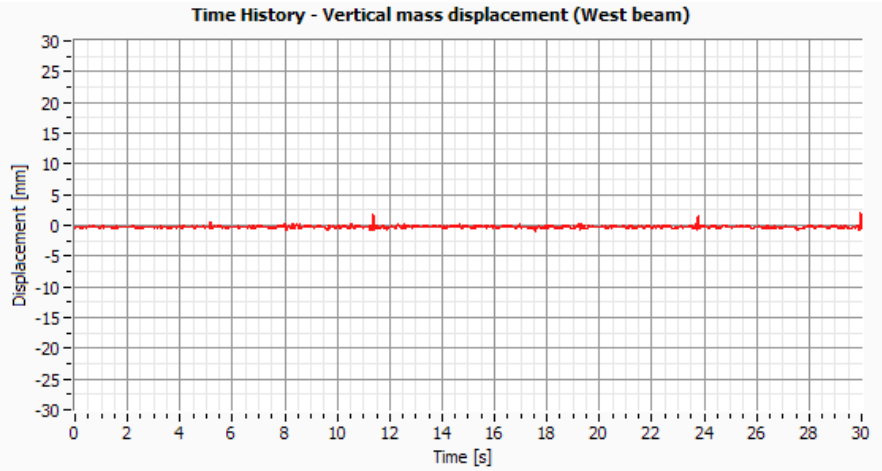

Figure IV.87: Vertical mass displacement in the West beam (Channel9).

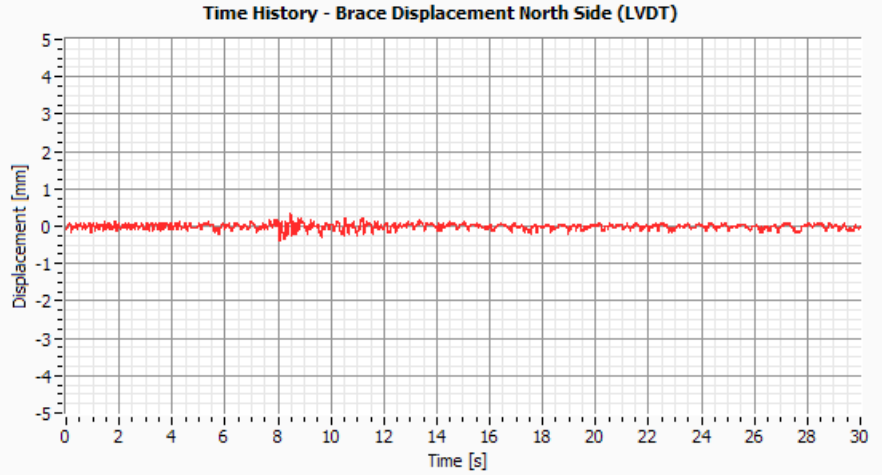

Figure IV.88: Brace displacement North side (Channel10).

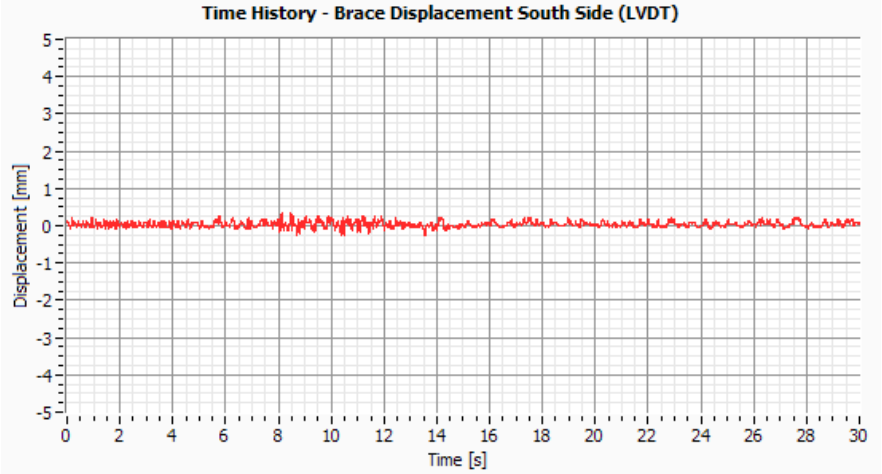

Figure IV.89: Brace displacement South side (Channel11).

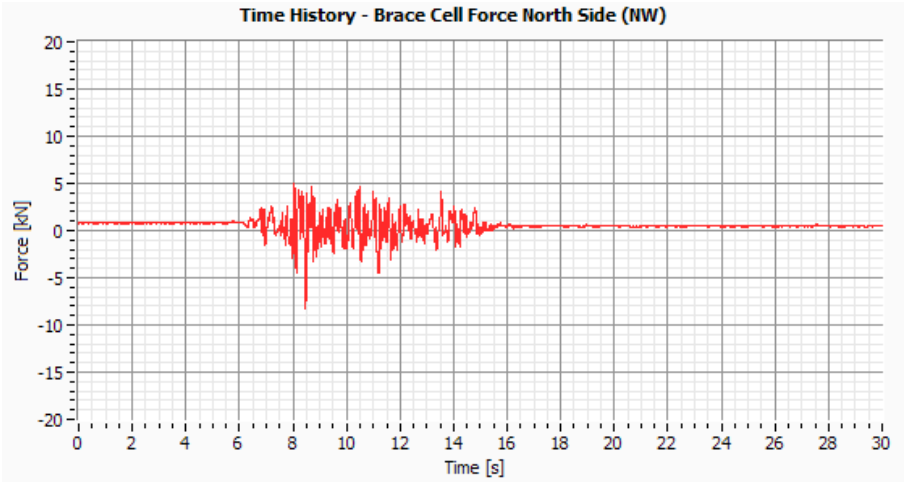

Figure IV.90: Brace cell force North Side – NW (Channel14).

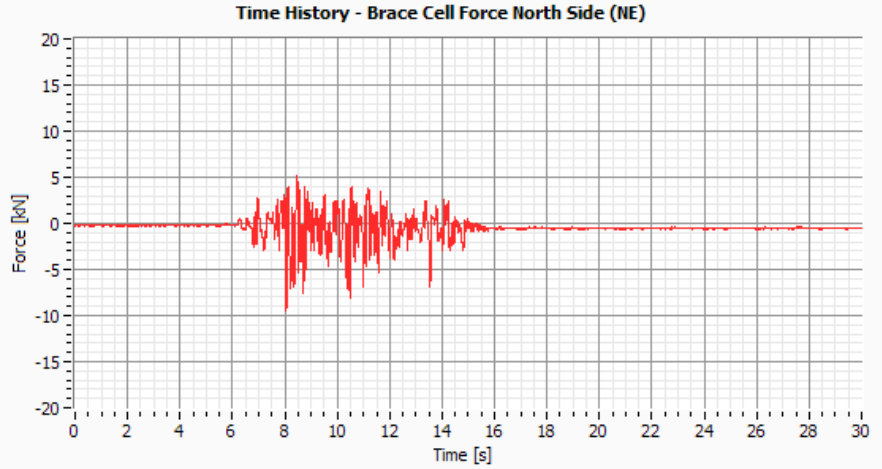

Figure IV.91: Brace cell force North Side – NE (Channel15).

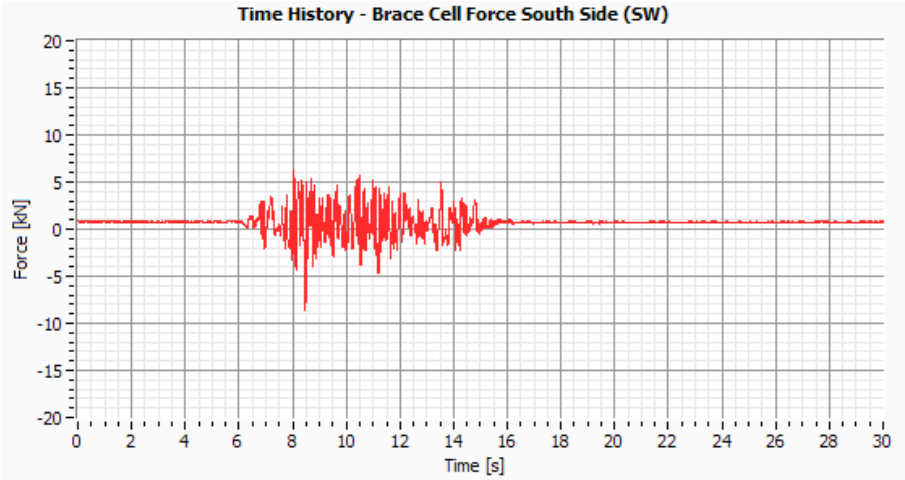

Figure IV.92: Brace cell force South Side – SW (Channel16).

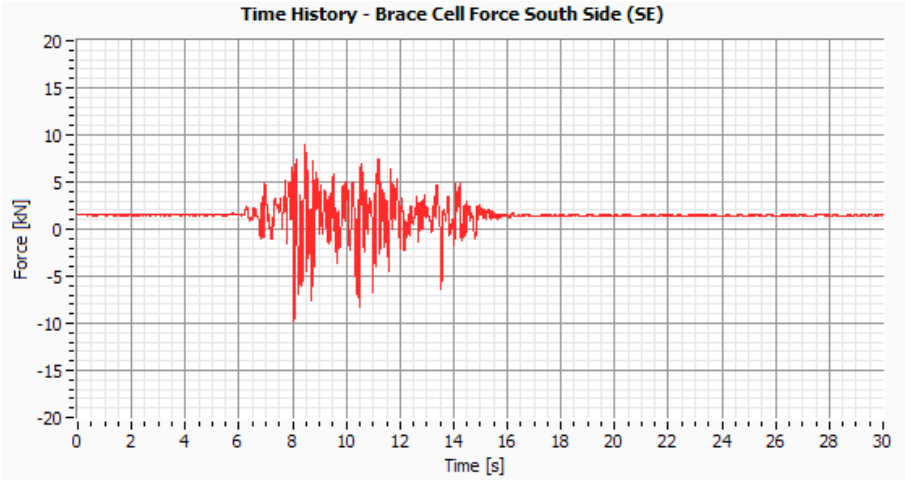

Figure IV.93: Brace cell force South Side – NE (Channel17).

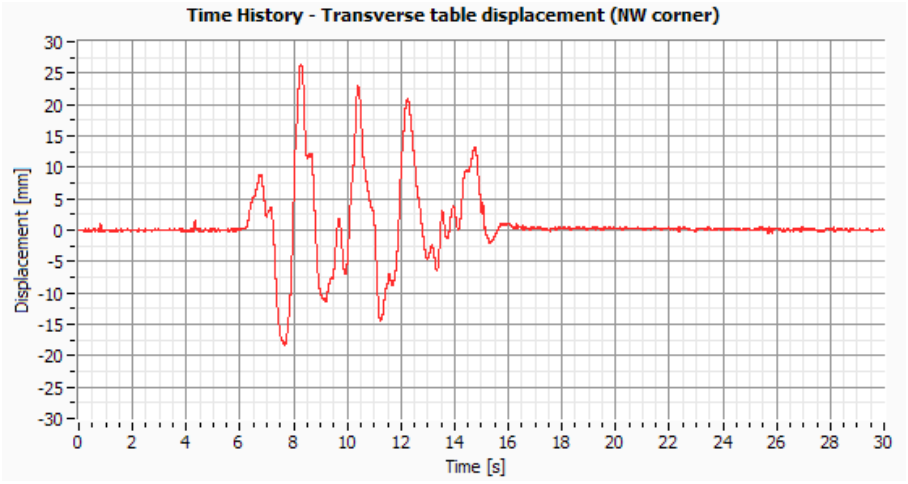

Figure IV.94: Transverse table displacement in the NW corner (Channel18).

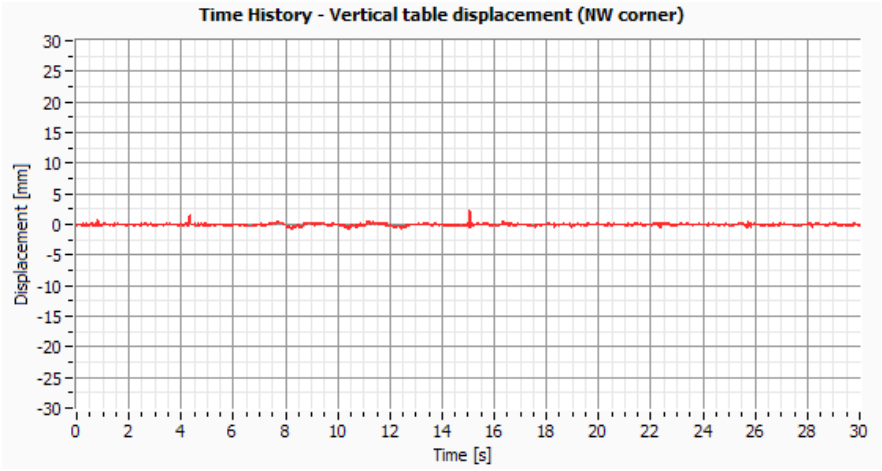

Figure IV.95: Vertical table displacement in the NW corner (Channel19).

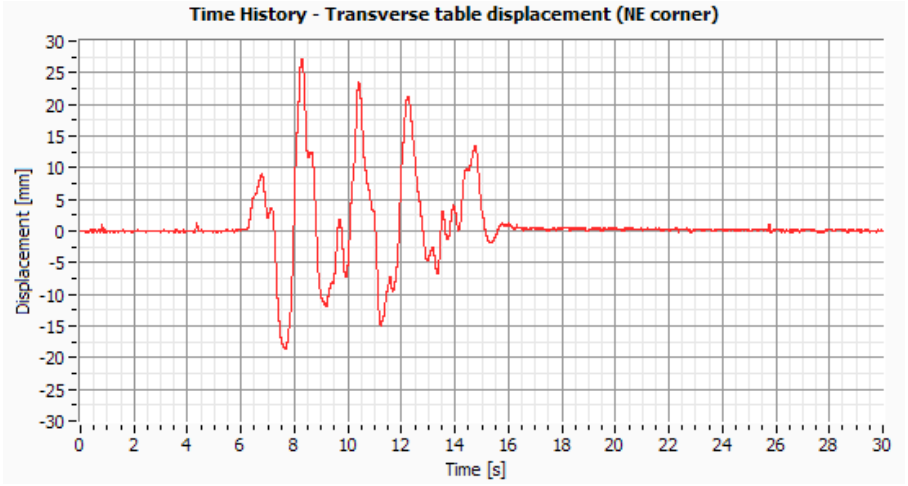

Figure IV.96: Transverse table displacement in the NE corner (Channel 20).

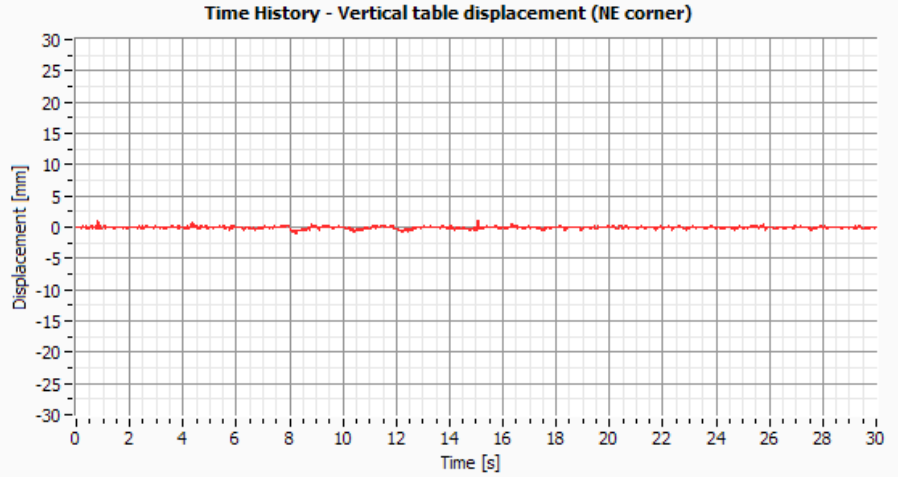

Figure IV.97: Vertical table displacement in the NE corner (Channel 21).

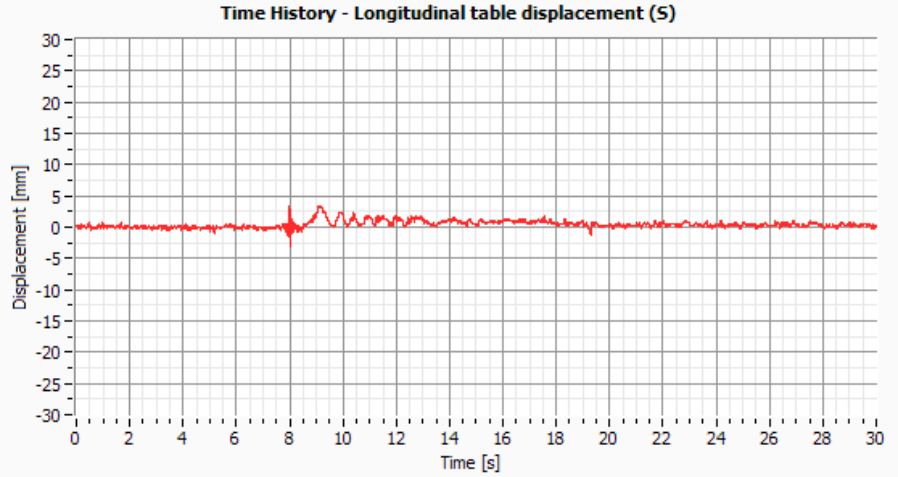

Figure IV.98: Longitudinal table displacement –S (Channel 22).

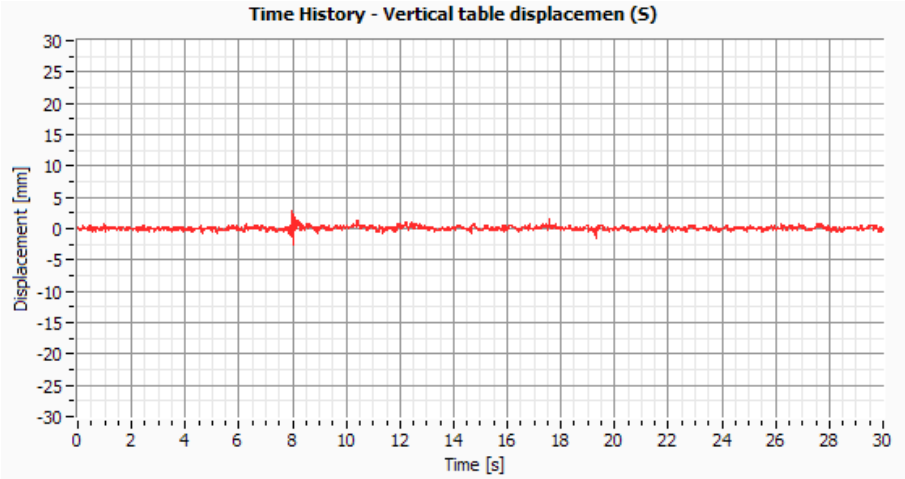

Figure IV.99: Vertical table displacement –S (Channel 23).

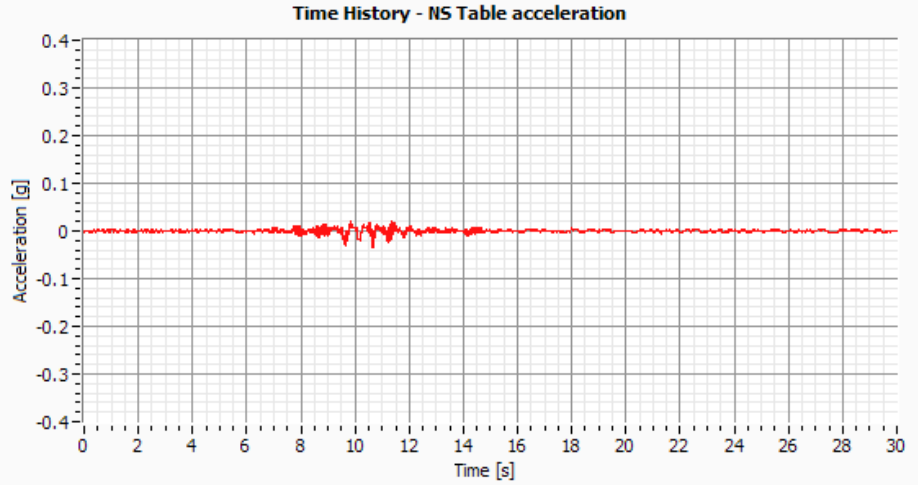

Figure IV.100: EW Table acceleration (Channel 24).

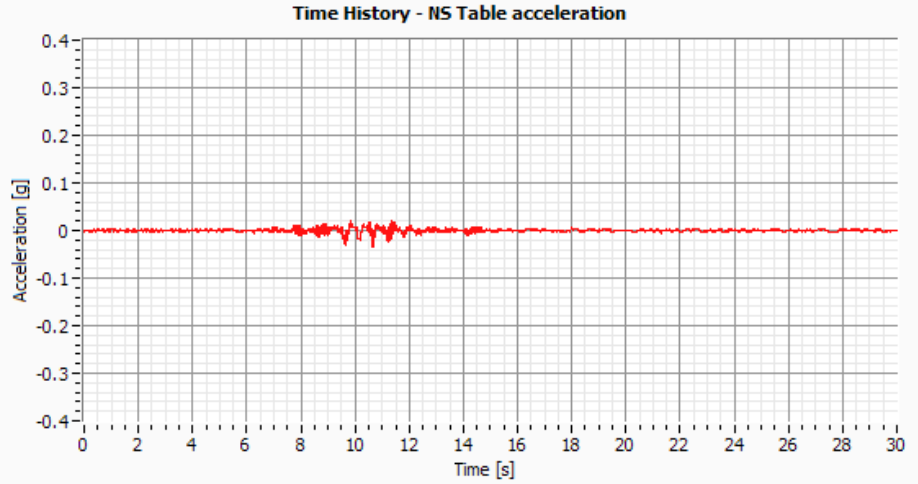

Figure IV.101: NS Table acceleration (Channel 25).

Test 8 – Sen 8.22Hz (EW PGA=0.05g)

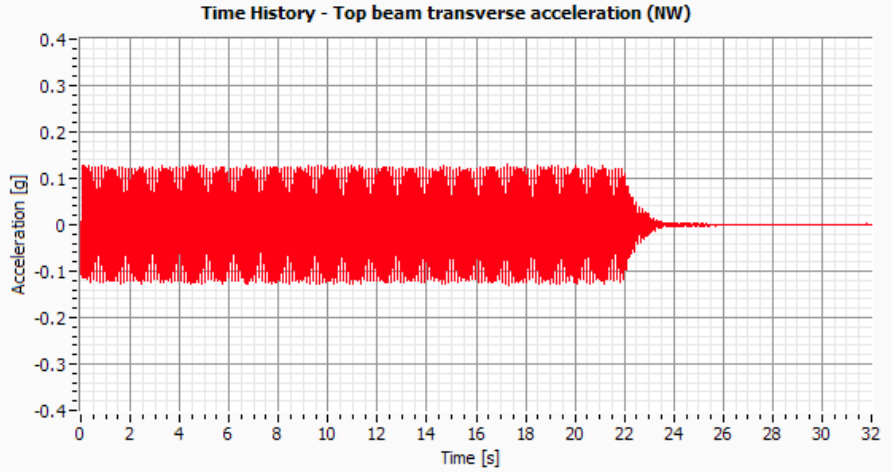

Figure IV.102: NW Top beam acceleration (Channel 1).

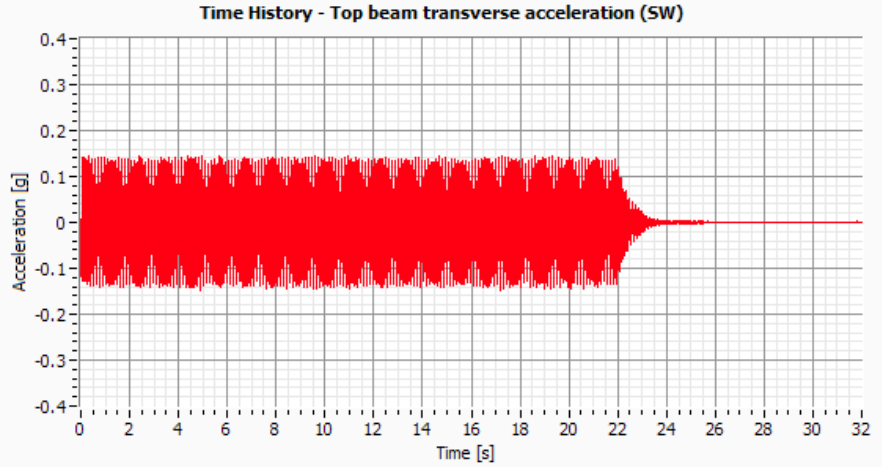

Figure IV.103: SW Top beam acceleration (Channel2).

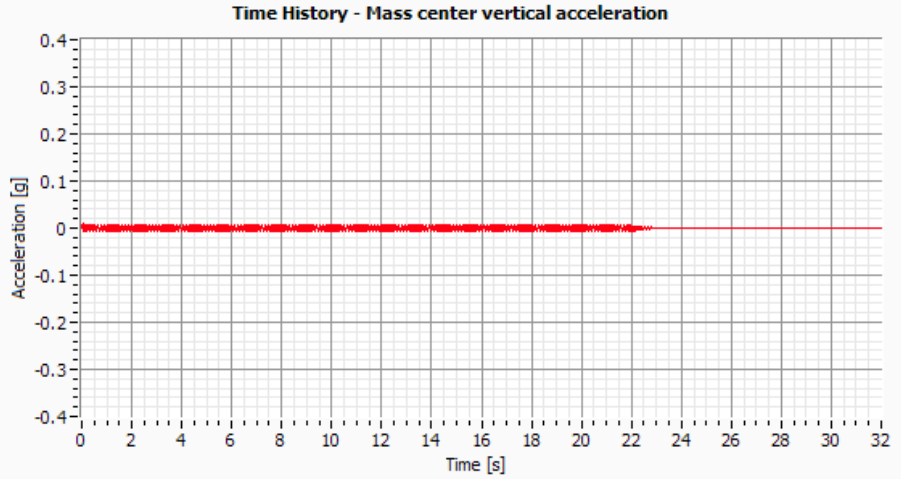

Figure IV.104: Mass center vertical acceleration (Channel 3).

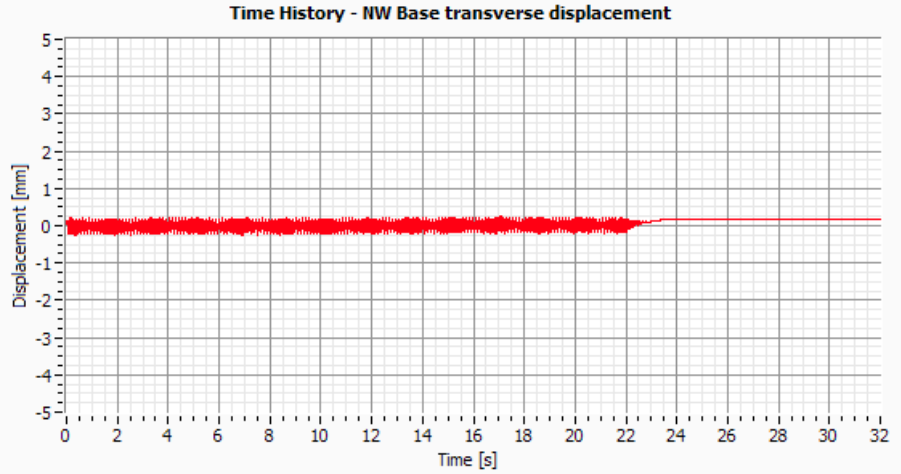

Figure IV.105: NW Base transverse displacement (Channel4).

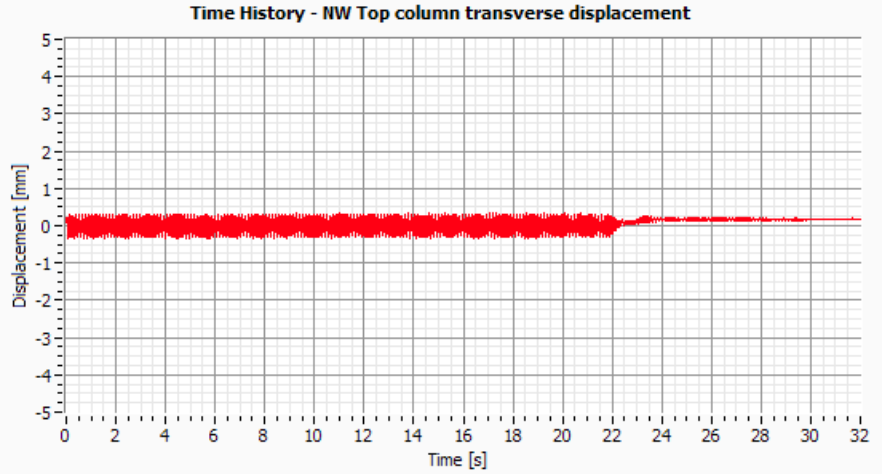

Figure IV.106: NW Top column transverse displacement (Channel5).

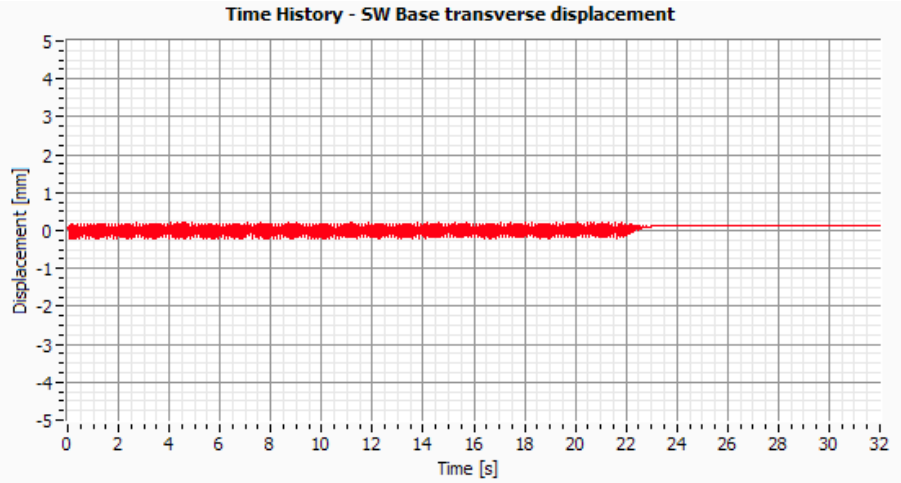

Figure IV.107: SW Base transverse displacement (Channel6).

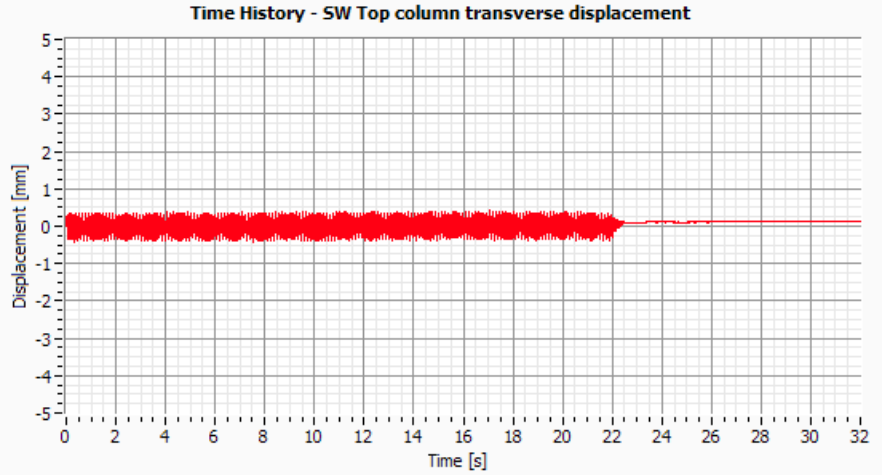

Figure IV.108: SW Top column transverse displacement (Channel7).

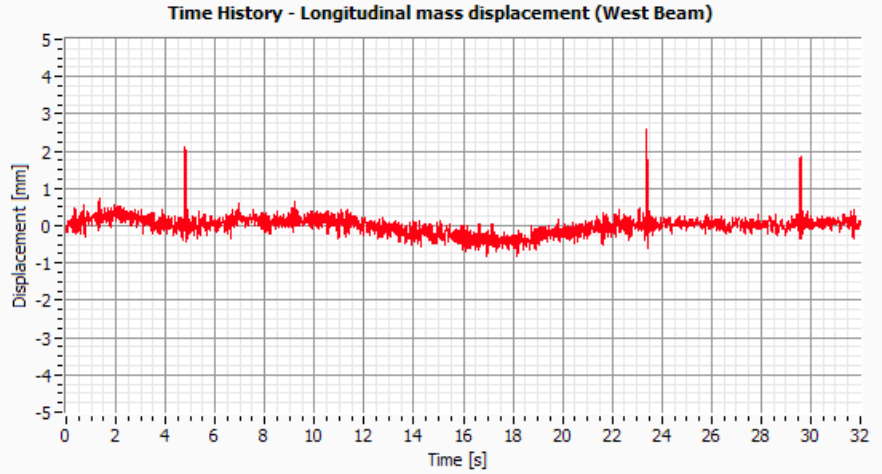

Figure IV.109: Longitudinal mass displacement in the West beam (Channel 8).

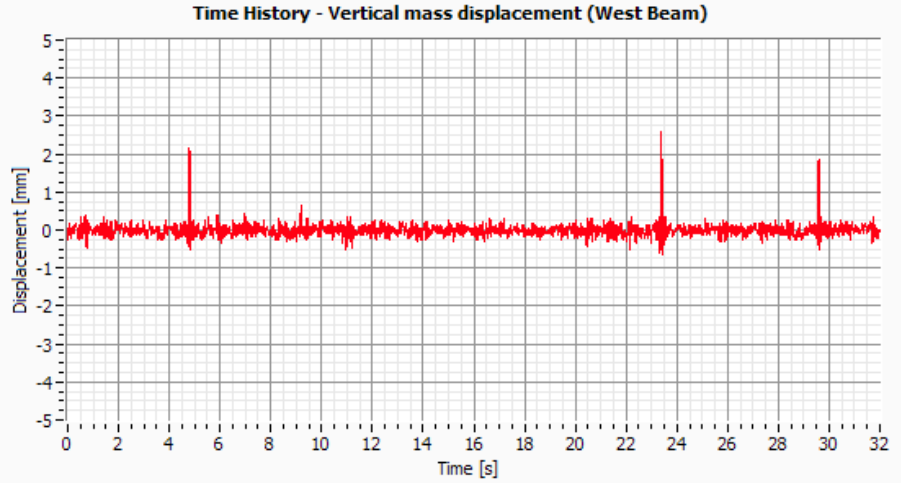

Figure IV.110: Vertical mass displacement in the West beam (Channel9).

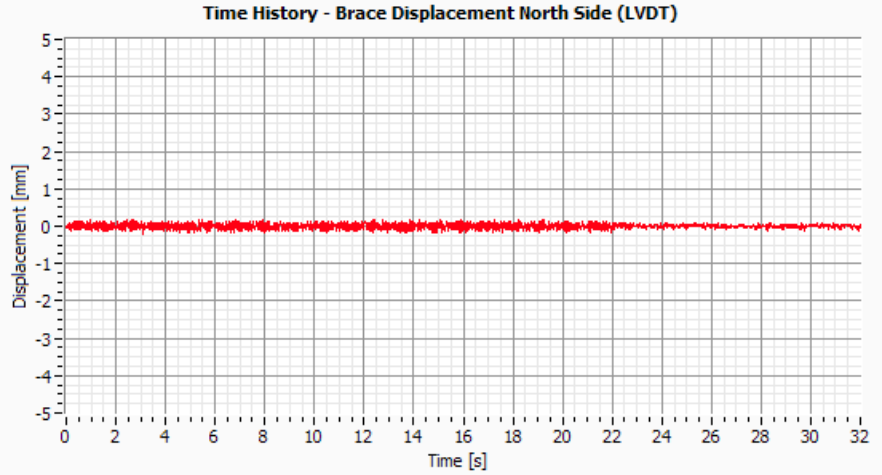

Figure IV.111: Brace displacement North side (Channel10).

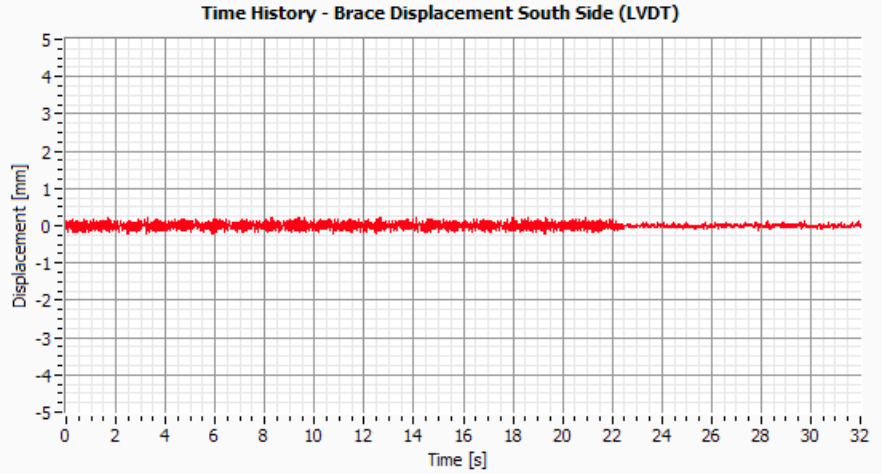

Figure IV.112: Brace displacement South side (Channel11).

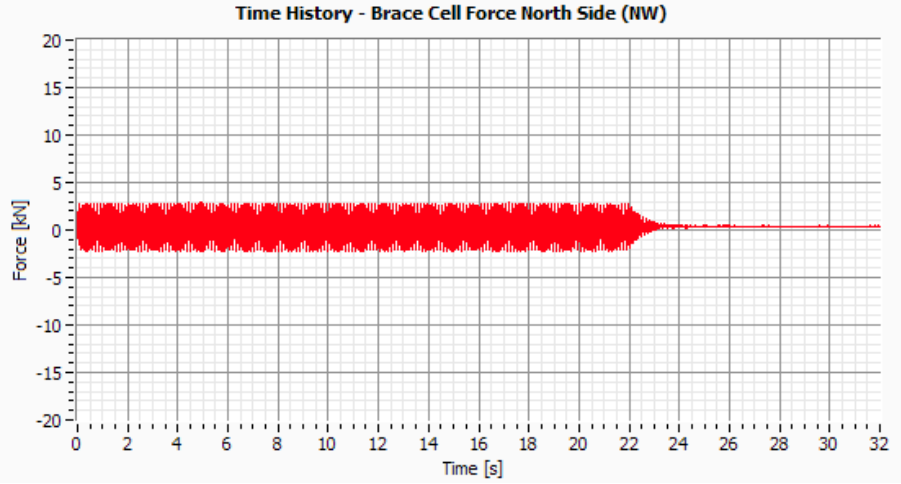

Figure IV.113: Brace cell force North Side – NW (Channel14).

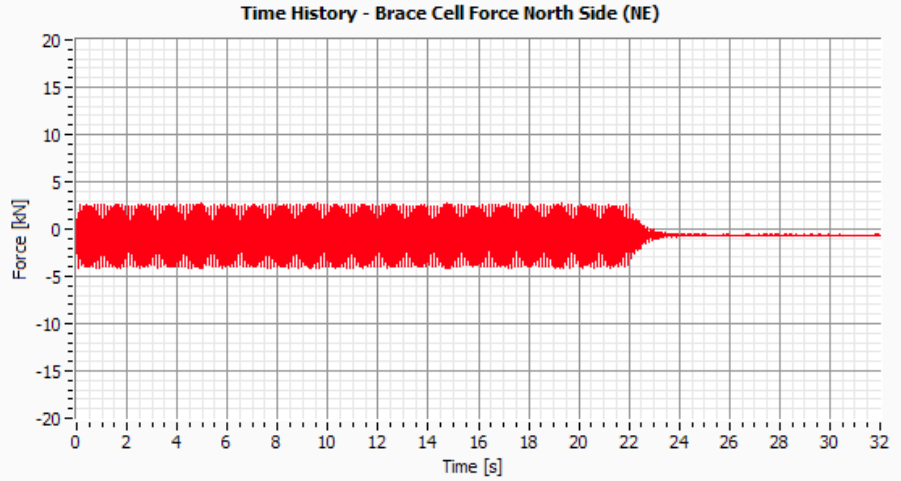

Figure IV.114: Brace cell force North Side – NE (Channel15).

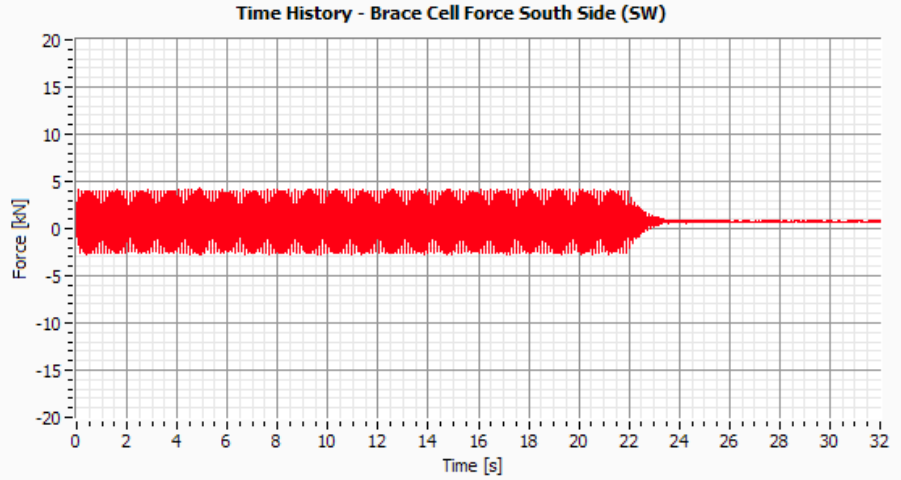

Figure IV.115: Brace cell force South Side – SW (Channel16).

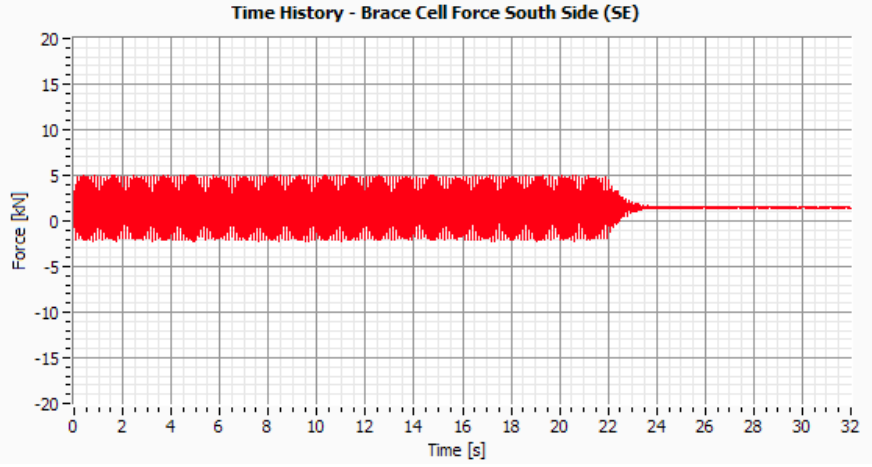

Figure IV.116: Brace cell force South Side – NE (Channel17).

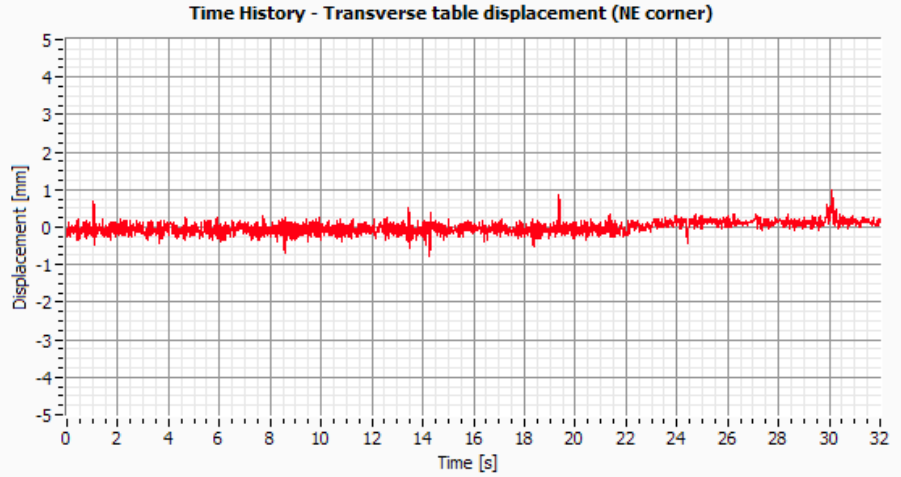

Figure IV.117: Transverse table displacement in the NW corner (Channel18).

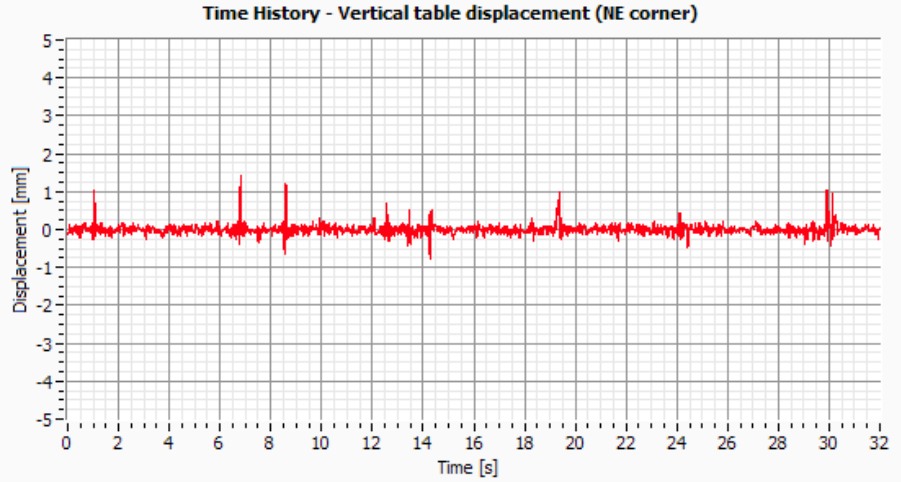

Figure IV.118: Vertical table displacement in the NW corner (Channel19).

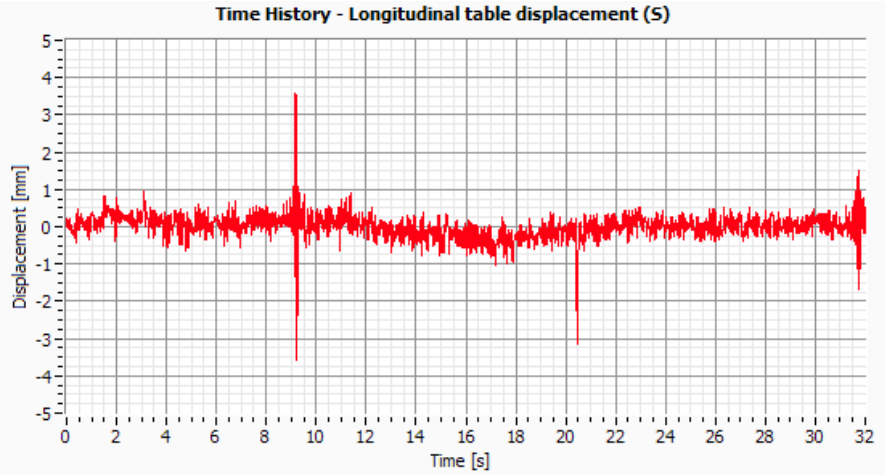

Figure IV.119: Transverse table displacement in the NE corner (Channel 20).

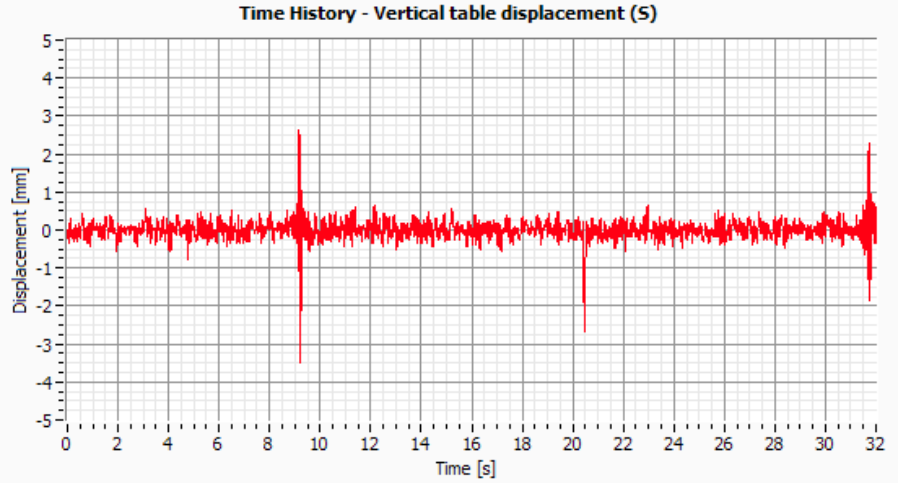

Figure IV.120: Vertical table displacement in the NE corner (Channel 21).

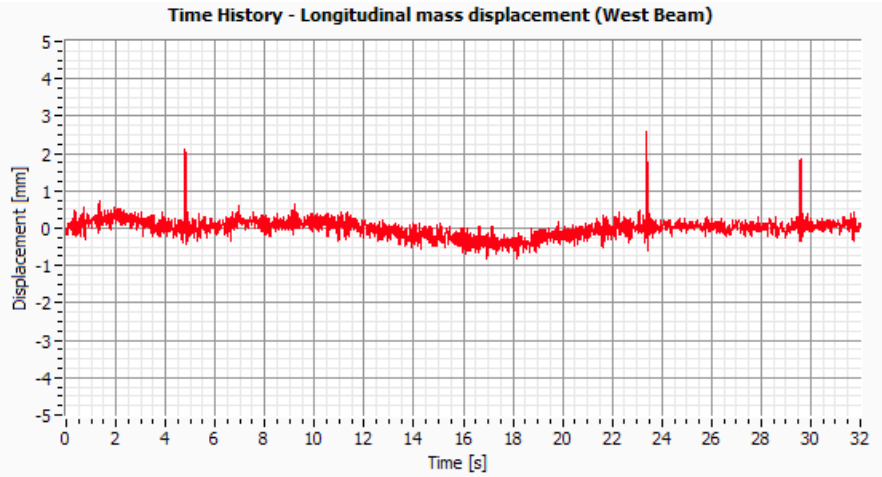

Figure IV.121: Longitudinal table displacement –S (Channel 22).

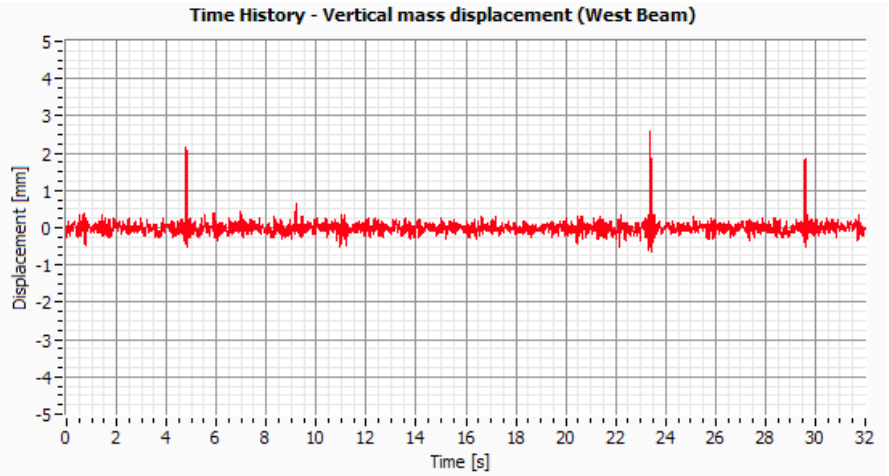

Figure IV.122: Vertical table displacement –S (Channel 23).

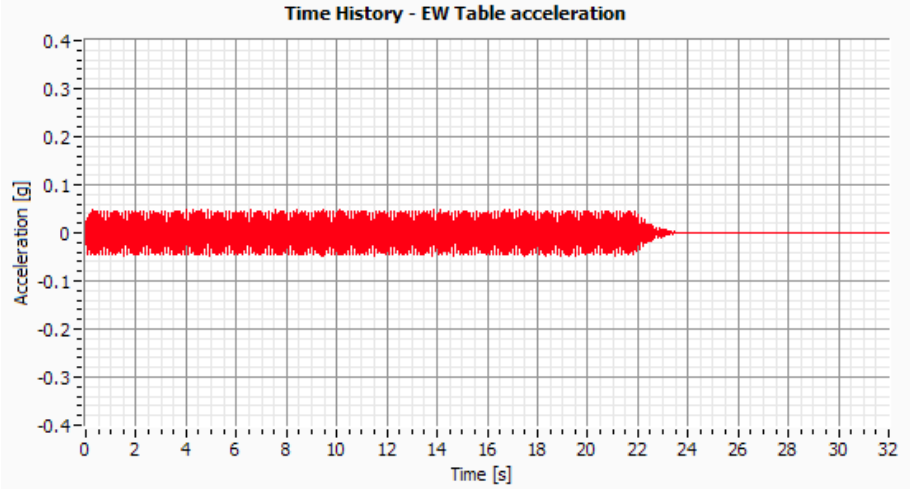

Figure IV.123: EW Table acceleration (Channel 24).

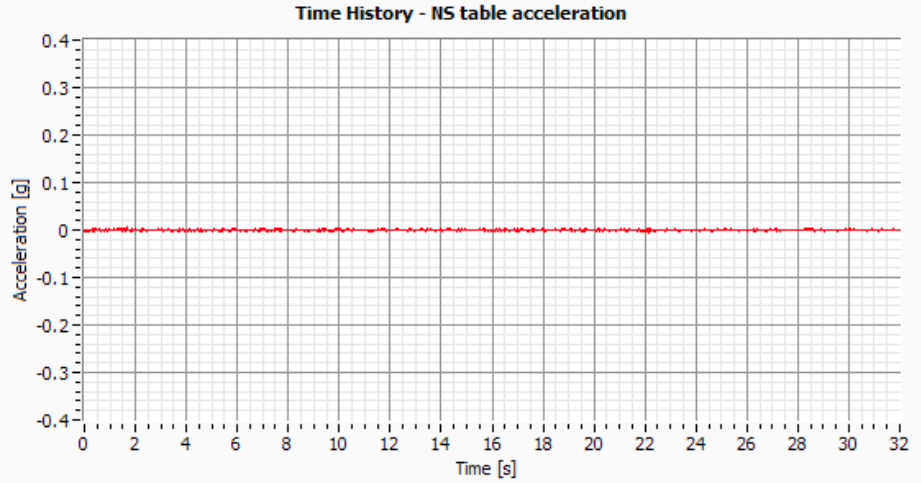

Figure IV.124: NS Table acceleration (Channel 25).

Test 9 – Cat03 (EW PGA=0.05g)

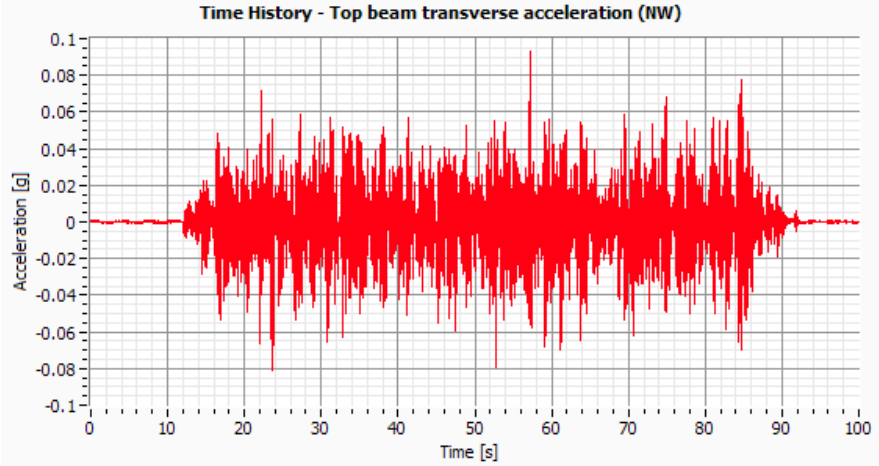

Figure IV.125: NW Top beam acceleration (Channel 1).

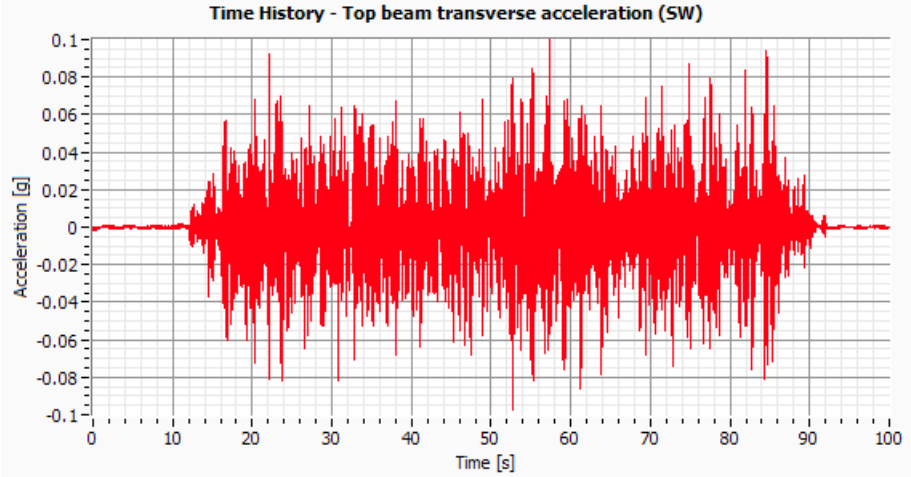

Figure IV.126: SW Top beam acceleration (Channel2).

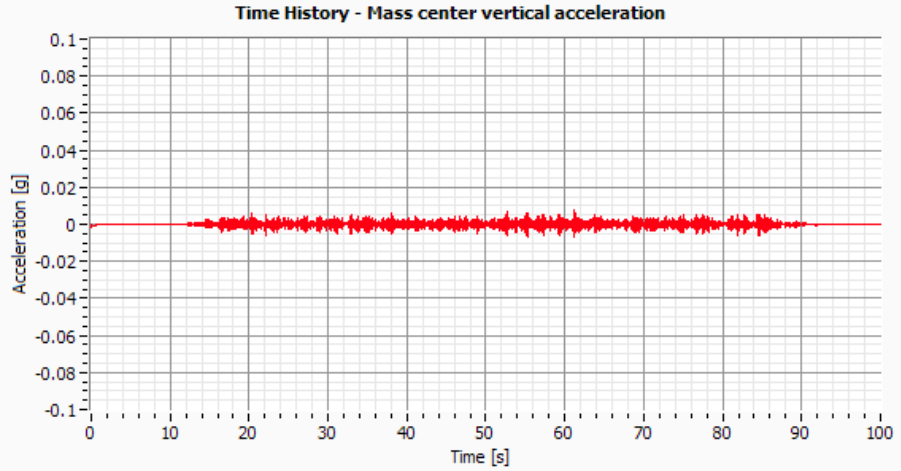

Figure IV.127: Mass center vertical acceleration (Channel 3).

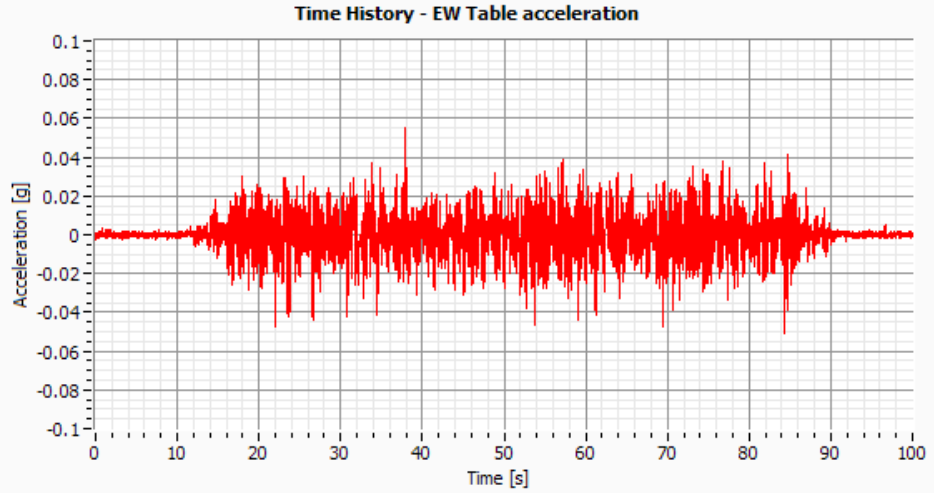

Figure IV.128: EW Table acceleration (Channel 24).

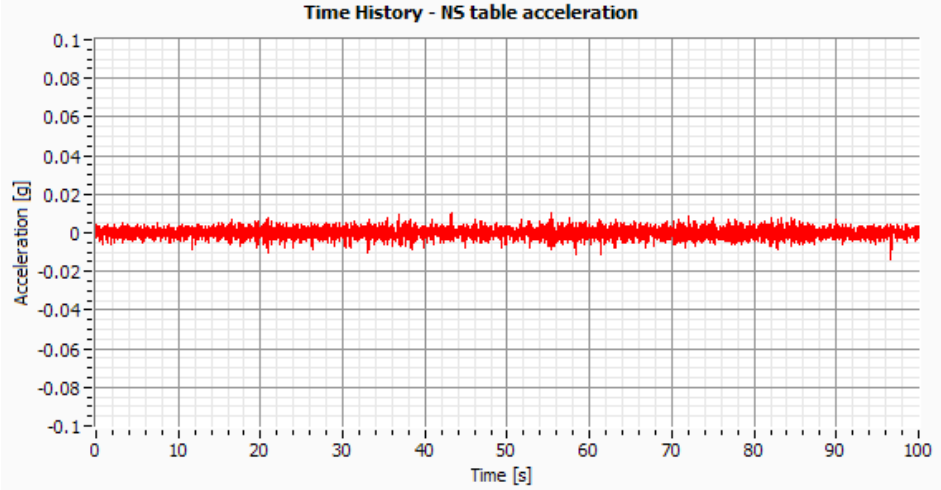

Figure IV.129: NS Table acceleration (Channel 25).

Test 10 – Artificial EC8 (EW PGA=0.60g)

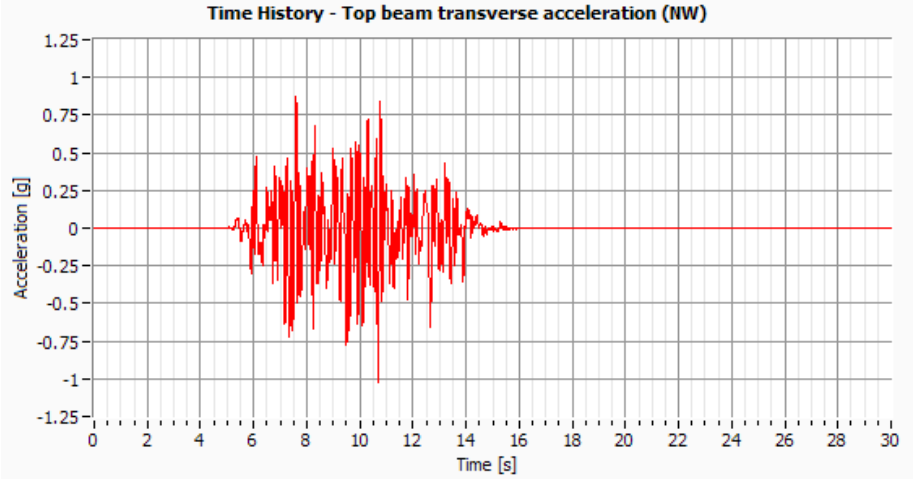

Figure IV.130: NW Top beam acceleration (Channel 1).

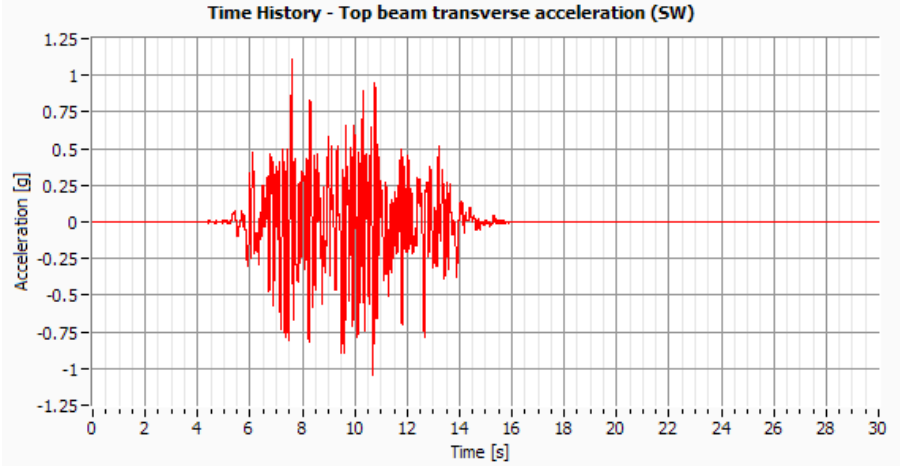

Figure IV.131: SW Top beam acceleration (Channel2).

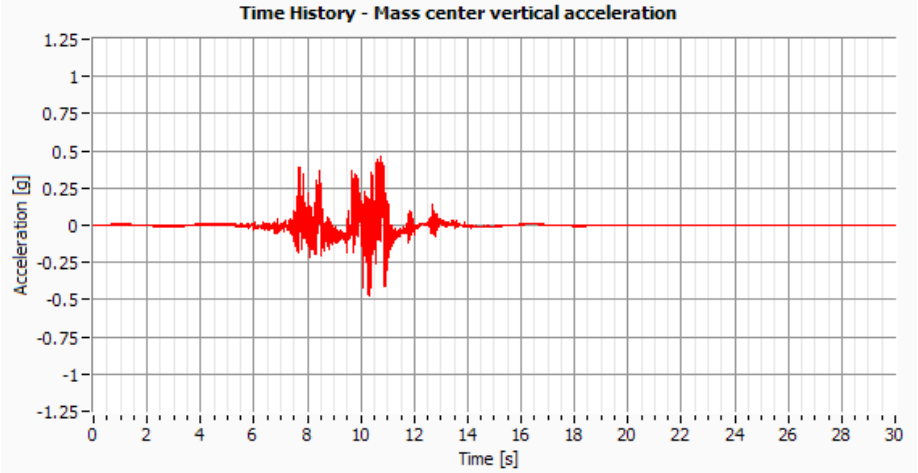

Figure IV.132: Mass center vertical acceleration (Channel 3).

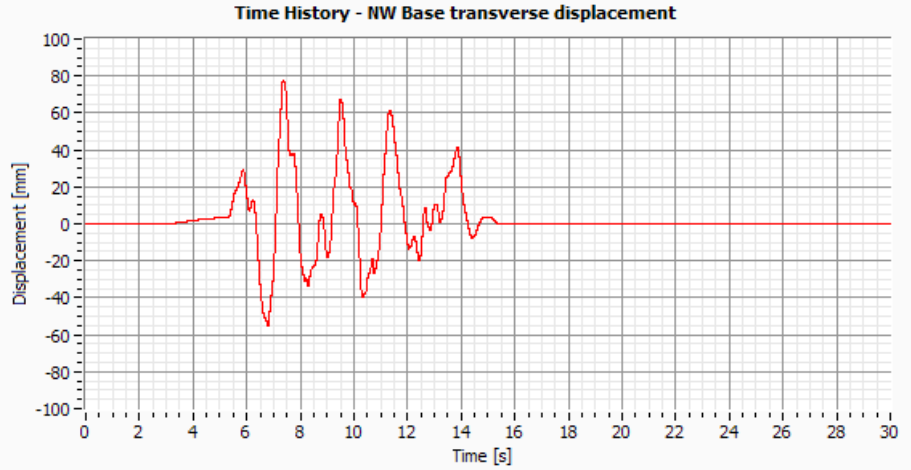

Figure IV.133: NW Base transverse displacement (Channel4).

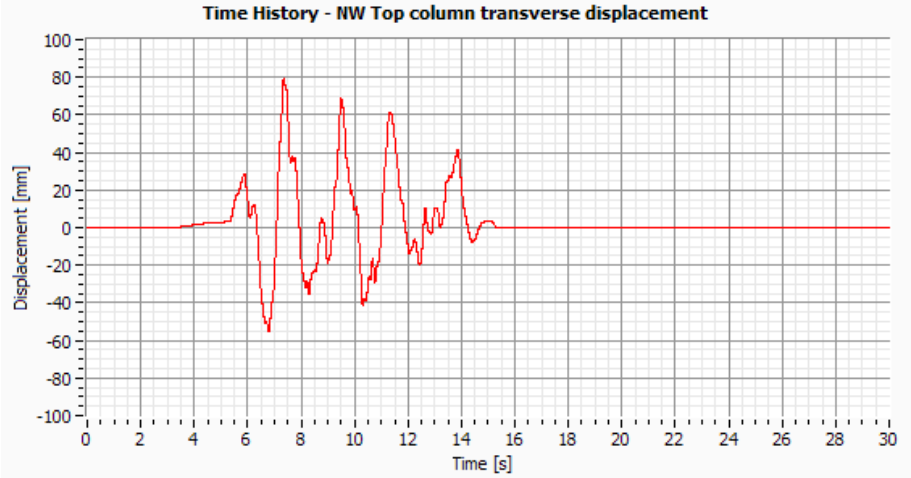

Figure IV.134: NW Top column transverse displacement (Channel5).

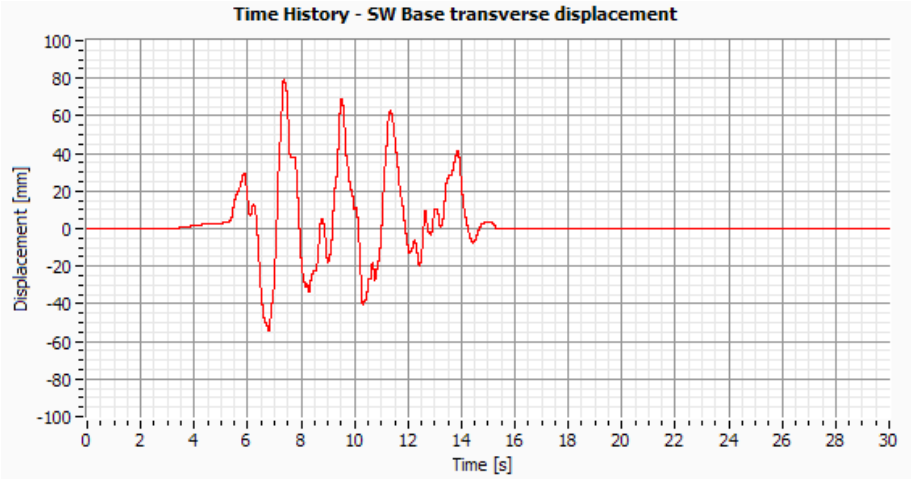

Figure IV.135: SW Base transverse displacement (Channel6).

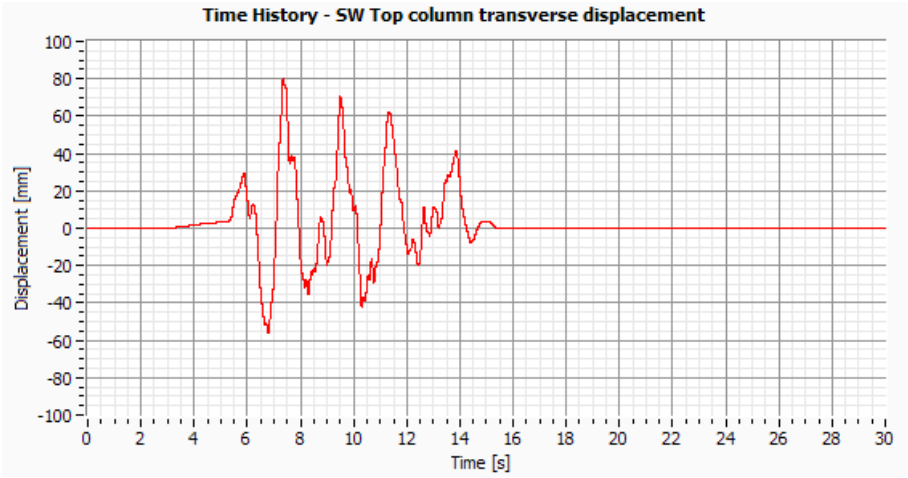

Figure IV.136: SW Top column transverse displacement (Channel7).

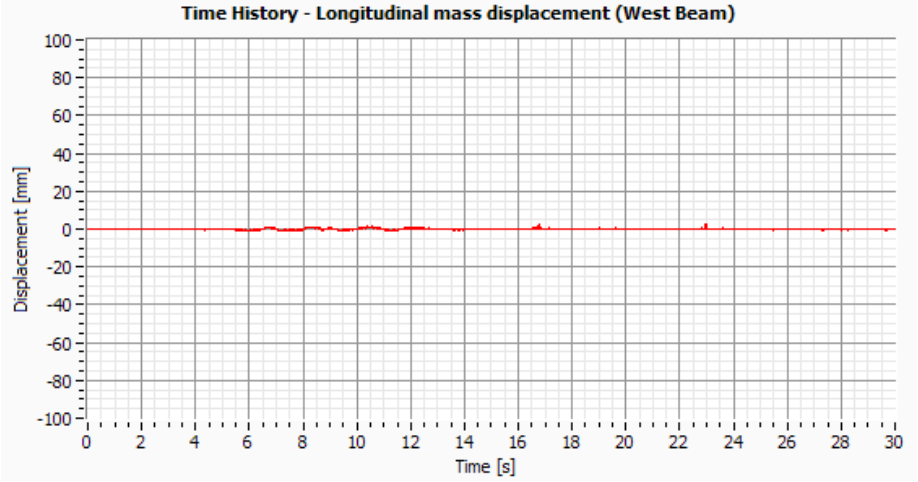

Figure IV.137: Longitudinal mass displacement in the West beam (Channel 8).

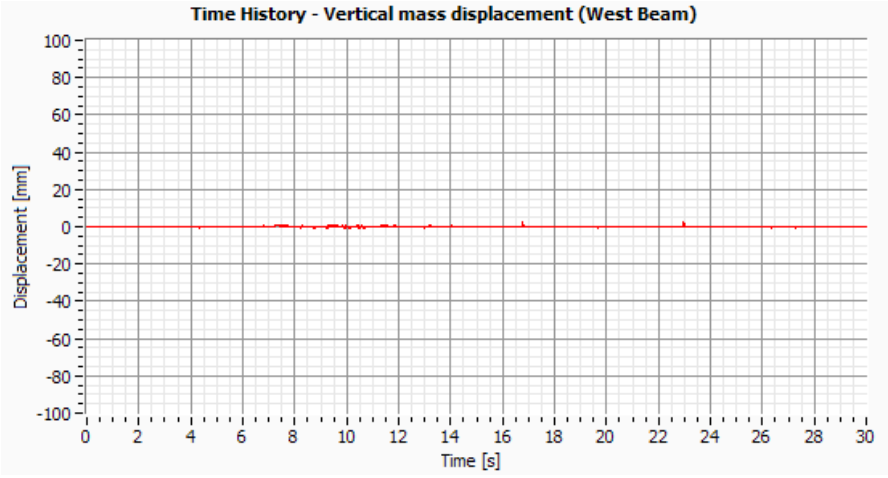

Figure IV.138: Vertical mass displacement in the West beam (Channel9).

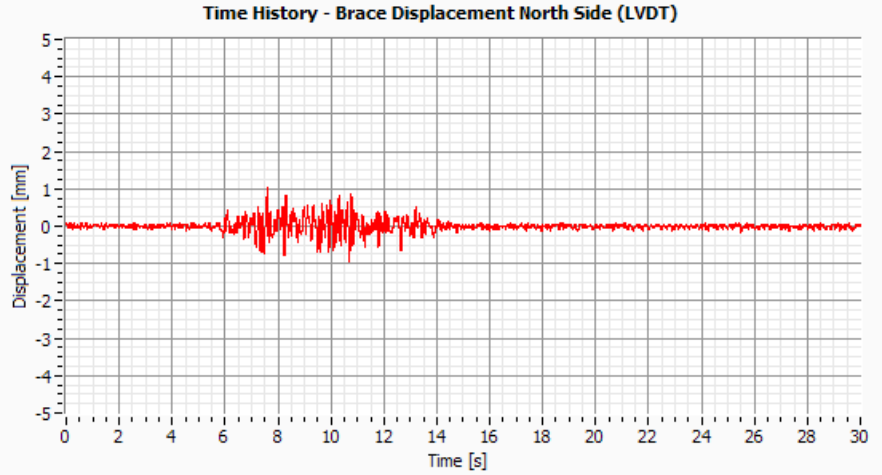

Figure IV.139: Brace displacement North side (Channel10).

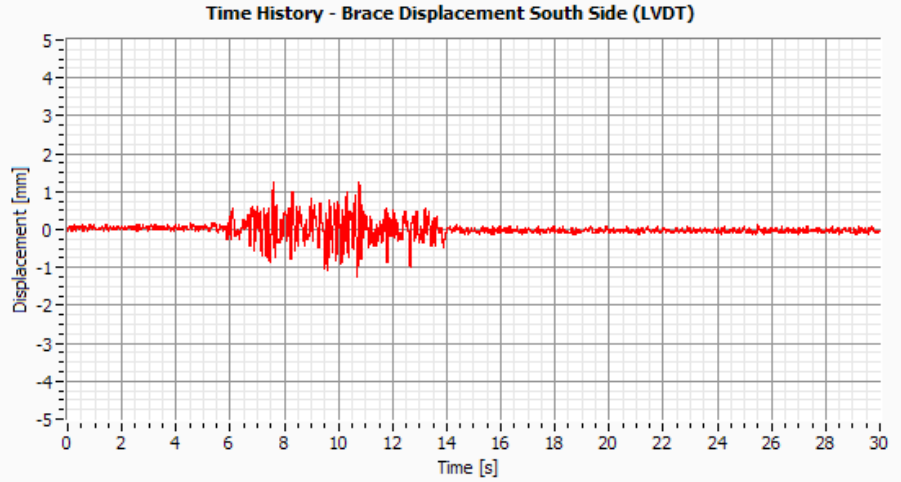

Figure IV.140: Brace displacement South side (Channel11).

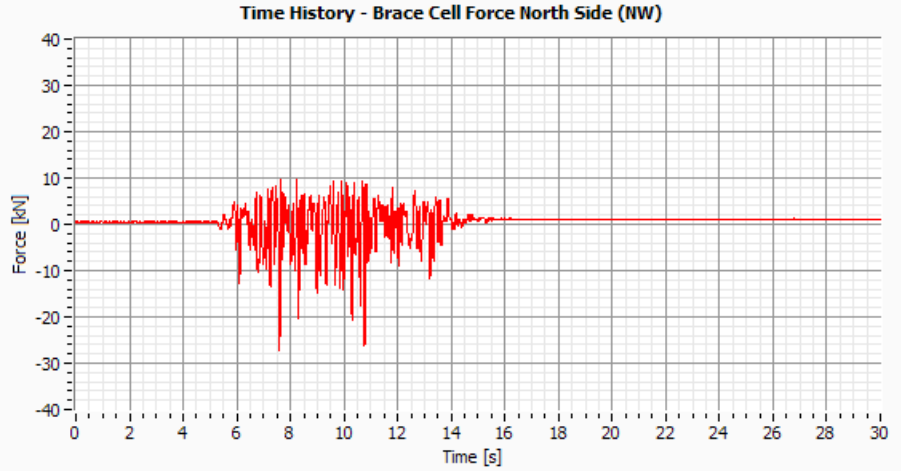

Figure IV.141: Brace cell force North Side – NW (Channel14).

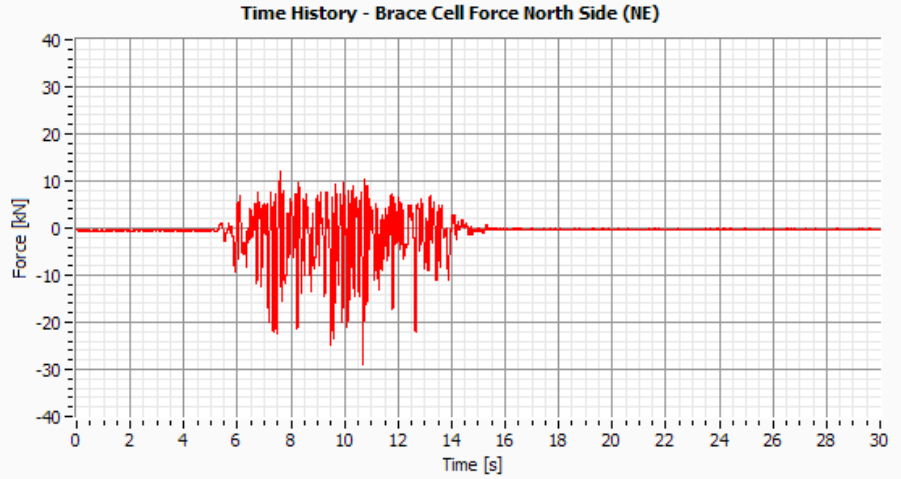

Figure IV.142: Brace cell force North Side – NE (Channel15).

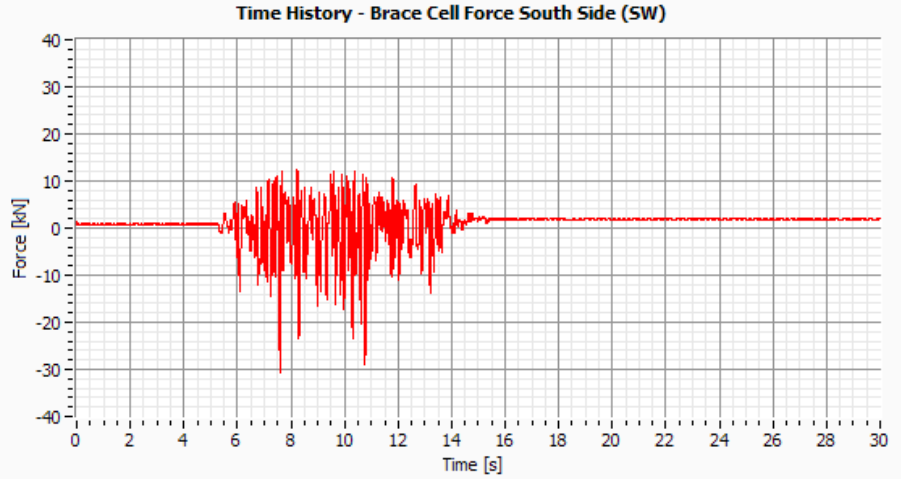

Figure IV.143: Brace cell force South Side – SW (Channel16).

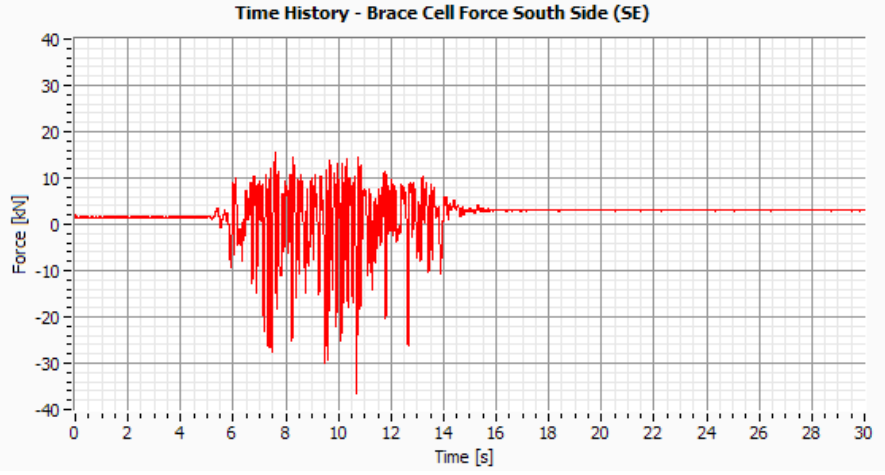

Figure IV.144: Brace cell force South Side – NE (Channel17).

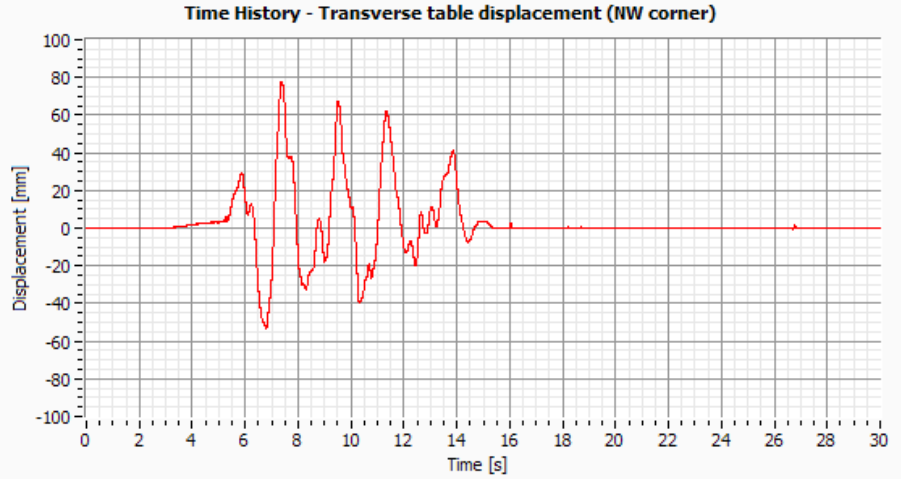

Figure IV.145: Transverse table displacement in the NW corner (Channel18).

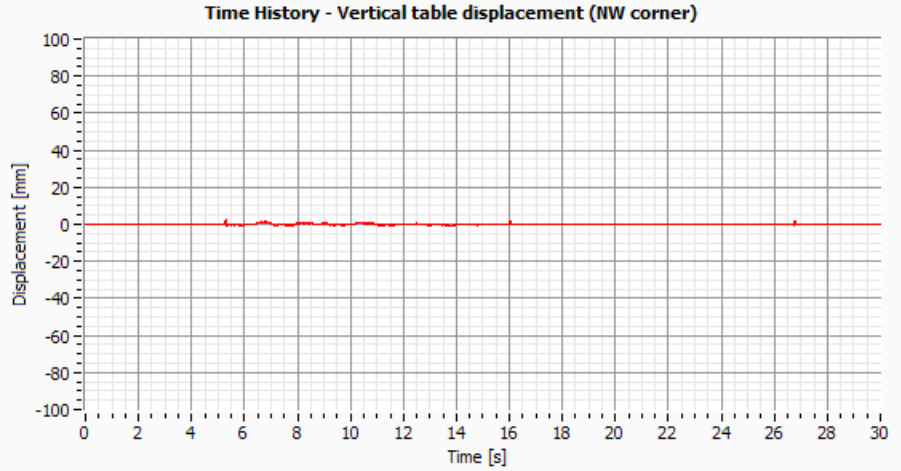

Figure IV.146: Vertical table displacement in the NW corner (Channel19).

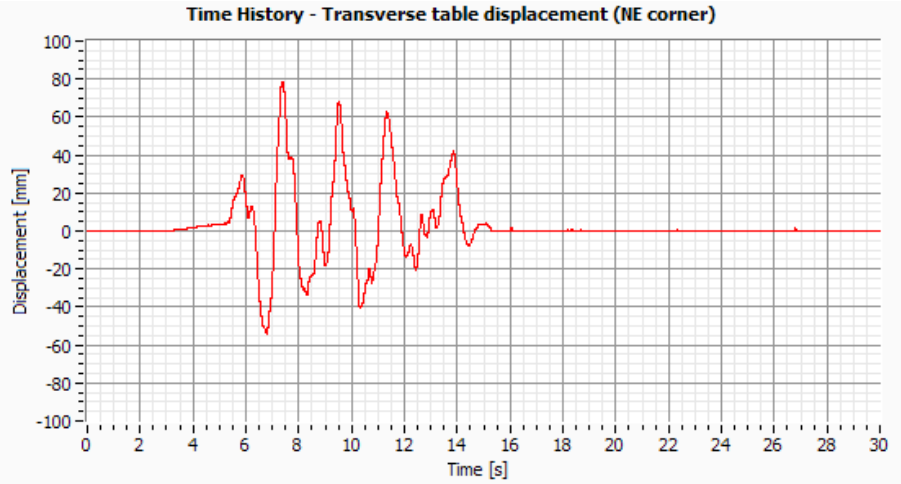

Figure IV.147: Transverse table displacement in the NE corner (Channel 20).

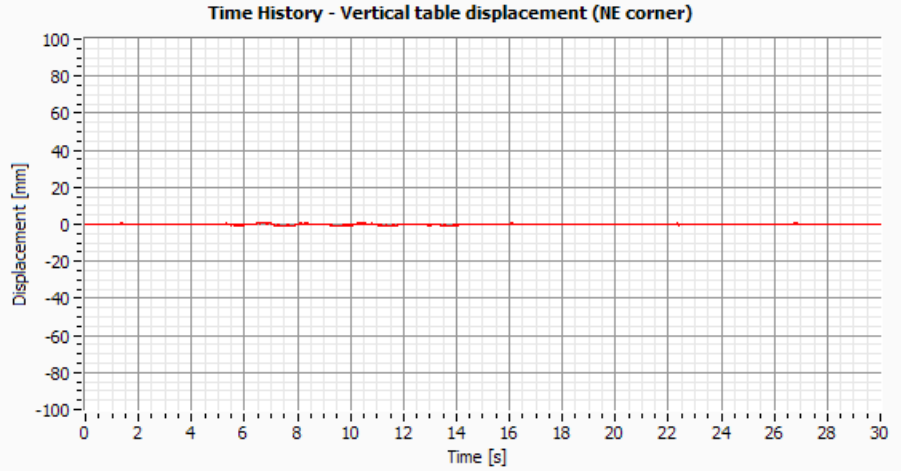

Figure IV.148: Vertical table displacement in the NE corner (Channel 21).

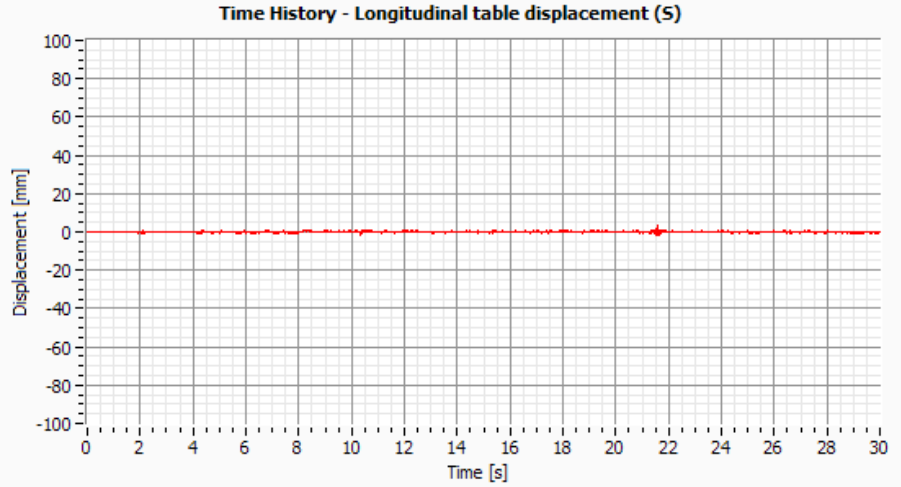

Figure IV.149: Longitudinal table displacement –S (Channel 22).

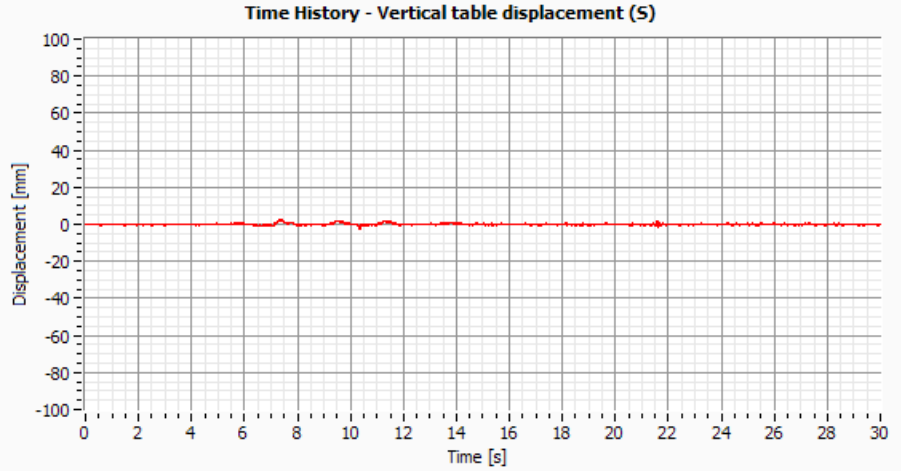

Figure IV.150: Vertical table displacement –S (Channel 23).

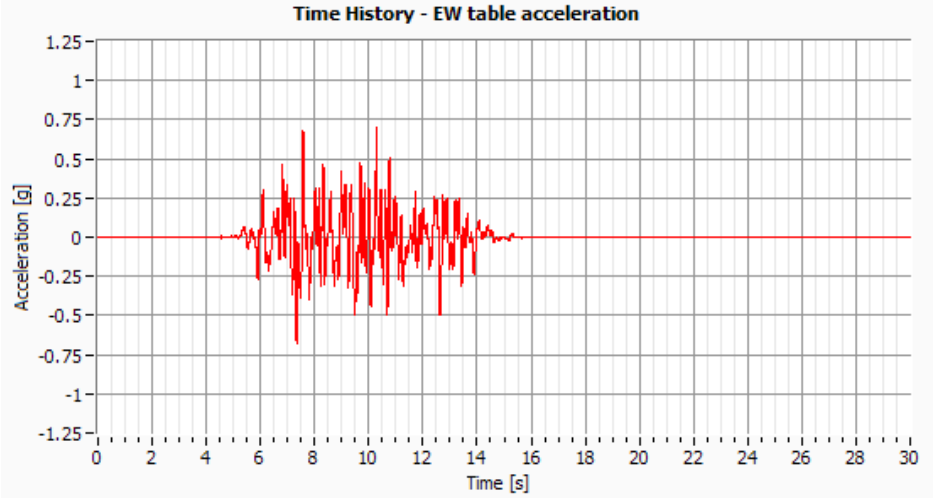

Figure IV.151: EW Table acceleration (Channel 24).

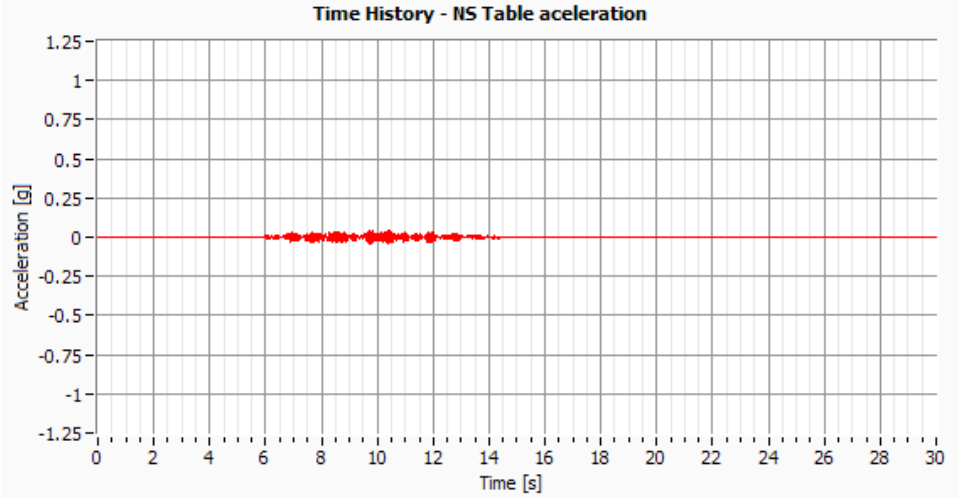

Figure IV.152: NS Table acceleration (Channel 25).

Test 11 – Cat04 (EW PGA=0.05g)

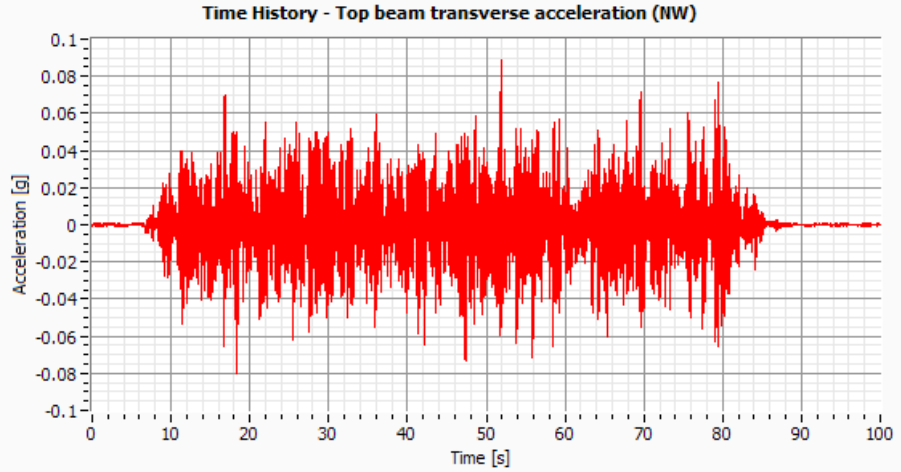

Figure IV.153: NW Top beam acceleration (Channel 1).

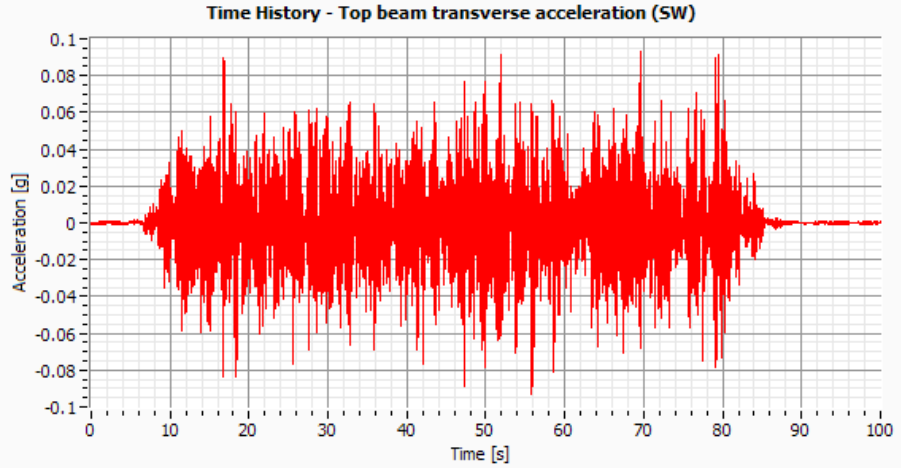

Figure IV.154: SW Top beam acceleration (Channel2).

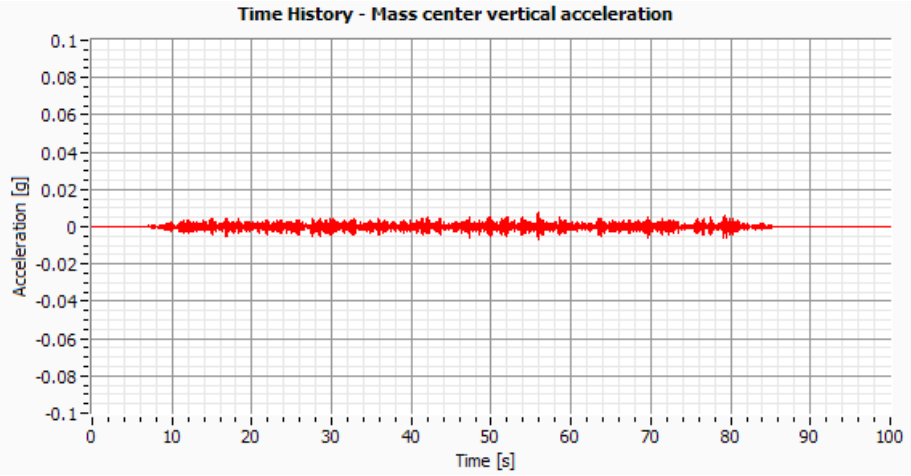

Figure IV.155: Mass center vertical acceleration (Channel 3).

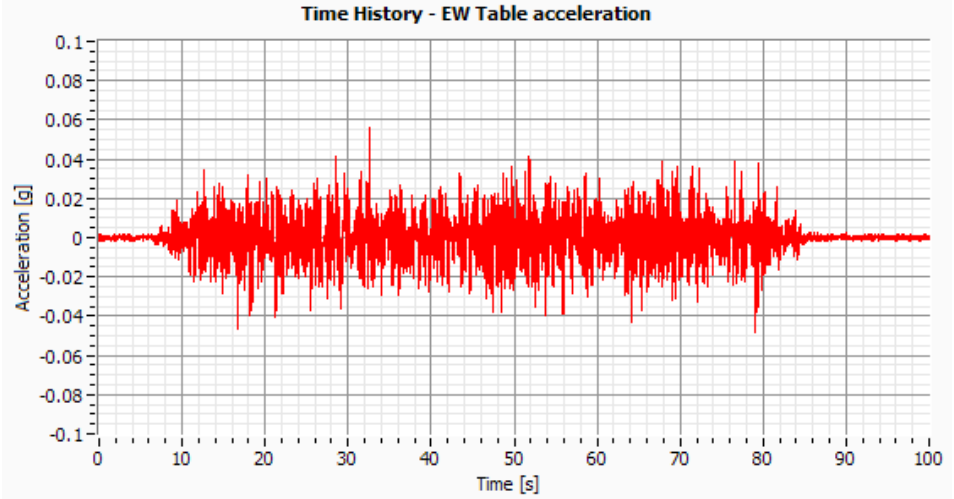

Figure IV.156: EW Table acceleration (Channel 24).

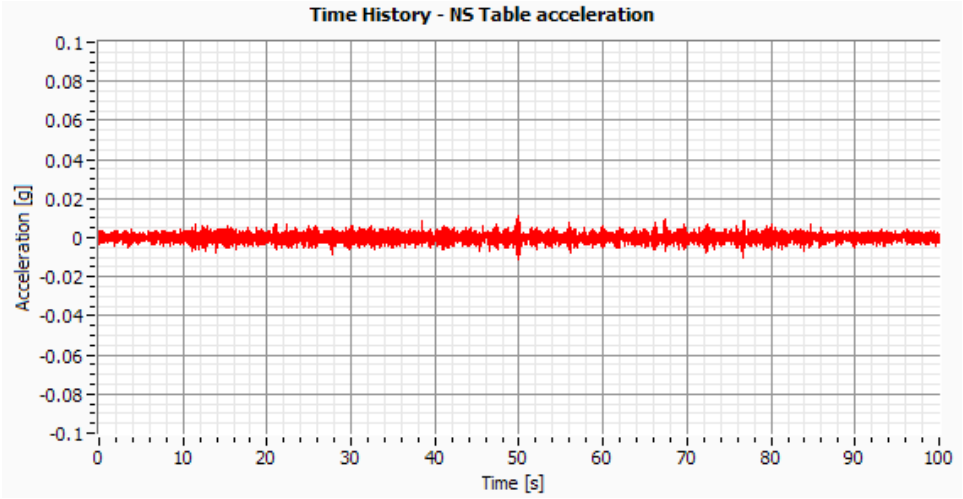

Figure IV.157: NS Table acceleration (Channel 25).

Test 12 – Artificial EC8 (EW PGA=0.80g)

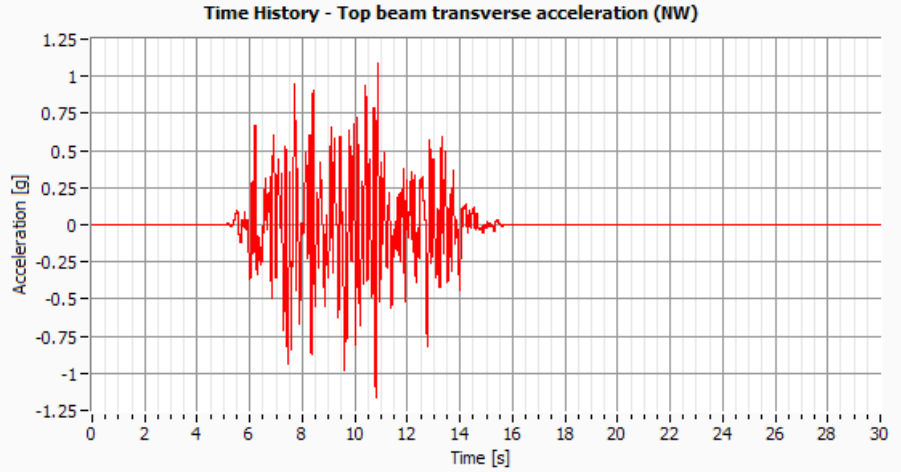

Figure IV.158: NW Top beam acceleration (Channel 1).

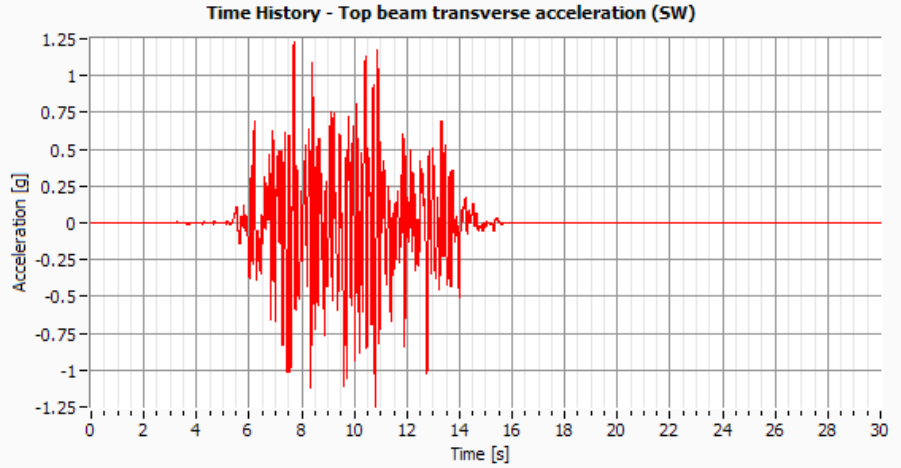

Figure IV.159: SW Top beam acceleration (Channel2).

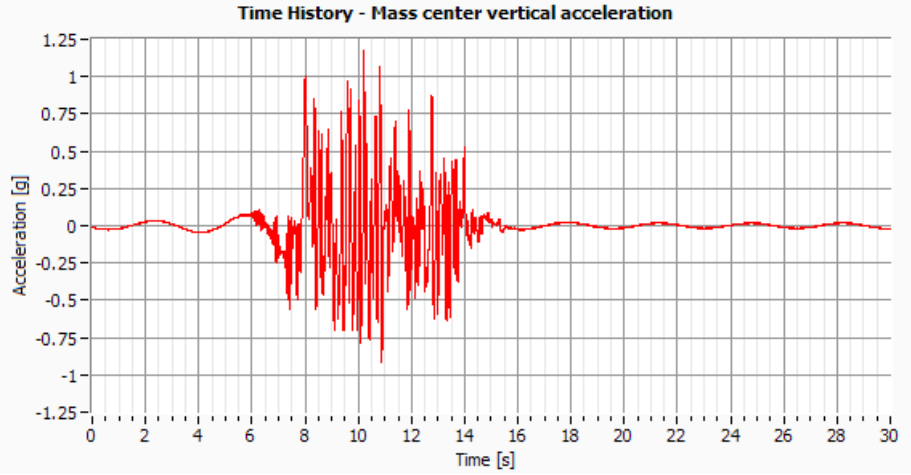

Figure IV.160: Mass center vertical acceleration (Channel 3).

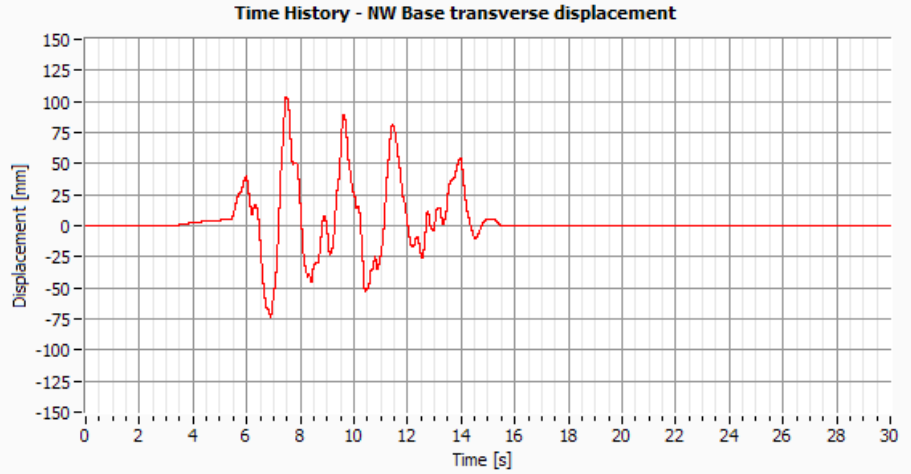

Figure IV.161: NW Base transverse displacement (Channel4).

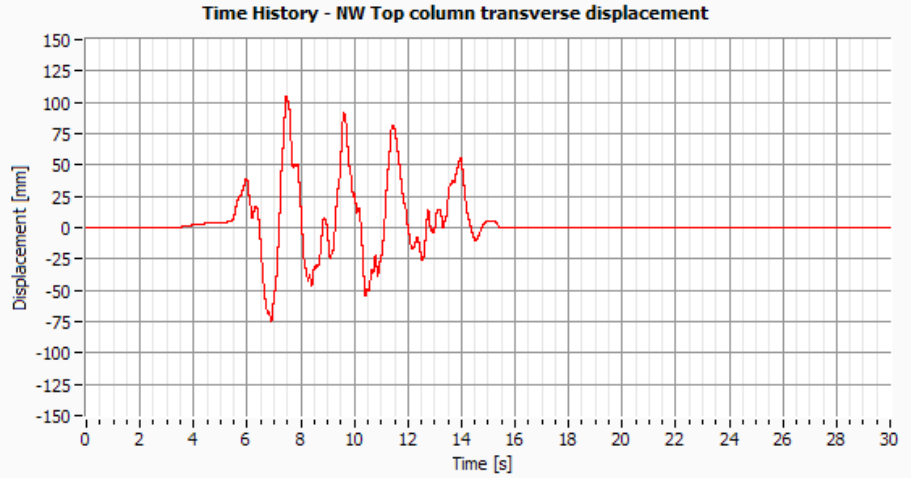

Figure IV.162: NW Top column transverse displacement (Channel5).

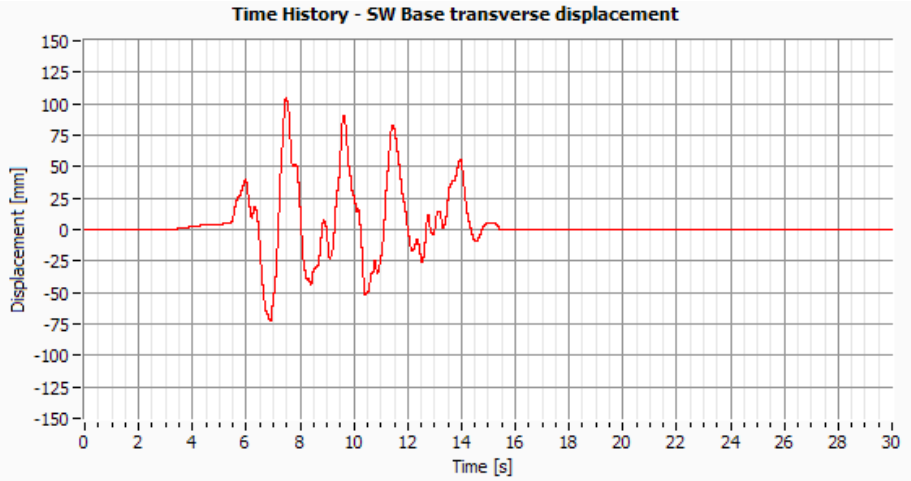

Figure IV.163: SW Base transverse displacement (Channel6).

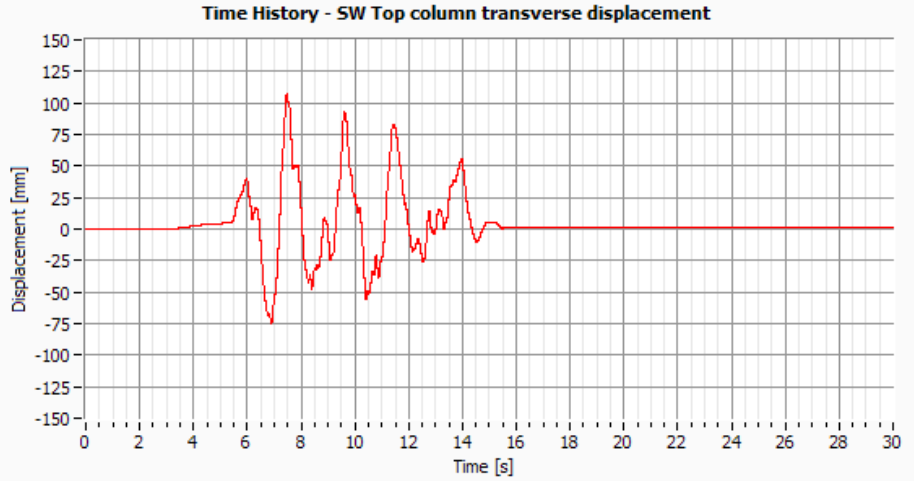

Figure IV.164: SW Top column transverse displacement (Channel7).

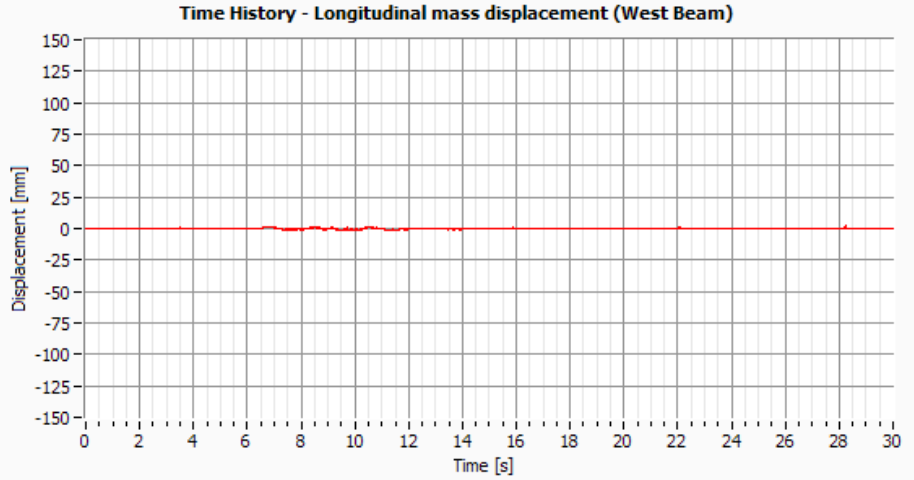

Figure IV.165: Longitudinal mass displacement in the West beam (Channel 8).

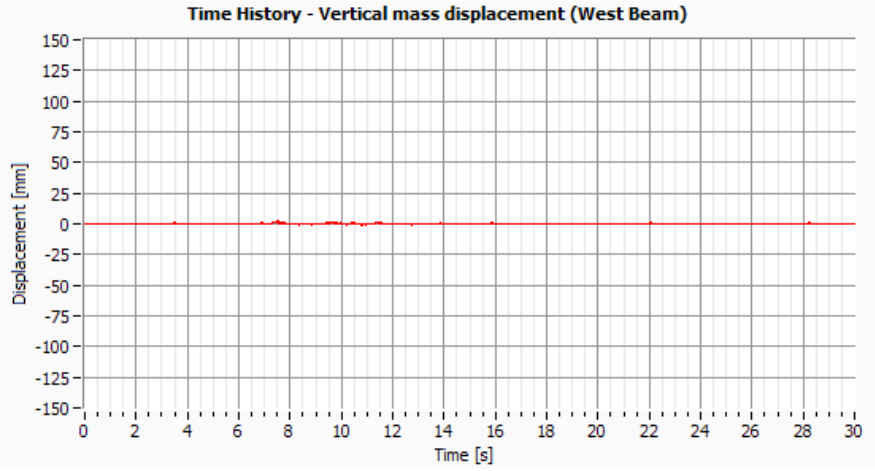

Figure IV.166: Vertical mass displacement in the West beam (Channel9).

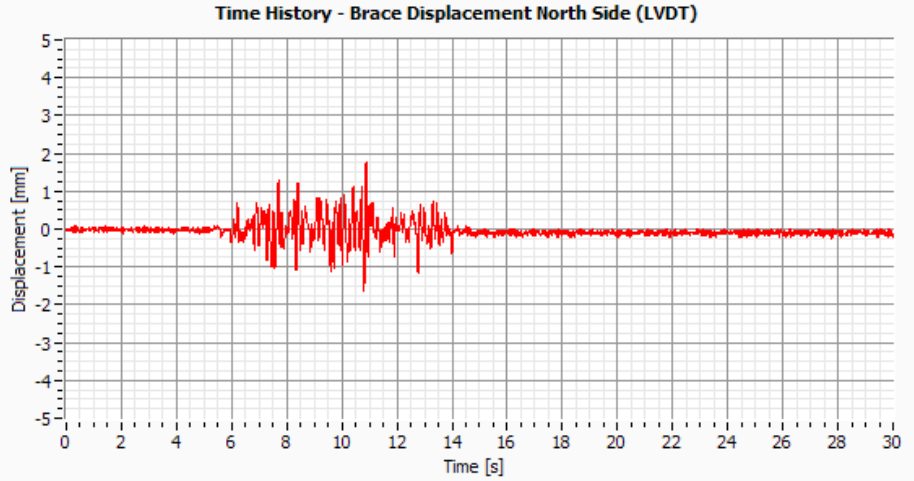

Figure IV.167: Brace displacement North side (Channel10).

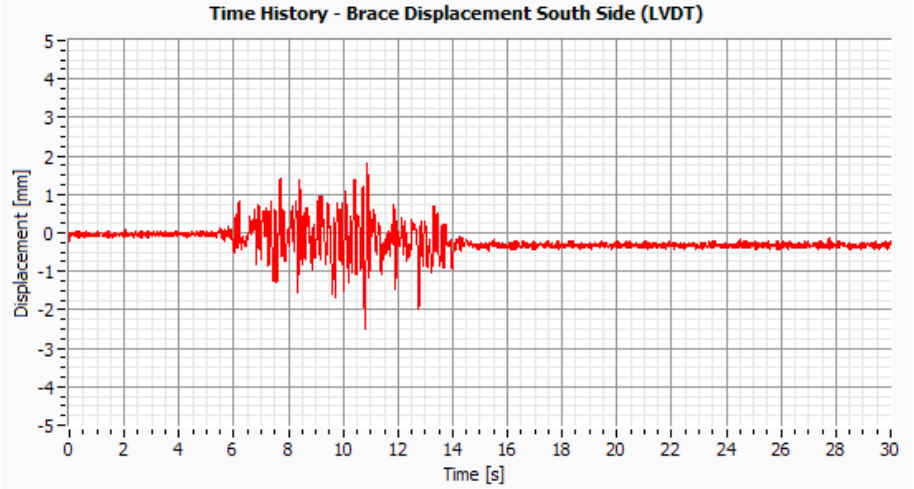

Figure IV.168: Brace displacement South side (Channel11).

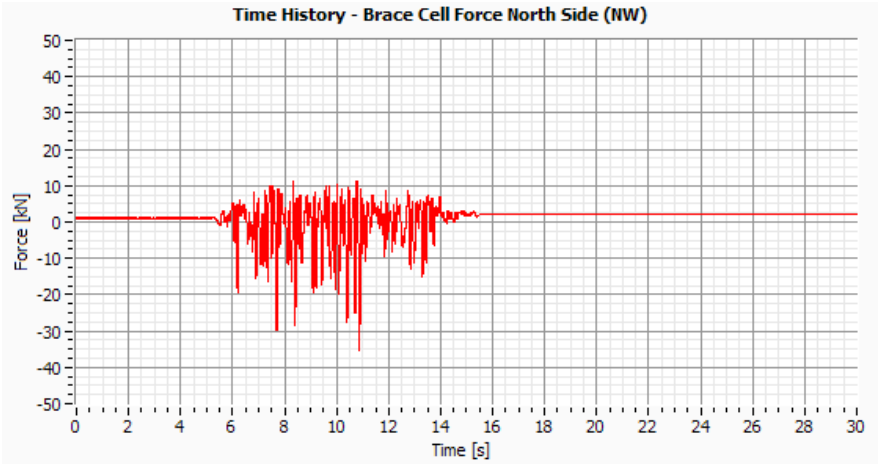

Figure IV.169: Brace cell force North Side – NW (Channel14).

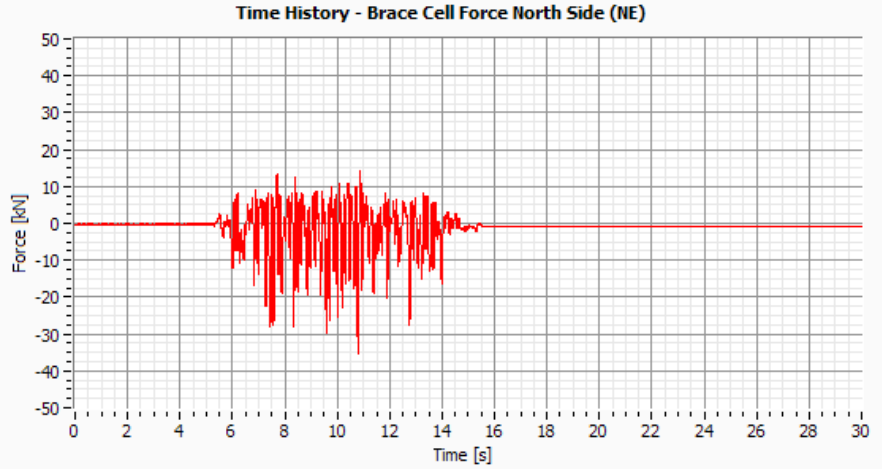

Figure IV.170: Brace cell force North Side – NE (Channel15).

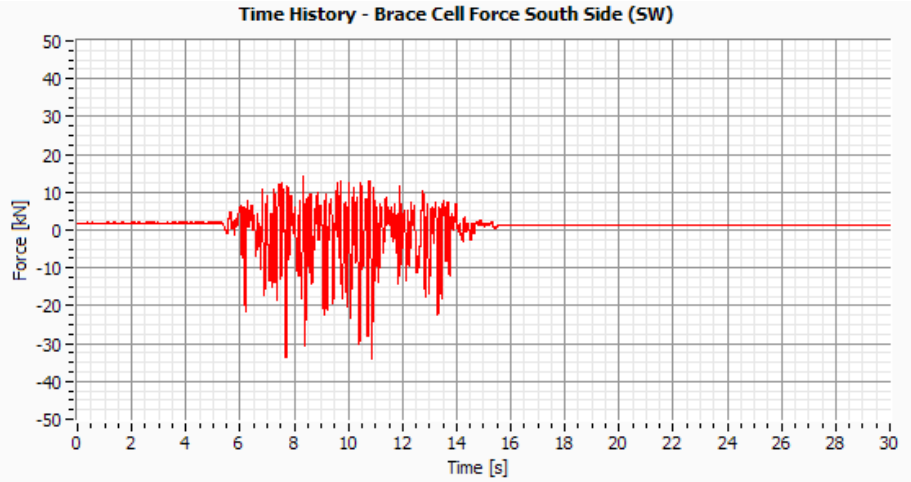

Figure IV.171: Brace cell force South Side – SW (Channel16).

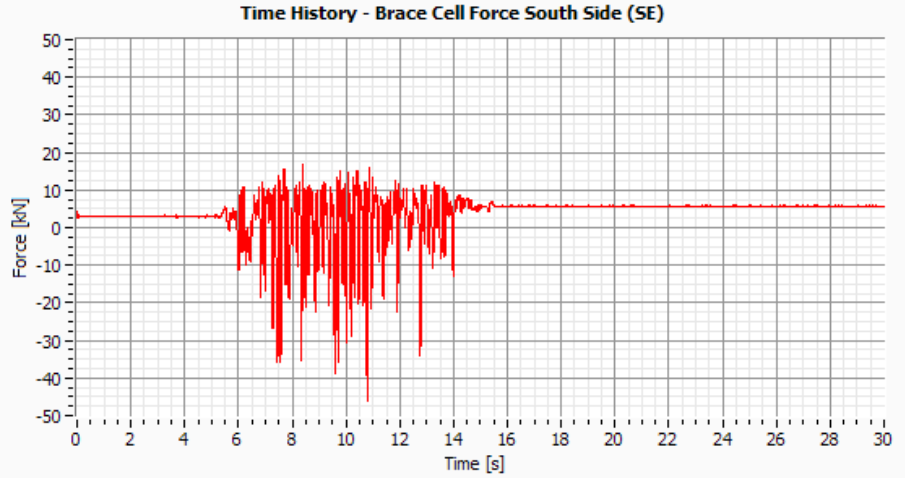

Figure IV.172: Brace cell force South Side – NE (Channel17).

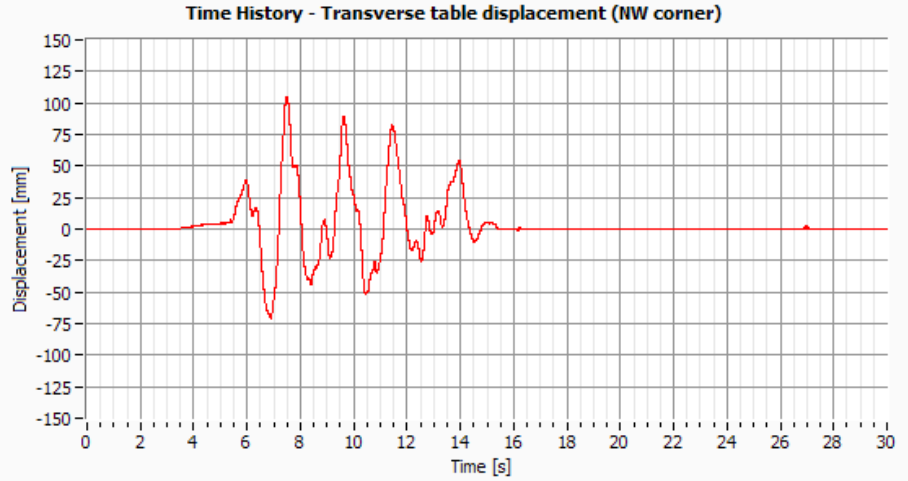

Figure IV.173: Transverse table displacement in the NW corner (Channel18).

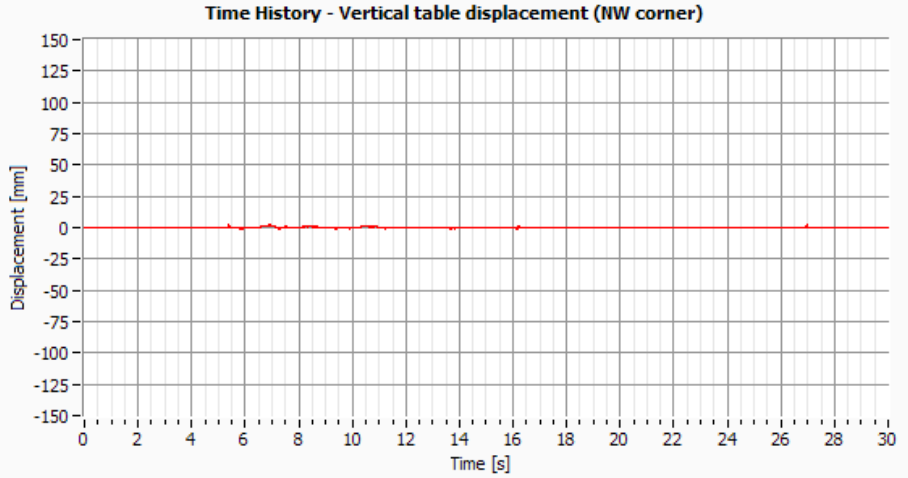

Figure IV.174: Vertical table displacement in the NW corner (Channel19).

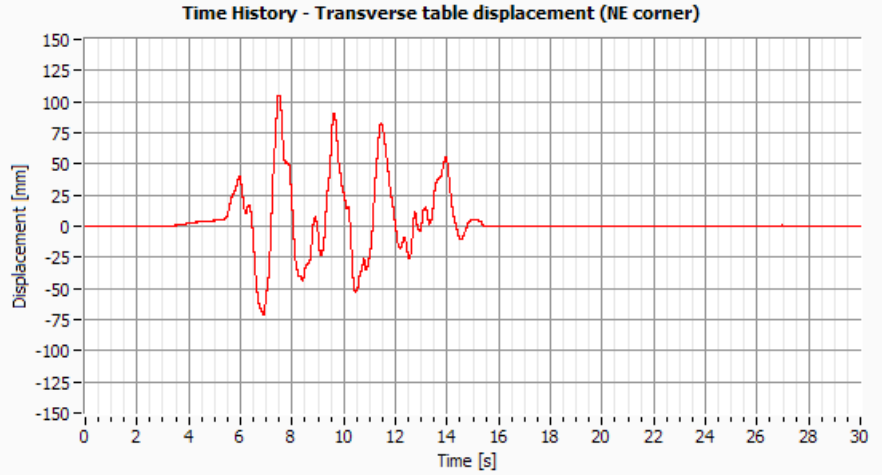

Figure IV.175: Transverse table displacement in the NE corner (Channel 20).

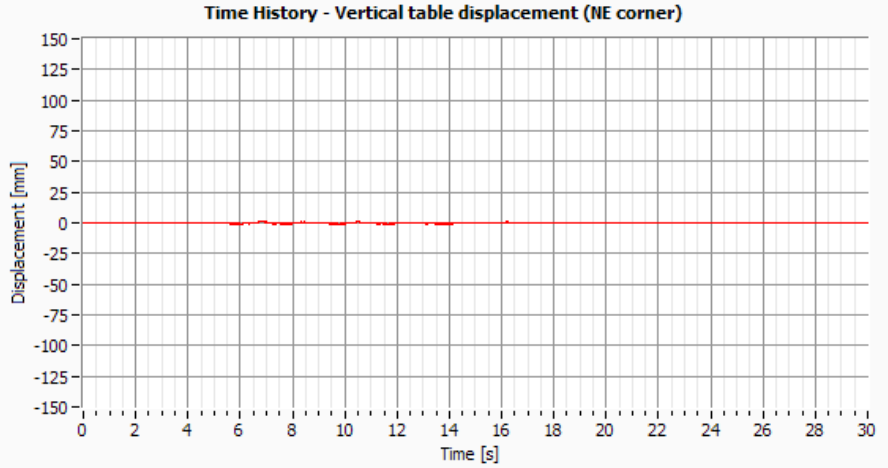

Figure IV.176: Vertical table displacement in the NE corner (Channel 21).

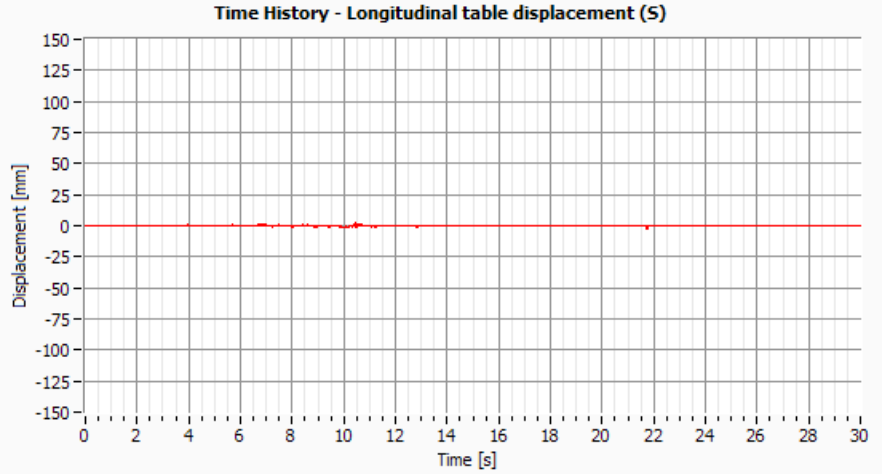

Figure IV.177: Longitudinal table displacement –S (Channel 22).

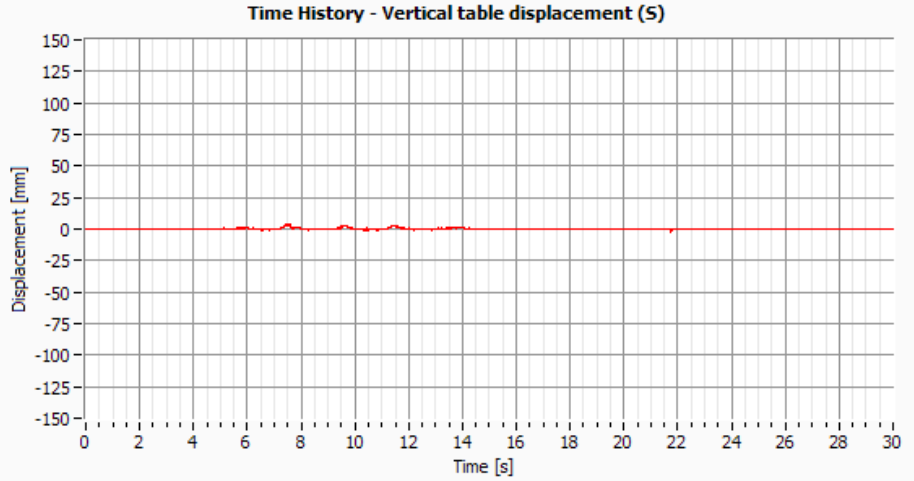

Figure IV.178: Vertical table displacement –S (Channel 23).

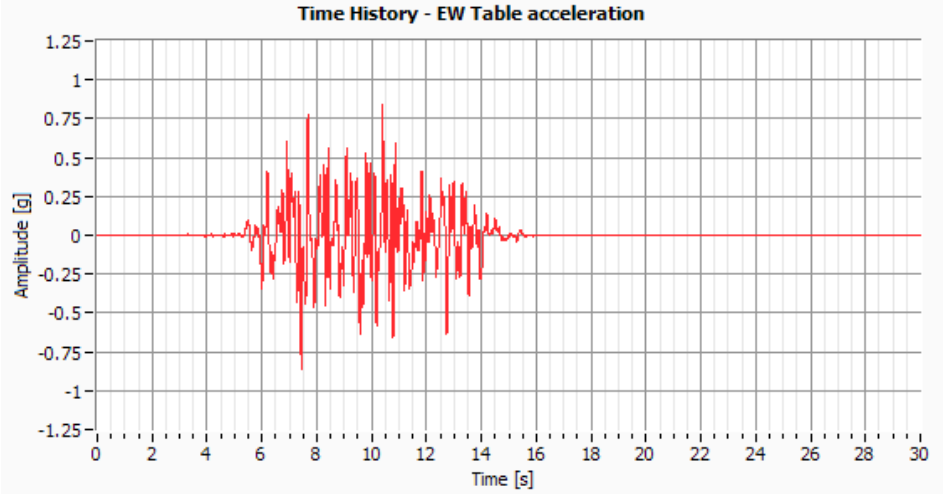

Figure IV.179: EW Table acceleration (Channel 24).

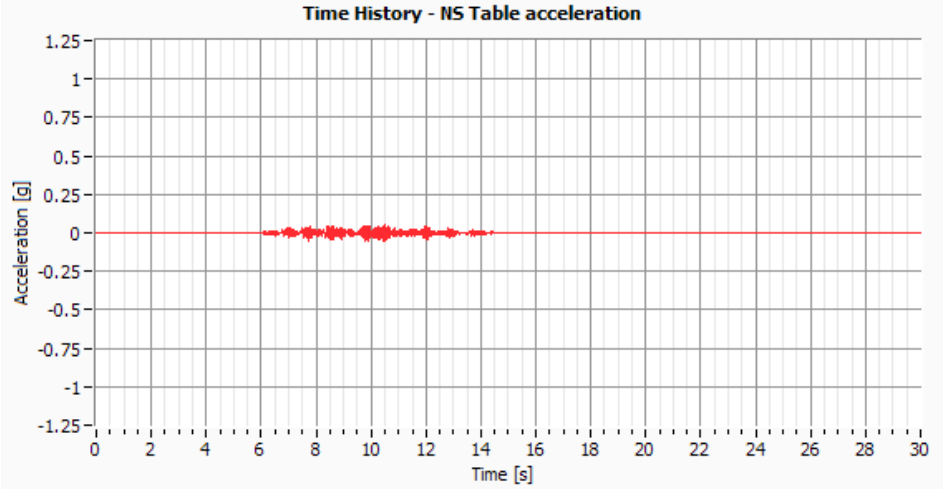

Figure IV.180: NS Table acceleration (Channel 25).

Test 13 – Cat05 (EW PGA=0.05g)

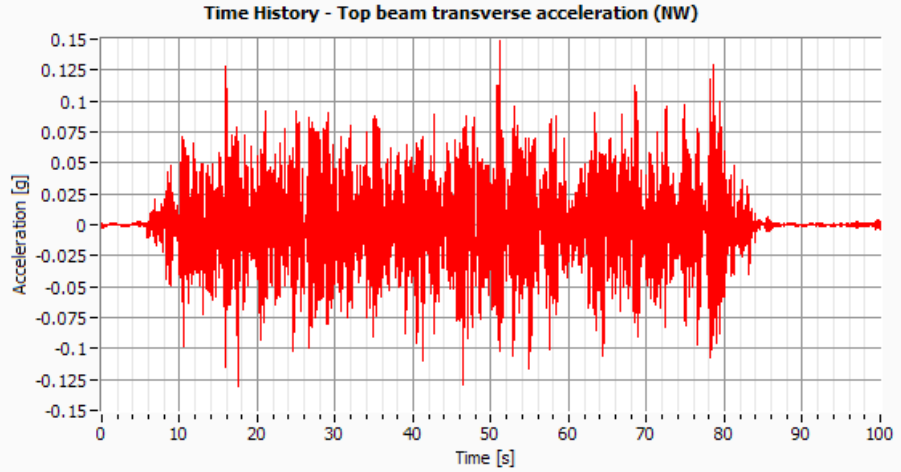

Figure IV.181: NW Top beam acceleration (Channel 1).

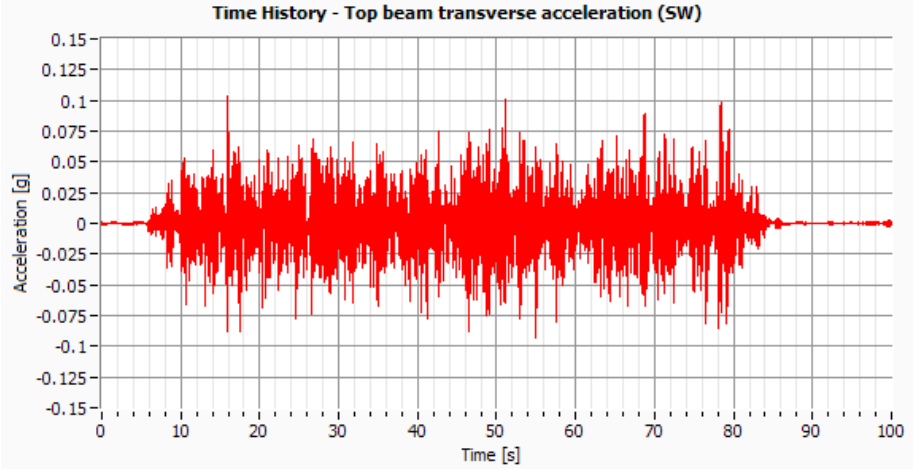

Figure IV.182: SW Top beam acceleration (Channel2).

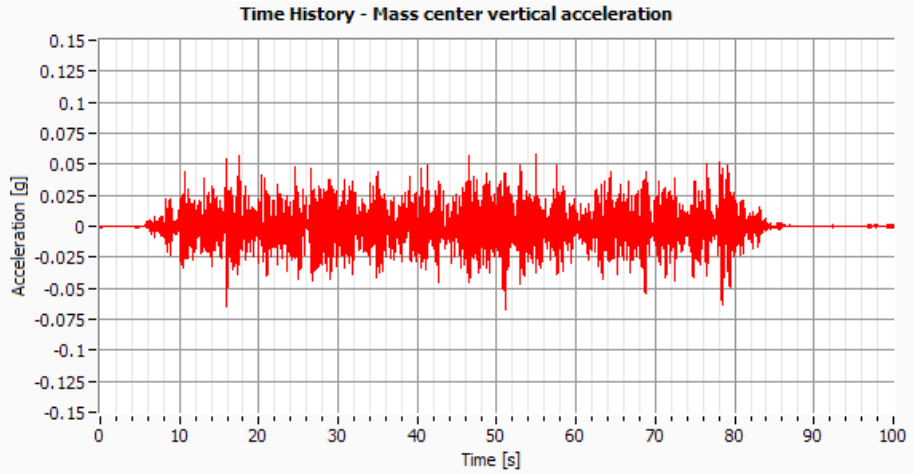

Figure IV.183: Mass center vertical acceleration (Channel 3).

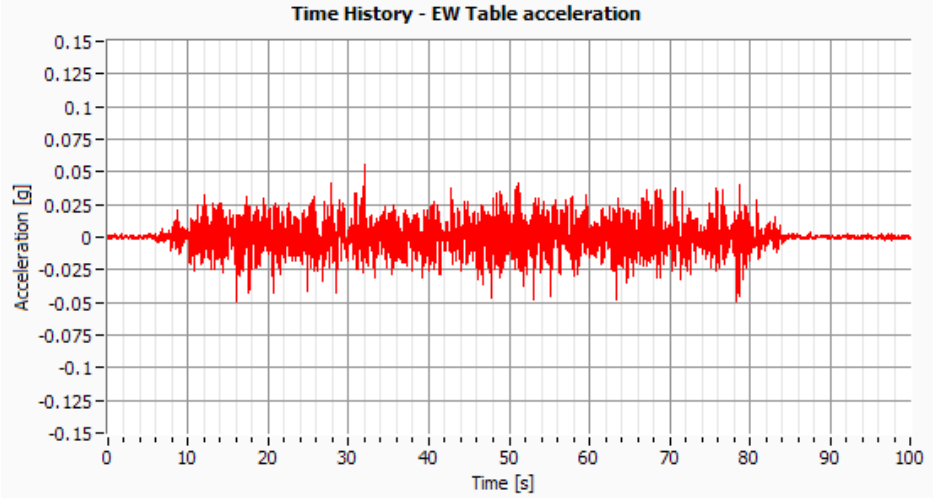

Figure IV.184: EW Table acceleration (Channel 24).

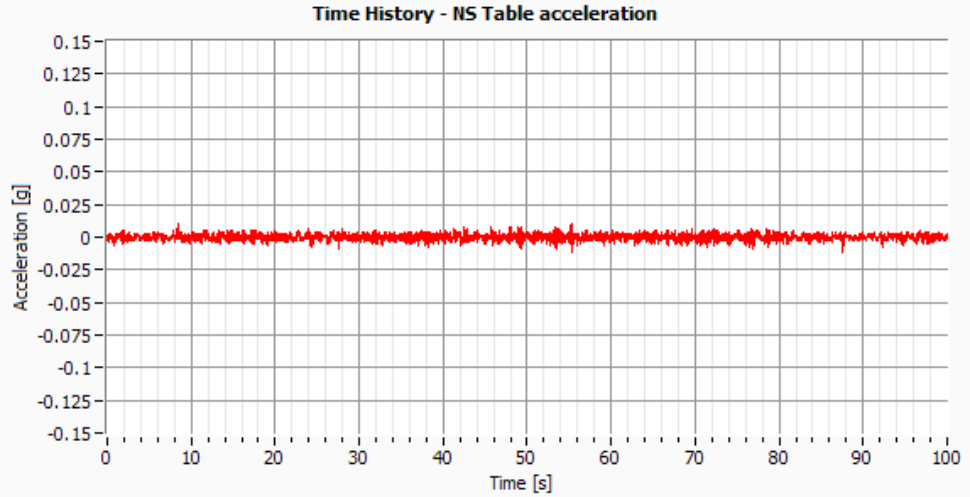

Figure IV.185: NS Table acceleration (Channel 25).

Test 14 – Artificial EC8 (EW PGA=1.0g)

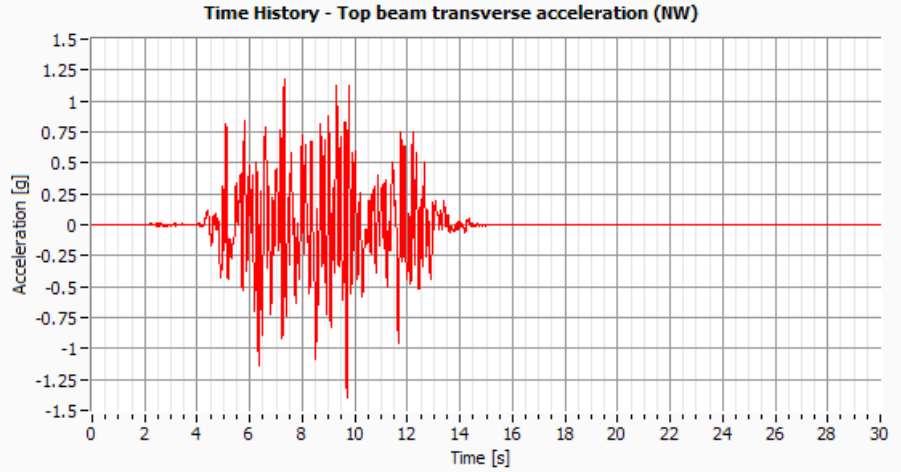

Figure IV.186: NW Top beam acceleration (Channel 1).

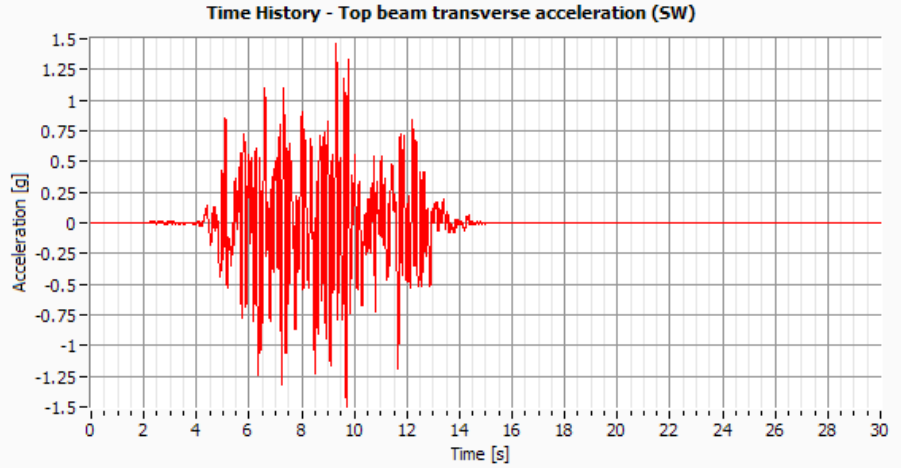

Figure IV.187: SW Top beam acceleration (Channel2).

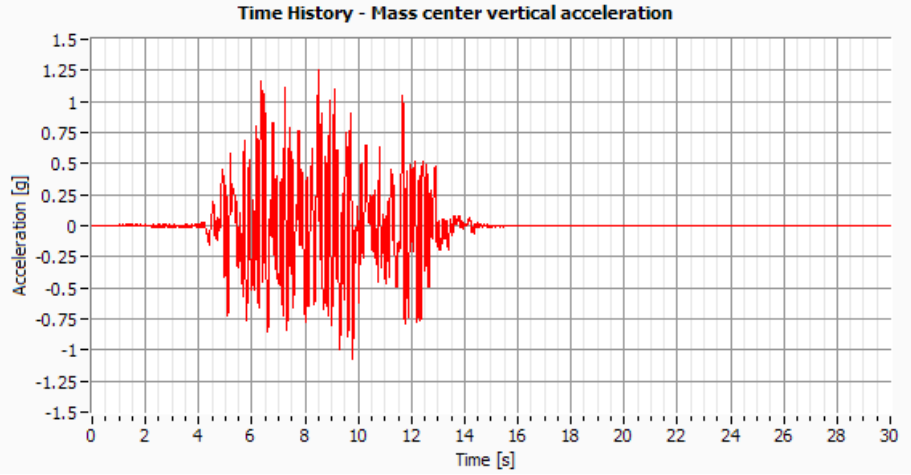

Figure IV.188: Mass center vertical acceleration (Channel 3).

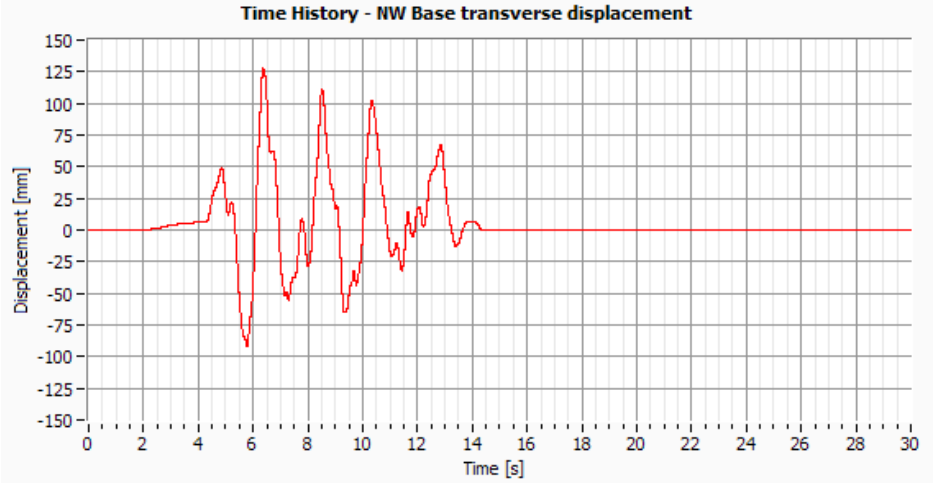

Figure IV.189: NW Base transverse displacement (Channel4).

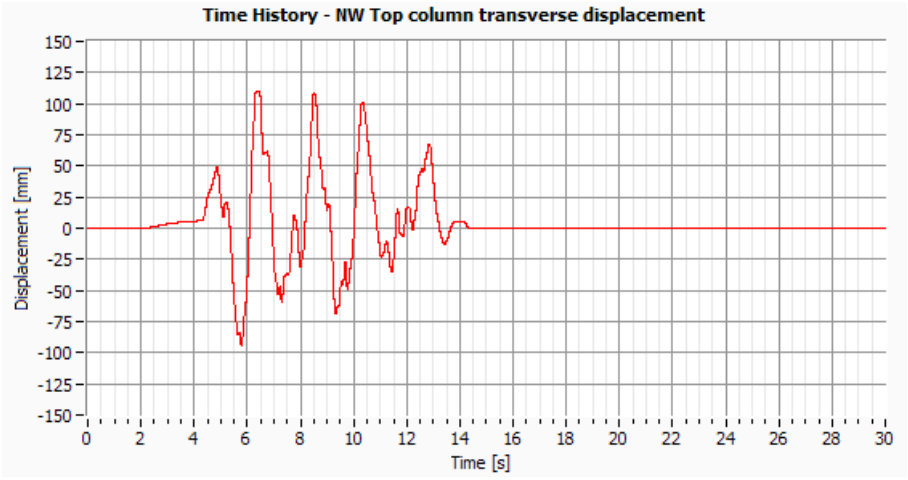

Figure IV.190: NW Top column transverse displacement (Channel5).

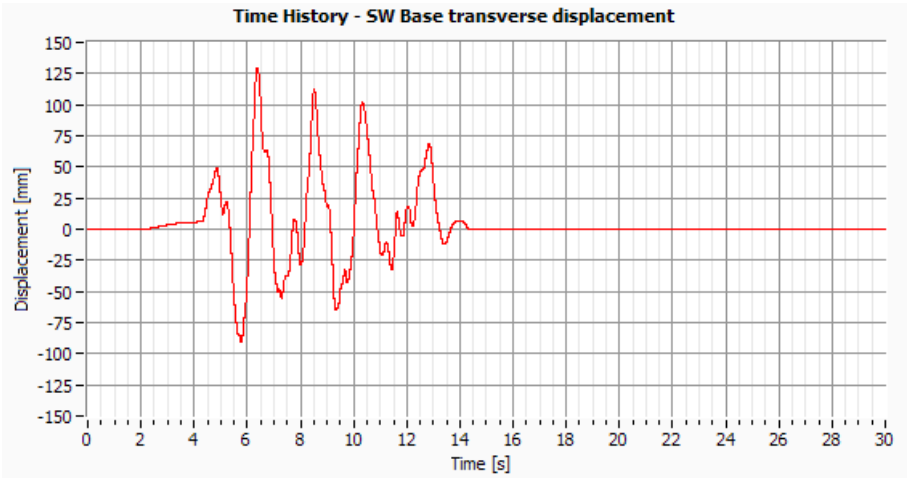

Figure IV.191: SW Base transverse displacement (Channel6).

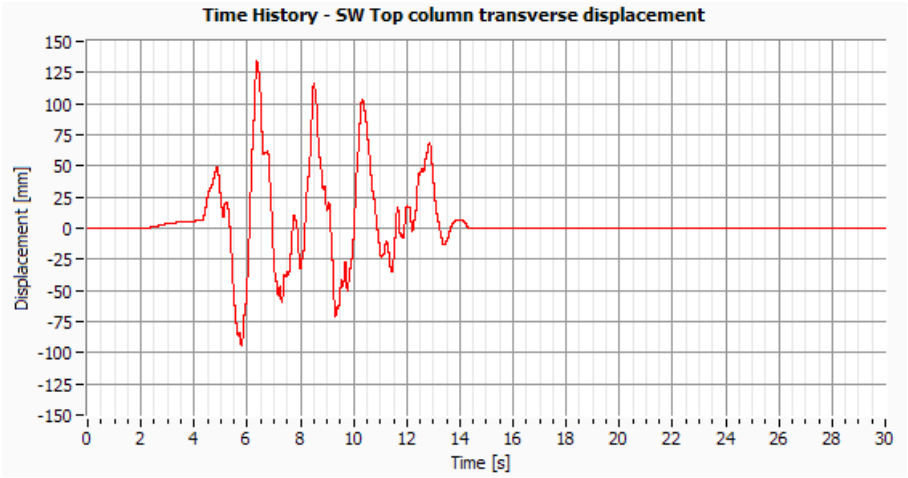

Figure IV.192: SW Top column transverse displacement (Channel7).

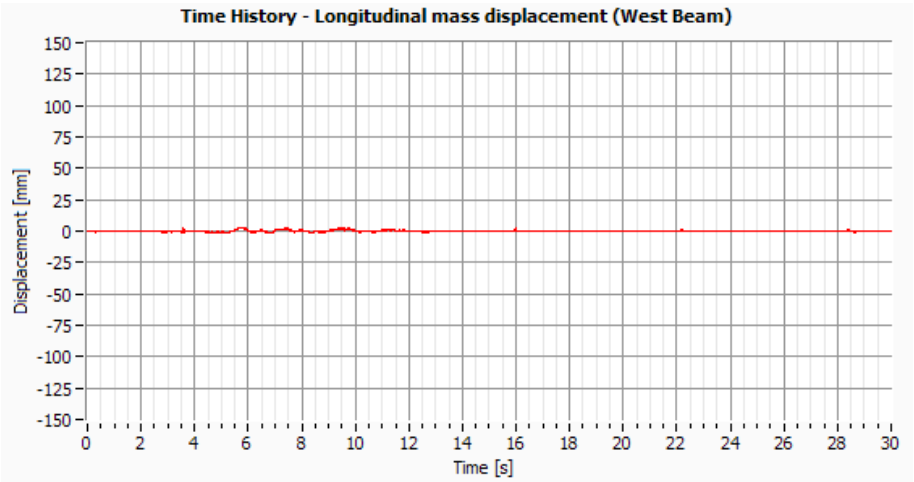

Figure IV.193: Longitudinal mass displacement in the West beam (Channel 8).

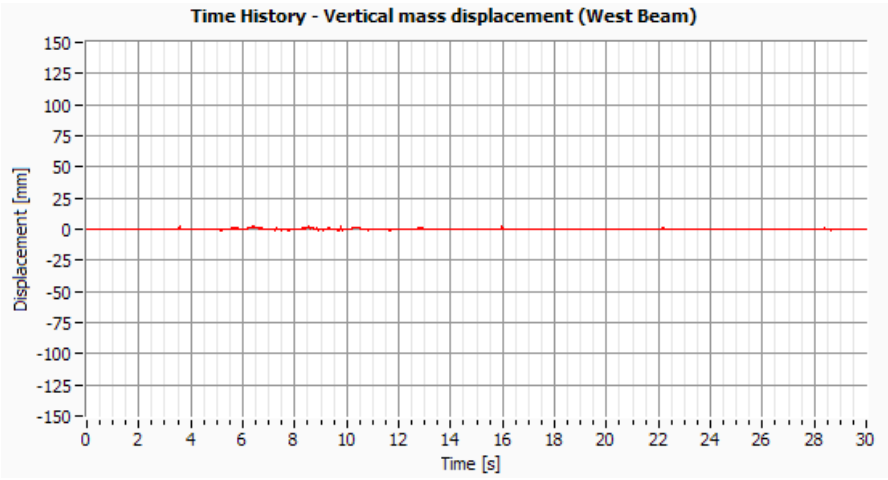

Figure IV.194: Vertical mass displacement in the West beam (Channel9).

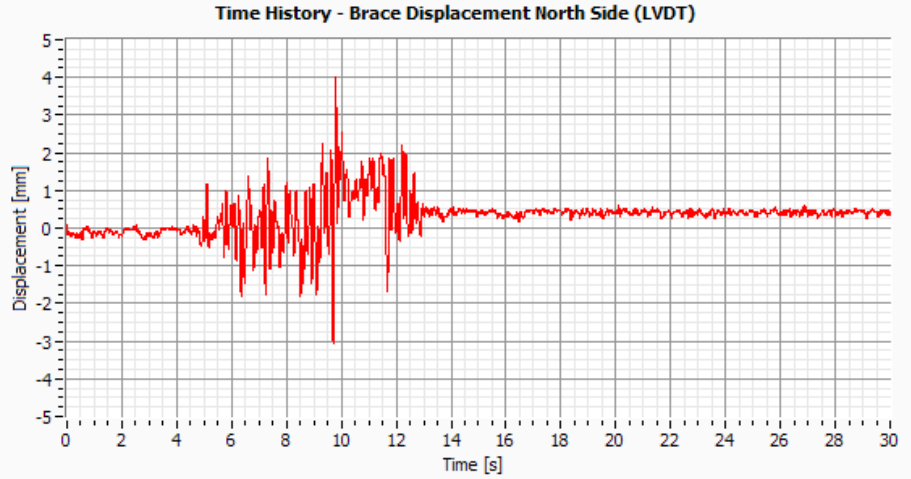

Figure IV.195: Brace displacement North side (Channel10).

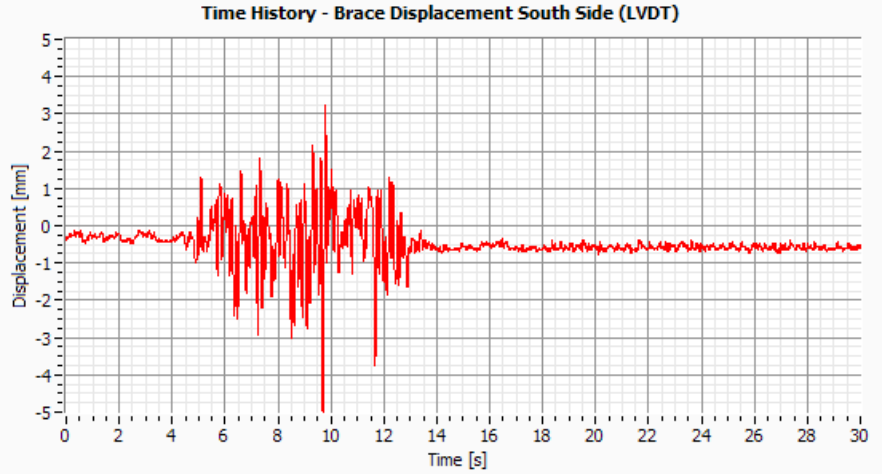

Figure IV.196: Brace displacement South side (Channel11).

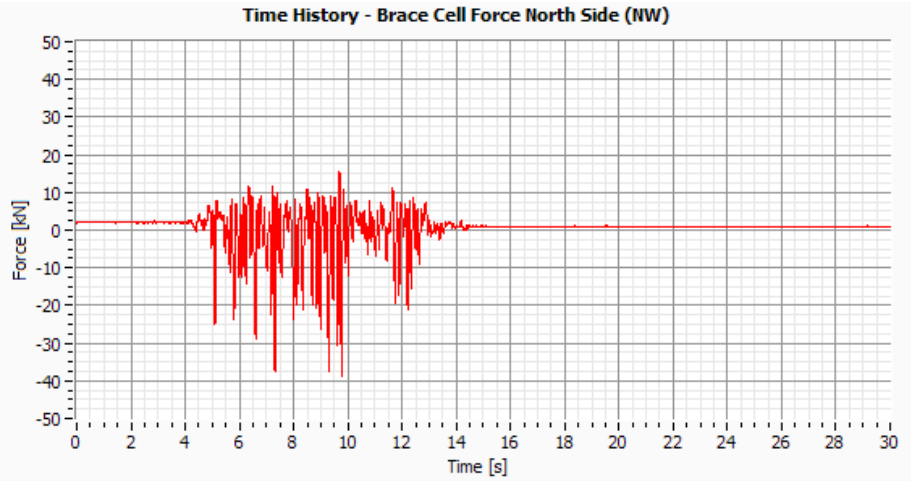

Figure IV.197: Brace cell force North Side – NW (Channel14).

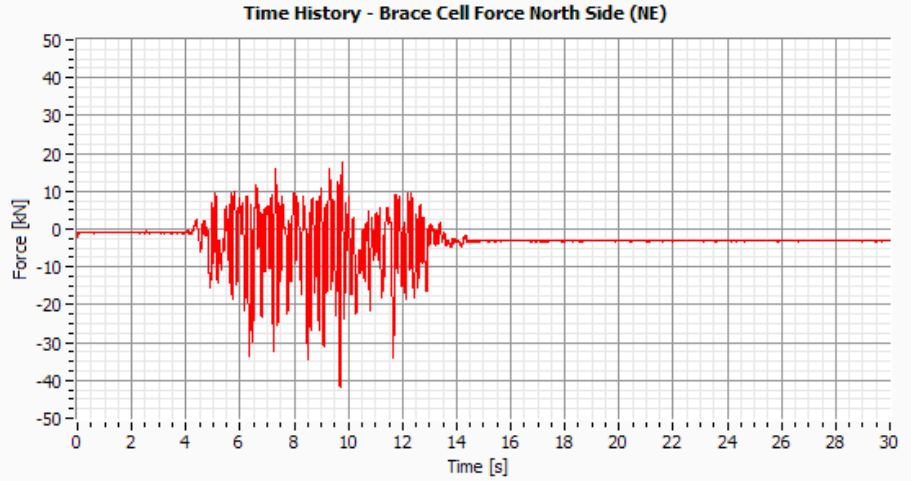

Figure IV.198: Brace cell force North Side – NE (Channel15).

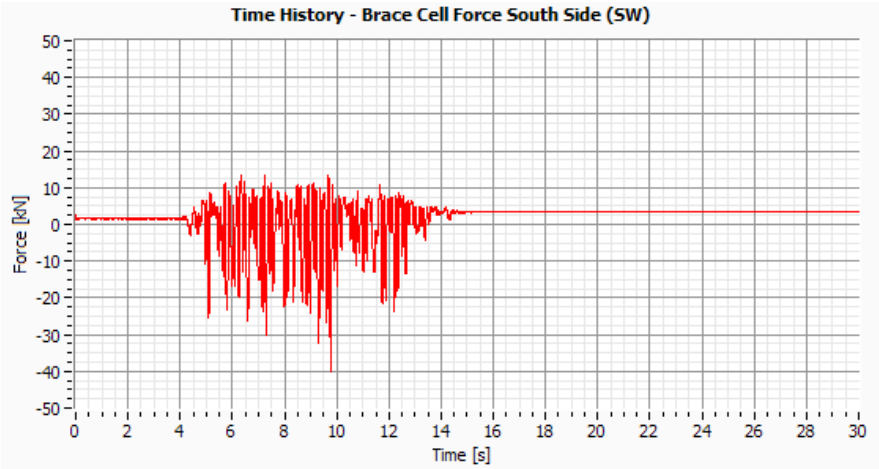

Figure IV.199: Brace cell force South Side – SW (Channel16).

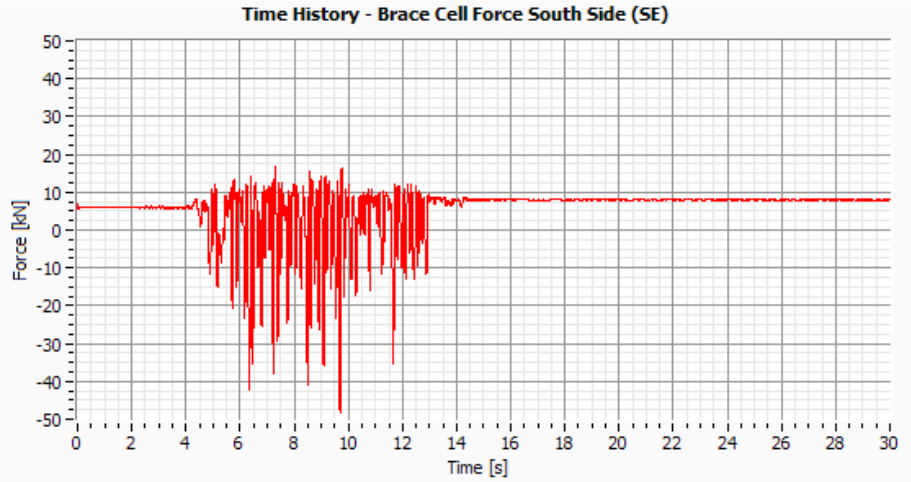

Figure IV.200: Brace cell force South Side – NE (Channel17).

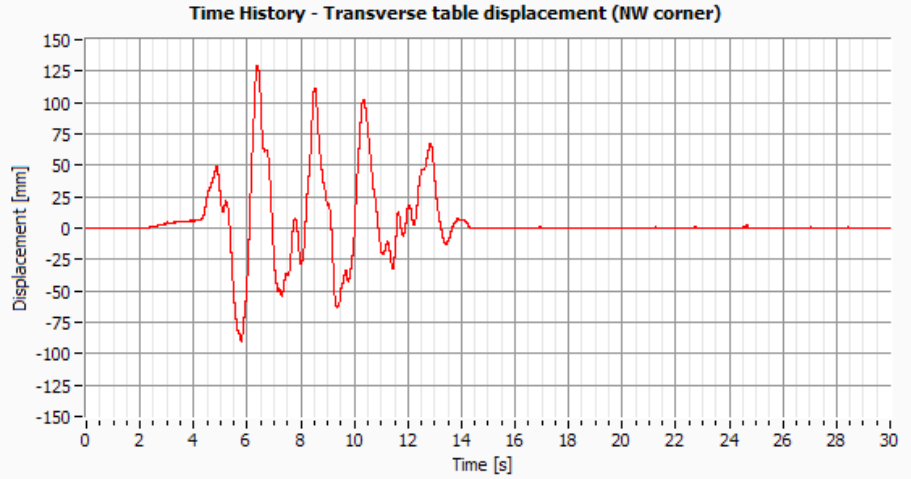

Figure IV.201: Transverse table displacement in the NW corner (Channel18).

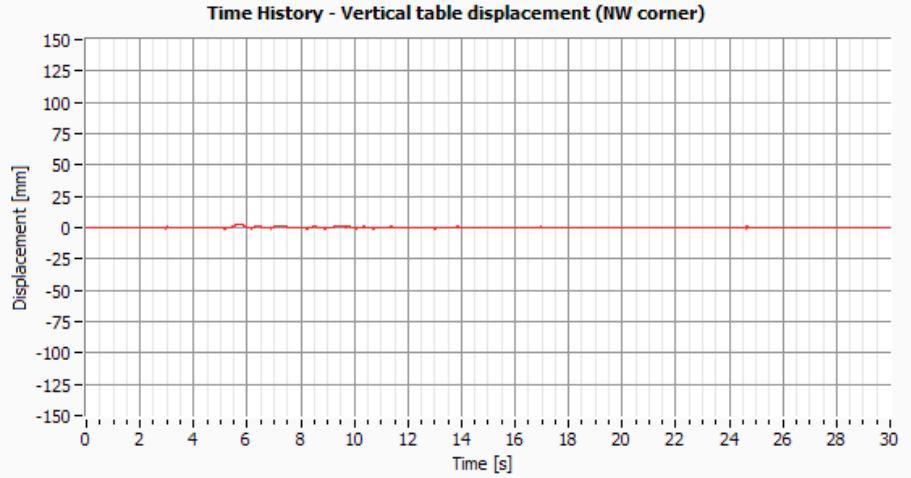

Figure IV.202: Vertical table displacement in the NW corner (Channel19).

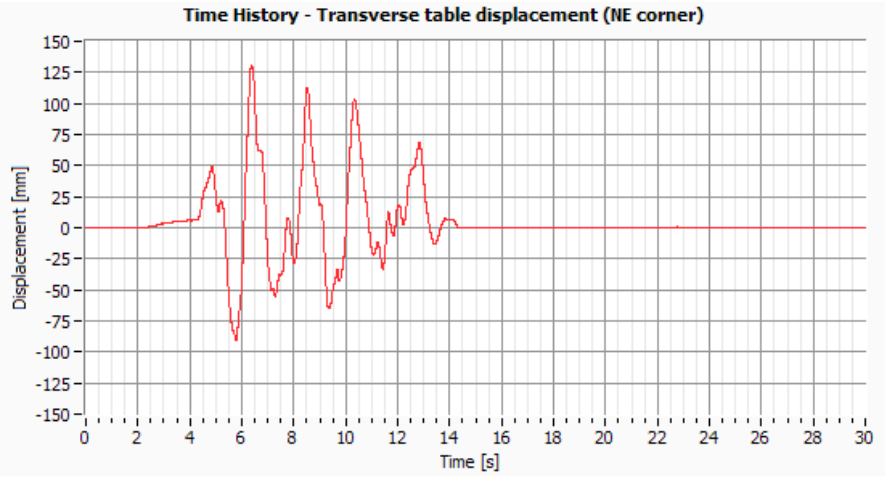

Figure IV.203: Transverse table displacement in the NE corner (Channel 20).

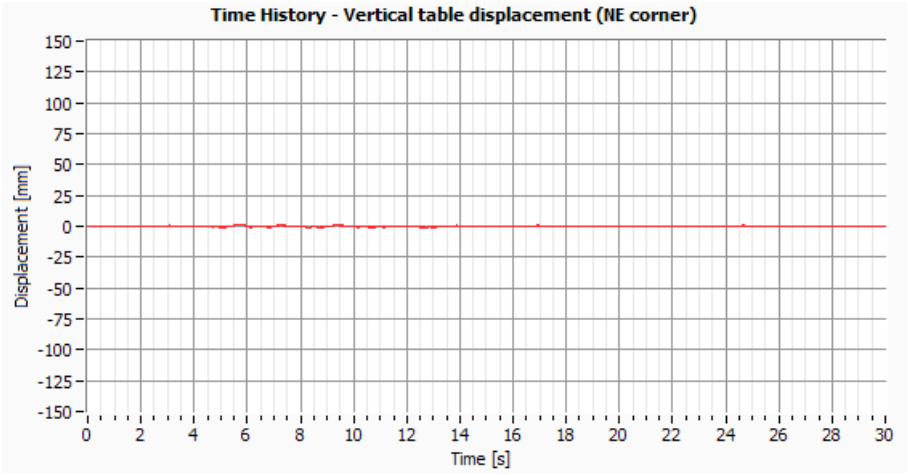

Figure IV.204: Vertical table displacement in the NE corner (Channel 21).

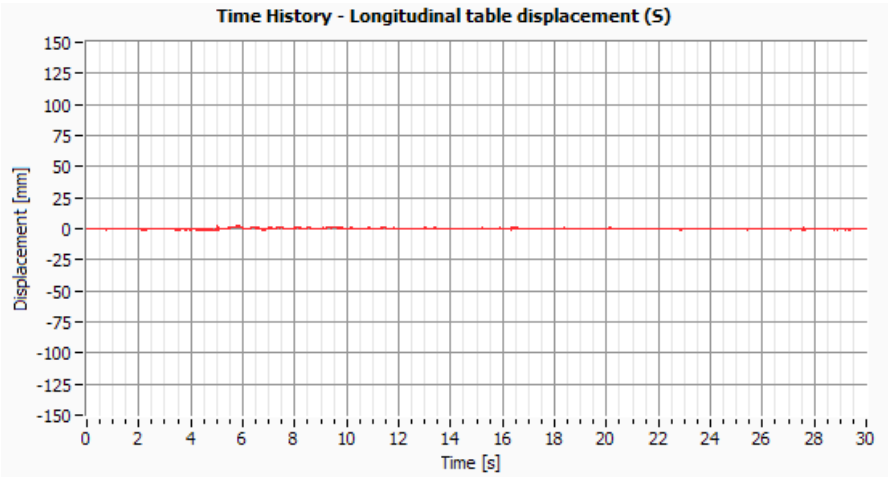

Figure IV.205: Longitudinal table displacement –S (Channel 22).

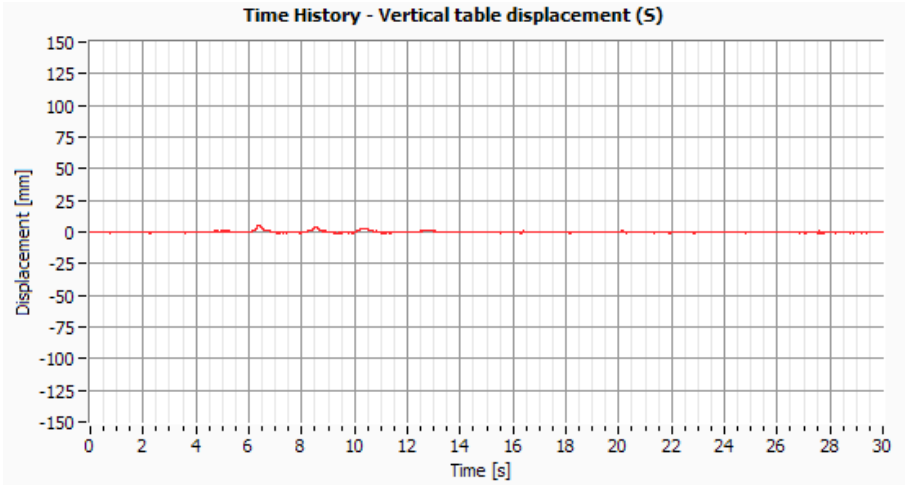

Figure IV.206: Vertical table displacement –S (Channel 23).

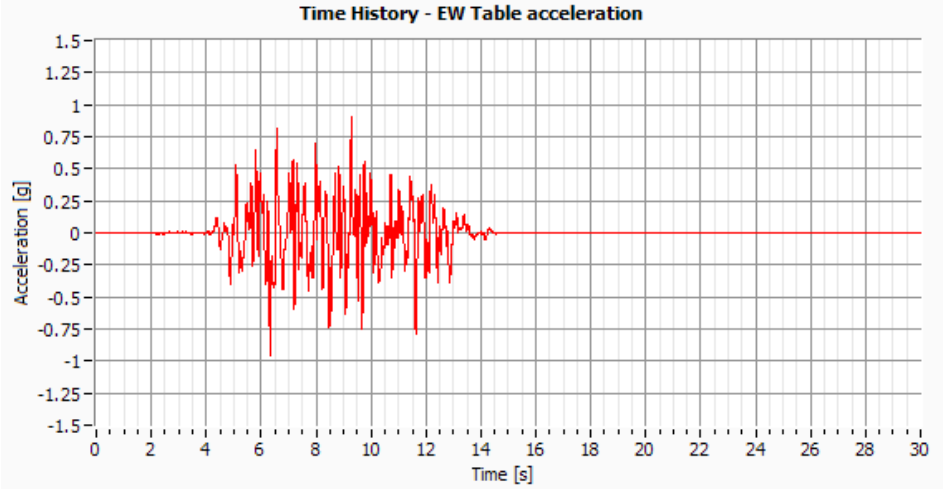

Figure IV.207: EW Table acceleration (Channel 24).

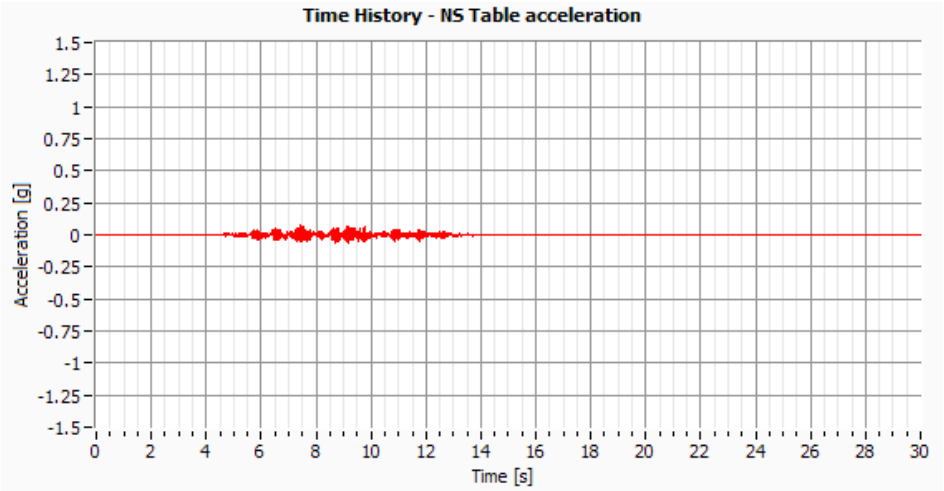

Figure IV.208: NS Table acceleration (Channel 25).

Test 15 – Cat06 (EW PGA=0.05g)

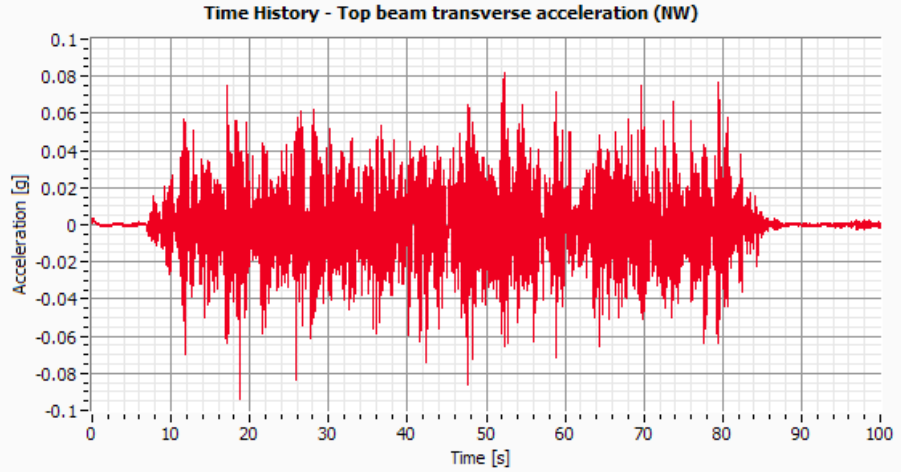

Figure IV.209: NW Top beam acceleration (Channel 1).

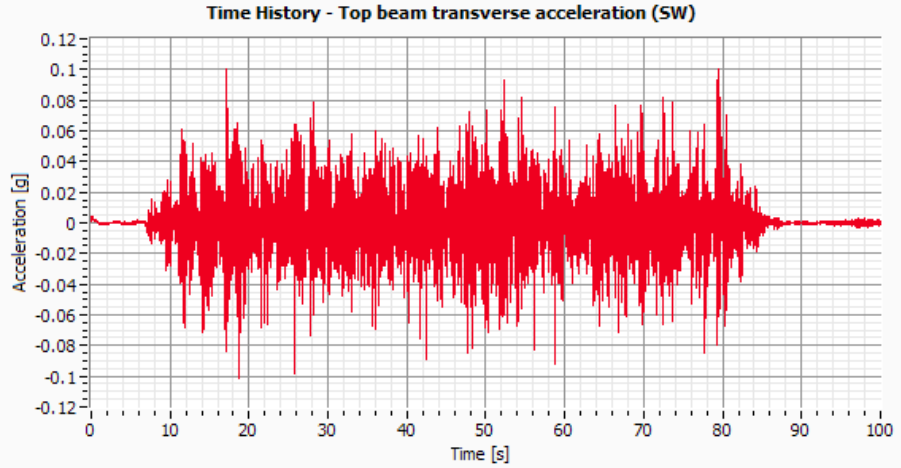

Figure IV.210: SW Top beam acceleration (Channel2).

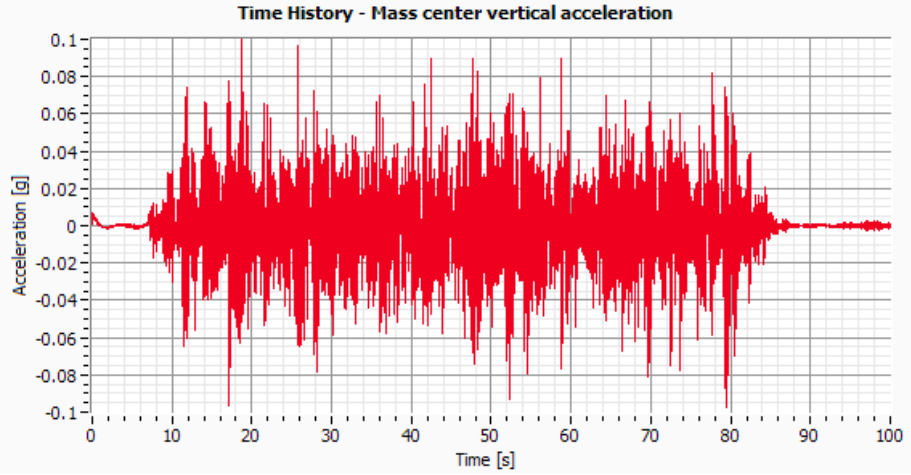

Figure IV.211: Mass center vertical acceleration (Channel 3).

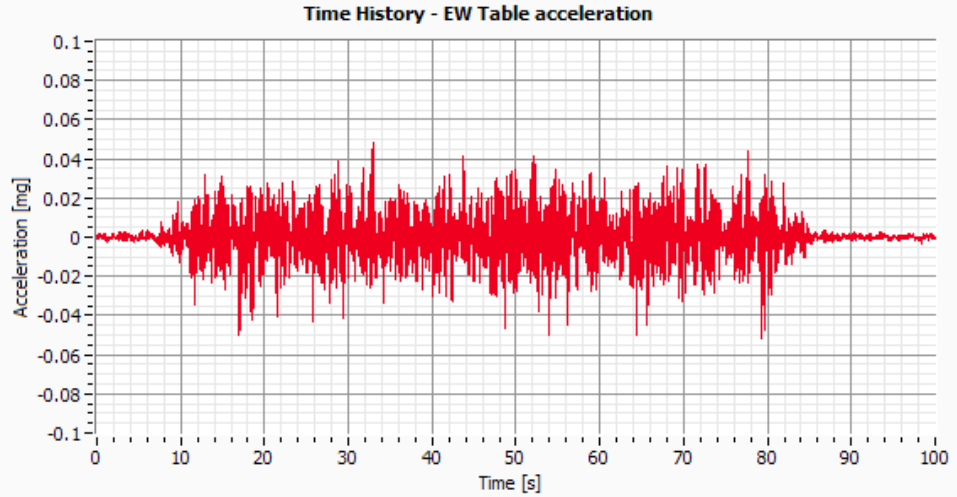

Figure IV.212: EW Table acceleration (Channel 24).

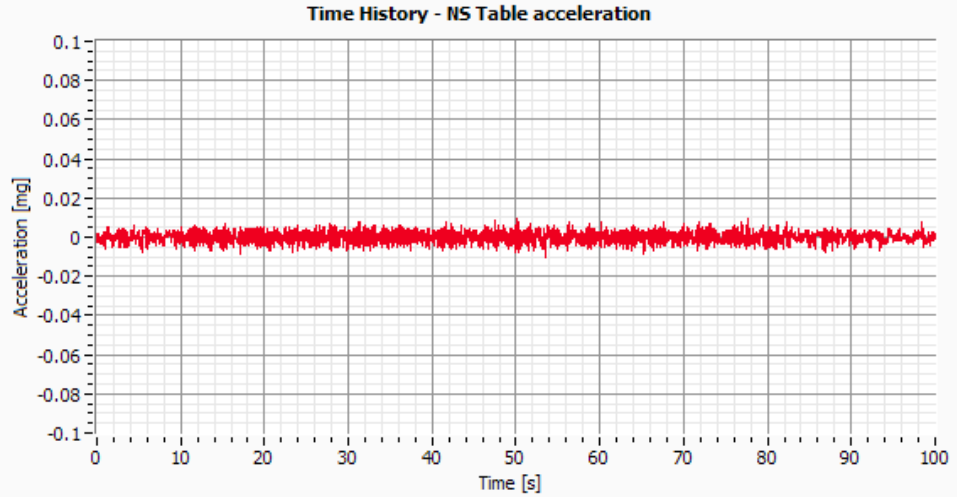

Figure IV.213: NS Table acceleration (Channel 25).

ANNEX V

Interstorey Drifts

INDEX OF FIGURES

Test 2 – ElCentro (EW PGA=0.20g)

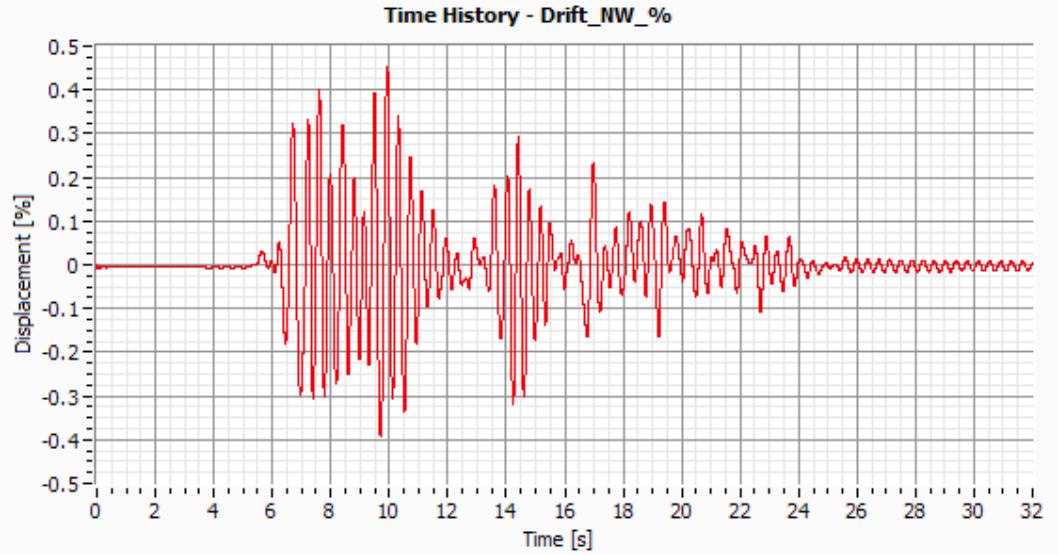

Figure II.1: Interstorey Drift NW column.

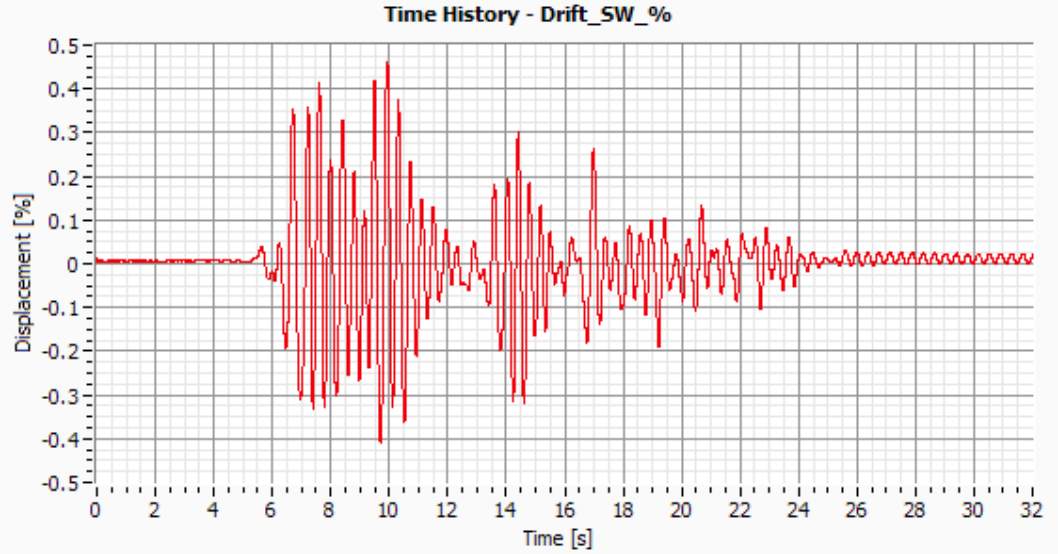

Figure V.1: Interstorey Drift SW column.

Test 5 – ElCentro (EW PGA=0.20g)

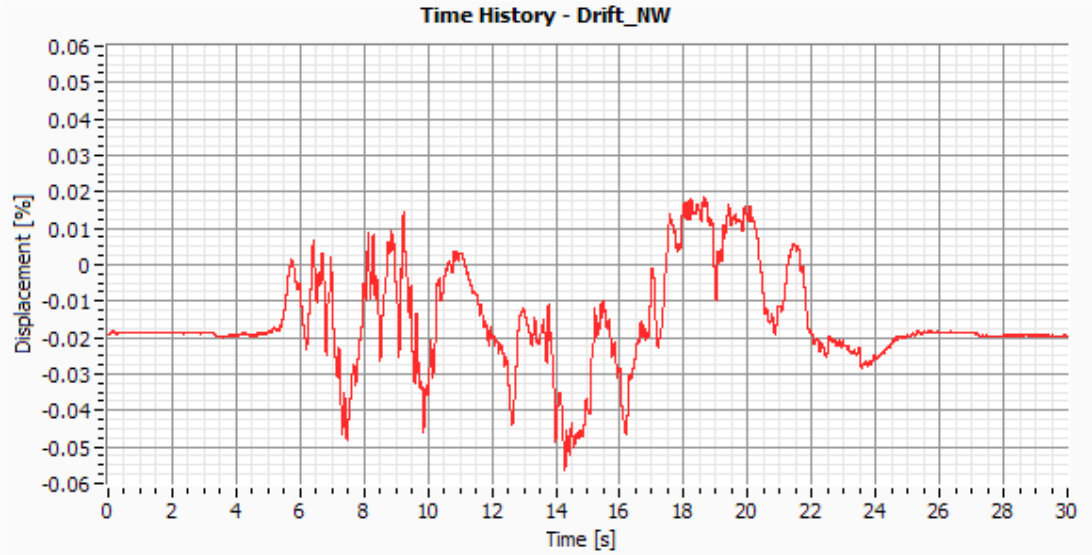

Figure V.2: Interstorey Drift NW column.

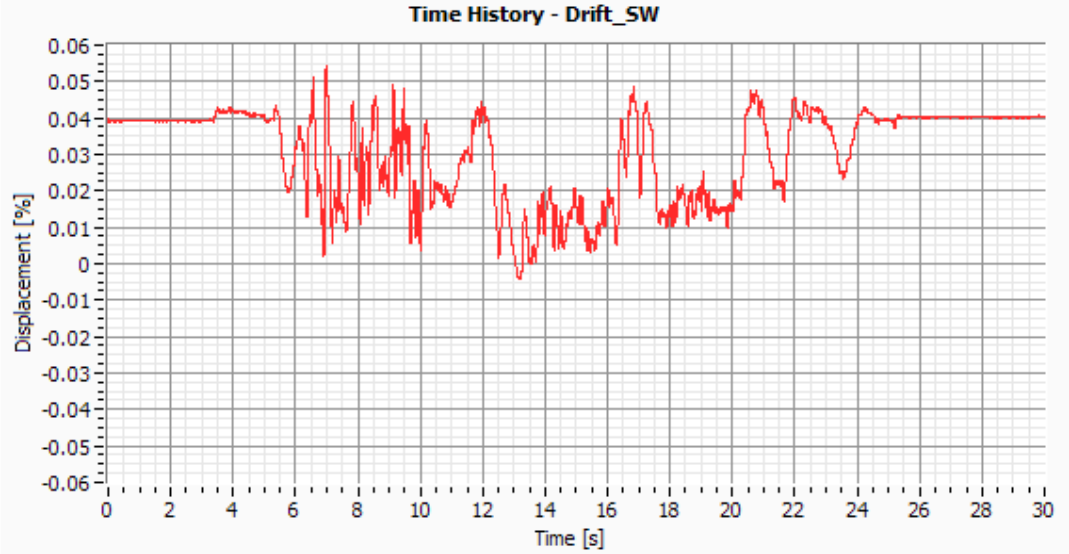

Figure V.3: Interstorey Drift SW column.

Test 6 – Sen 10.28Hz (EW PGA=0.05g)

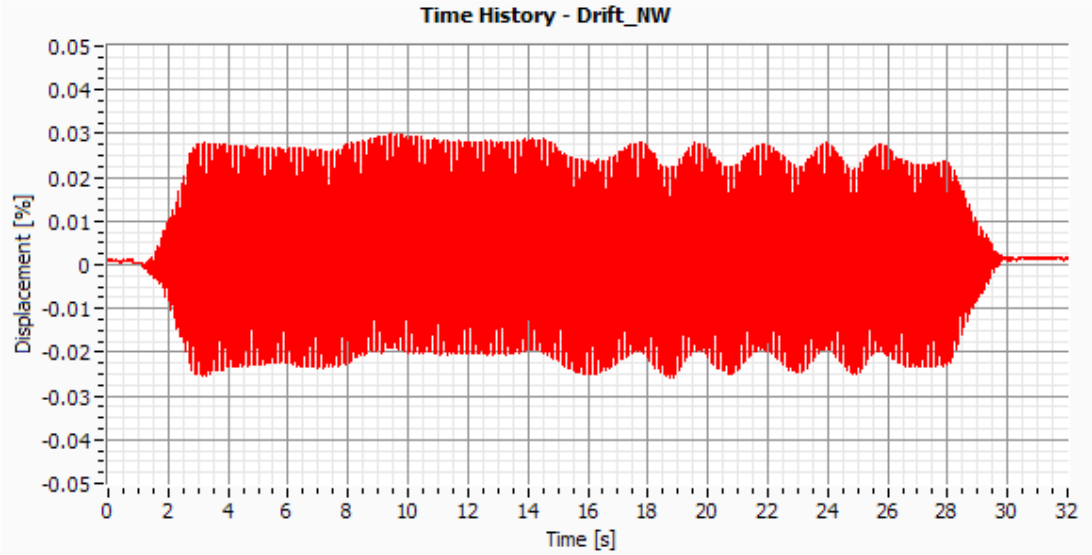

Figure V.4: Interstorey Drift NW column.

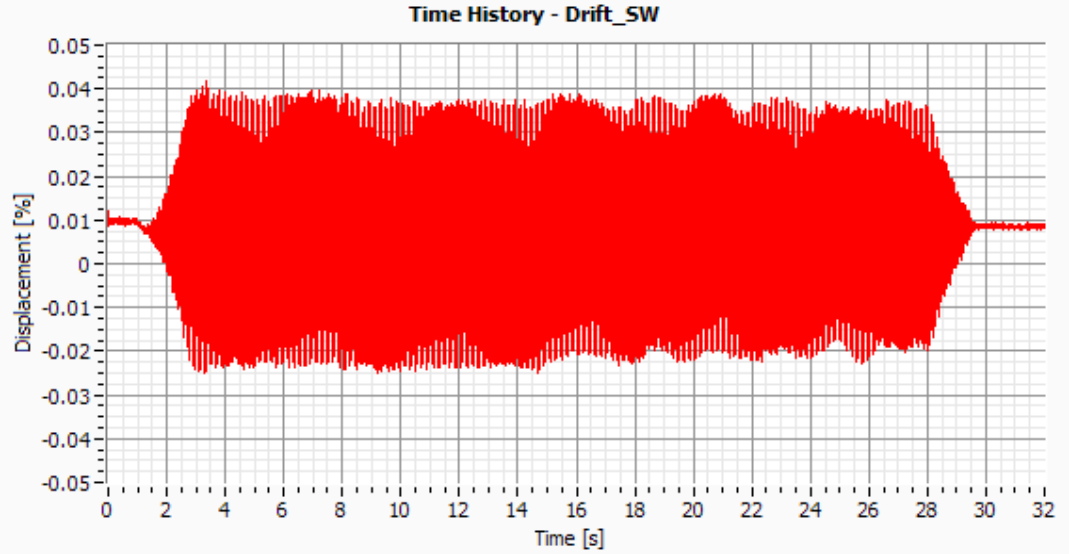

Figure V.5: Interstorey Drift SW column.

Test 7 – Artificial EC8 (EW PGA=0.20g)

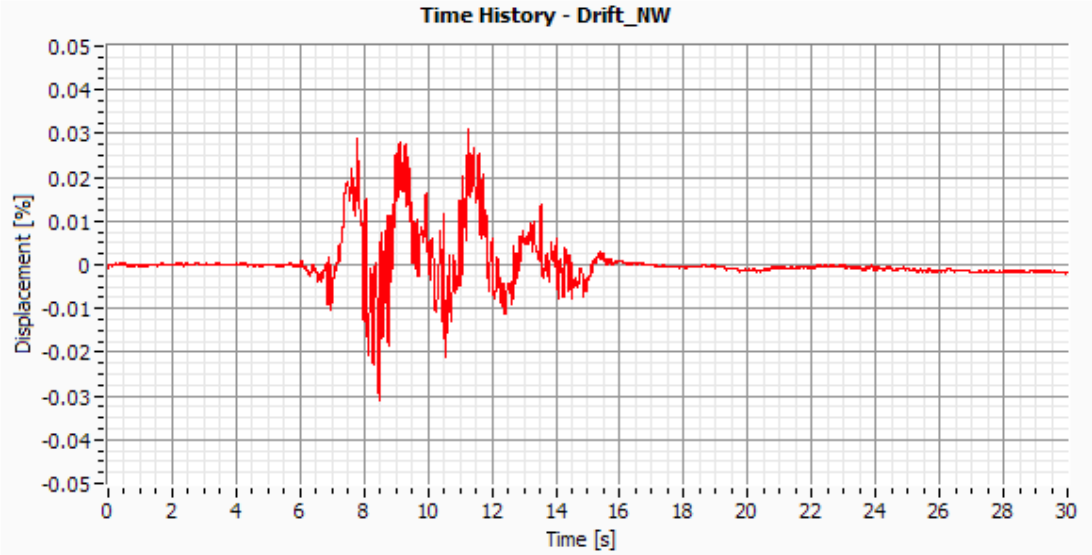

Figure V.6: Interstorey Drift NW column.

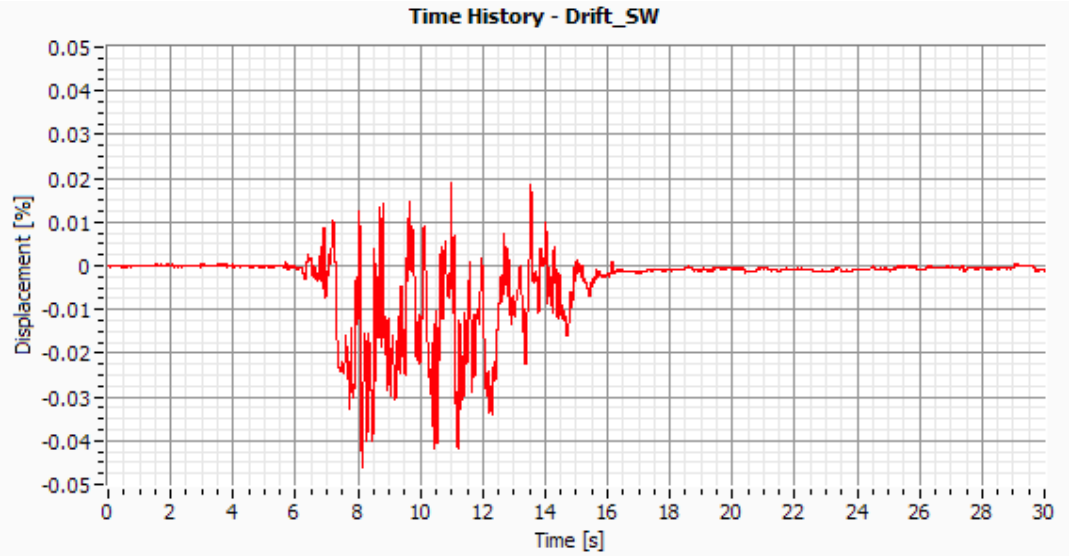

Figure V.7: Interstorey Drift SW column.

Test 8 – Sen 8.22Hz (EW PGA=0.05g)

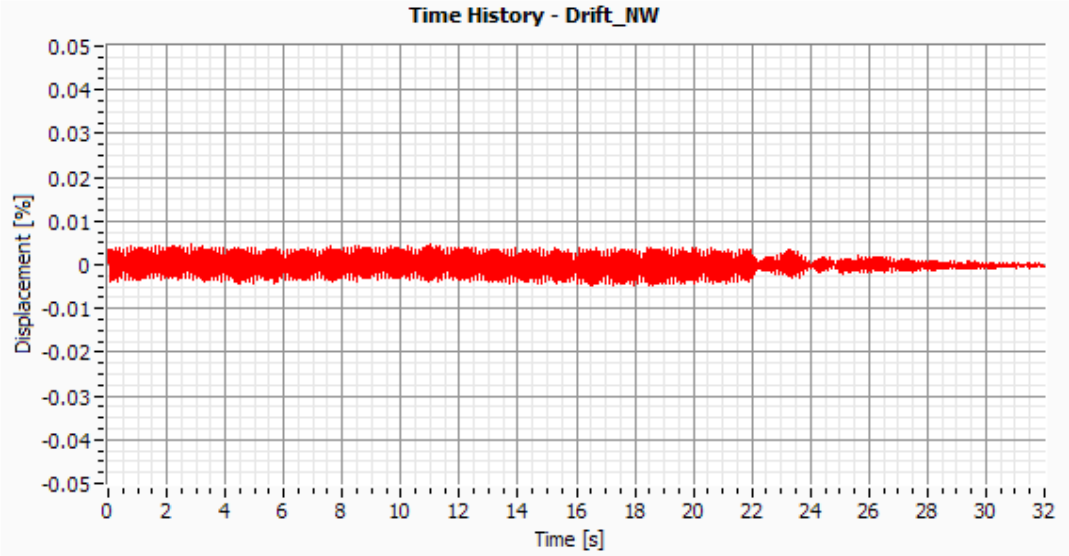

Figure V.8: Interstorey Drift NW column.

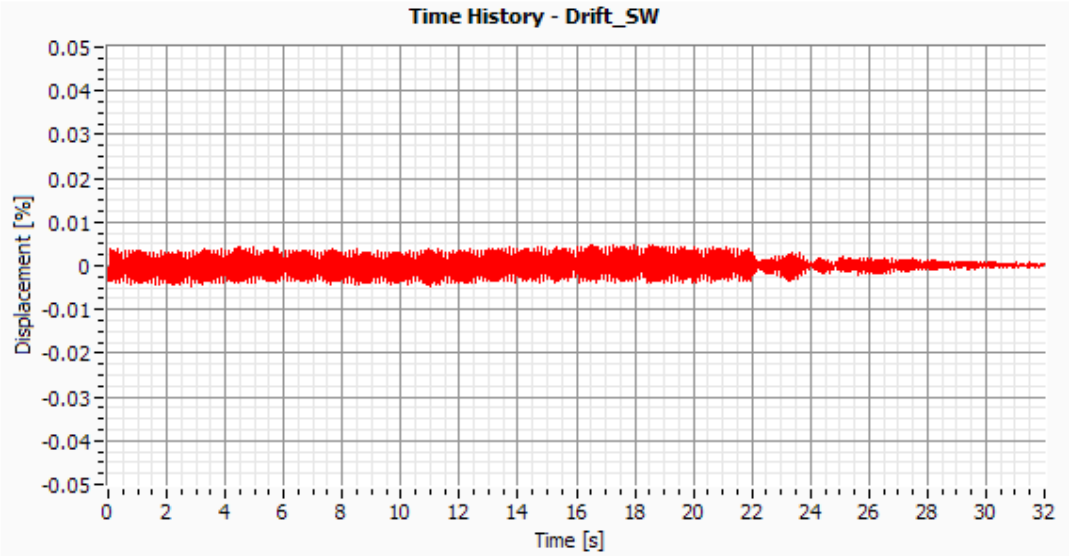

Figure V.9: Interstorey Drift SW column.

Test 10 – Artificial EC8 (EW PGA=0.60g)

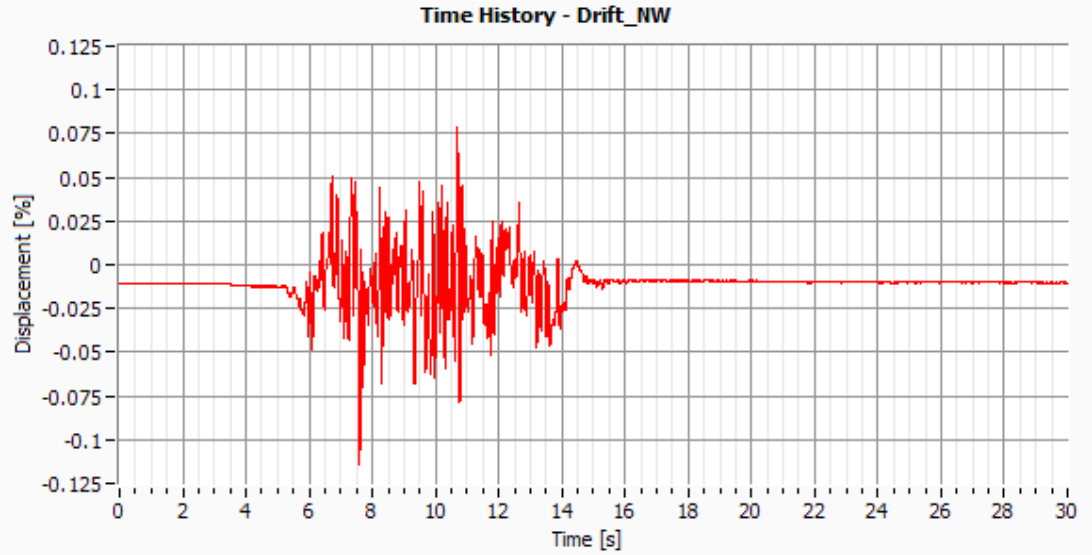

Figure V.10: Interstorey Drift NW column.

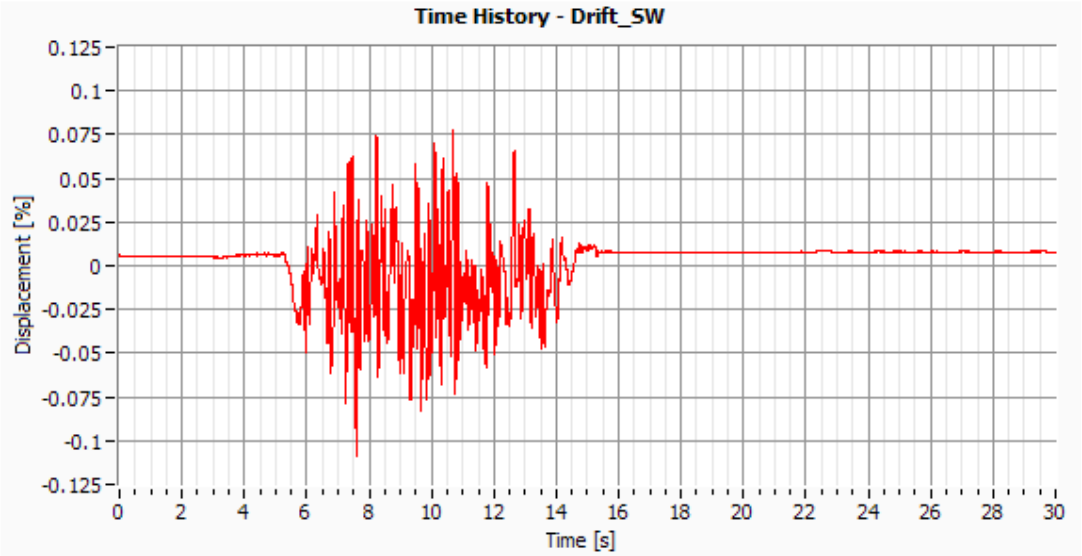

Figure V.11: Interstorey Drift SW column.

Test 12 – Artificial EC8 (EW PGA=0.80g)

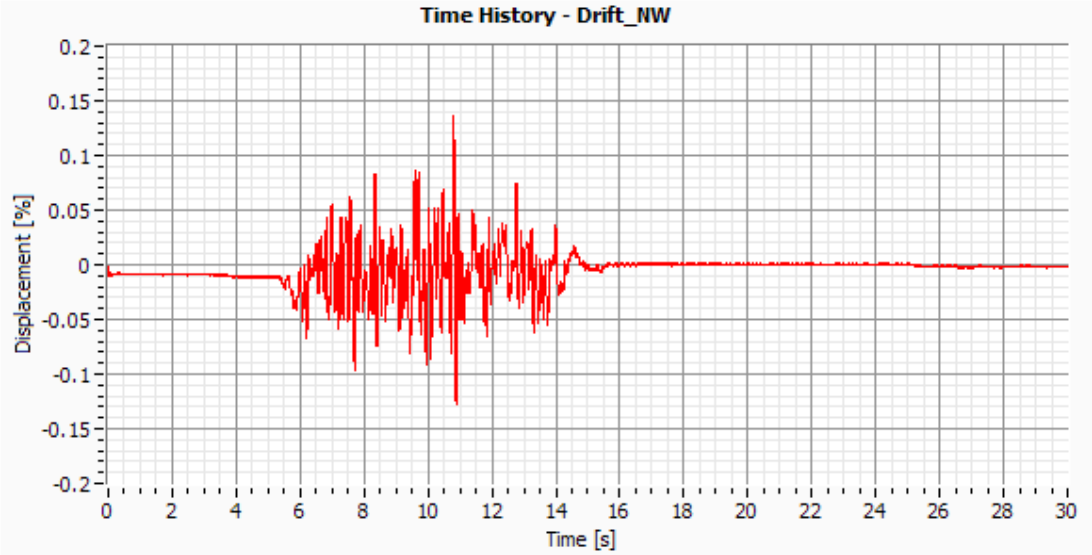

Figure V.12: Interstorey Drift NW column.

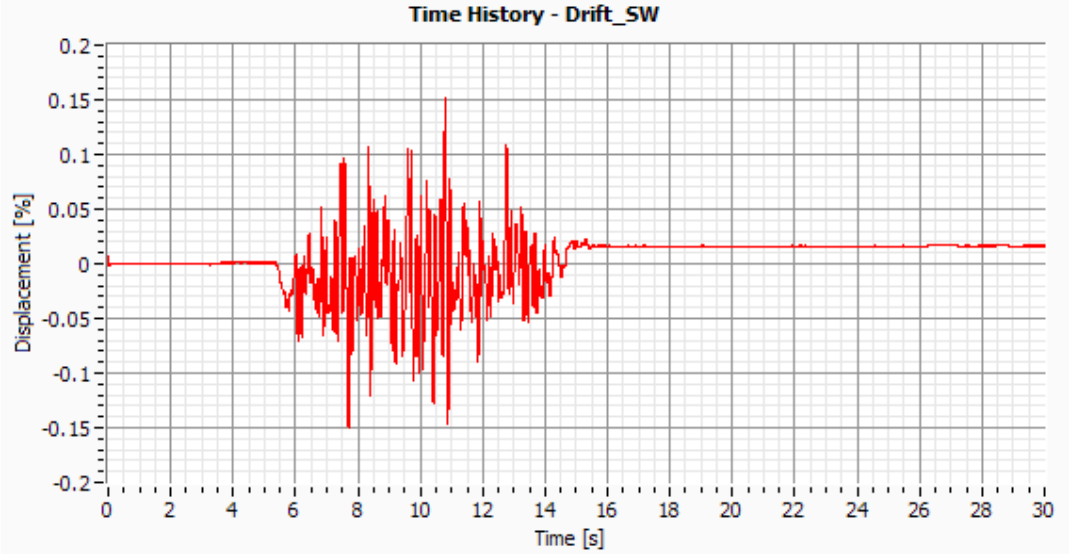

Figure V.13: Interstorey Drift SW column.

Test 14 – Artificial EC8 (EW PGA=1.0g)

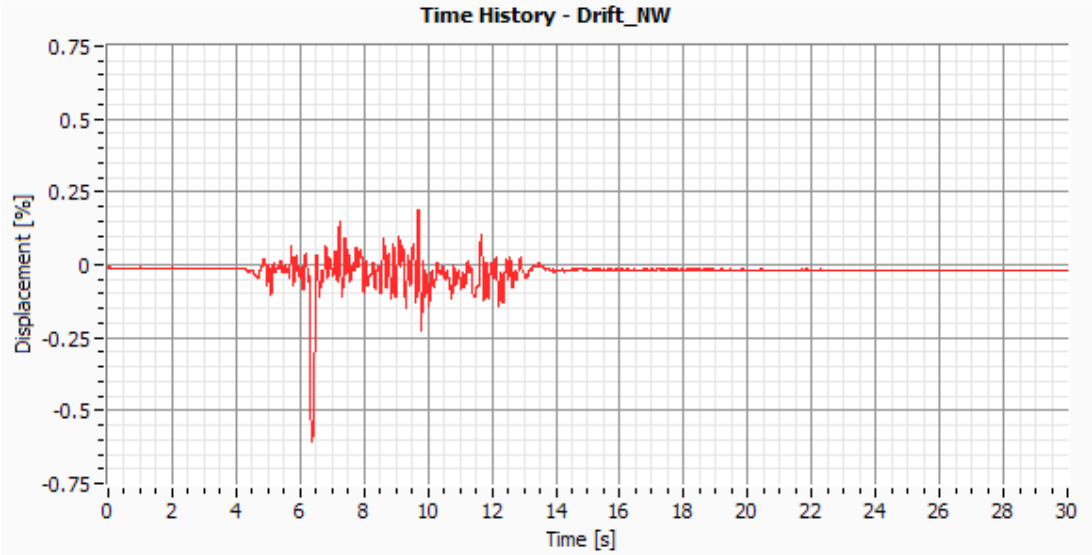

Figure V.14: Interstorey Drift NW column.

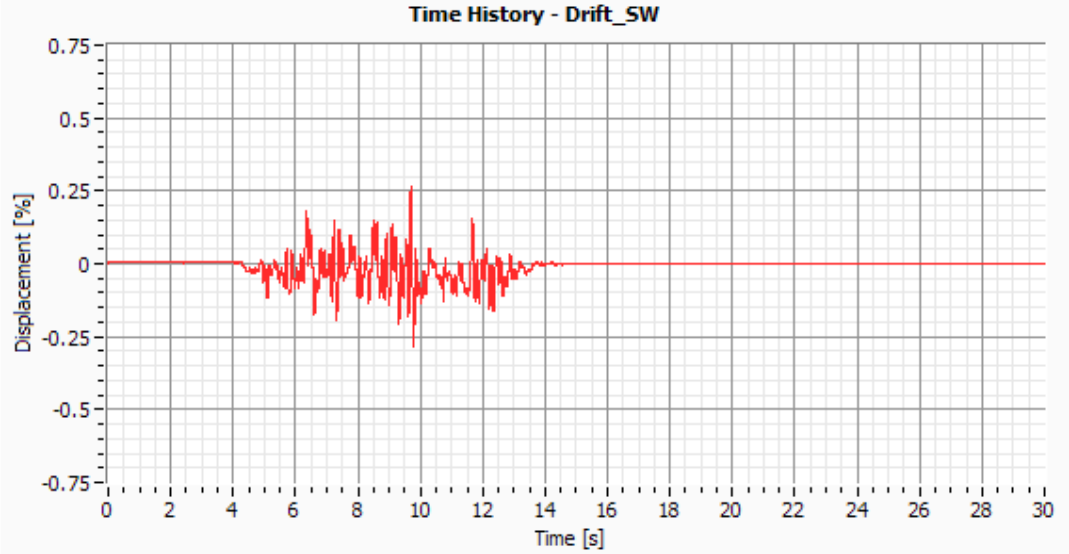

Figure V.15: Interstorey Drift SW column.

Test 17 – ElCentro (EW PGA=0.20g)

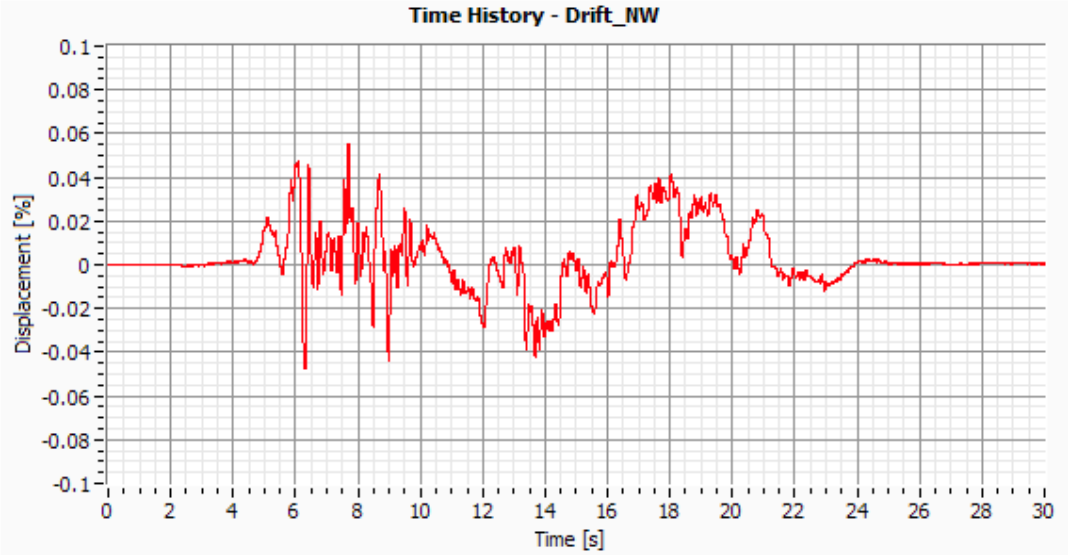

Figure V.16: Interstorey Drift NW column.

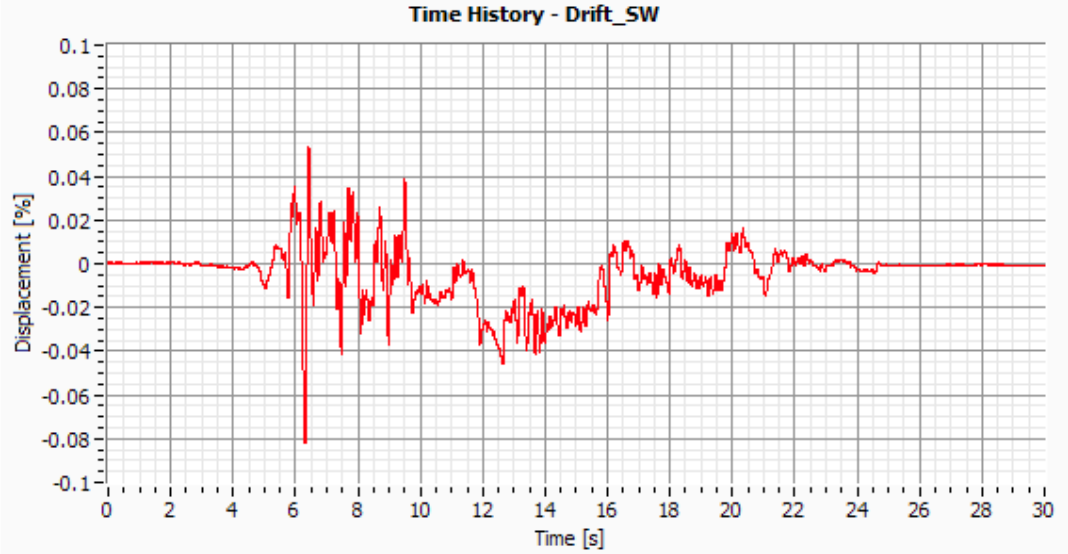

Figure V.17: Interstorey Drift SW column.

Test 18 – Sen 9.48Hz (EW PGA=0.05g)

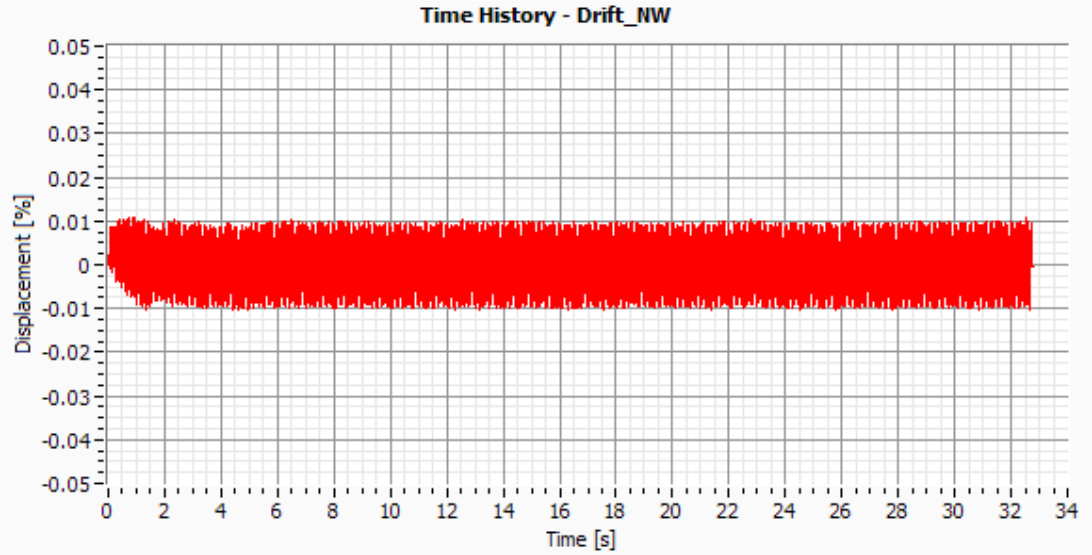

Figure V.18: Interstorey Drift NW column.

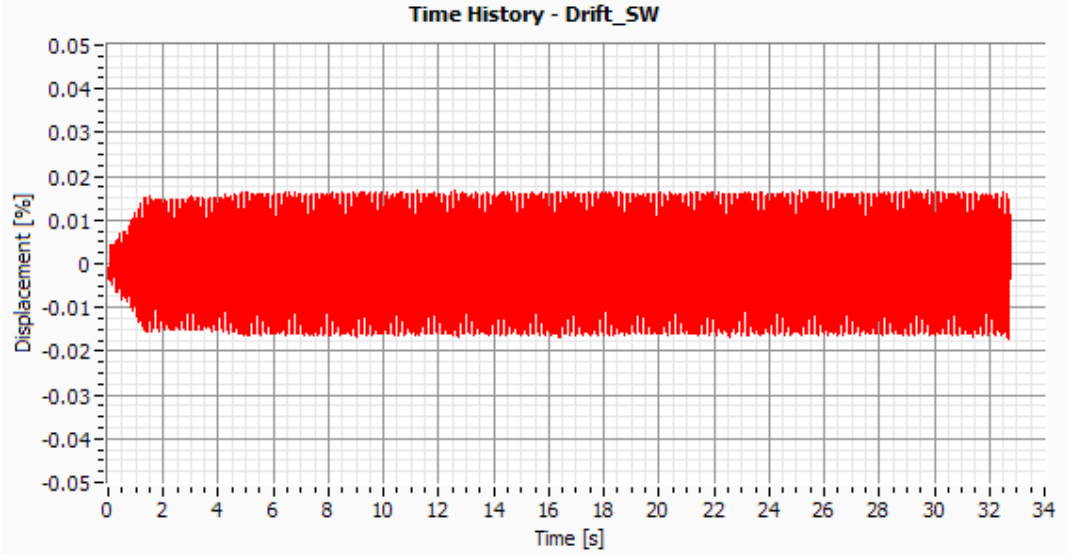

Figure V.19: Interstorey Drift SW column.

Test 19 – Artificial EC8 (EW PGA=0.20g)

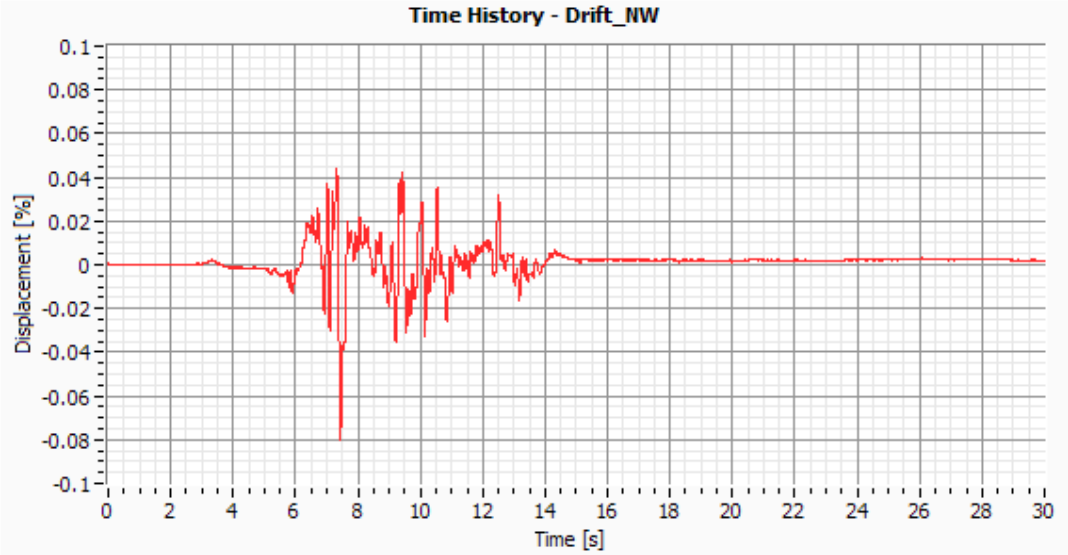

Figure V.20: Interstorey Drift NW column.

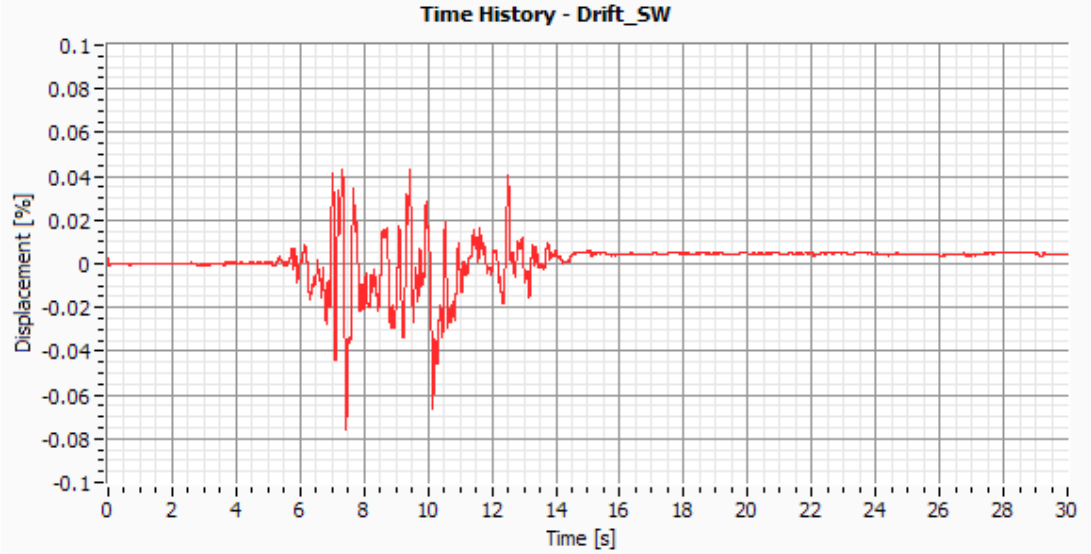

Figure V.21: Interstorey Drift SW column.

Test 22 – Artificial EC8 (EW PGA=0.60g)

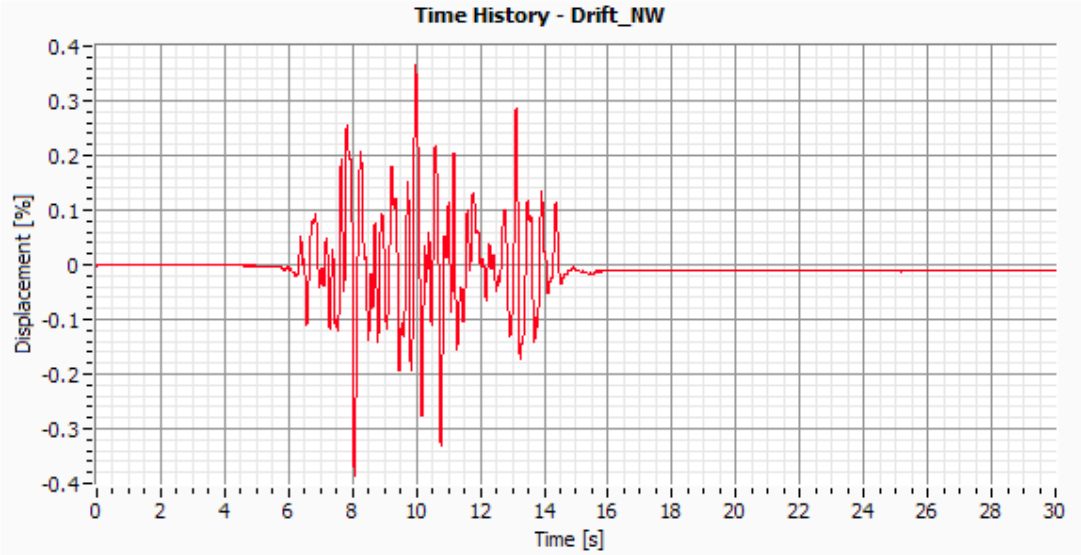

Figure V.22: Interstorey Drift NW column.

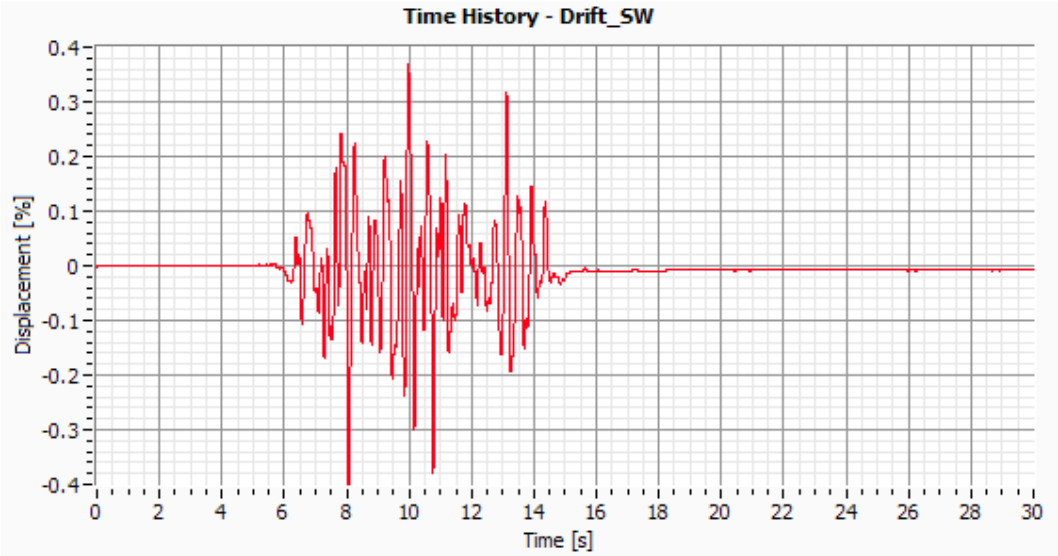

Figure V.23: Interstorey Drift SW column.

Test 24 – Artificial EC8 (EW PGA=0.80g)

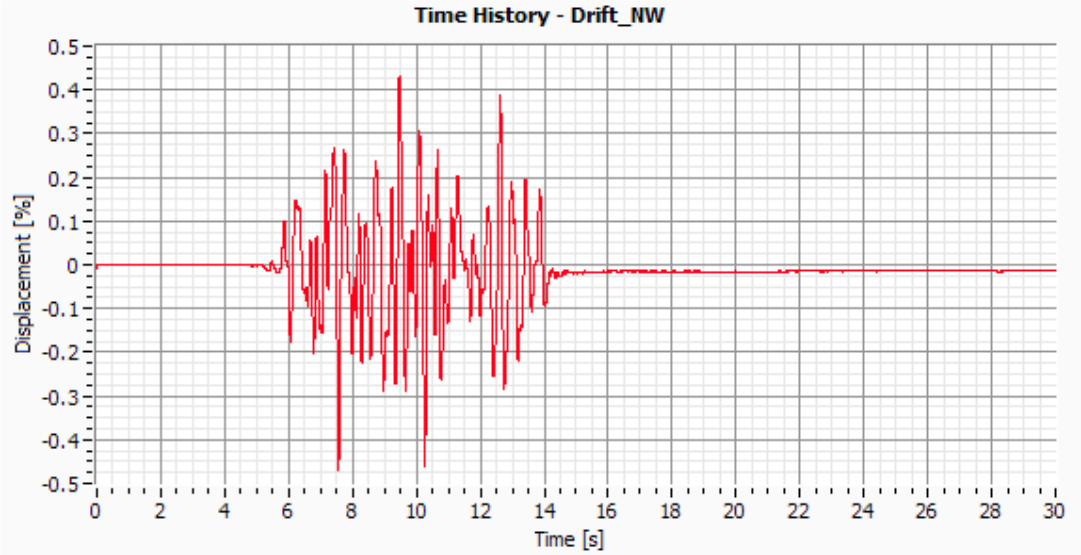

Figure V.24: Interstorey Drift NW column.

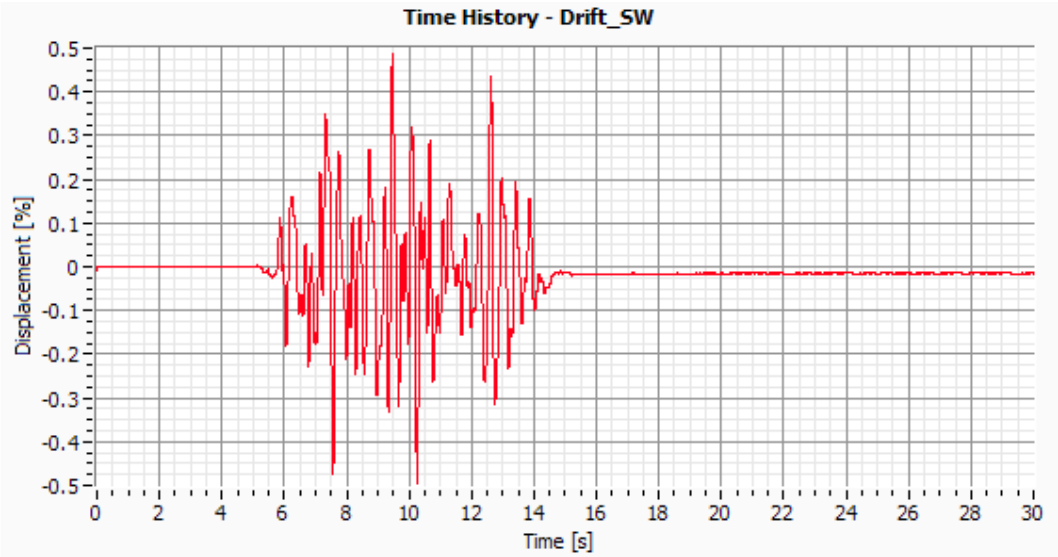

Figure V.25: Interstorey Drift SW column.

Test 26 – Artificial EC8 (EW PGA=1.0g)

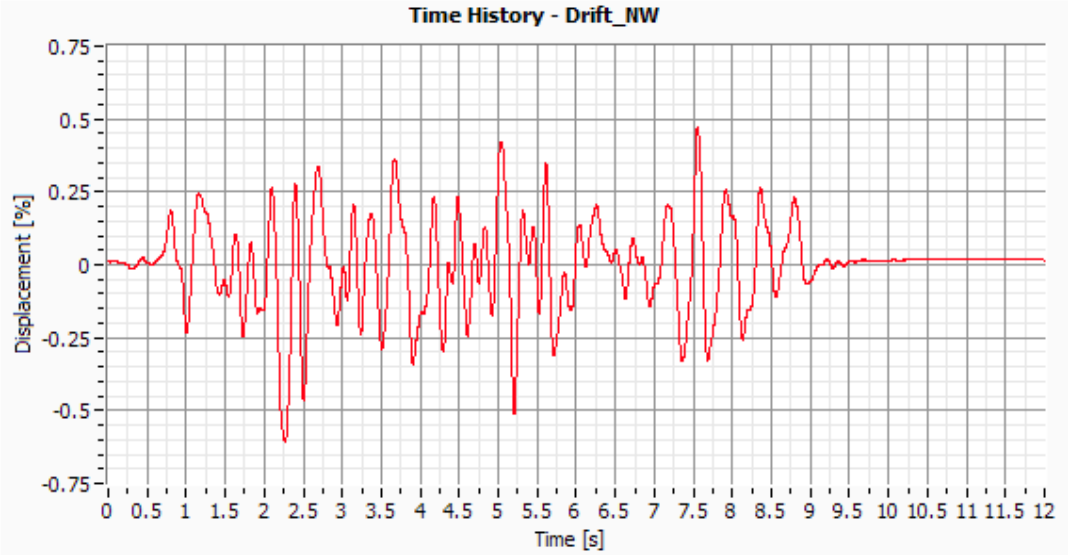

Figure V.26: Interstorey Drift NW column.

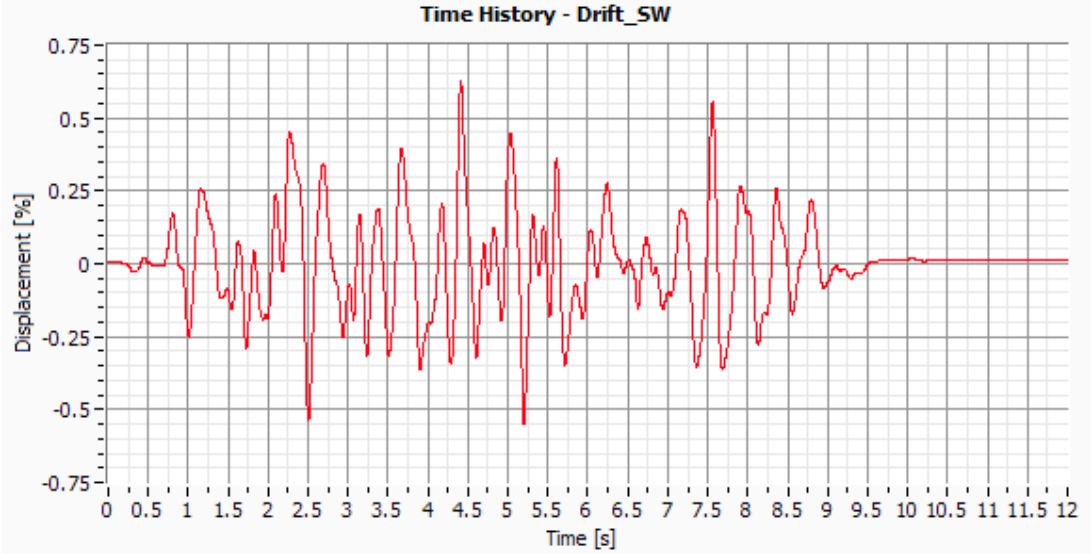

Figure V.27: Interstorey Drift SW column.

ANNEX VI

Global Forces in the Dissipation Devices

INDEX OF FIGURES

Test 5 – ElCentro (EW PGA=0.20g)

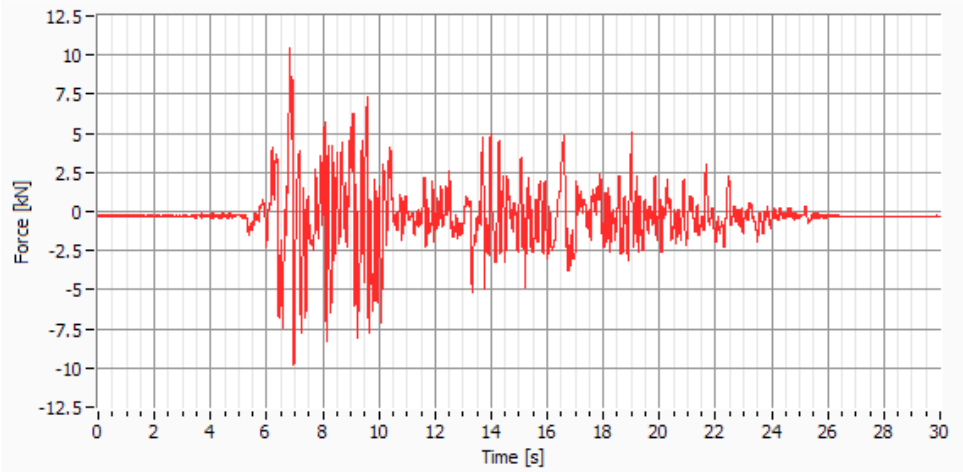

Figure VI.1: Global Force in the North side

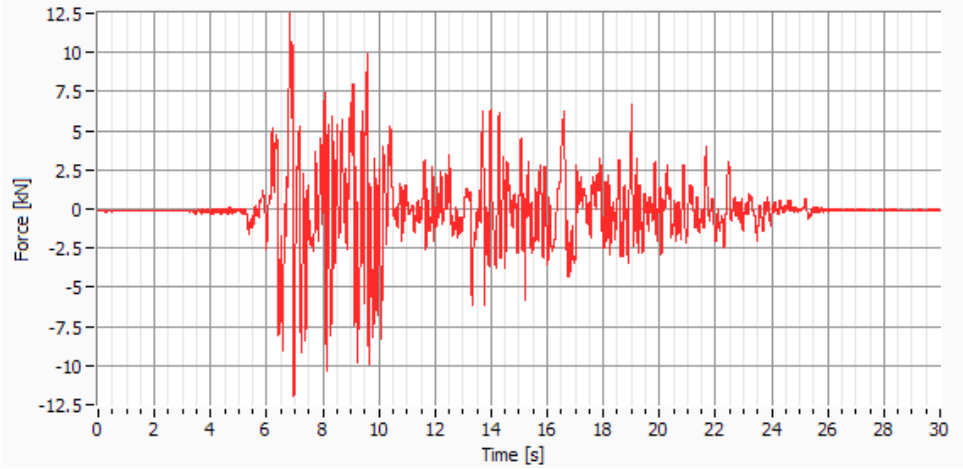

Figure VI.2: Global Force in the South side.

Test 6 – Sinusoidal 10.28Hz (EW PGA=0.05g)

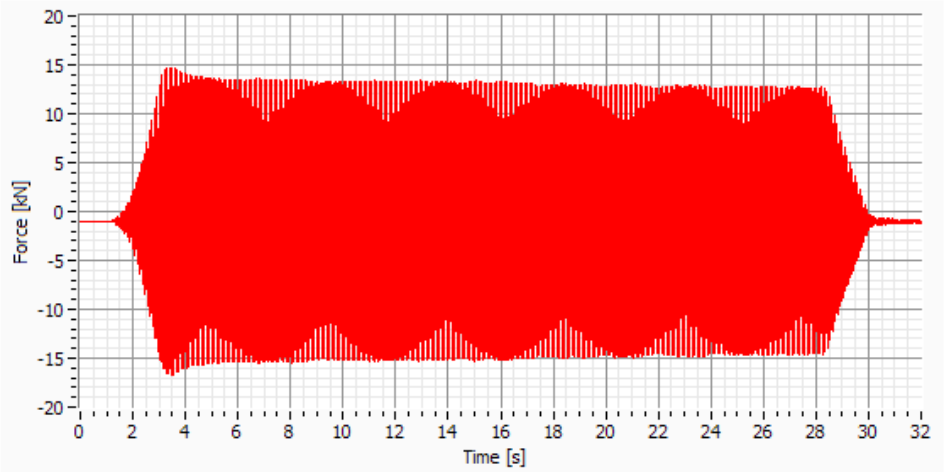

Figure VI.3: Global force in the North side.

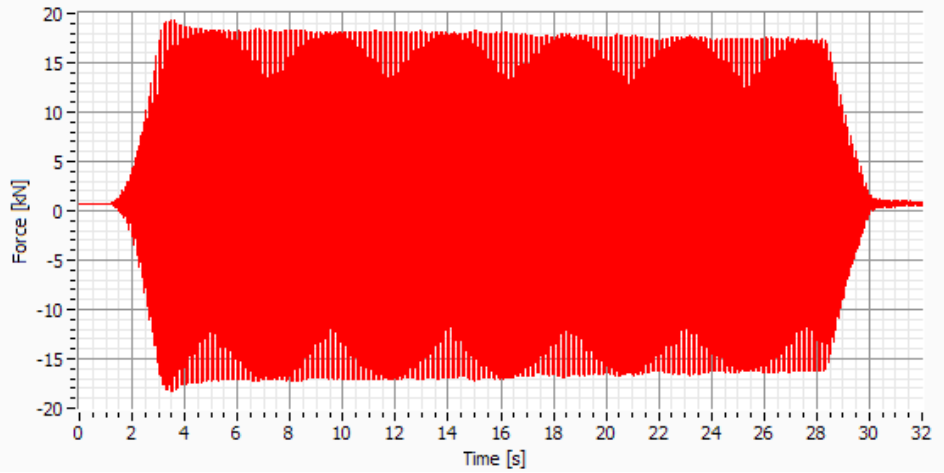

Figure VI.4: Global force in the South side.

Test 7 – Artificial EC8 (EW PGA=0.20g)

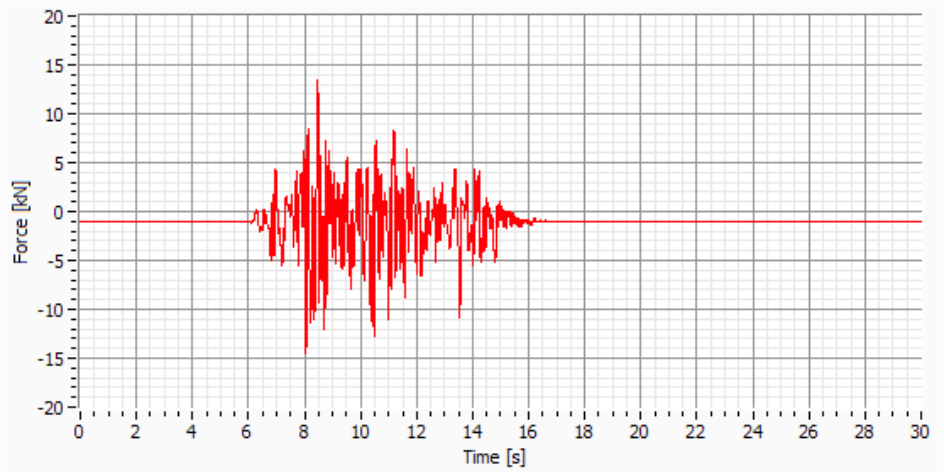

Figure VI.5: Global force in the North side.

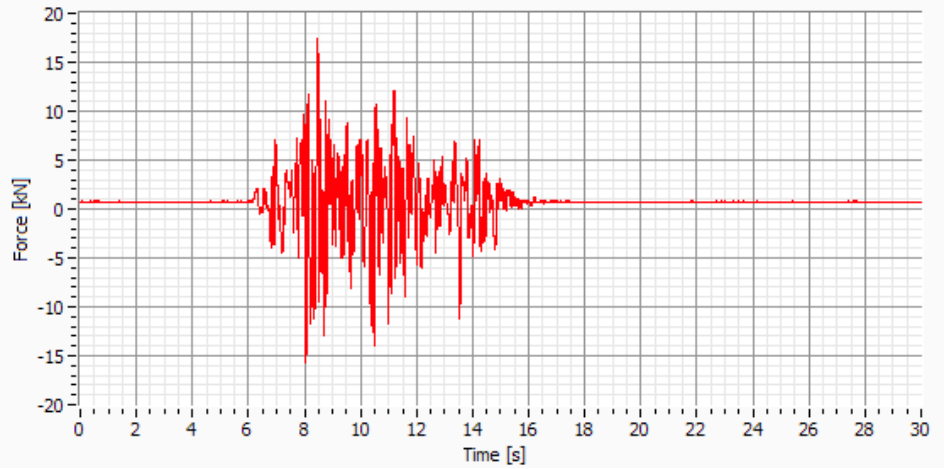

Figure VI.6: Global force in the South side.

Test 8 – Sen 8.22Hz (EW PGA=0.05g)

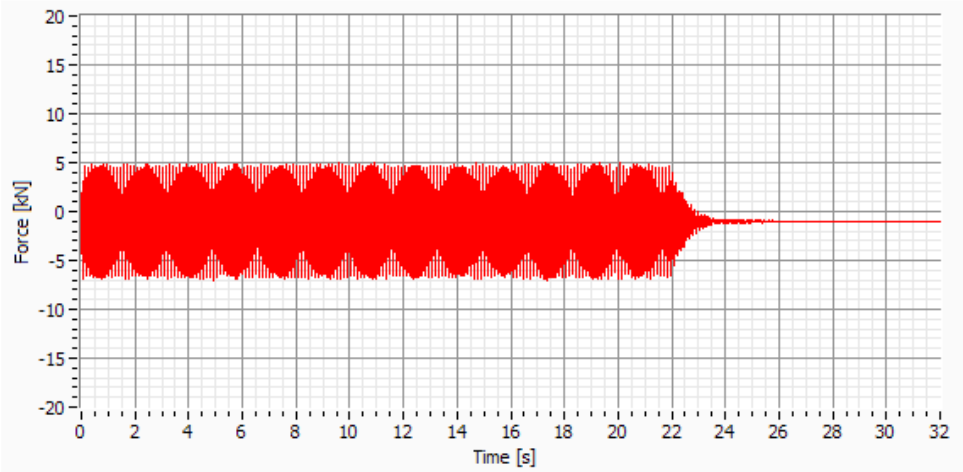

Figure VI.7: Global force in the North side.

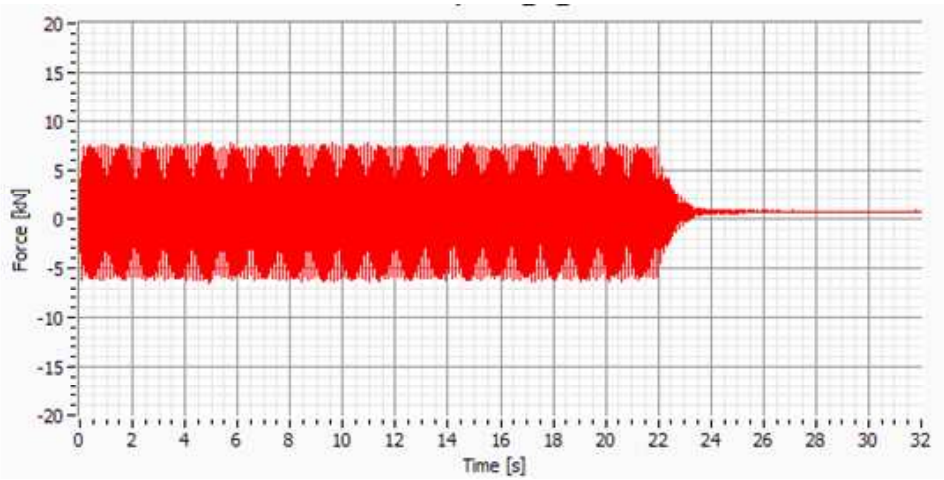

Figure VI.8: Global force in the South side.

Test 10 – Artificial EC8 (EW PGA=0.60g)

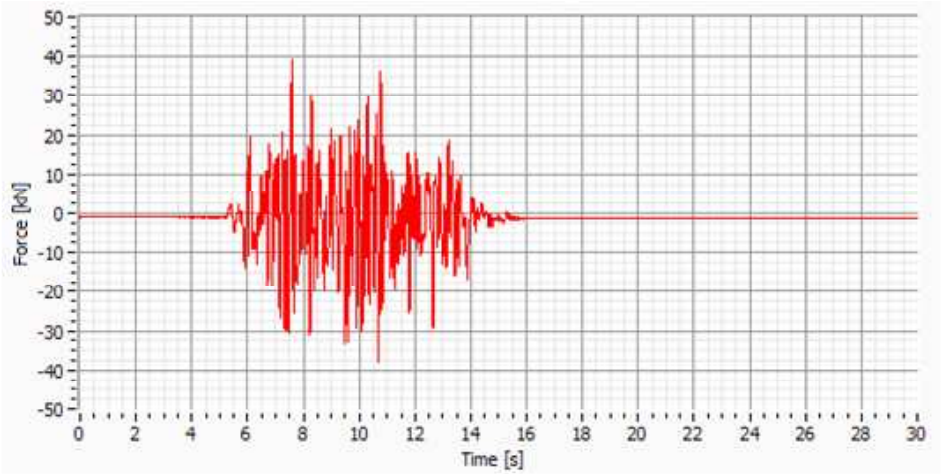

Figure VI.9: Global force in the North side.

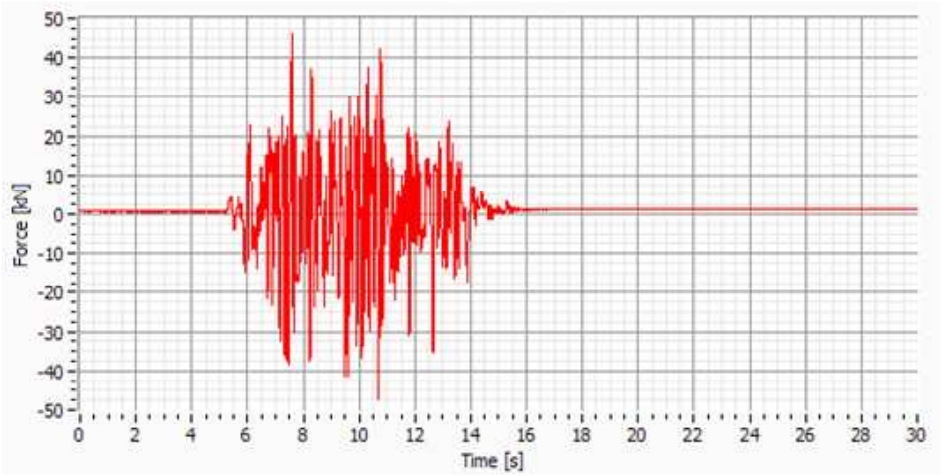

Figure VI.10: Global force in the South side.

Test 10 – Artificial EC8 (EW PGA=0.80g)

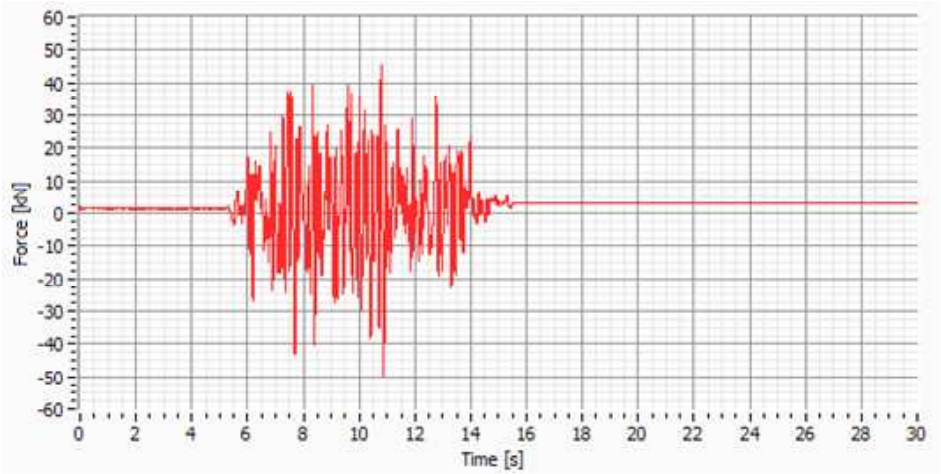

Figure VI.11: Global force in the North side.

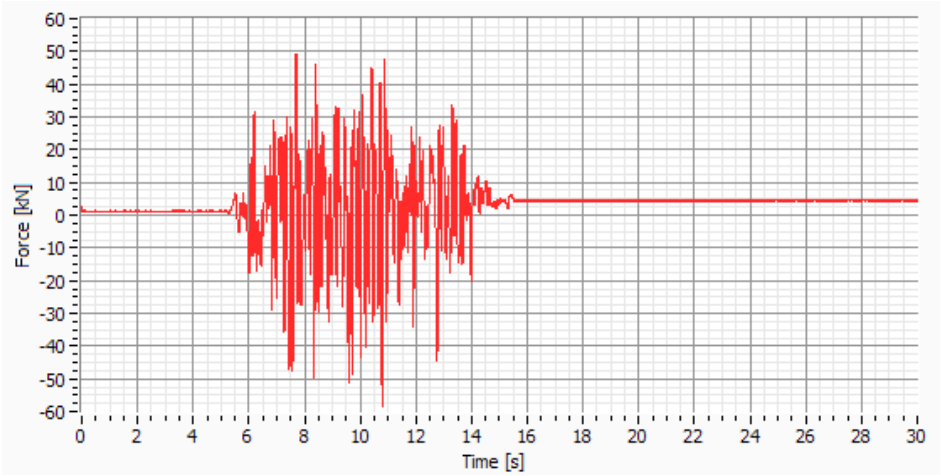

Figure VI.12: Global force in the South side.

Test 14 – Artificial EC8 (EW PGA=1.0g)

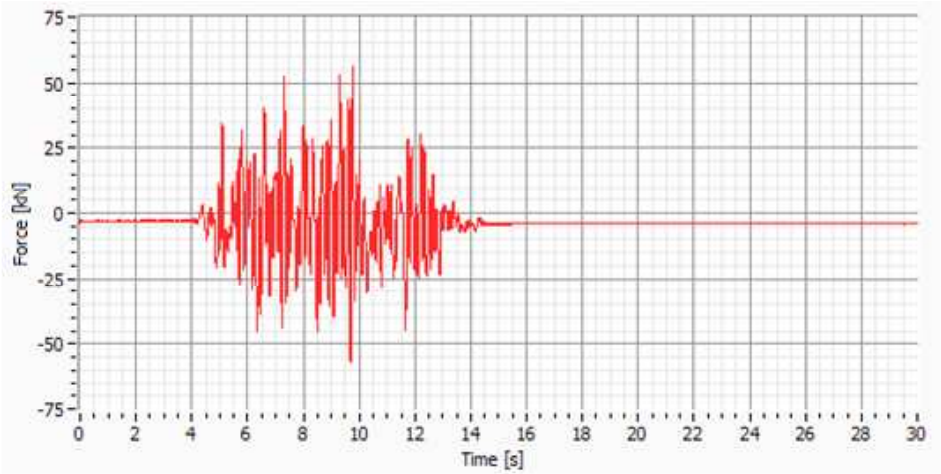

Figure VI.13: Global force in the North side.

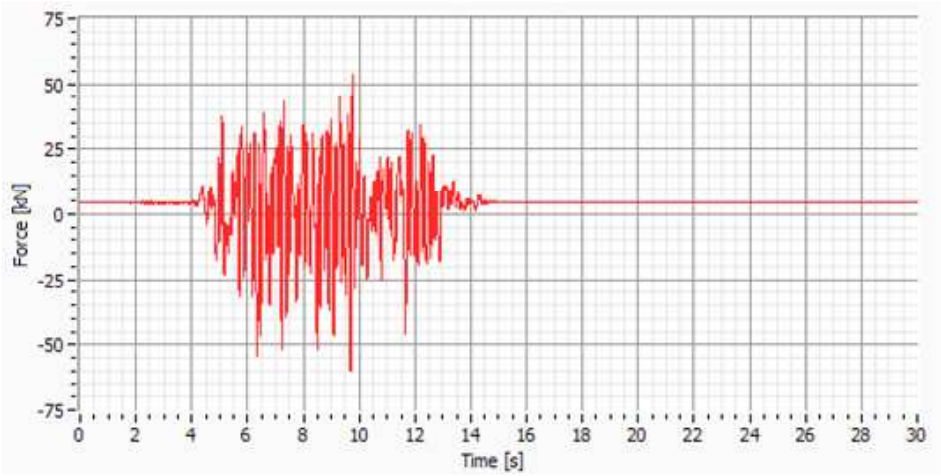

Figure VI.14: Global force in the South side.

Test 17 – ElCentro (EW PGA=0.20g)

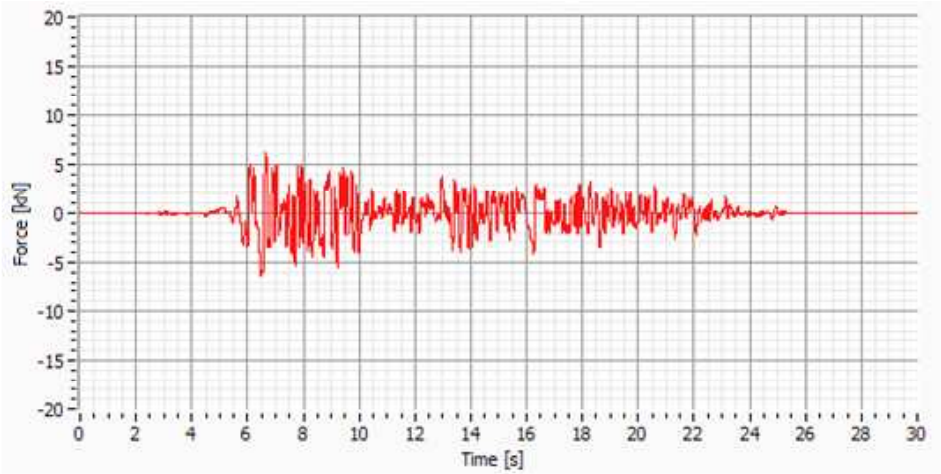

Figure VI.15: Global force in the North side.

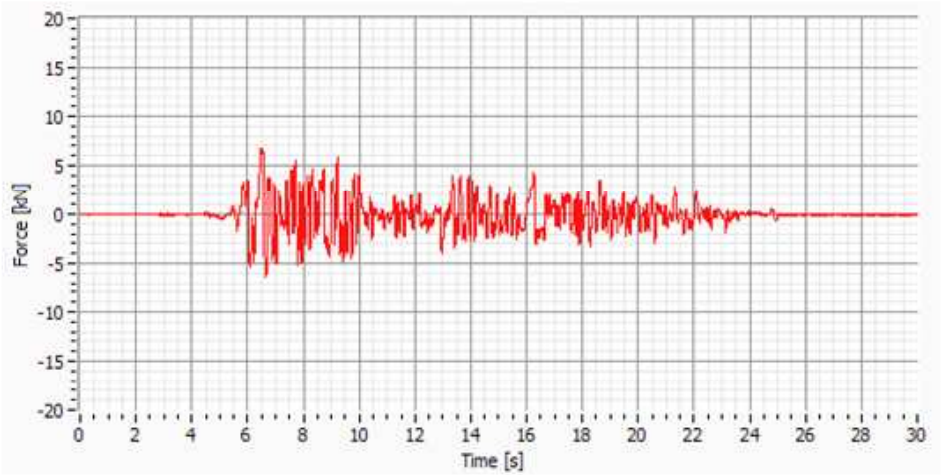

Figure VI.16: Global force in the South side.

Test 18 – Sen 9.48Hz (EW PGA=0.05g)

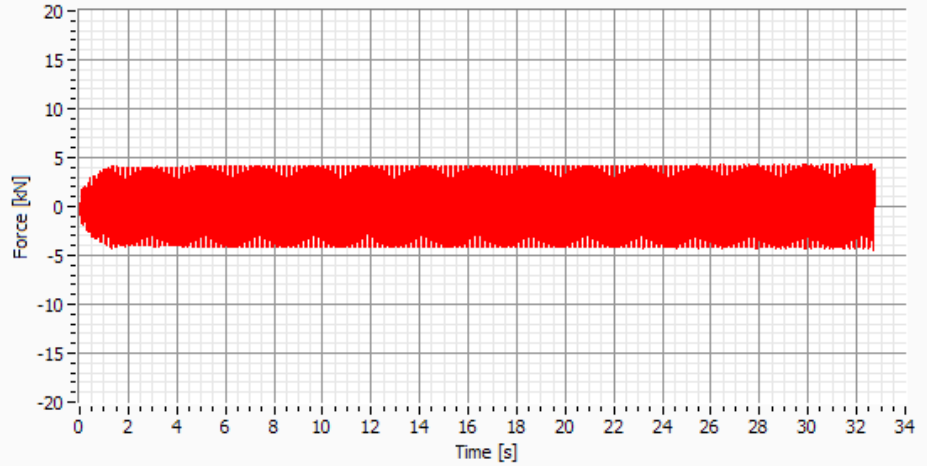

Figure VI.17: Global force in the North side.

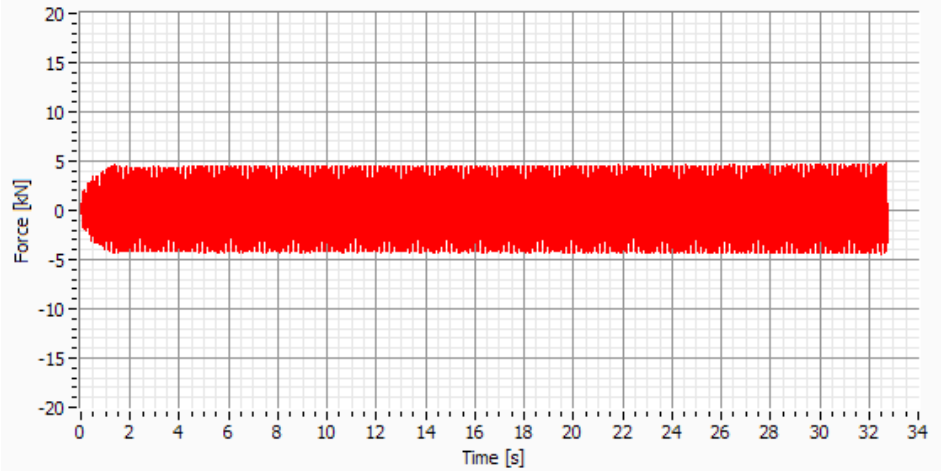

Figure VI.18: Global force in the South side.

Test 19 – Artificial EC8 (EW PGA=0.20g)

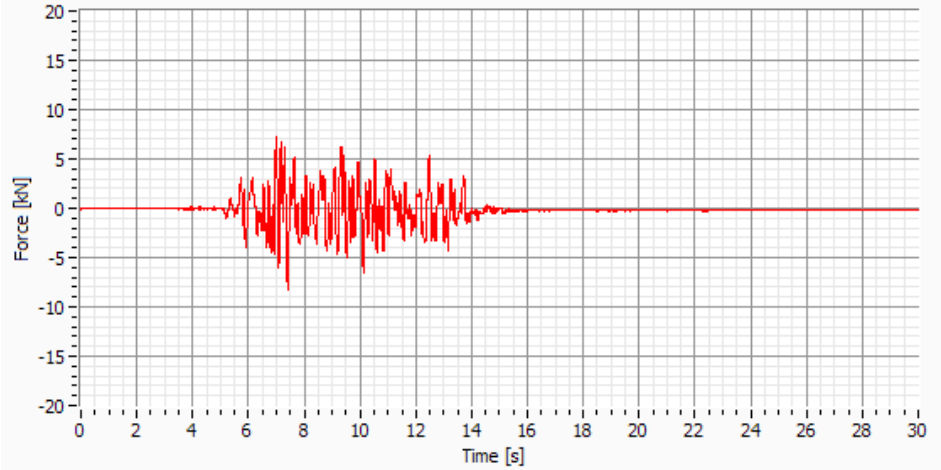

Figure VI.19: Global force in the North side.

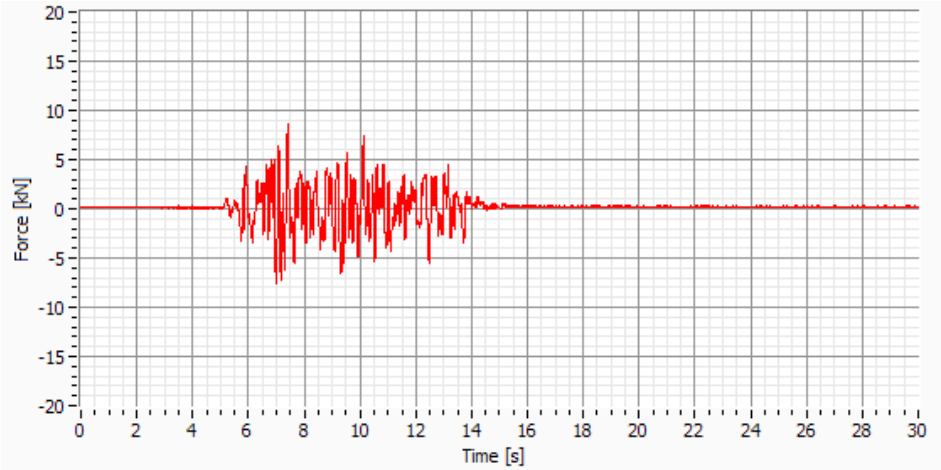

Figure VI.20: Global force in the South side.

Test 20 – Sen 7.58Hz (EW PGA=0.05g)

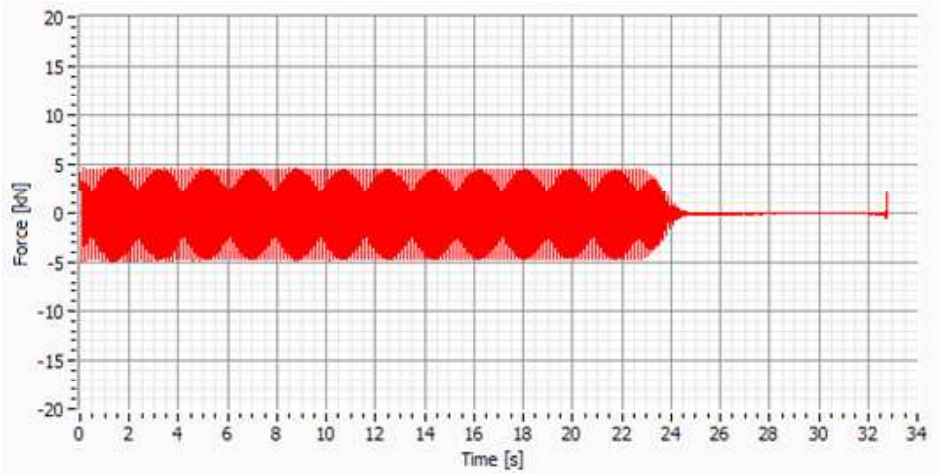

Figure VI.21: Global force in the North side.

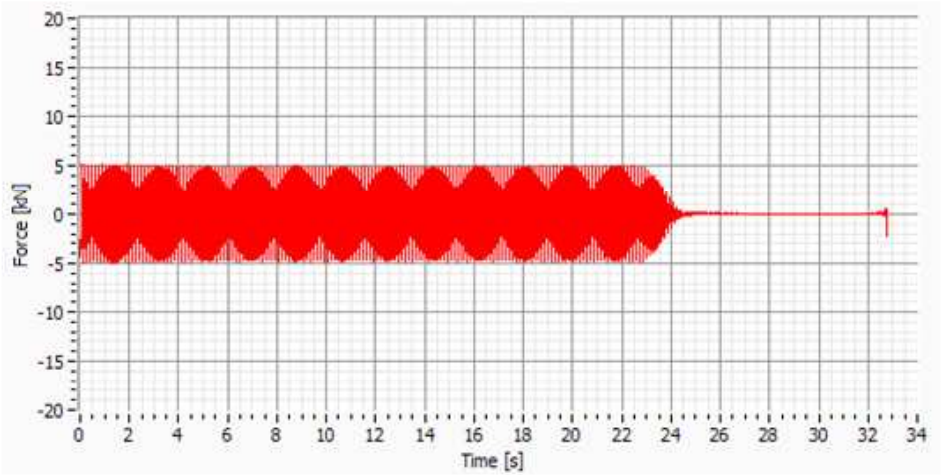

Figure VI.22: Global force in the South side.

Test 22 – Artificial EC8 (EW PGA=0.60g)

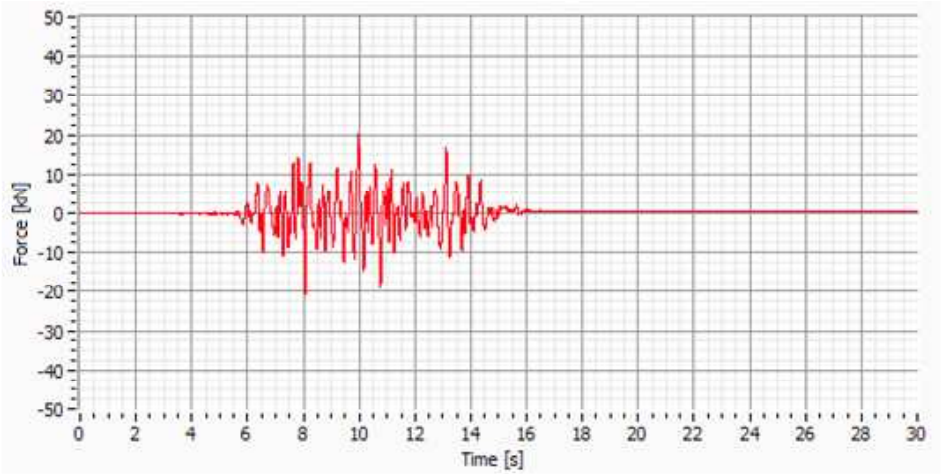

Figure VI.23: Global force in the North side.

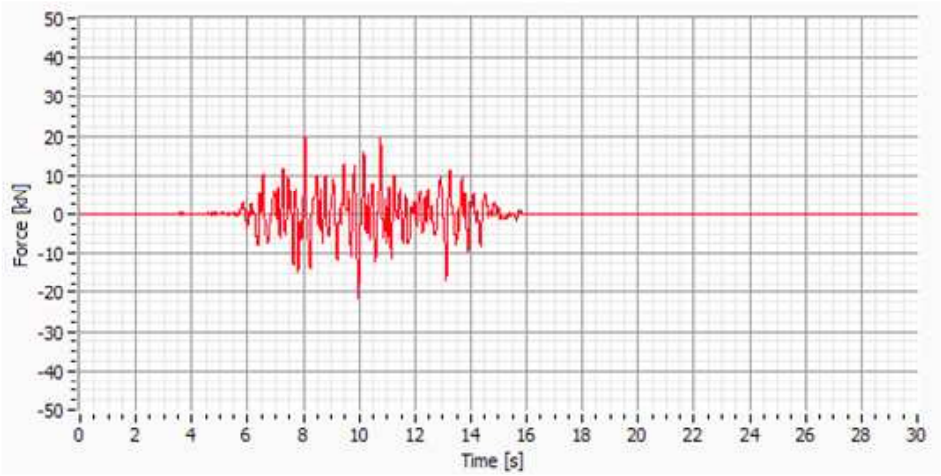

Figure VI.24: Global force in the South side.

Test 24 – Artificial EC8 (EW PGA=0.80g)

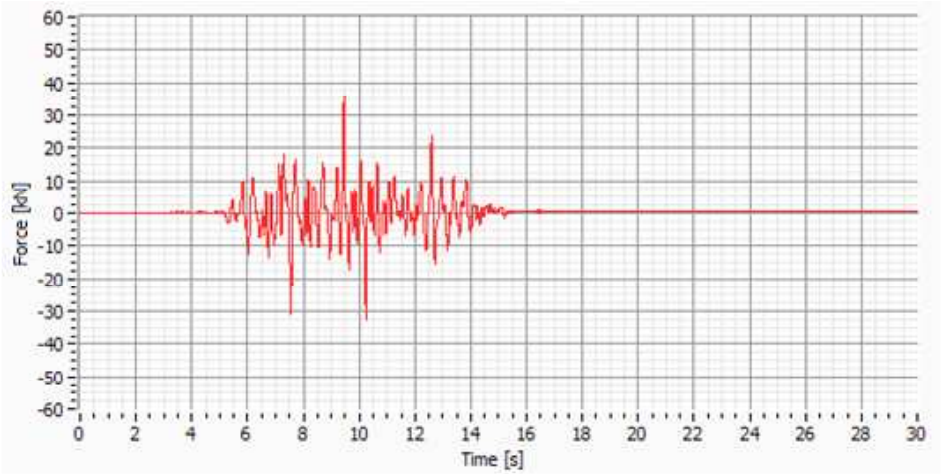

Figure VI.25: Global force in the North side.

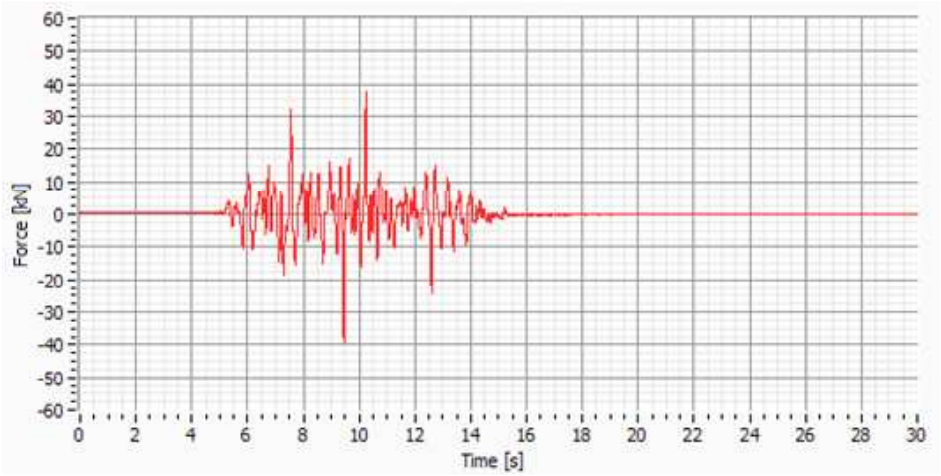

Figure VI.26: Global force in the South side.

Test 26 – Artificial EC8 (EW PGA=1.0g)

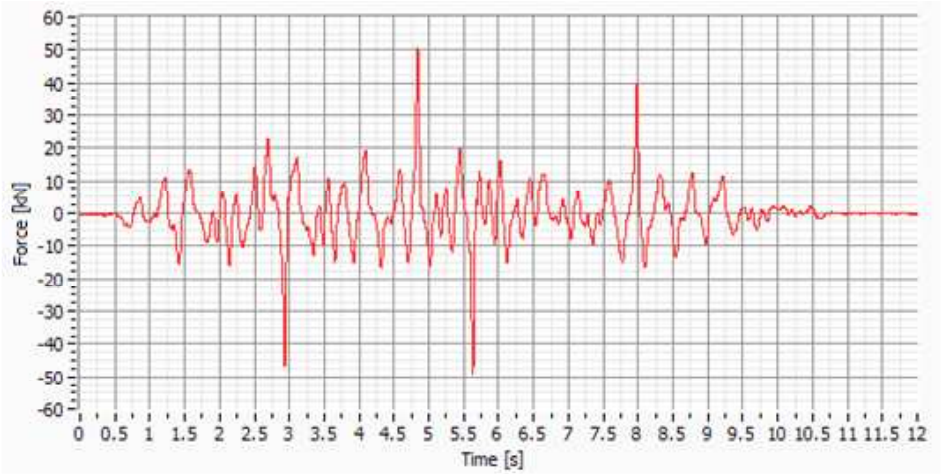

Figure VI.27: Global force in the North side.

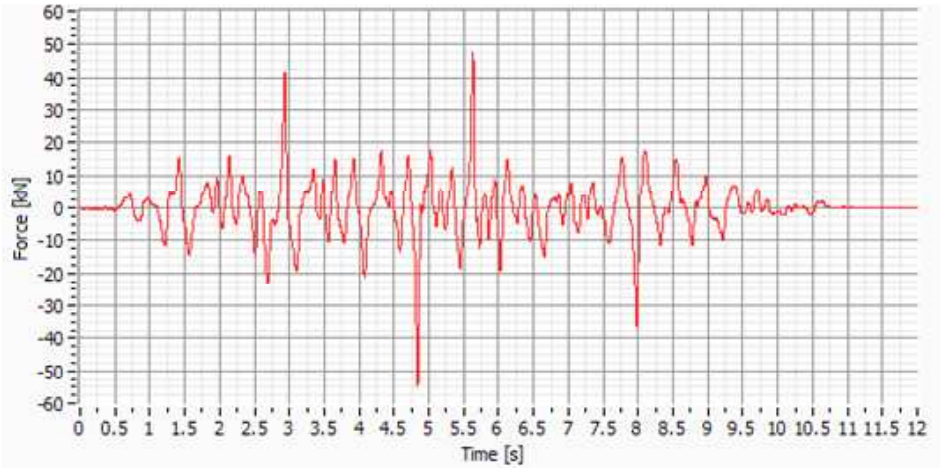

Figure VI.28: Global force in the South side.

ANNEX VII

Global Hysteretic Loops in the Dissipation Devices

INDEX OF FIGURES

Test 5 – ElCentro (EW PGA=0.20g)

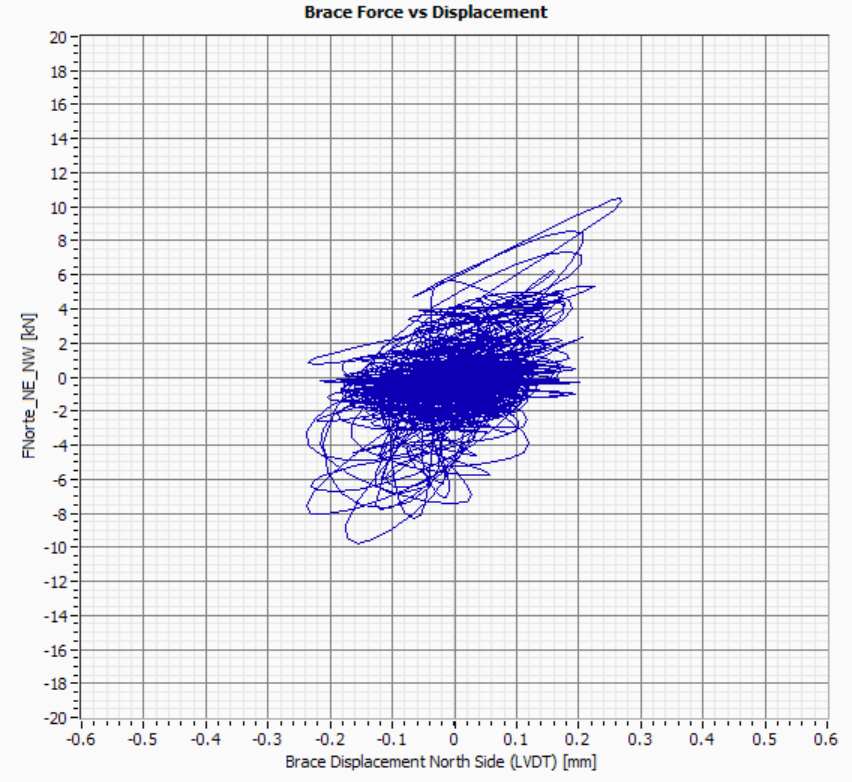

Figure VII.1: Shear Force – Brace displacement in the North side.

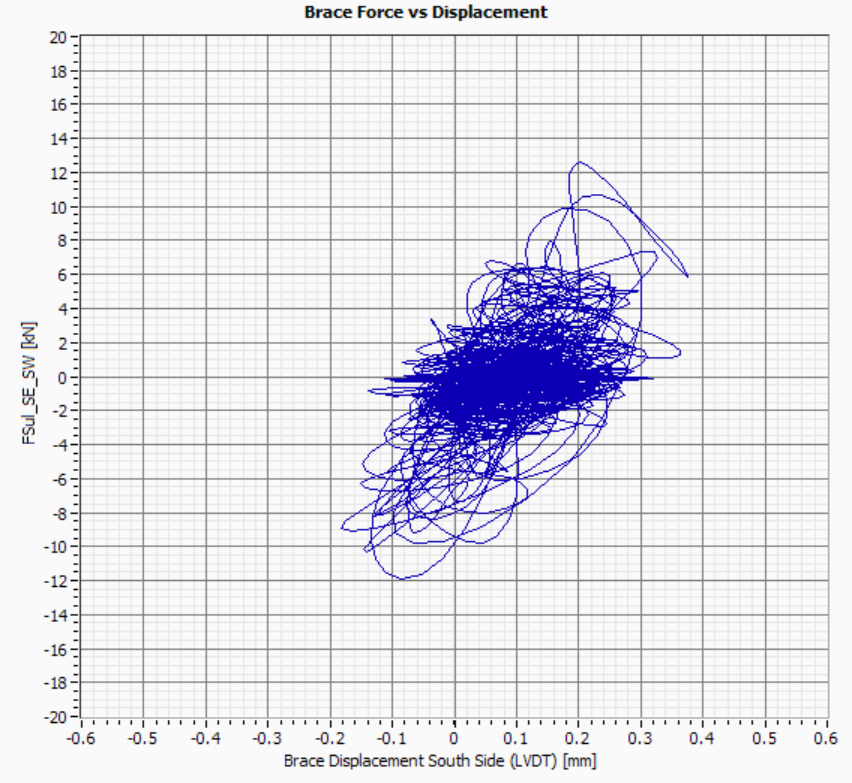

Figure VII.2: Shear Force – Brace displacement in the South side.

Test 6 – Sen 10.28Hz (EW PGA=0.05g)

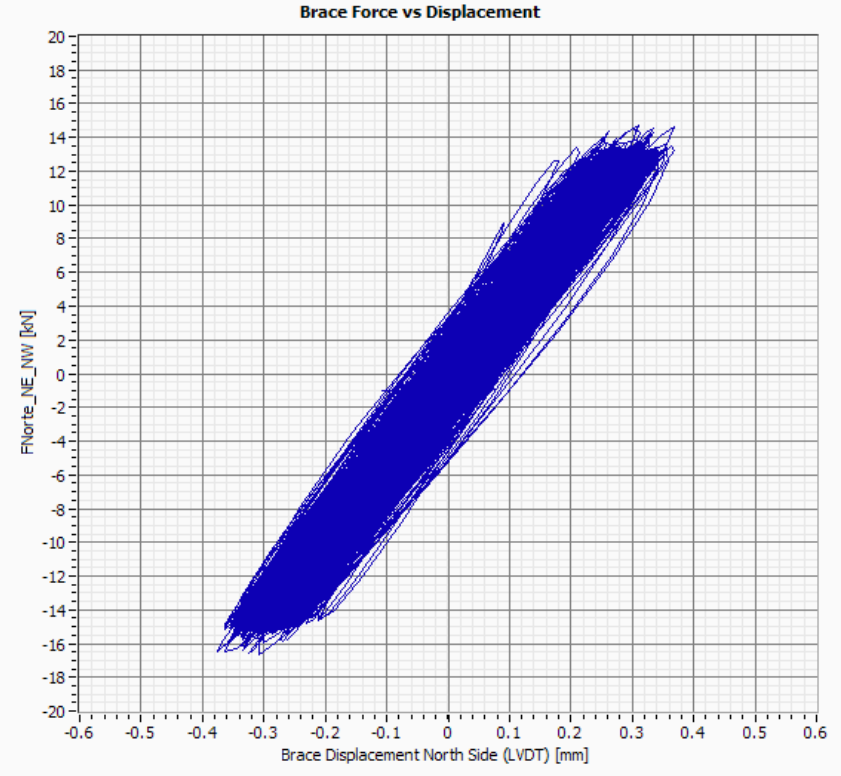

Figure VII.3: Shear Force – Brace displacement in the North side.

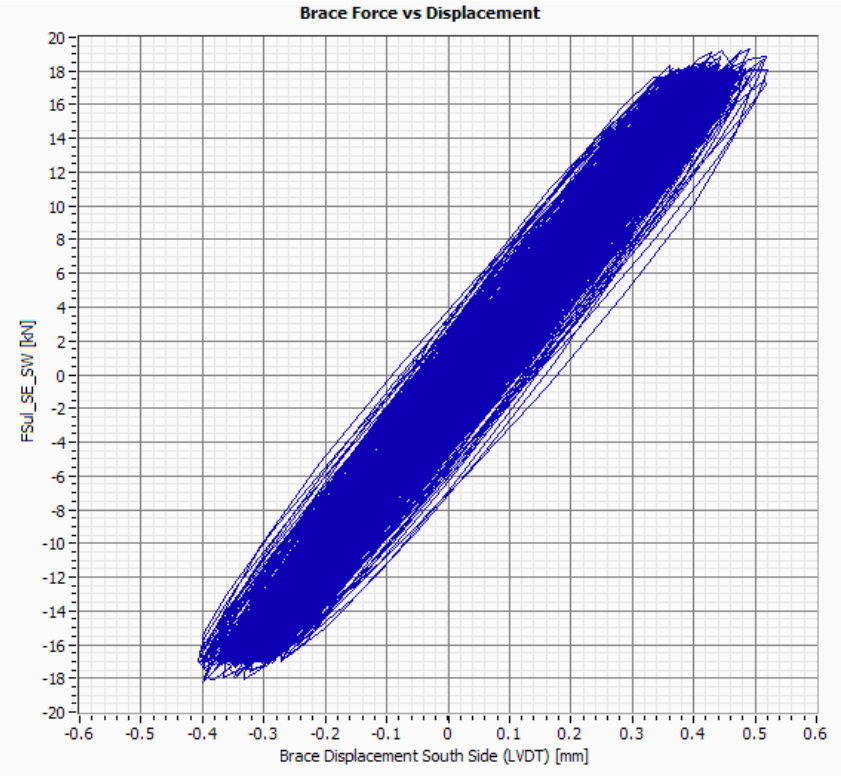

Figure VII.4: Shear Force – Brace displacement in the South side.

Test 7 – Artificial EC8 (EW PGA=0.20g)

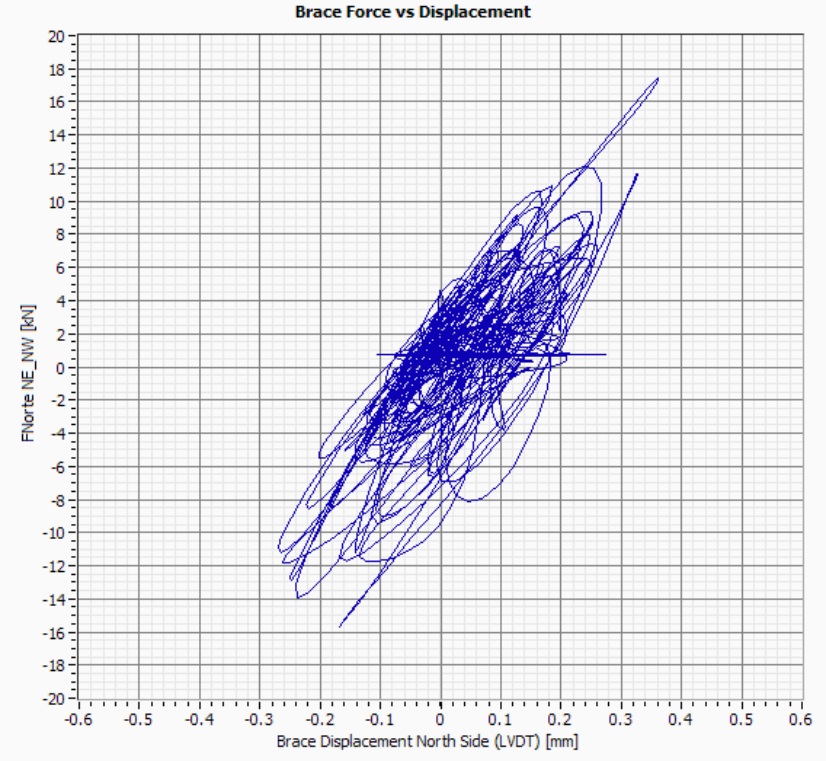

Figure VII.5: Shear Force – Brace displacement in the North side.

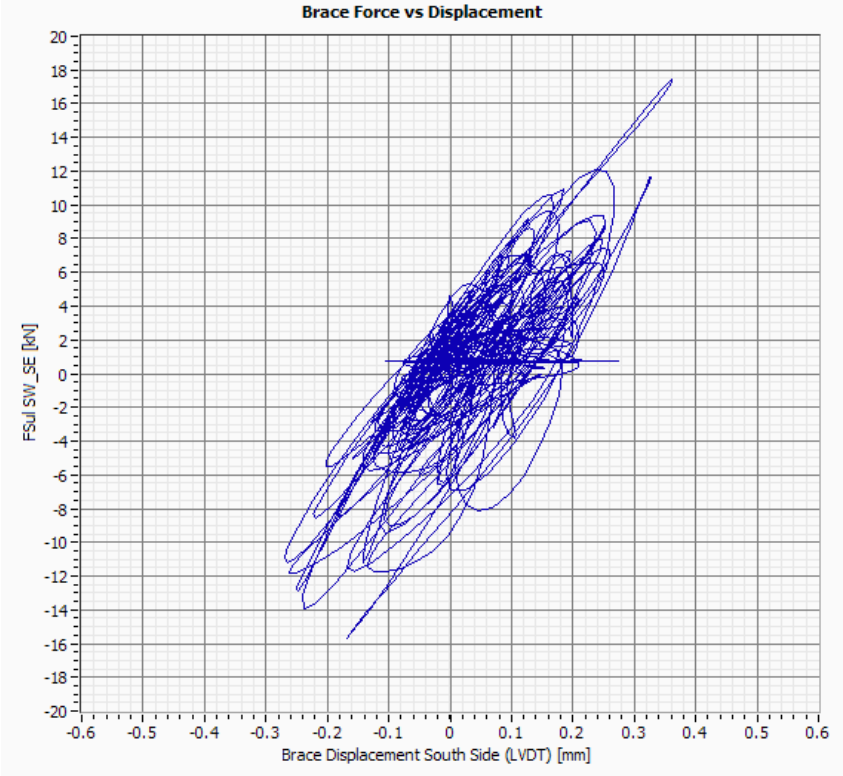

Figure VII.6: Shear Force – Brace displacement in the South side.

Test 8 – Sen 8.22Hz (EW PGA=0.05g)

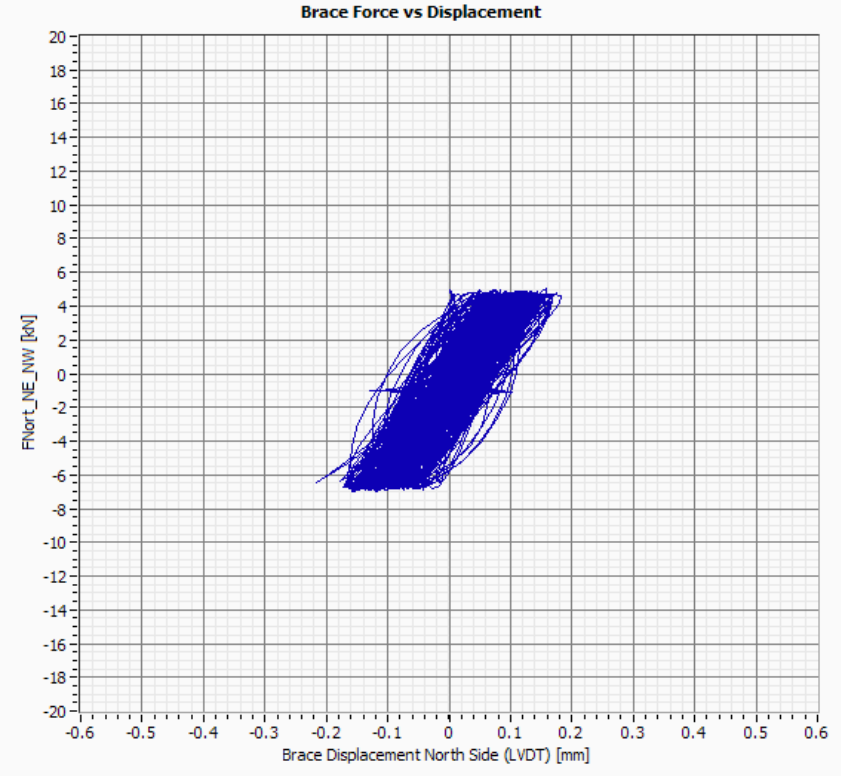

Figure VII.7: Shear Force – Brace displacement in the North side.

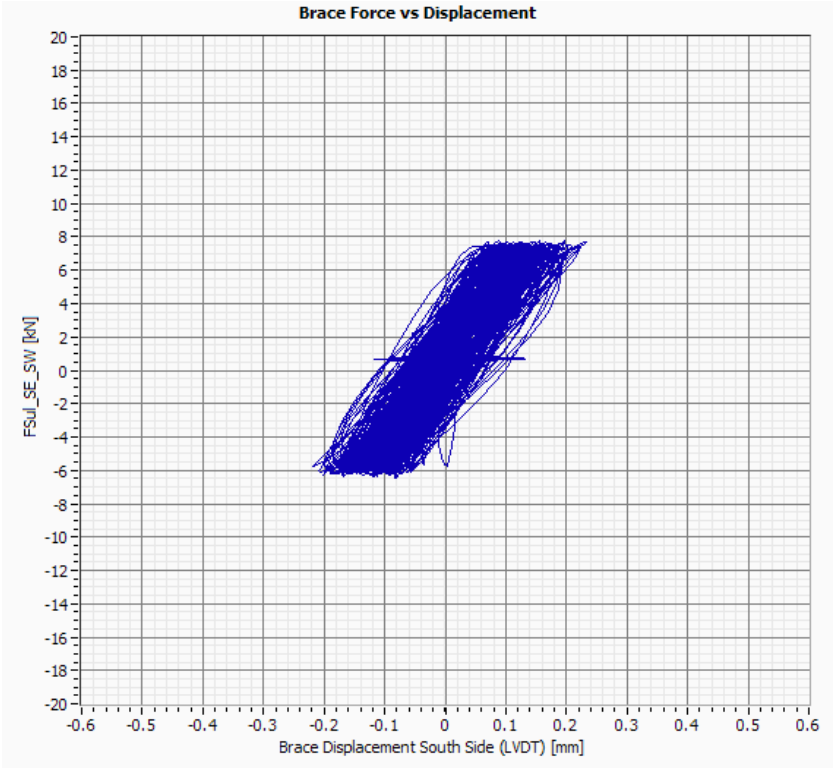

Figure VII.8: Shear Force – Brace displacement in the South side.

Test 10 – Artificial EC8 (EW PGA=0.60g)

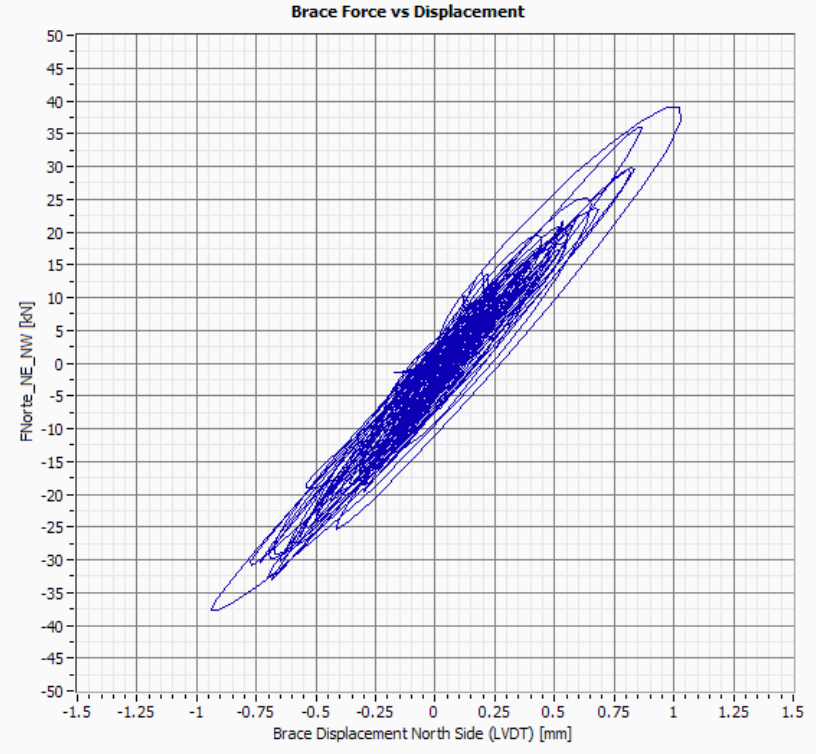

Figure VII.9: Shear Force – Brace displacement in the North side.

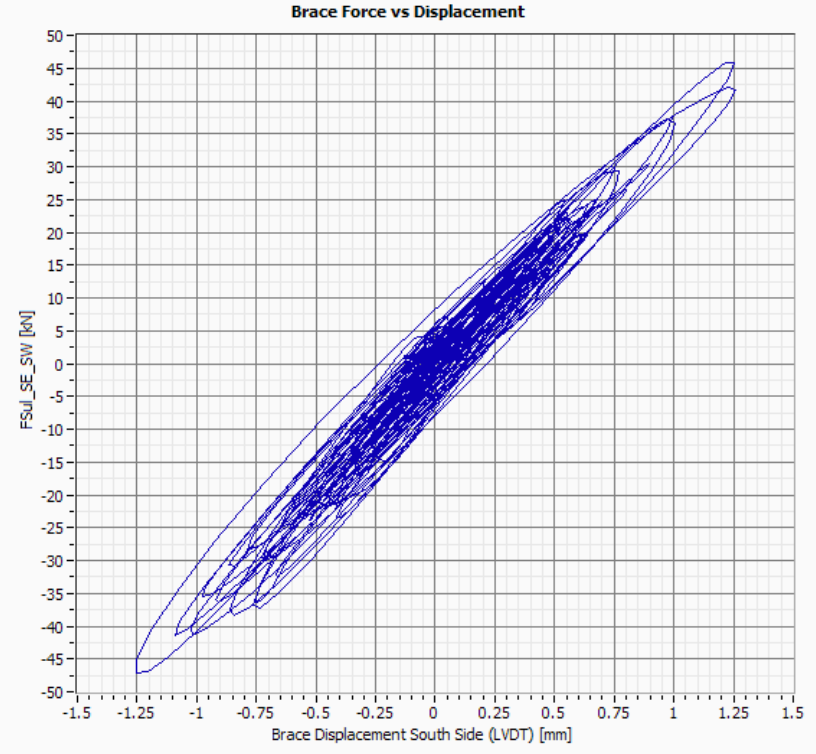

Figure VII.10: Shear Force – Brace displacement in the South side.

Test 12 – Artificial EC8 (EW PGA=0.80g)

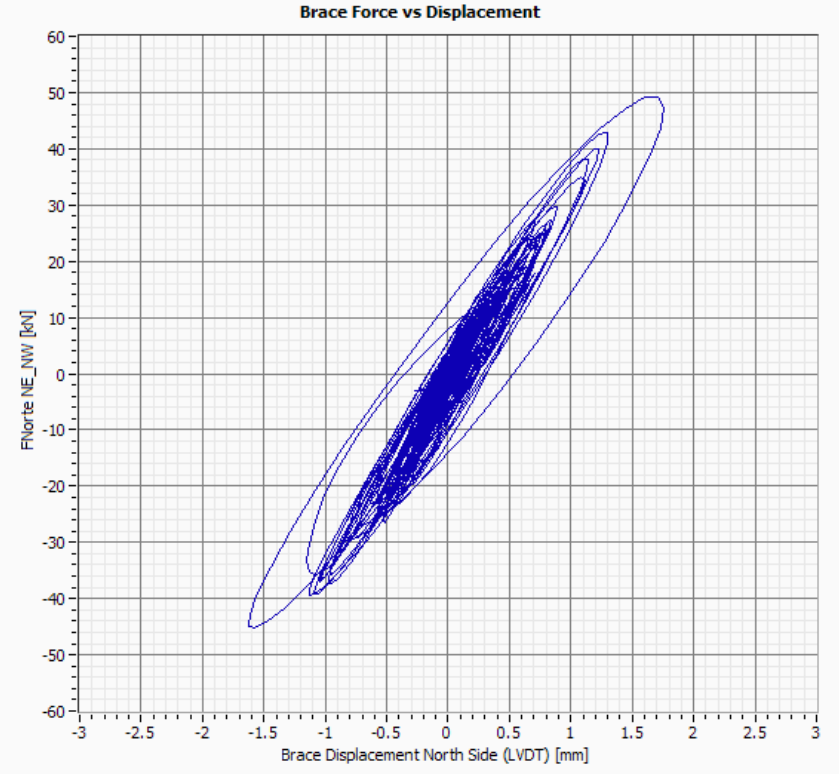

Figure VII.11: Shear Force – Brace displacement in the North side.

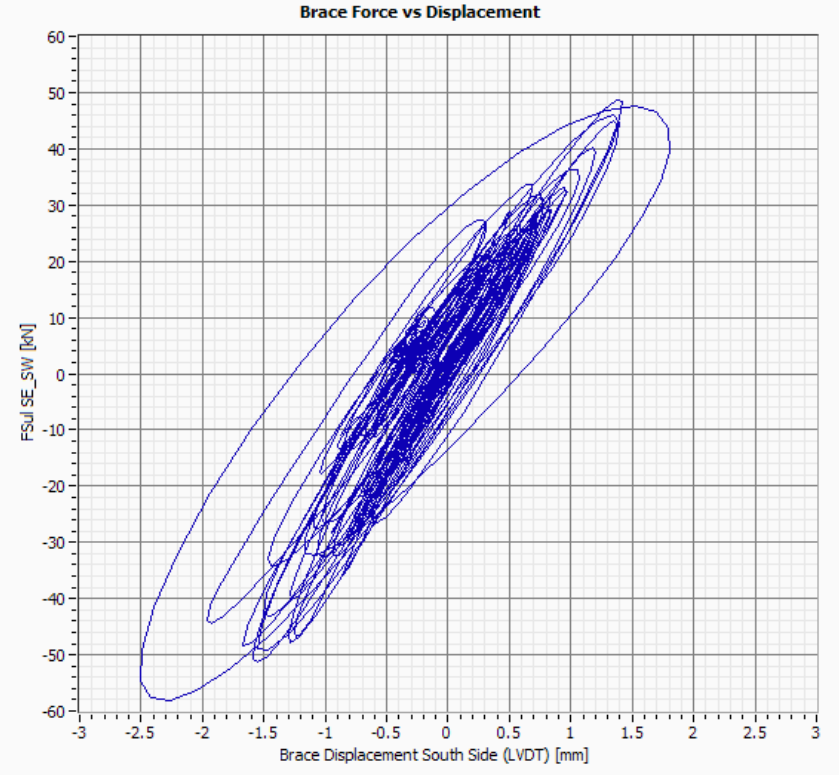

Figure VII.12: Shear Force – Brace displacement in the South side.

Test 14 – Artificial EC8 (EW PGA=1.0g)

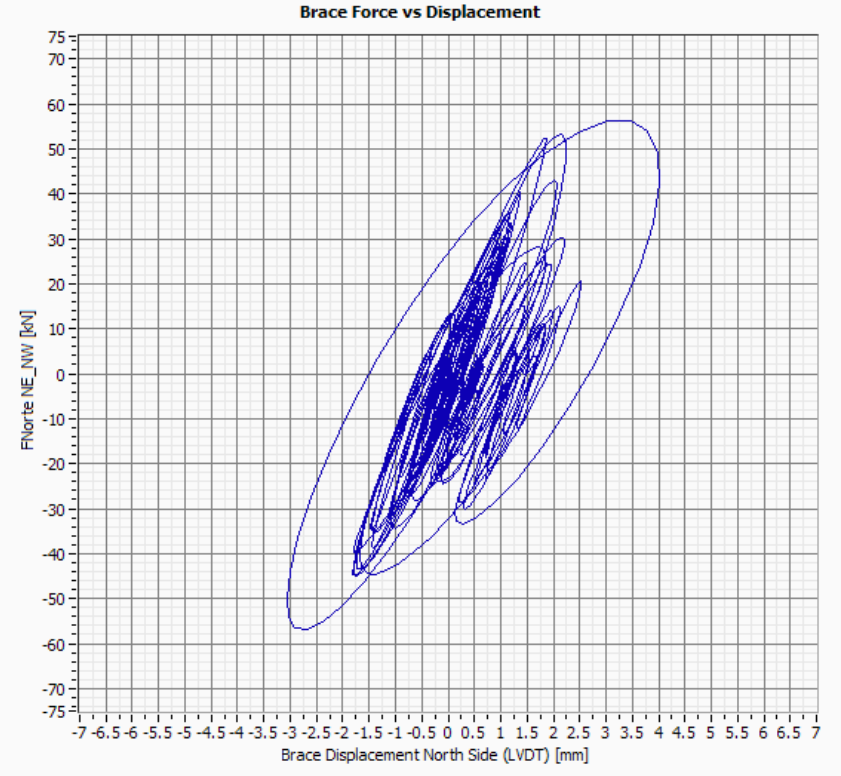

Figure VII.13: Shear Force – Brace displacement in the North side.

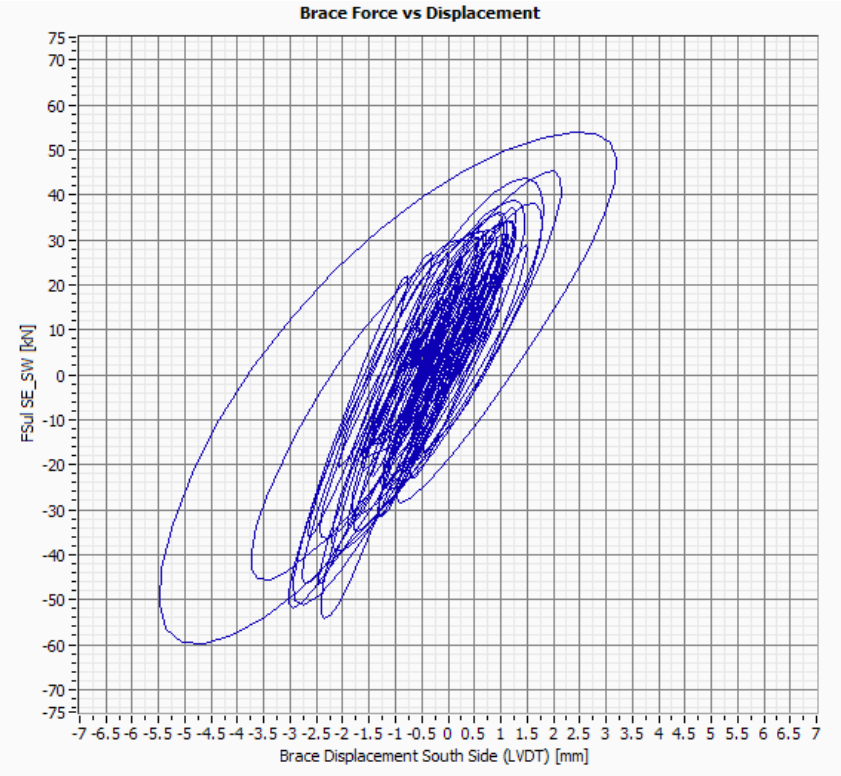

Figure VII.14: Shear Force – Brace displacement in the South side.

Test 17 – ElCentro (EW PGA=0.20g)

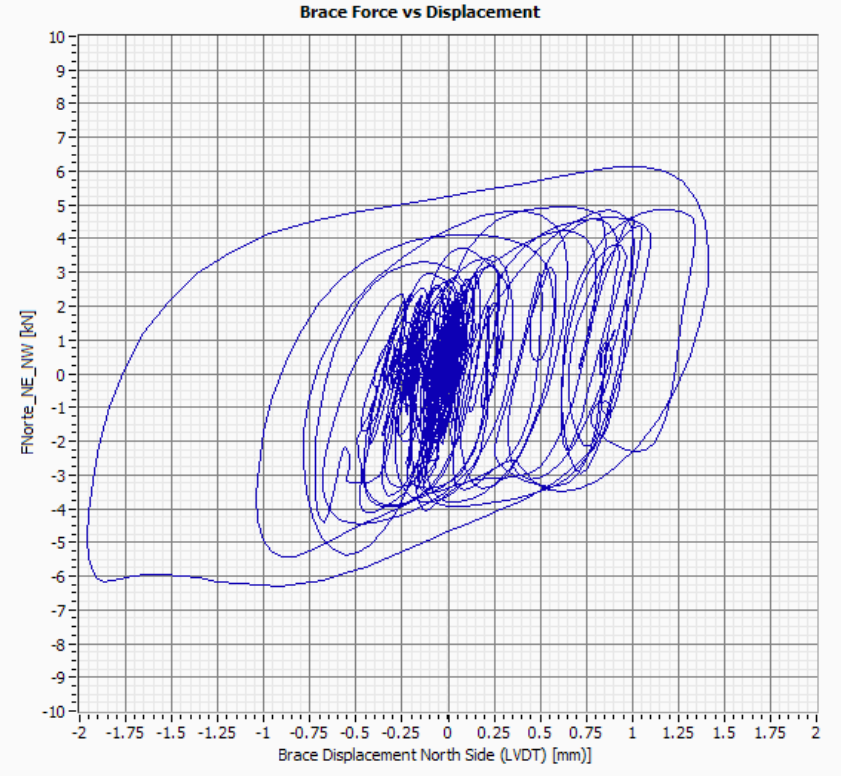

Figure VII.15: Shear Force – Brace displacement in the North side.

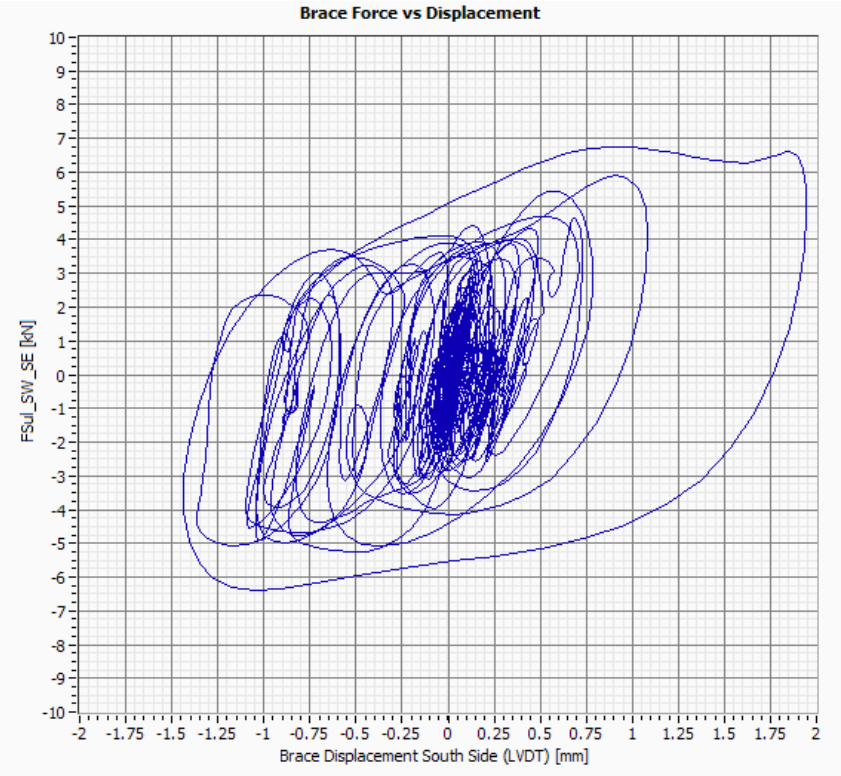

Figure VII.16: Shear Force – Brace displacement in the South side.

Test 18 – Sen 9.48Hz (EW PGA=0.05g)

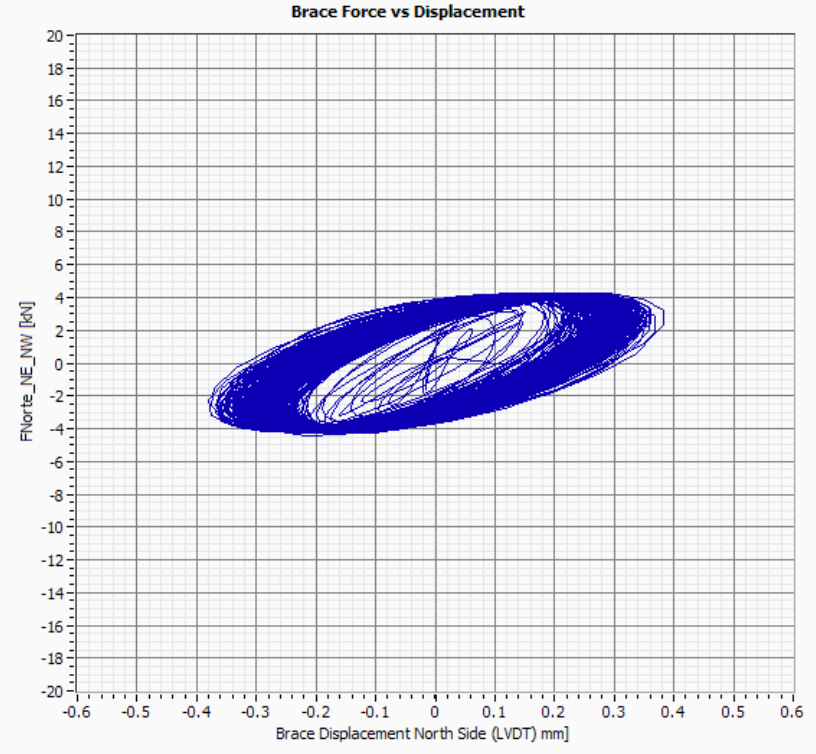

Figure VII.17: Shear Force – Brace displacement in the North side.

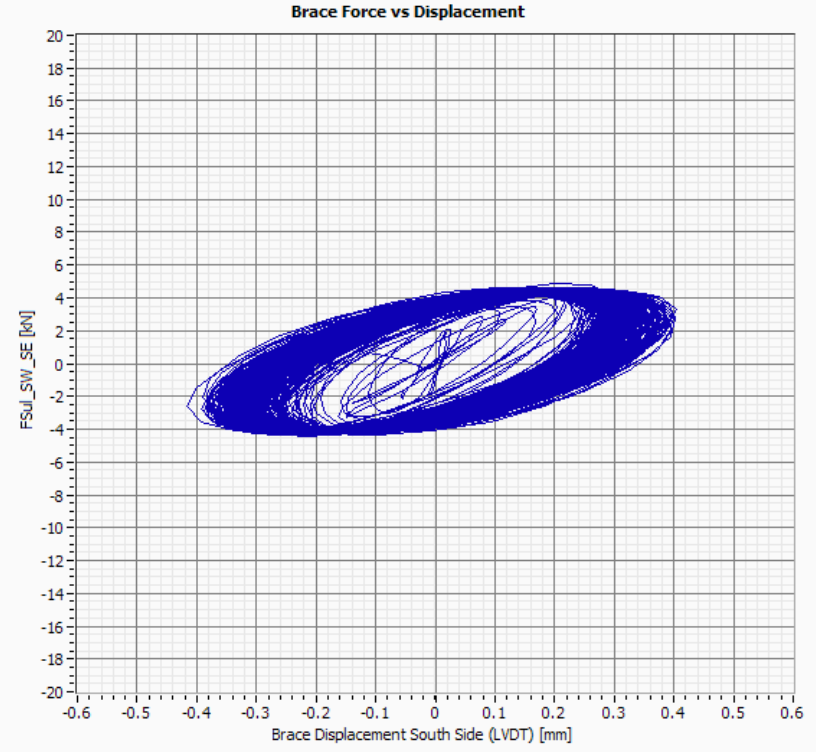

Figure VII.18: Shear Force – Brace displacement in the South side.

Test 19 – Artificial EC8 (EW PGA=0.20g)

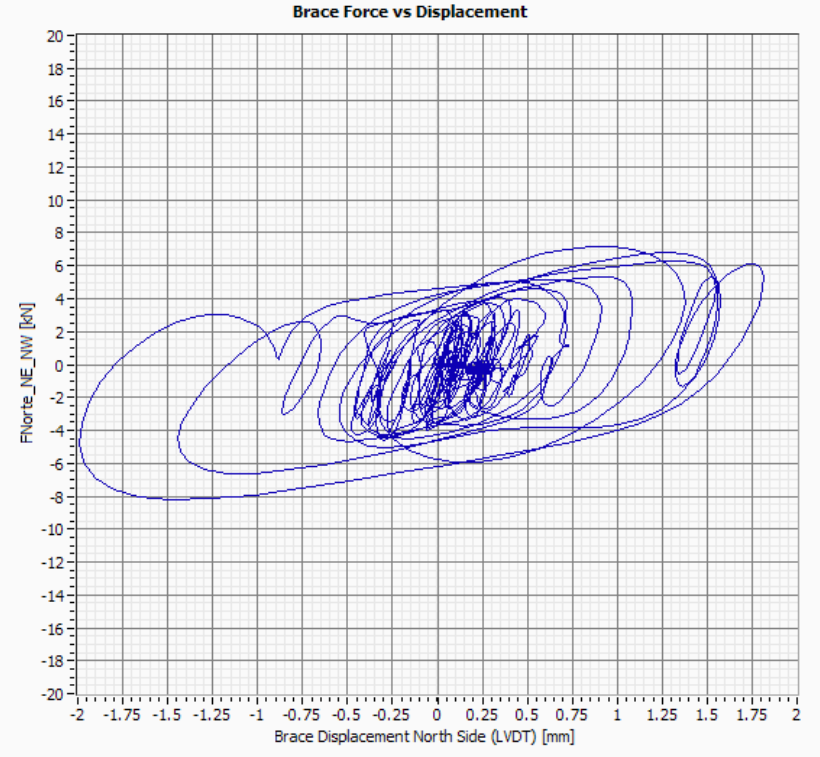

Figure VII.19: Shear Force – Brace displacement in the North side.

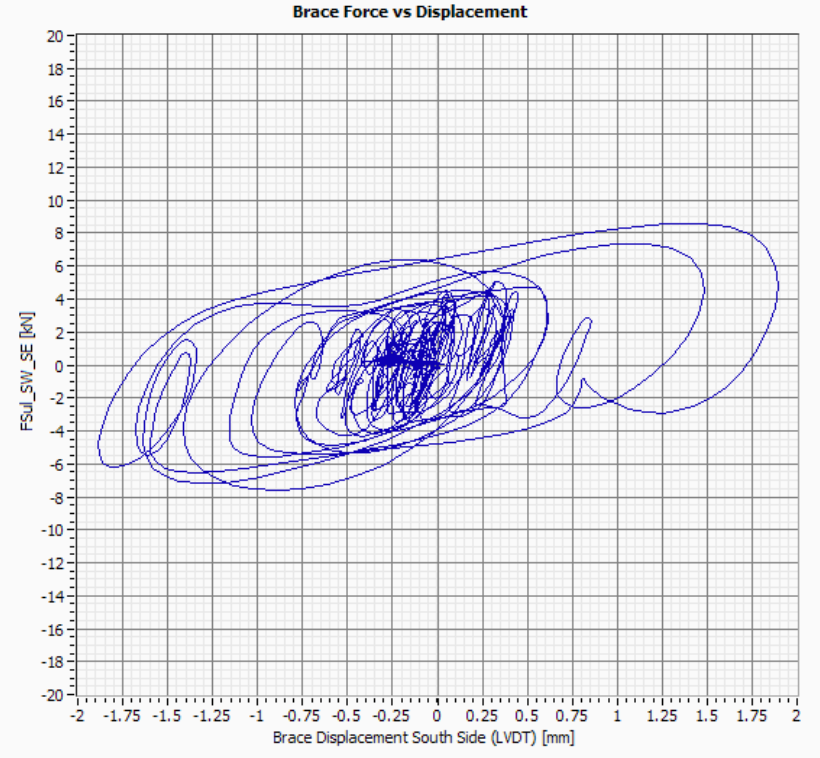

Figure VII.20: Shear Force – Brace displacement in the South side.

Test 20 – Sen 7.58Hz (EW PGA=0.05g)

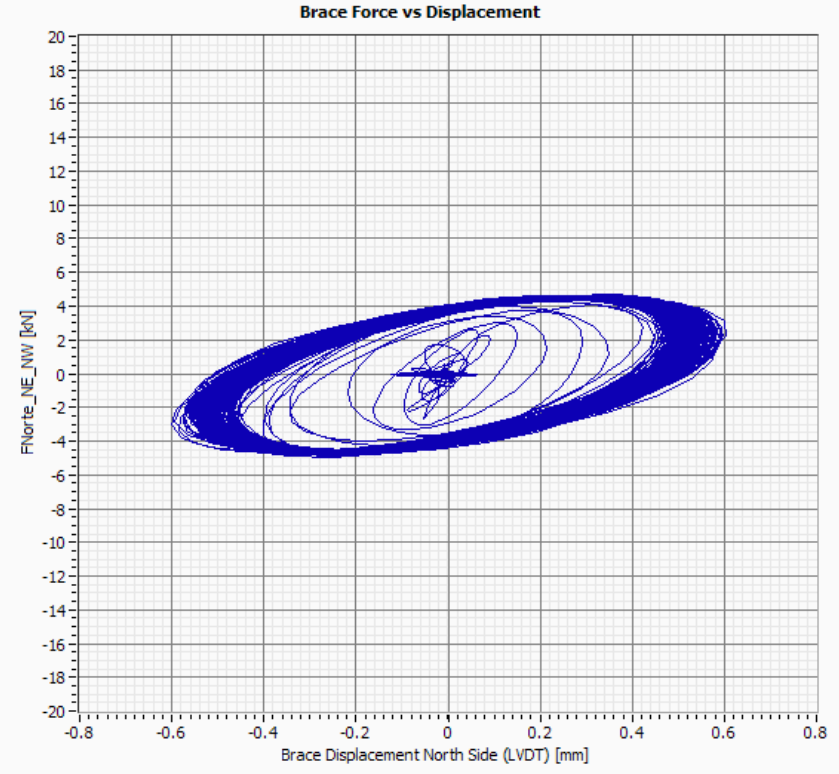

Figure VII.21: Shear Force – Brace displacement in the North side.

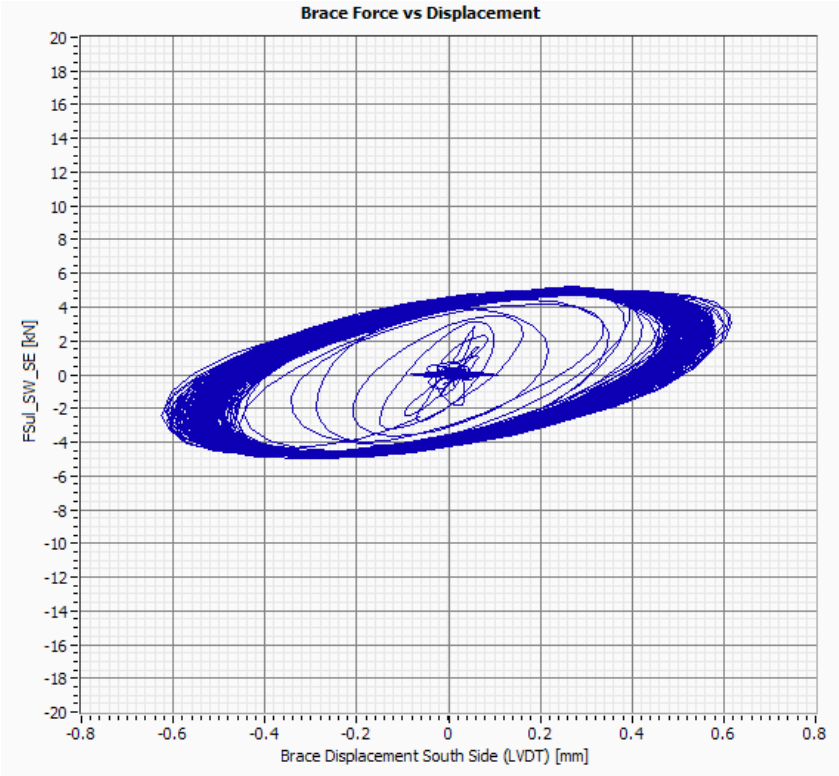

Figure VII.22: Shear Force – Brace displacement in the South side.

Test 22 – Artificial EC8 (EW PGA=0.60g)

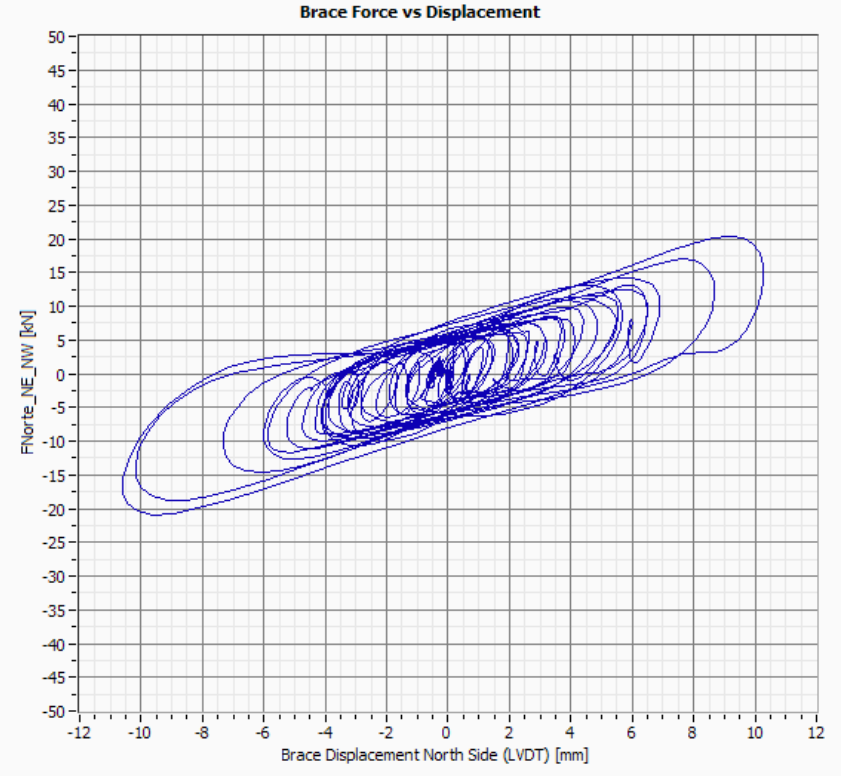

Figure VII.23: Shear Force – Brace displacement in the North side.

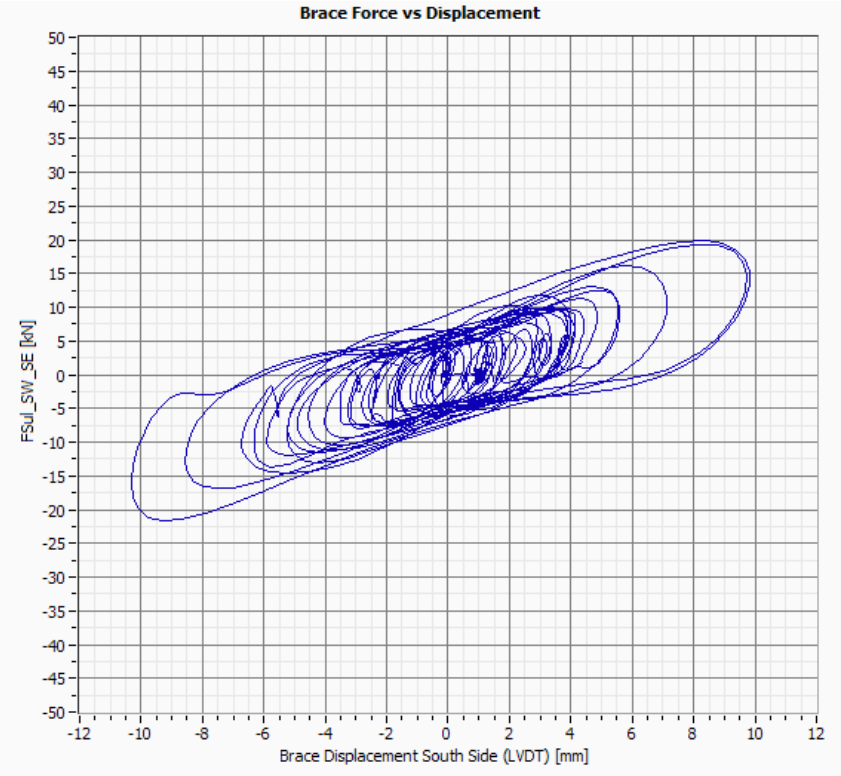

Figure VII.24: Shear Force – Brace displacement in the South side.

Test 24 – Artificial EC8 (EW PGA=0.80g)

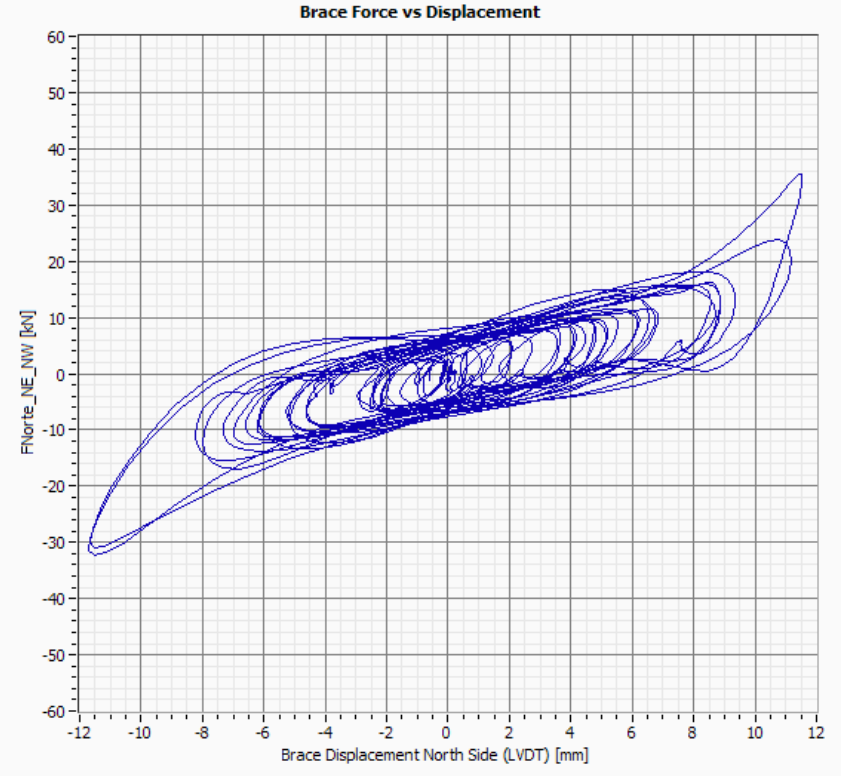

Figure VII.25: Shear Force – Brace displacement in the North side.

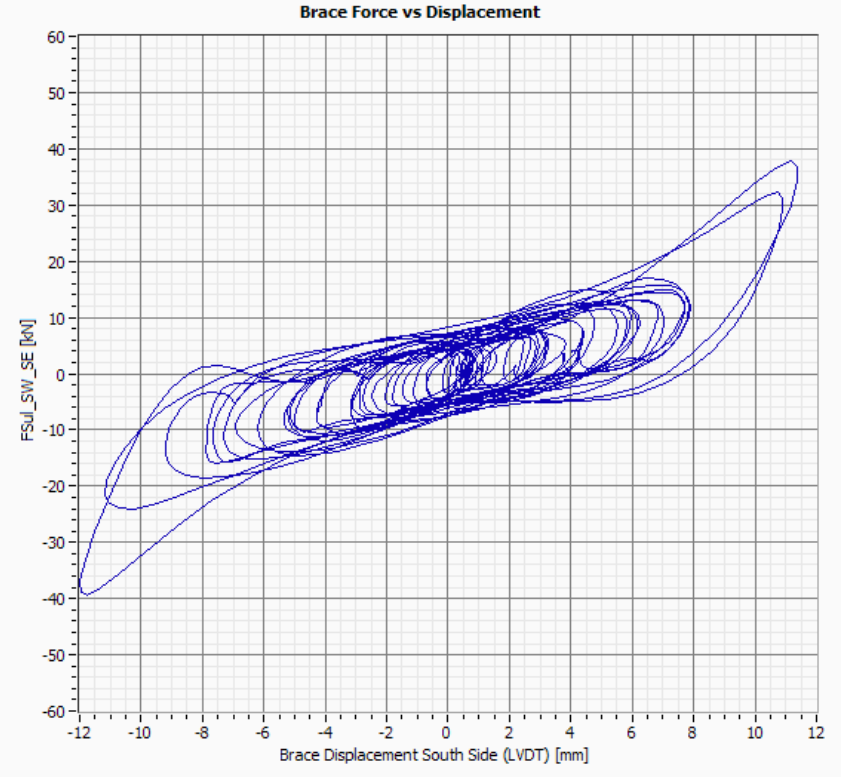

Figure VII.26: Shear Force – Brace displacement in the South side.

Test 26 – Artificial EC8 (EW PGA=1.0g)

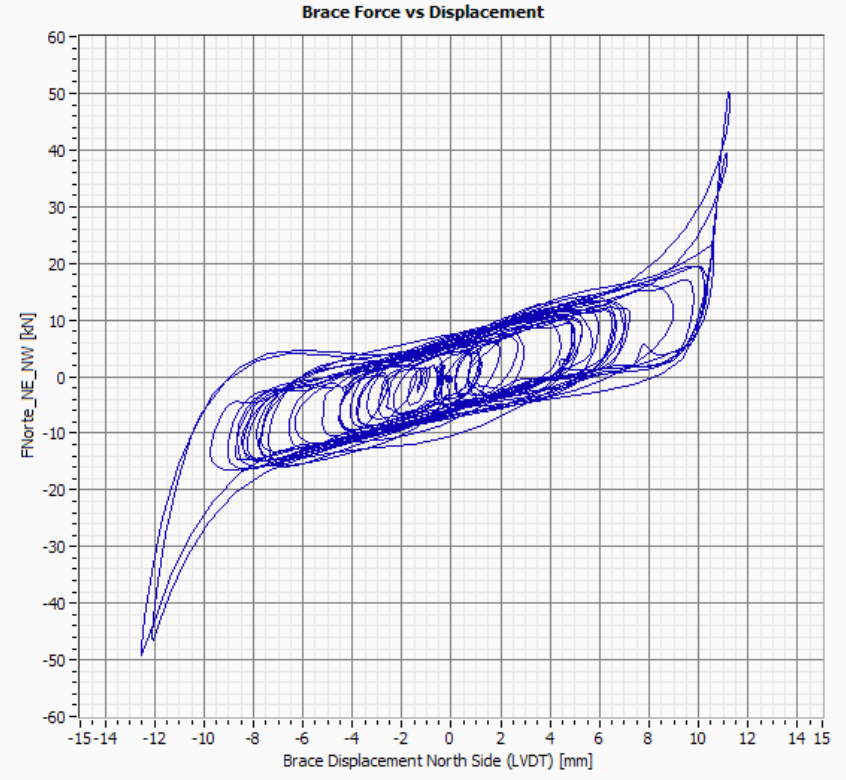

Figure VII.27: Shear Force – Brace displacement in the North side.

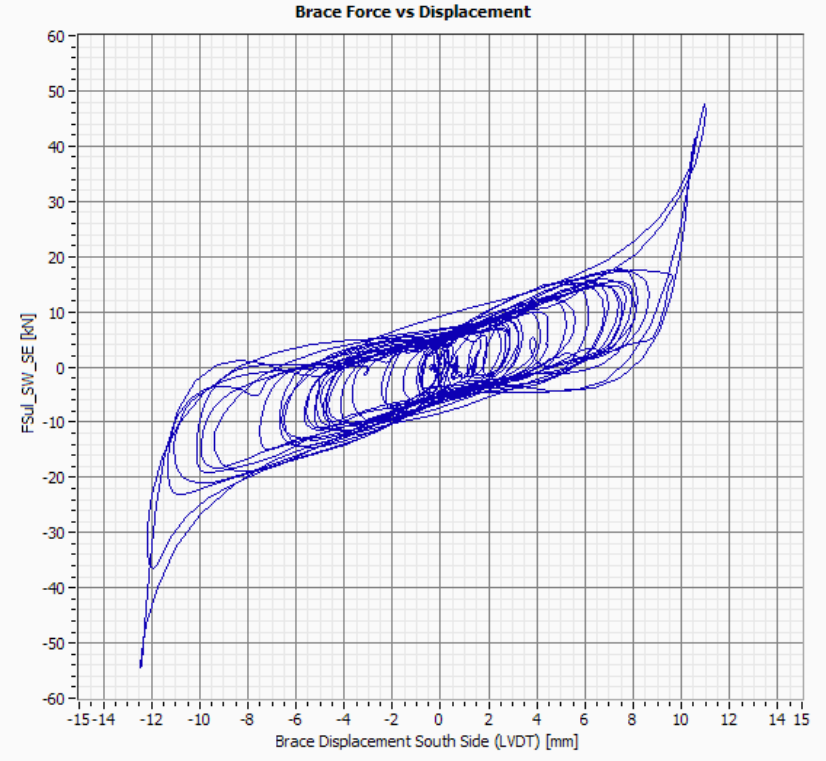

Figure VII.28: Shear Force – Brace displacement in the South side.

ANNEX VIII

Energy Dissipation in the Devices

INDEX OF FIGURES

Test 5 – ElCentro (EW PGA=0.20g)

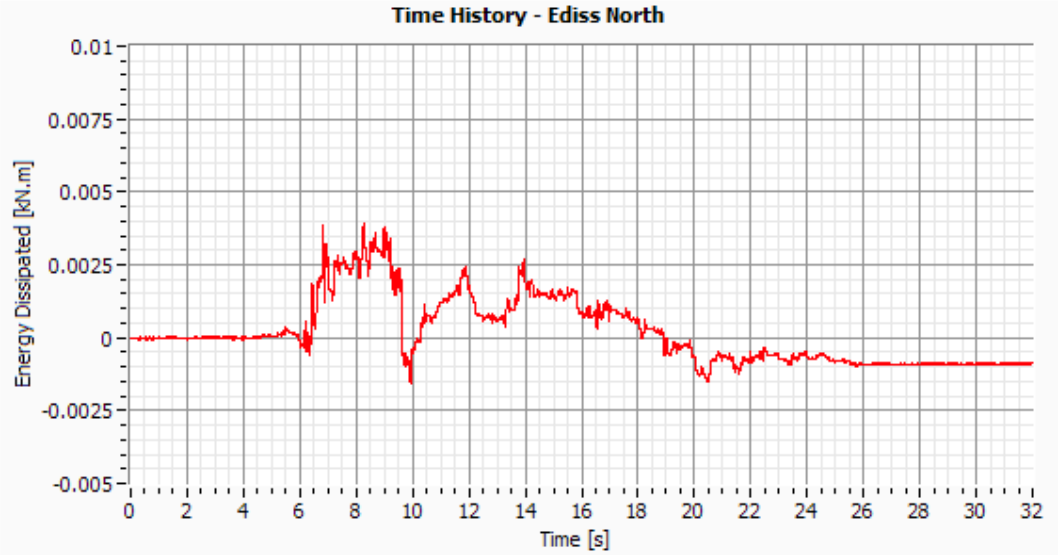

Figure VIII.1: Energy dissipation in the North side.

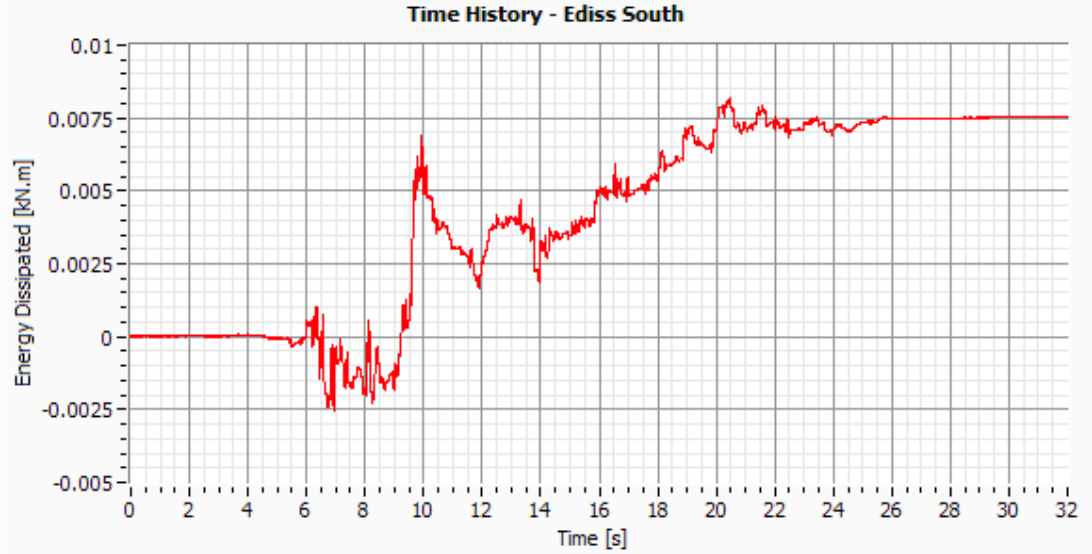

Figure VIII.2: Energy dissipation in the South side.

Test 6 – Sen 10.28Hz (EW PGA=0.05g)

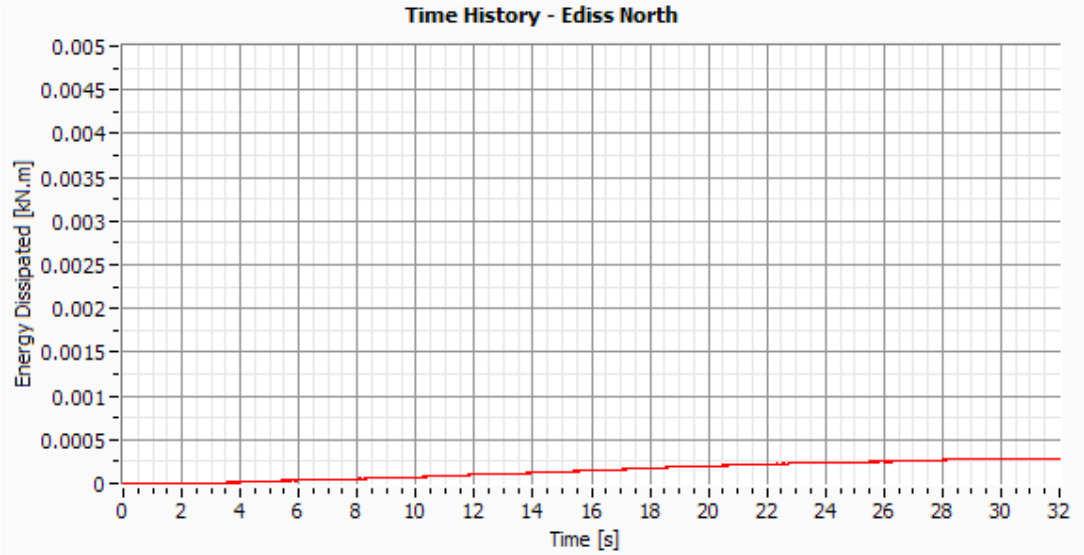

Figure VIII.3: Energy dissipation in the North side.

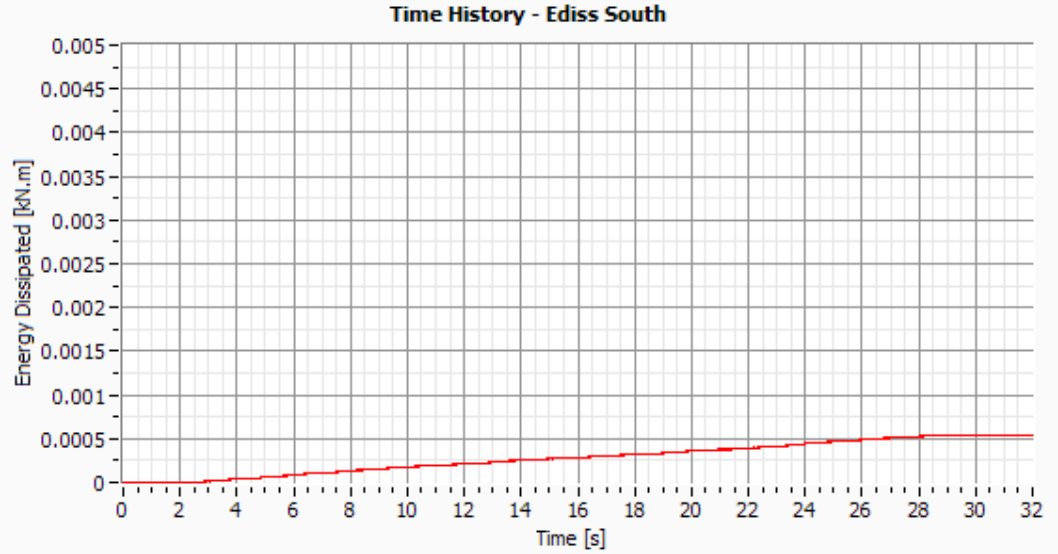

Figure VIII.4: Energy dissipation in the South side.

Test 7 – Artificial EC8 (EW PGA=0.20g)

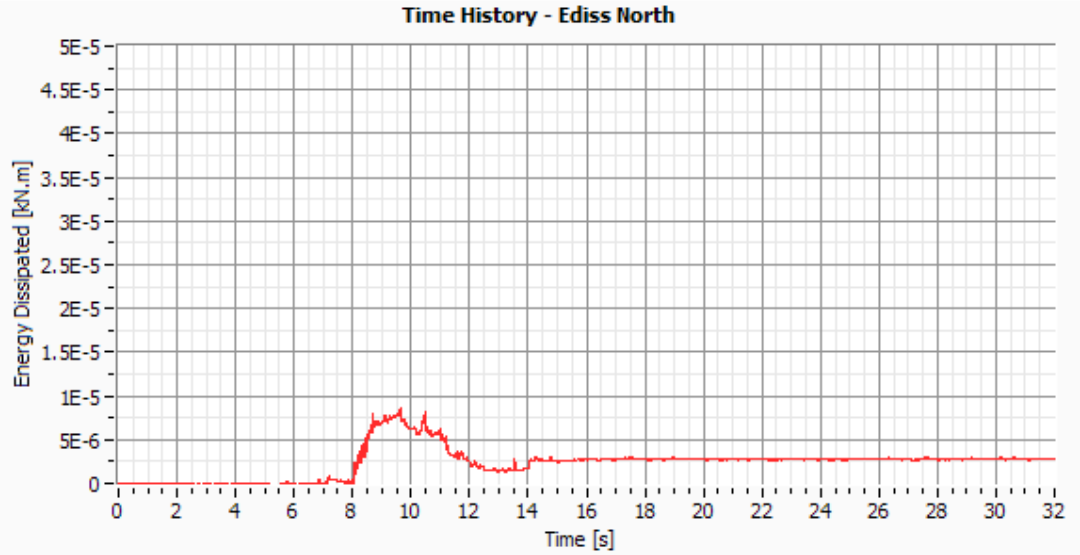

Figure VIII.5: Energy dissipation in the North side.

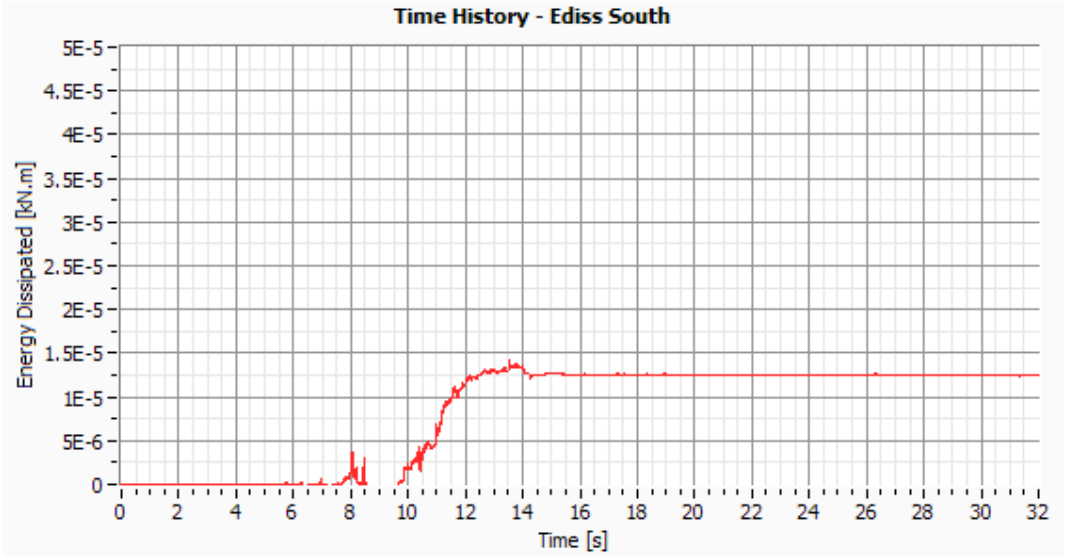

Figure VIII.6: Energy dissipation in the South side.

Test 8 – Sen 8.22Hz (EW PGA=0.05g)

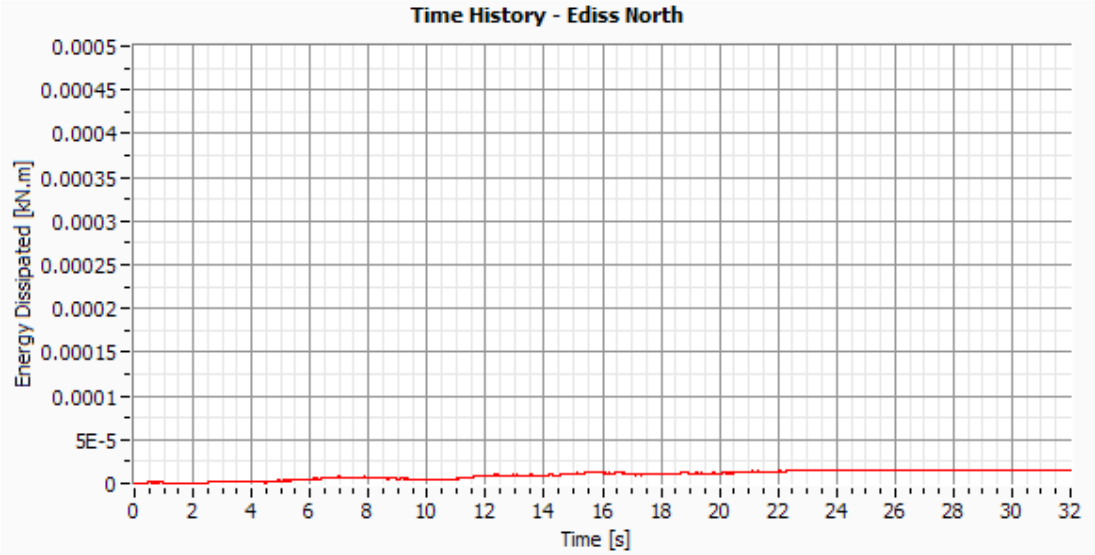

Figure VIII.7: Energy dissipation in the North side.

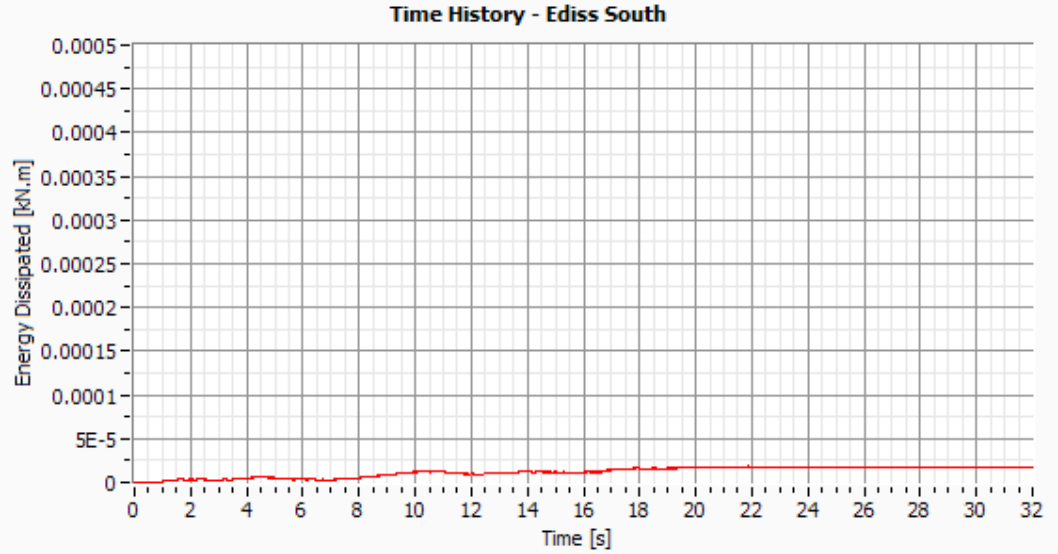

Figure VIII.8: Energy dissipation in the South side.

Test 10 – Artificial EC8 (EW PGA=0.60g)

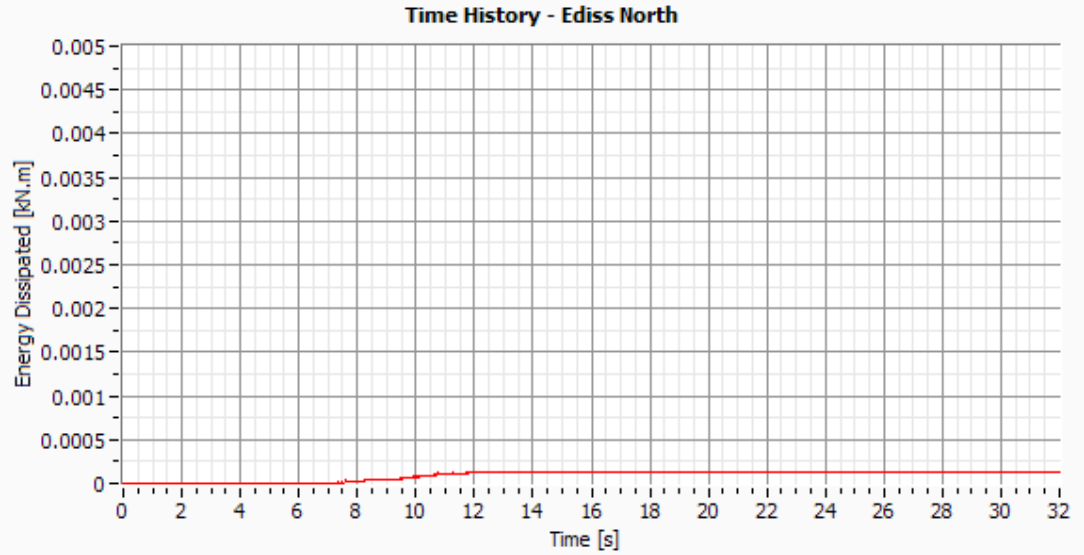

Figure VIII.9: Energy dissipation in the North side.

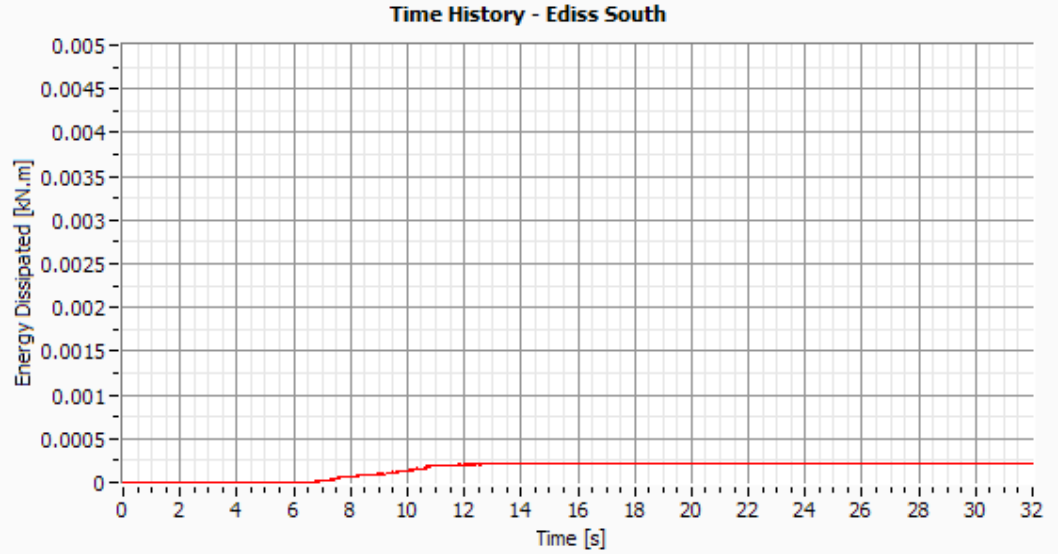

Figure VIII.10: Energy dissipation in the South side.

Test 12 – Artificial EC8 (EW PGA=0.80g)

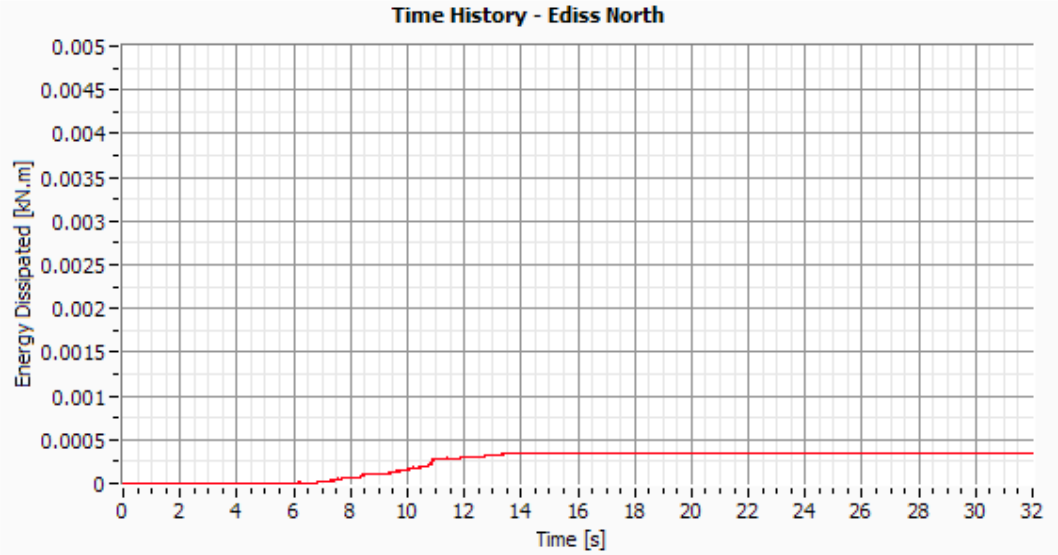

Figure VIII.11: Energy dissipation in the North side.

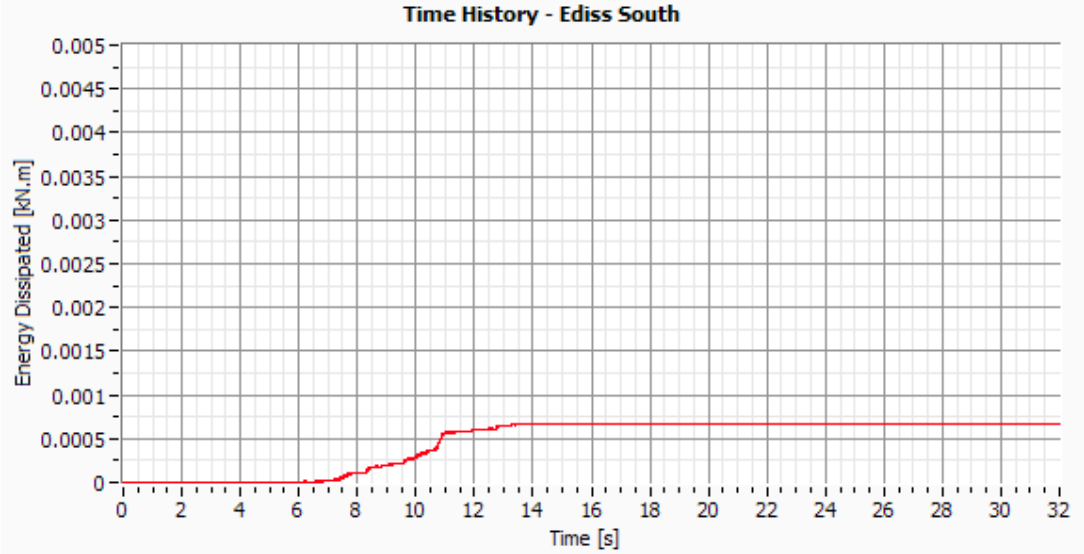

Figure VIII.12: Energy dissipation in the South side.

Test 14 – Artificial EC8 (EW PGA=1.0g)

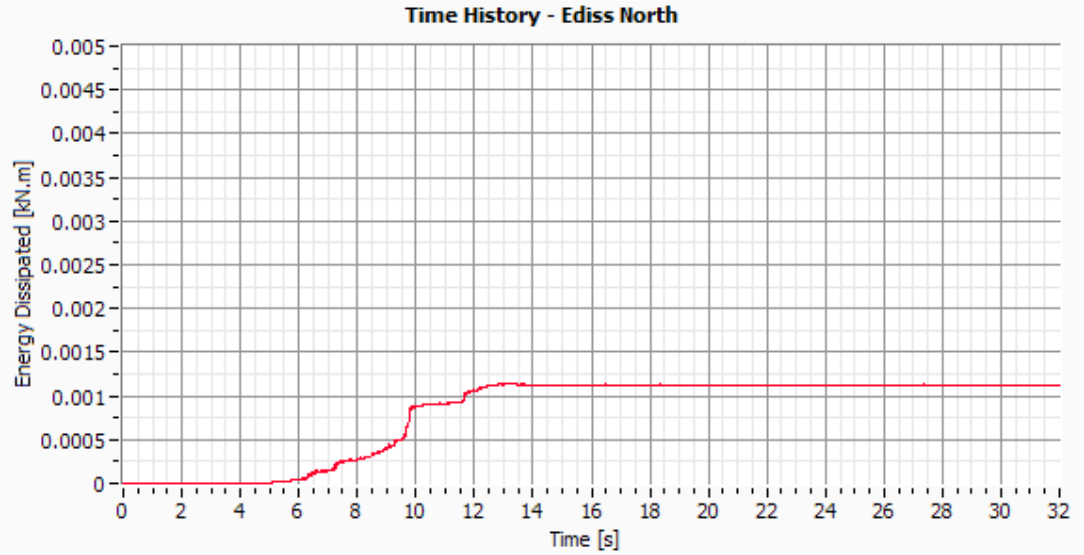

Figure VIII.13: Energy dissipation in the North side.

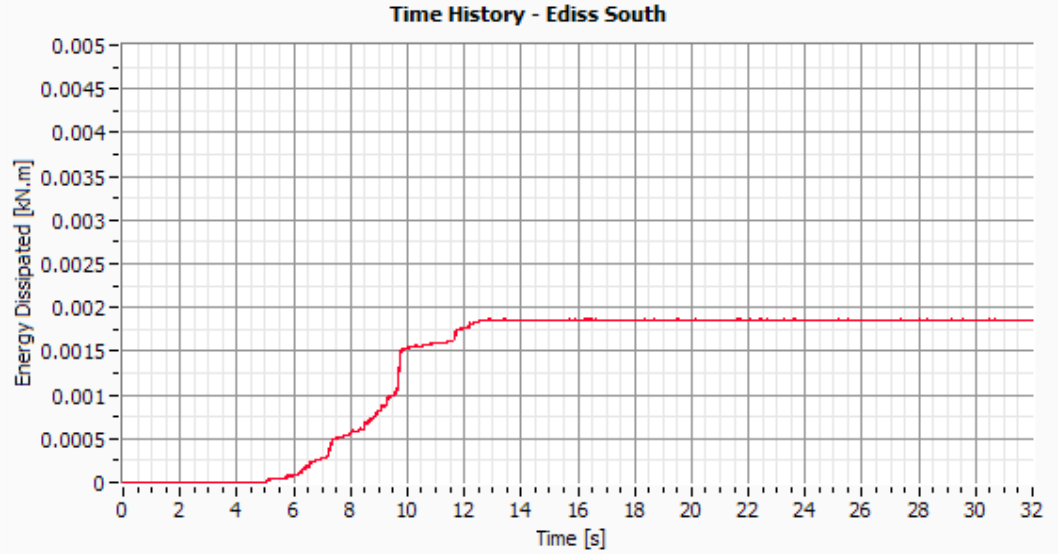

Figure VIII.14: Energy dissipation in the South side.

Test 17 – ElCentro (EW PGA=0.20g)

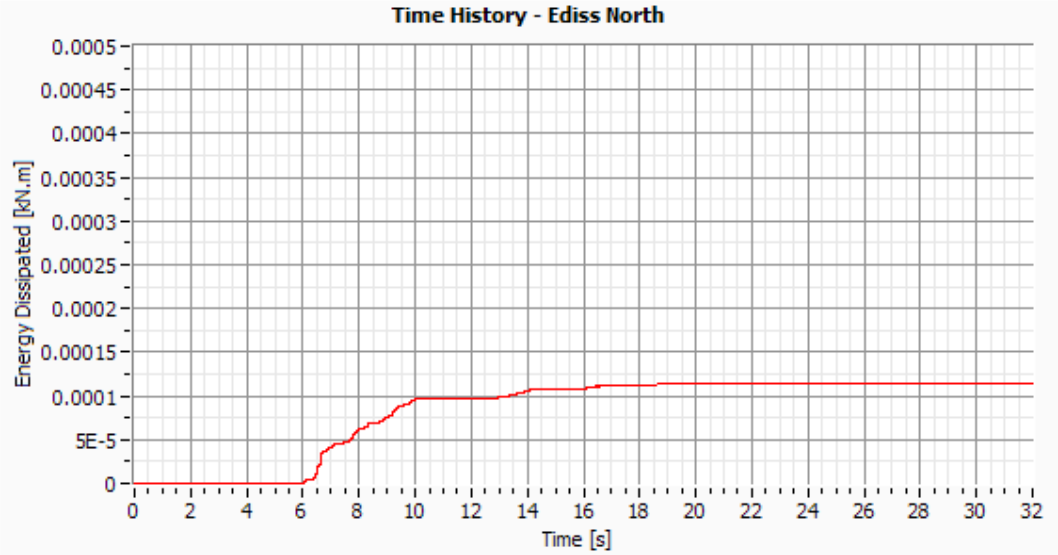

Figure VIII.15: Energy Dissipation in the North side.

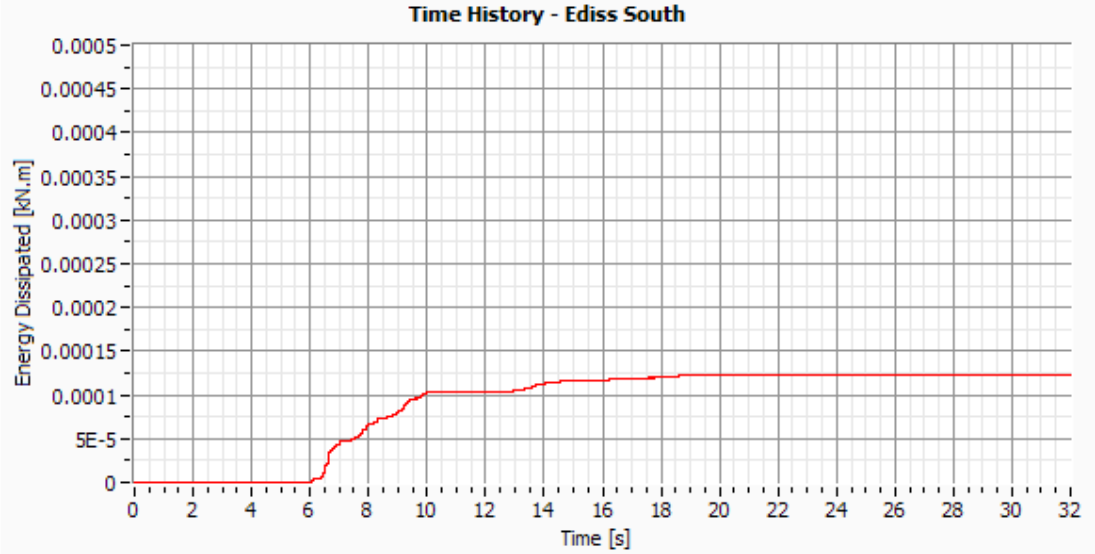

Figure VIII.16: Energy Dissipation in the South side.

Test 18 – Sen 9.48Hz (EW PGA=0.05g)

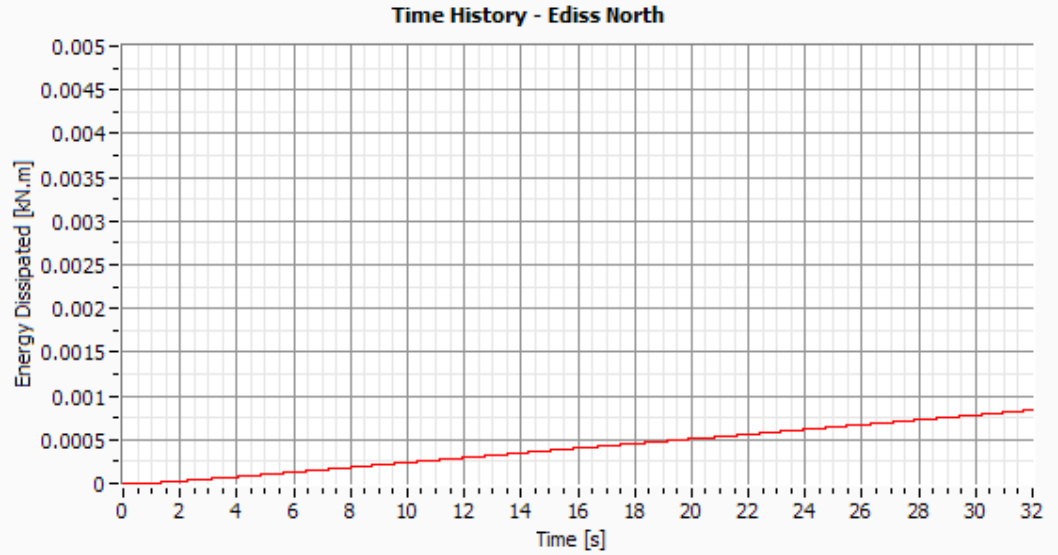

Figure VIII.17: Energy Dissipation in the North side.

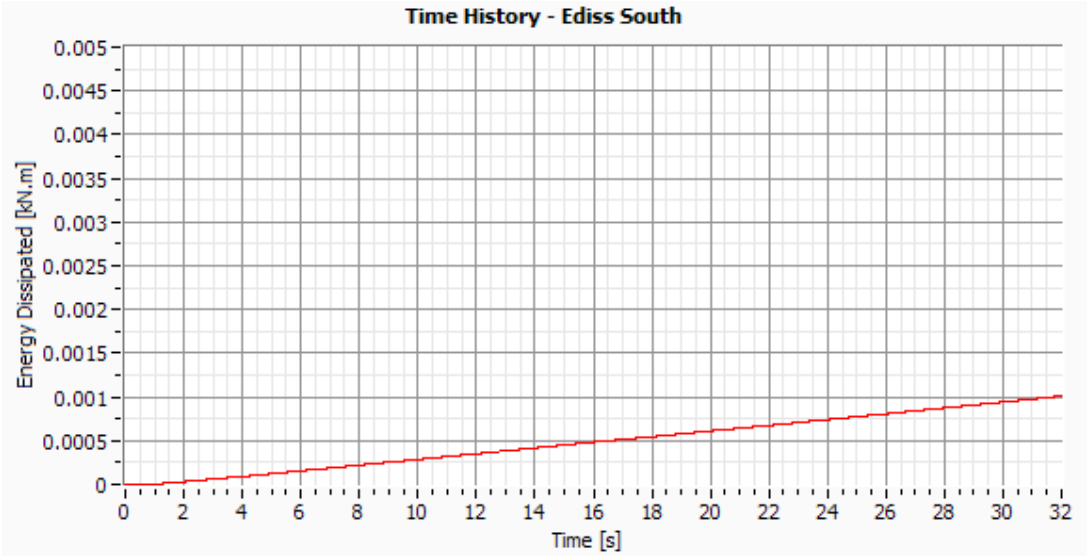

Figure VIII.18: Energy Dissipation in the South side.

Test 19 – Artificial EC8 (EW PGA=0.20g)

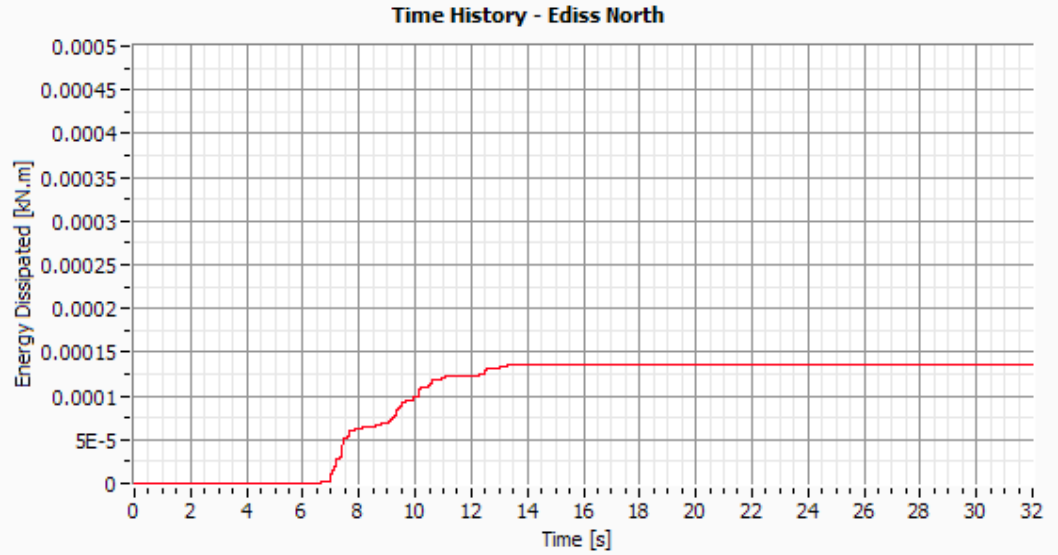

Figure VIII.19: Energy Dissipation in the North side.

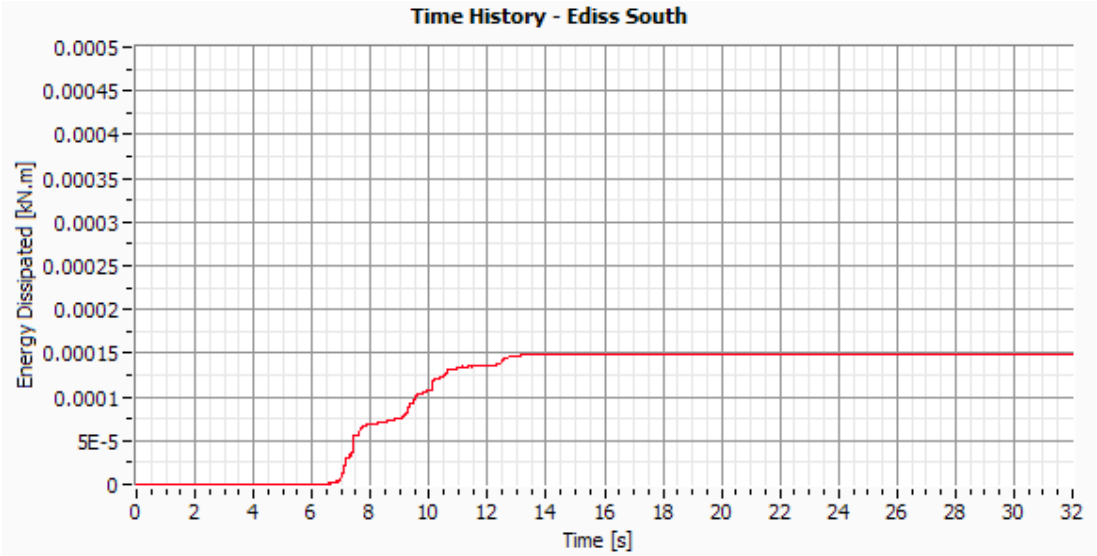

Figure VIII.20: Energy Dissipation in the South side.

Test 20 – Sen 7.58Hz (EW PGA=0.05g)

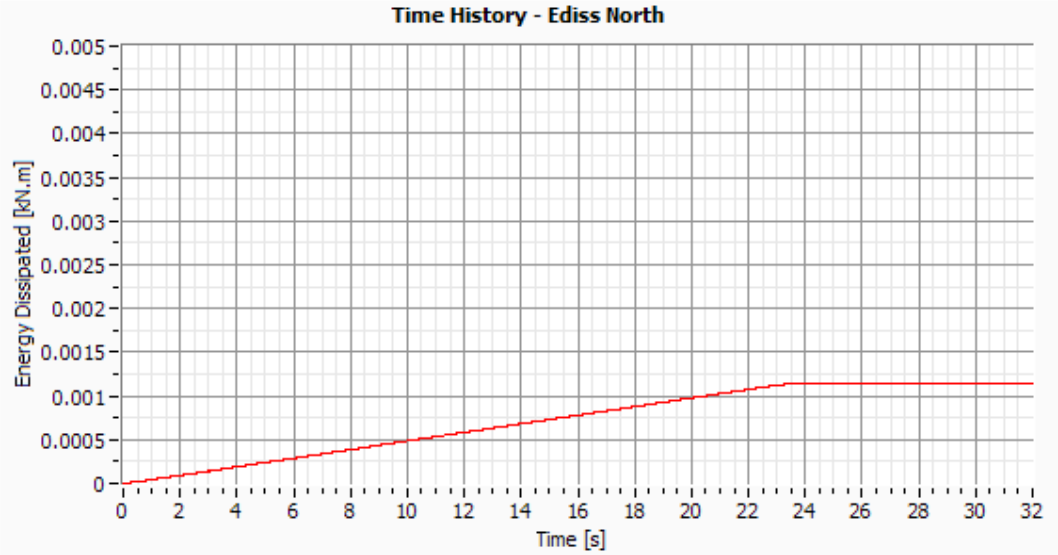

Figure VIII.21: Energy Dissipation in the North side.

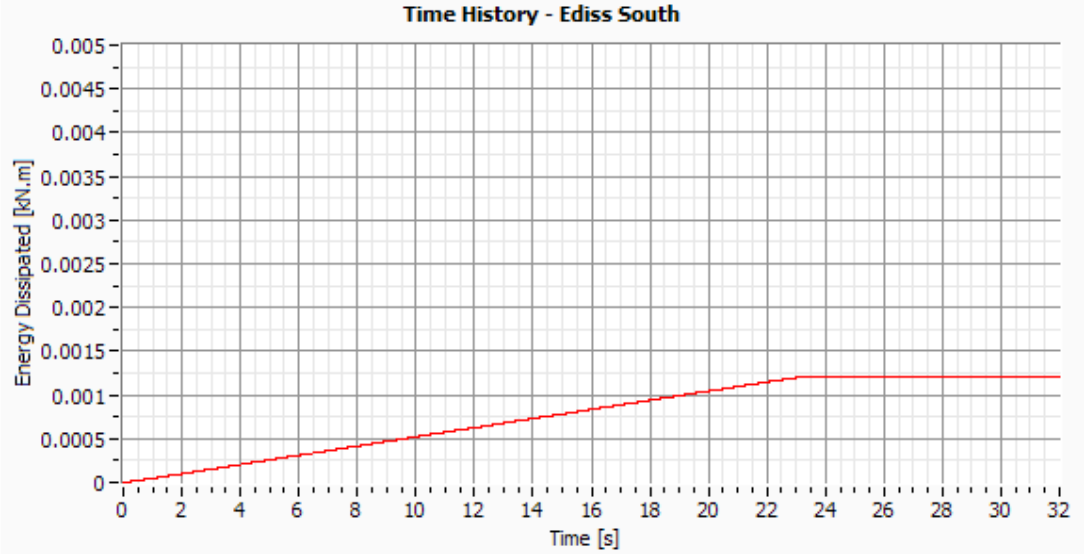

Figure VIII.22: Energy Dissipation in the South side.

Test 22 – Artificial EC8 (EW PGA=0.60g)

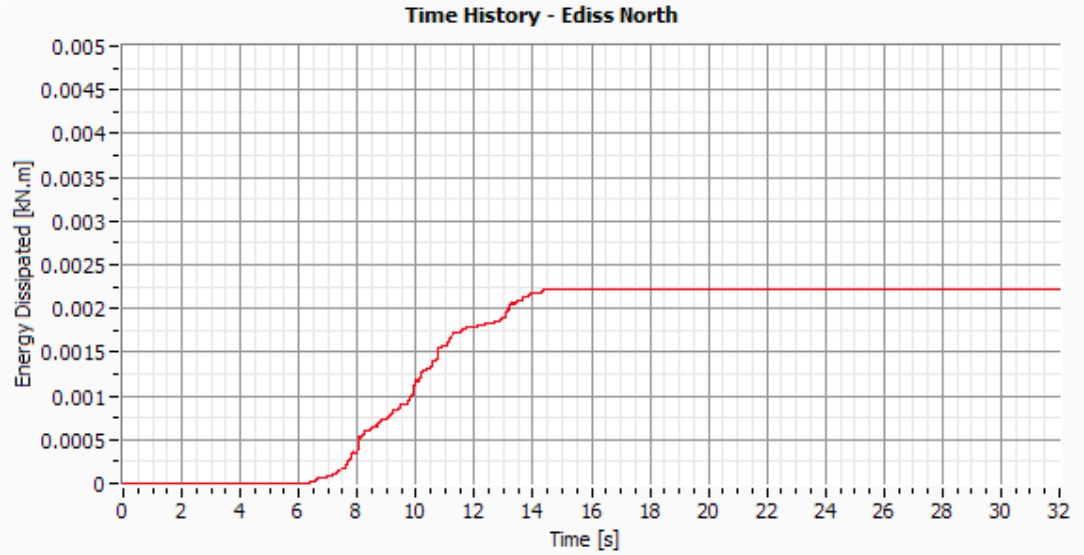

Figure VIII.23: Energy Dissipation in the North side.

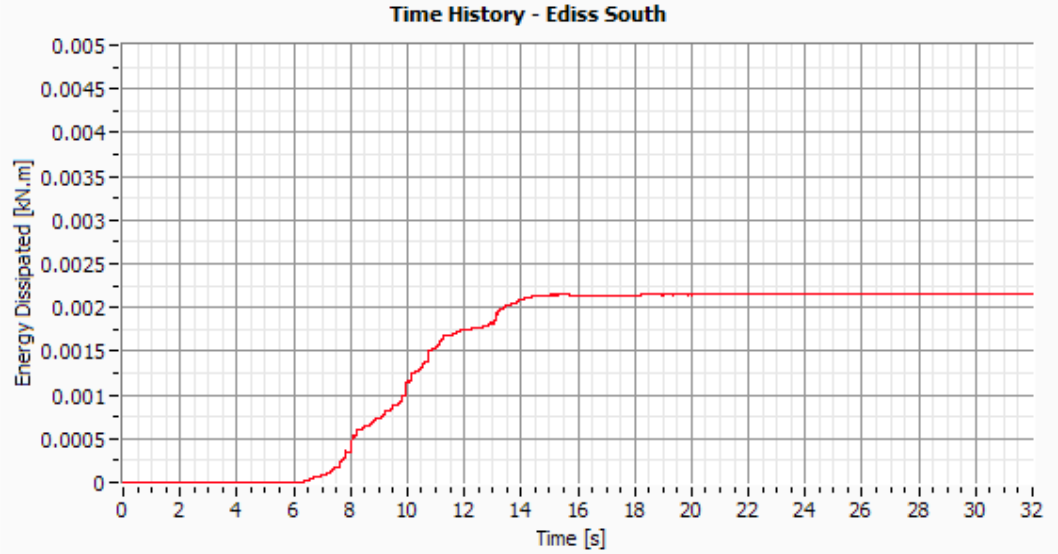

Figure VIII.24: Energy Dissipation in the South side.

Test 24 – Artificial EC8 (EW PGA=0.80g)

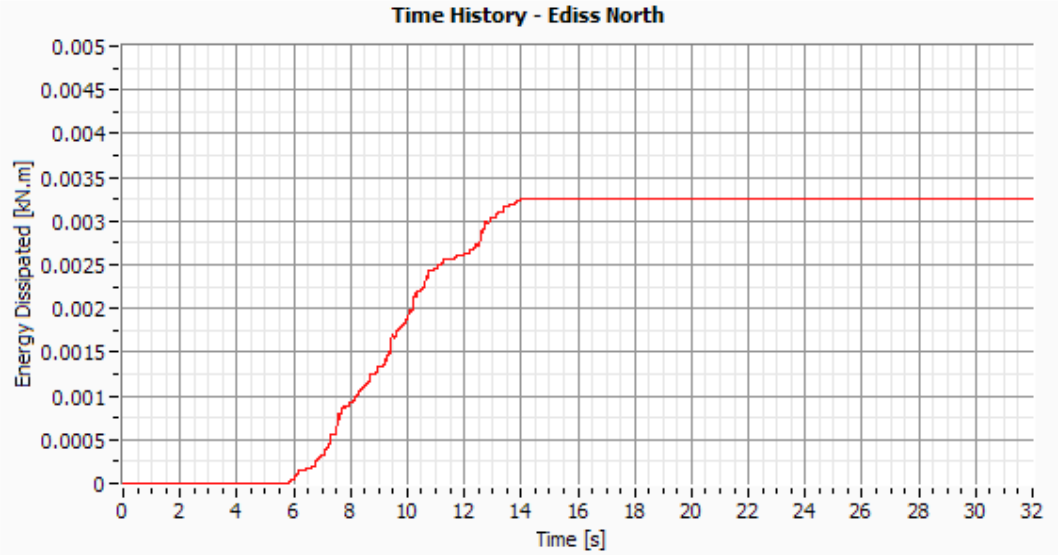

Figure VIII.25: Energy Dissipation in the North side.

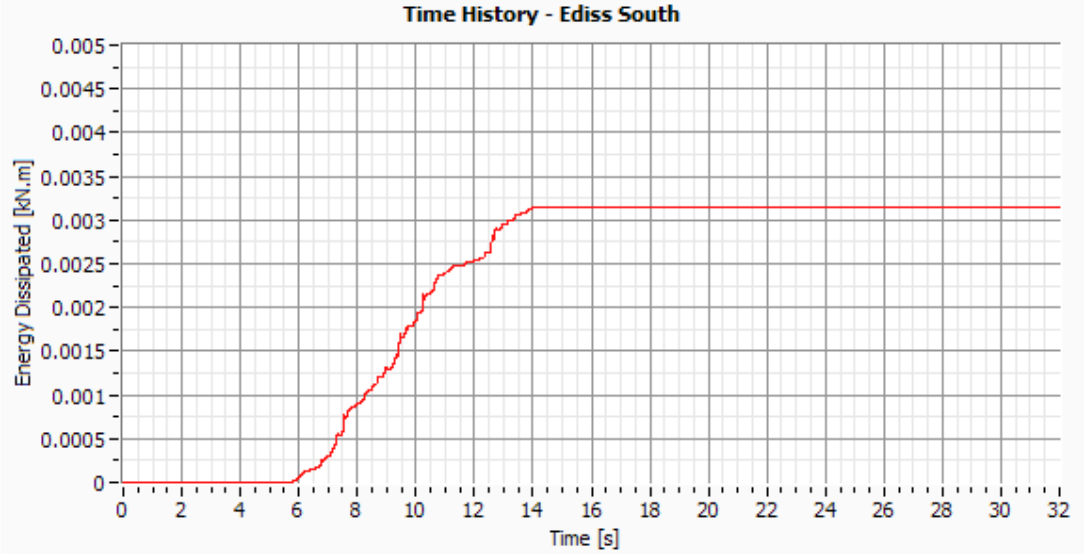

Figure VIII.26: Energy Dissipation in the South side.

Test 26 – Artificial EC8 (EW PGA=1.0g)

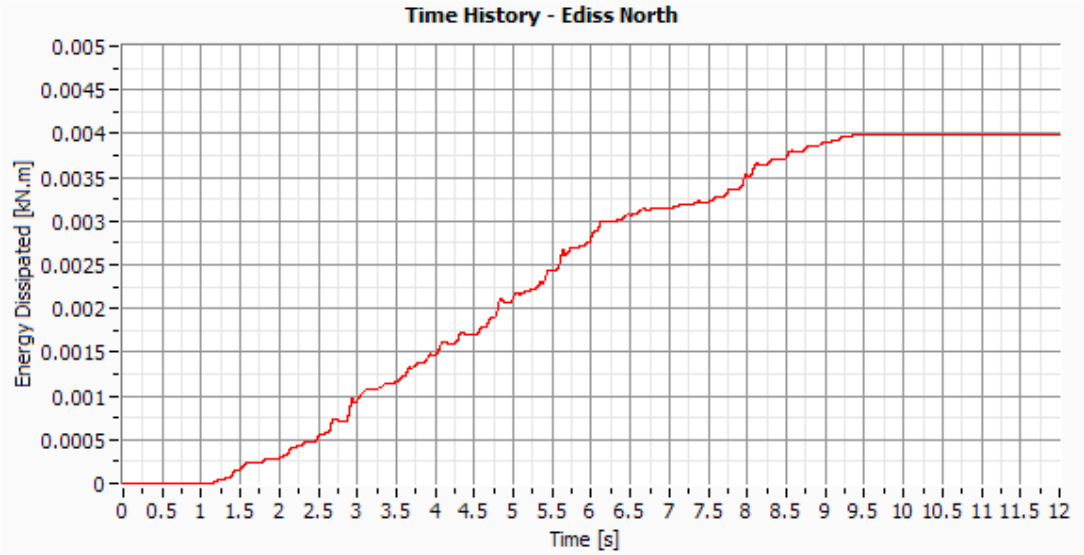

Figure VIII.27: Energy Dissipation in the North side.

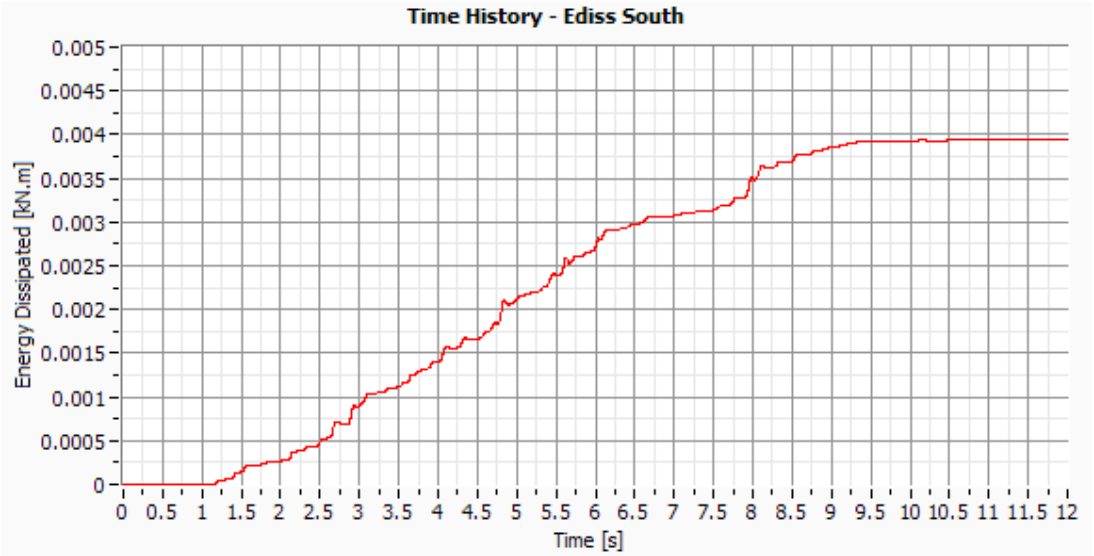

Figure VIII.28: Energy Dissipation in the South side.